IRRIGATION PERFORMANCE OF CENTRE PIVOT END-GUNS OPERATING IN WINDY CONDITIONS

A Thesis submitted by

Mohammed Salim YOUNUS

B.Sc., M.Sc.

For the award of

Doctor of Philosophy

2019

Abstract

Sprinkler irrigated areas are increasing rapidly around Australia and the world. Wind is the main factor that affects sprinkler irrigation performance of all systems, especially those sprinklers that throw into higher elevations above the ground or crop surface. Two sprinkler irrigation systems that are most prone to being impacted by wind are travelling big gun irrigation machines, and end-guns on centre pivot machines.

A lot of research has been conducted to identify the effect of wind for the large impact sprinklers, for solid set sprinkler systems, and movable sprinkler system, using different approaches. The TravGUN irrigation model was developed to simulate big-gun irrigation performance, and has the capability to calculate the radial leg and calibrate the model, from three measured sets of data, one in quiescent wind, and two in different wind speed and directions, and then simulate the wind effect for any wind speed and direction, for a limited combination of wetted sector and side sector angles.

End-guns are a large impact sprinkler which are commonly attached on the distal end of the centre pivot machine to extend the irrigated radius by up to 50 metres. The end-gun sprinkler configurations are very similar to travelling big guns. But, there are two main differences between them. The first difference is that the end-gun side sector angle is perpendicular and asymmetrical to the direction of travel, while big guns have side sector angles parallel to the direction of travel. The second difference is that end-gun on centre pivot travels on curved path, while big guns travel on straight paths.

The literature review addressed low irrigation performance under end-gun irrigated areas, comparing to the irrigated area under regular sprinklers on the centre pivot machine. In addition, there is a lack of studies that investigate the end-gun performance

as a separate pattern from the regular sprinkler pattern on the centre pivot under different windy conditions. Therefore, the research problem that is addressed in this dissertation, aims to develop a new methodology and software tools in order to simulate end-gun performance under different wind speed and directions. The special focus is on a new mathematical model and a new methodology for data collection, to overcome research limitations and answer the research question: Does TravGUN have the capability to simulate end-gun performance in windy conditions?.

Six research objectives have been identified to achieve the main aim of this dissertation:

- First, there is a need to develop a new mathematical model (for inclusion in TravGUN V3.1) to produce radial leg data for end-gun and big gun sprinklers from transect data of any combination of wetted sector and side sector angles.
- Second, there is a need to develop a new methodology for data collection for an end-gun on centre pivots under different wind conditions.
- Third, any new model should be validated by comparing simulated radial leg data for different transect data sets from a range of wetted sector and side sector angles, with measured radial leg data of the same configuration.
- Fourth, simulate end-gun patterns under a constant wind speed and direction for the eight cardinal points of the compass, to represent a full irrigated rotation for all end-gun travel directions on a centre pivot machine, and calculate the application uniformity at each of these eight end-gun travel directions.
- Fifth, the effect of the curved movement on the simulated water depth in the transect data, need to be corrected according to the value of the centre pivot radius.

- Finally, the combined and overlapped normalised end-gun and regular sprinkler patterns from zero wind conditions should be analysed, to evaluate the irrigation performance of both patterns. Then the combined results from eight simulated and corrected end-gun patterns under constant wind speed and direction with eight simulated and normalised regular sprinkler patterns for a centre pivot in the same wind conditions can be simulated, in order to calculate the application uniformity for the entire irrigation system at each the eight cardinal compass points.

The novelty of research lies in developing a new version of TravGUN software to simulate end-gun pattern in different wind conditions. The study concluded that the empirical simulation result under zero wind speed from TravGUN V3.1 for the combination of a wetted sector angle of 130° and side sector angle of 60°, provides the optimum transect for an end-gun on a centre pivot. These simulation results for a centre pivot operating with an end-gun at the eight cardinal positions of the compass under constant speed and direction revealed that the application patterns were distorted, the length of the transect was greatly shortened, and the coefficient of uniformity decreased when the end-gun was travelling crosswind, and upwind. The simulated results adjusted, by the correction factor for curved movement, revealed that the applied water depth decreased. This depth decrease depended on the radius of the centre pivot. The results of the correction factor for three different pivot radii revealed that the curved movement of pivots with radii equal to and less than 400 m have a significant effect, of up to 8.8 % decrease, in the applied water depths.

Thesis Certification

This Thesis is entirely the work of Mohammed Salim Younus YOUNUS except where otherwise acknowledged. The work is original and has not previously been submitted for any other award, except where acknowledged.

Signature of Candidature_____ / / 2019

Mohammed Salim Younus YOUNUS

Principal Supervisor: _____ / / 2019

Associate Professor Joseph Patrick FOLEY

Associate Supervisor: _____ / / 2019

Dr Malcolm GILLIES

Student and supervisors signatures of endorsement are held at the University.

Acknowledgments

This thesis would not have been possible without the many institutes and people who helped me complete my PhD project. First, thanks to God, the Iraqi government, the University of Southern Queensland for giving me this opportunity and the research training scheme provided by Australian government.

I would like to express my deepest appreciation to my principal supervisor, Dr Joseph Foley, for his guidance, remarks and engagement throughout the process of my learning in the field of sprinkler irrigation. Thanks for their valuable, useful solutions to the great number of challenges during the period of field tests through borrowing me, his own irrigator machine and the equipment. I would like to thank him also for providing me with centre pivot simulated patterns in zero wind and in simulated wind to investigate the combined patterns for end-gun and centre pivot at overlapping area. I am highly grateful to my associate supervisor Dr Malcolm Gillies for his great time and effort in providing the code of TravGUN software and his guidance during the development of the algorithms. Thanks are also due to my colleague Dr Omar Hazem Salim, who helped me to learn and use MATLAB program in solving a complicated mathematical calculations. Further, I would like to express my thanks to all my colleagues who supporting me during this studying journey. I would like my thanks go to Roy from the (the word whisperer) website for helping me in proofreading the thesis.

Finally, I would thank my loving wife and children for their patience, love and support while, enduring significant absence of my time during the period of this dissertation.

I would like to dedicate this dissertation to my mother and father, whom never had a formal education but have taught me more in life than anyone else, whom always encouraged me to challenge the travel and achieve highest degree.

Contributions to theory and practice from this research

This dissertation has covered a wide range of topic areas in developing a methodology to measure, simulate and optimize the irrigation performance of end-guns on centre pivots under different wind conditions. A summary of the major contributions to theory and practice arising from this research is as follows:

- Collection of an extensive field test data set from more than twenty five trails of a Nelson SR100 end-gun in quiescent and windy conditions that captures radial leg information, and transect data sets from this moving irrigation sprinkler.
- Development of a new mathematical model to predict radial leg data from end-gun transect data, for any combination of wetted sector and side sector angles.
- Validation of this new sub-model in a new version of the TravGUN simulation model (TravGUN V3.1), to predict radial leg data from end-gun transect data for any combination of wetted sector and side sector angles, against the measured field data sets.
- Simulation of the irrigation performance of an end-gun on a centre pivot at the eight cardinal point of the compass, in a wind of constant speed and direction, to represent the full irrigation rotation of centre pivot irrigation machine.
- Investigation and determination of a correction factor for the simulated transect data and irrigation performance due to the effect of the curved movement of an end-gun on centre pivots different radii.
- Evaluation of the irrigation performance of the combinations of corrected, simulated end-gun patterns with simulated regular sprinkler patterns on centre pivot at the eight cardinal compass points for the wind constant direction and

speed. Recommendation and suggestions to improve the irrigation performance of end-guns on centre pivots under different wind conditions, have been made

This research has led to the development of a new end-gun test methodology, and a new version of the TravGUN model (V3.1) that now allows for the evaluation of the irrigation performance of end-guns on centre pivots under different wind conditions. This, will serve as a practical tool, and a theoretical platform for improving irrigation performance of end-guns on centre pivots into the future.

Contents

Abstract i
Thesis Certification v
Acknowledgments vii
Contents xi
List of Figures xix
List of Tables xxxiii
List of Abbreviations xxxv
1 CHAPTER ONE Introduction 1
1.1 Background 1
1.2 The Hypothesis 2
1.3 TravGun limitations 2
1.4 Objectives 3
1.5 Thesis Structure 4
2 CHAPTER TWO Literature Review 7
2.1 Introduction 7
2.2 The similarities and the differences between end-guns and travelling big-gun sprinklers 7
2.2.1 End-gun on centre pivot irrigation systems 8
2.2.2 Travelling big-gun sprinkler 10
2.3 Sprinkler characteristics 13
2.3.1 Wetted distribution pattern 13
2.3.2 Radial leg 14
2.4 Irrigation Performance (Application Uniformity) 14
2.5 The factors that affect the performance (application uniformity) 16
2.5.1 Sprinkler machine operating adjustments 16
- Sector angle 16
- Side sector angle 17
- Trajectory angle 17
- Nozzle pressure 18
- Nozzle shape 19
- Nozzle size 20

- Nozzle height 21
- Machine speed 21
- Lane spacing 22

2.5.2 Weather condition 22

2.6 Models that predict the distortion in wetted distribution pattern under wind conditions for large sprinklers 24

2.6.1 Empirical models 25

2.6.2 Semi-empirical models 25

2.6.3 Ballistic models 31

2.7 Measurement methodology 32

2.7.1 Transect measurement 32

2.7.2 Full grid measurement 33

2.7.3 Drop size distribution measurement method 34

2.8 Review of research conducted on end-gun performance 35

2.8.1 Analysing the motion of the wetted distribution pattern of end-guns on a centre pivot systems 35

2.8.2 The performance of end-guns in centre pivot systems 37

2.9 Summary and the Research Gap 38

3 CHAPTER THREE Development of a new TravGUN sub-model ..41

3.1 Introduction 41

3.2 Development of a new mathematical model 42

3.3 Calculation of segment lengths for three combinations of sector and side sector angles 48

3.3.1 Case 1: Segment length L for $90° < \theta < 180°$ and $225° < \phi < 315°$ 48

3.3.2 Case 2: Segment length L for $90° \leq \Theta < 180°$ and $-315° \leq \phi < 45°$ 51

3.3.3 Case 3: Segment length L for $0° < \Theta < 90°$ and $180° < \phi < 270°$ 56

3.4 Calculating the application rate at each segment or fragment of segment .61

3.4.1 Calculating the application rate for a sector angle of less than 180° with side sector angle symmetrical to the direction of travel 62

3.4.2 Calculating the application rate for a sector angle of less than 180° with the side sector asymmetrical to the direction of travel 72

3.5 Boundaries of sector angles calculation in the model 76

3.6 Summary 80

4 CHAPTER FOUR Material and Methods 81
4.1. Introduction 81
4.2. Characteristics of Testing Site 81
4.3. Machine and Equipment Used and Setup 83
4.3.1 Adjusting the pump pressure 85
4.3.2 Adjusting sector and side sector angles 86
4.3.3 Adjusting machine speed and consistency 87
4.3.4 Measured data and modification 88
4.3.5 Measuring wind speed and direction during tests 88
4.4. Selecting appropriate local climate condition for open field measurements 90
4.5. Measuring radial leg and transect data in the field 94
4.6. Measuring radial leg data from stationary full circle 95
4.7. Measuring transects of different wetted sector and side sector angles 98
4.8. Measuring transects in curve movement 100
4.9. Methodologies for validation, and simulation of end-gun patterns in wind using new sub-model 102
4.10 Summary 103
5 CHAPTER FIVE Field measurement and data analysis 105
5.1 Introduction 105
5.2 Measuring radial leg data from a stationary full circle 105
5.2.1 Measured radial leg data in Test Four 106
5.2.2 Measured radial leg data from Test Six 111
5.2.3 Measured radial leg data from Test Seven 113
5.2.4 Measured radial leg data from Test Eight 118
5.2.5 Identifying the radial leg for validation processes 122
5.3 Measured transect data 124
5.4 Measured transects for straight travel 125
5.4.1 Measuring transect Test Number Four 125
5.4.2 Measured transect data Test Number Seven 128
5.4.3 Measured transect data from Test Number Eleven 130
5.4.4 Measured transect data from Test Number Ten 133
5.4.5 Measured transect data for Test Number Thirteen 136

5.5 Measured transects on curved paths 139
5.5.1 Measured transect from Test Number Fourteen 139
5.5.2 Measured transect data Test Number Fifteen 142
5.5.3 Measured transect data from Test Number Seventeen 145
5.6 Recording zero wind speed during the measurements.....149
5.6.1 First Record of zero wind speed 149
5.7 Summary.....154

6 CHAPTER SIX Validation of the new sub-model to estimate the sprinkler radial leg.....155
6.1 Introduction.....155
6.2 Validation of the predicted radial leg for combinations of different wetted sector angles perpendicular to travel direction 156
6.2.1 Validation of predicted radial leg from transect of wetted sector angle $\theta =$ 180° and side sector, $\phi =$ 270° 156
6.2.2 Validation of predicted radial leg from transect of wetted sector angle 140° and side sector 270° 158
6.2.3 Validation of predicted radial leg from transect of wetted sector angle 105° and side sector 270° 159
6.2.4 Validation of predicted radial leg from transect of wetted sector angle 80° and side sector 270° 160
6.3 Validation of the combination of wetted sector angles not perpendicular to travel direction 161
6.4 The comparison of different curved movement for wetted sector angle of 180° and a side sector angle of 270°.....162
6.4.1 Comparison of transect from curved and straight movement at a 200-metre radius.....163
6.4.2 Comparison of transect from curved and straight movement at a 300-metre radius.....164
6.4.3 Comparison of transect from curved and straight movement at a 400-metre radius.....165
6.4.4 Comparison of three curved transects.....167
6.5 Discussion and conclusions 168
6.5.1 Validation of the new sub-model in TravGUN.....168

6.5.2 Impact of the curved movement of the end-gun 168
7 CHAPTER SEVEN Optimising End-Gun Performance under Windy Conditions 171
7.1 Introduction.....171
7.2 Optimizing wetted sector and side sector angles under no-wind conditions.....172
7.3 Simulated end-gun transect of Θ = 130° and ϕ = 60° in no-wind for a machine speed of 50 m/h 179
7.4 Simulating the optimum sector and side sector angles under windy conditions.....180
7.4.1 Simulation results for an end-gun travelling directly into the wind .183
7.4.2 Simulation results for an end-gun travelling across the incoming wind by 45°.....185
7.4.3 Simulation results for the end-gun travelling south in an Easterly wind 187
7.4.4 Simulating the pattern for end-gun travel in a direction of 225° 189
7.4.5 Simulating the pattern for end-gun travel direction of 270° in an easterly wind.....191
7.4.6 Simulating the pattern for end-gun travel direction of 315° 193
7.4.7 Simulating the pattern for end-gun travel direction of 360° 195
7.4.8 Simulating the pattern for end-gun travel direction of 45° 197
7.4.9 Simulation outcomes.....199
7.5 Correction factor for arced movement.....199
7.6 Determining the significance of the curved movement.....203
7.6.1 Correcting the water depth for a centre pivot of 250 m radius 203
7.6.2 Correcting the water depth for centre pivot of 400 metre radius 204
7.6.3 Correcting the water depth for centre pivot of 550 m radius 204
7.7 Combining the end-gun pattern with regular centre pivot sprinkler patterns in zero wind 205
7.8 Combining the end-gun wetted pattern with regular centre pivot sprinkler patterns in windy conditions.....207
7.8.1 Simulating both patterns for a travel direction of 90° 207
7.8.2 Simulating both patterns for a travel direction of 135° 208

7.8.3 Simulating both patterns for a travel direction of 180° 209
7.8.4 Simulating both patterns for a travel direction of 225° 210
7.8.5 Simulating both patterns for a travel direction of 270° 211
7.8.6 Simulating both patterns for a travel direction of 315° 211
7.8.7 Simulating both patterns for a travel direction of 360° 212
7.8.8 Simulating both patterns for a travel direction of 45° 213
7.9 The general shapes for different wetted sector angle perpendicular to the direction of travel 214
7.10 Simulating end-gun patterns for curved movement 215
7.11 Conclusions 219
8 CHAPTER EIGHT Discussion 223
8.1 Introduction 223
8.2 Evaluation of the performance of end-guns on centre pivots 223
8.3 TravGUN limitations 225
8.4 Developing a new mathematical model for big gun sprinklers 226
8.5 New methodology for field tests 228
8.6 Field measurements for end-gun configuration 229
8.6.1 Radial leg data 229
8.6.2 Transect data from straight movement 230
8.6.3 Transect data with curved movement 231
8.7 Validation of the new TravGUN sub-model 232
8.8 Correction the curved movement 233
8.9 Using the new model (to solve the problem) 235
8.10 Simulating end-gun pattern in windy conditions 235
8.11 The combination of end-gun and centre pivot patterns 236
8.12 Conclusion 238
9 CHAPTER NINE Conclusions and Future Study 239
9.1 Conclusions 239
9.2 Recommended Future research 240
References 243
A. Appendix A Radial Leg at Wind 251
A.1 Introduction 251
A.2 Measuring radial leg data from stationary full circle 251

A.2.1 Measuring radial leg data test one on 15/3/2015 at 7:20 pm.....251
A.2.2 Measuring radial leg data test two on 18/3/2015 at 4:00 am.....253
A.2.3 Measuring radial leg data test three on 18/3/2015 at 6:30 pm.....255
A.2.4 Measuring radial leg data test five on 18/3/2015 at 9:30 pm 257
B. Appendix B Transect data at Wind.....261
B.1 Introduction.....261
B.2 Measuring transects in straight movement.....261
B.2.1 Transect test number eight.....261
B.2.2 Transect test number nine.....263
B.2.3 Transect test number twelve.....265
B.2.4 Transect test number five 267
B.2.5 Transect test number six.....269
B.2.6 Transect test number one.....271
B.2.7 Transect test number two.....273
B.2.8 Transect test number three.....275
B.3 Measuring transect in curve movement 277
B.3.1 Transect test number sixteen 277
C. Appendix C Record Zero Wind Speed.....281
C.1 Introduction.....281
C.1.1 Second record of zero wind speed.....281
C.1.2 Third record of zero wind speed.....283
C.1.3 Fourth record of zero wind speed.....286
C.1.4 Fifth record of zero wind speed.....290
C.1.5 Sixth record of zero wind speed 293

List of Figures

Figure 2-1: Main components of the Nelson SR100 large impact sprinkler, used in travelling big-guns and in end-guns on centre pivots (Nelson Irrigation, 2010) 8

Figure 2-2:The shape of an irrigated field using a centre pivot system with an end-gun attached to the outer end of the pivot, where (a) is the fixed centre tower, (b) number of spans of the centre pivot attached to the end-gun, (c) end-gun on centre pivot system (Centralstation, 2014) (Lindsay Corporation, 2011, 2012) (Google Image, 2014) 9

Figure 2-3: Diagram of the end-gun on centre pivot shows wetted sector and travel path (Nelson Irrigation, 2018) 10

Figure 2-4: A travelling big gun sprinkler machine consists of a big gun on a cart wheel (1), distribution hose (2) and self-propelled stationary hose reel (3) and central pressurised supply water pipe (4) (Google Image, 2015) (Wade Rain, 2018) . 11

Figure 2-5: Diagram of travelling big-gun showing wetted sector and travel path (Lacey, 2006) 12

Figure 2-6: Distribution patterns as visual form full circle during (left) calm conditions and (right) wind speed of 4.5 m/s, the dark colour refer to more water depth (Newell, 2003) 13

Figure 2-7: A radial leg from stationary gun from Newell et al. (2003) 14

Figure 2-8: Sector and side sector angles. A- Sector angle 340° and Side sector parallel to travel direction. B- Sector angle 220° and Side sector perpendicular to travel direction 17

Figure 2-9: Large sprinklers with adjustable trajectory angle (Nelson Irrigation, 2014) (India Mart, 2014) 18

Figure 2-10: Different nozzle types (A) taper nozzle, (B) taper ring nozzle and (C) ring nozzle (Newell et al., 2002) and (Nelson Irrigation Australia, 2016) 20

Figure 2-11: The distribution behaviours of droplets from different nozzle shapes (A) Ring nozzle, (B) Taper nozzle (Nelson Irrigation, 2016) 20

Figure 2-12: Movement of sprinkler patterns due to wind from Newell et al. (2003) 27

Figure 2-13: The angles used in the model by Al-Naeem (1993) 28

Figure 2-14: Procedure for determining the radial leg pattern from the measured transect (Smith et al., 2008) 30

Figure 3-1: Scheme showing the main angles used in developing the TravGUN sub-model. 43

Figure 3-2: Procedure for determining the radial leg pattern from the measured transect for case 1 (when the sector angle is between 0° and 180° and the side sector angle is perpendicular to the direction of travel). 43

Figure 3-3: Summary of the calculation process for length segment area for two separate quarters (first case). 46

Figure 3-4: Diagram showing the value of the α angle. 48

Figure 3-5: Diagram showing the value of the β angle. 50

Figure 3-6: Procedure for determining the radial leg pattern from the measured transect for case 2 (when sector angle less than 180° and greater than 0° and side sector angle parallel to the direction of travel) 54

Figure 3-7: Summarisation of the calculation process of length of segment area from two separate quarters (second case). 55

Figure 3-8: Procedure for determining the radial leg pattern from the measured transect for case 3 (when the sector angle less than 90° and greater than 0° and the side sector angle changes from 180° to 270° for each quarter to the direction of travel). 57

Figure 3-9: Summarisation of the calculation process of length of segment area from two separate quarters (third case). 59

Figure 3-10: An irrigation pattern scheme showing different areas where the mathematical calculations are undertaken to calculate the application rate for sector angles less than 180° with a side sector symmetrical to the direction of travel. 64

Figure 3-11: Procedure showing the critical points (LKω1 , LKω2) and a spatial distribution of the indicators ($K\alpha_{ij}$ and $K\beta_{ij}$) for sector angles less than 180° with side sector symmetrical to the direction of travel. 65

Figure 3-12: Summarisation of the calculation process of application rates at each segment area from two separate quarters 68

Figure 3-13: Summarisation of the calculation process of application rates at each segment area from two separate quarters 69

Figure 3-14: A scheme showing three different areas: blue area is equal on both sides, pink area received part pattern from the α side and full pattern from the β side, orange area received part pattern on both the α and β sides. 73

Figure 3-15: Summarisation of the calculation process of application rates at each segment area from two separate quarters..... 74

Figure 3-16: Summarisation of the calculation process of application rates at each segment area from two separate quarters..... 75

Figure 3-17: Three different areas: orange represents dry angle; the blue area from ω_1 to ω_2 represents wetted sector angle; and green (between 0° to 180°) represents the area where the calculation process takes place. 76

Figure 3-18: Two different areas: the orange area represents dry angle; and the green area between ω_1 and ω_2 represents wetted sector angle corresponding with the first edge of calculation process and the second edge of the calculation process (20° to 140°) respectively. 77

Figure 3-19: Three different areas: orange represents the dry angle; blue area from ω_1 to ω_2 represents wetted sector angle; and green area between ω_1 to 180° represents the area where the calculation process takes place..... 78

Figure 3-20: Three different areas: orange represents the dry angle; blue area from ω_1 to ω_2 represents wetted sector angle; and green area between 0° to ω_2 represents the area where the calculation process takes place. 79

Figure 4-1: Map of experiment site shows the buildings and institutions surrounding the experiment site (Google Maps, 2016)..... 82

Figure 4-2: Experiment site and location of equipment and all facilities relating to measurement (Google Maps, 2015)..... 83

Figure 4-3: Travelling-gun irrigator machine (Trailco T200-2, 2018). 84

Figure 4-4: Big-gun water sprinkler (Nelson Irrigation, 2015). 85

Figure 4-5 : Pressure gauge fixed close to the big gun, and two hoses fixed to redirect the water from the two small speed control nozzles. 86

Figure 4-6: Large protractor drawn on plastic sheet to adjust sector and side sector angles. 87

Figure 4-7: Three weather stations were used to measure wind speed and direction at the experimental site, and two close to the field site are shown here. 89

Figure 4-8: Photo of Weather Zone forecasts toolbars show minimum wind speed and wind direction change at same time (Weatherzone, 2015b). 90

Figure 4-9: Shot-screen (snapshot) from smartphone for Mean Sea Level Pressure map (Bureau of Meteorology, 2015a). 91

Figure 4-10 : Two different atmosphere pressure maps, letter (T) refer to experimental region influence under neutral pressure, letter (H) centre of high pressure zone and letter (L) centre of low pressure zone (Bureau of Meteorology, 2015a). .. 92

Figure 4-11 : Snapshot (shot-screen) from smartphone for online current weather condition at different times in the same day (Weatherzone, 2015a). 94

Figure 4-12: A photo of the irrigation machine and the four lines of collectors, setup for stationary tests. 96

Figure 4-13: Experimental layout for stationary tests; three lines of collectors were placed radially from the centre of the sprinkler 120° intervals..... 97

Figure 4-14: The second experimental layout for stationary tests with four lines of collectors placed radially from the centre of sprinkler 90° intervals. 97

Figure 4-15: Experimental layout for testing where three lines of collectors were placed perpendicular to the machine travel direction, with a sector angle less than 180°, and with a side sector of 270° to the travel direction. 99

Figure 4-16 : Photo of the experimental field is shown with three lines of collectors placed perpendicular to the travel direction from one side of irrigated area by travelling machine..... 99

Figure 4-17: Experimental layout showing three lines of collectors which were placed perpendicular to the machine's travel direction, with sector angles less than 180°, and side sector angle not perpendicular ($\phi \neq 270°$) to the travel direction. ... 100

Figure 4-18 : Experimental layout, where three lines of collectors were placed perpendicular to the machine travel direction, and a sector angle of 180°, and a side sector angle perpendicular and asymmetrical to the travel direction was used for a sprinkler travelling on a curved path. 101

Figure 4-19: Photo of real experimental layout, while three lines of collectors were placed perpendicular to machine travel direction, using a sector angle of 180°, and a side sector angle perpendicular to the travel direction, while the machine is traveling in curved movement. 102

Figure 5-1: Radial leg data Test Four, collected from three lines of collectors placed around a stationary sprinkler..... 107

Figure 5-2: Weather conditions (wind speed and direction) for radial leg test four. 108

Figure 5-3: Surface plot for radial leg Test Four shows the effect of wind on sprinkler distortion pattern. 110

Figure 5-4: Radial leg data from Test Six collected from three lines of collectors placed around a stationary sprinkler. 111

Figure 5-5: Weather conditions (wind speed and direction) for radial leg Test six. 112

Figure 5-6: Interpolated full circle applied depth plot for radial leg Test Six shows the effect of wind direction on the sprinkler pattern. 113

Figure 5-7: Radial leg data from Test Seven collected from four lines of collectors placed around the stationary sprinkler. 114

Figure 5-8: Weather condition (wind speed and direction) for radial leg collection in the Test Seven. 115

Figure 5-9: Surface interpolation plot of applied depths for radial leg Test Seven shows the effect of wind distortion on the sprinkler pattern. 117

Figure 5-10: Radial leg data from Test Eight collected from four lines of collectors placed around a stationary sprinkler. 119

Figure 5-11: Weather conditions (wind speed and direction) for radial leg Test Eight. 120

Figure 5-12: Surface interpolation plot for radial leg data Test Eight showing the effect of wind distortion on the sprinkler pattern. 122

Figure 5-13: Radial water distribution profile of Nelson SR 100 Big Gun sprinkler operating at 490 kPa with a 25.4 mm taper ring nozzle on an 18° trajectory angle as determined on tests Seven and Eight. 123

Figure 5-14: Transect Test Number Four shows test layout, the combination of wetted sector and side sector angles and other directions relevant to that test. 125

Figure 5-15: Weather conditions (wind speed and direction) for transect Test Number Four. 126

Figure 5-16: Transect data for Test Number Four for the combination of 180° wetted sector angle and 270° side sector angle. 127

Figure 5-17: Transect Test Number Seven shows test layout, the combination of wetted sector and side sector angles and other directions relevant to the test. 128

Figure 5-18: Weather conditions (wind speed and direction) for transect Test Number Seven 129

Figure 5-19: Transect data for Test Number Seven for the combination of 140° wetted sector angle and 270° side sector angle. 130

Figure 5-20: Transect Test Number Eleven shows test layout, the combination of wetted sector and side sector angle and other directions relevant to the test. 131

Figure 5-21: Weather conditions (wind speed and direction) for transect Test Number Eleven. 132

Figure 5-22: Transect data for Test Number Eleven for the combination of 105° wetted sector angle and 270° side sector angle. 133

Figure 5-23: Transect Test Number Ten shows test layout, the combination of wetted sector and side sector angle and other directions relevant to the test. 134

Figure 5-24: Weather conditions (wind speed and direction) for transect Test Number ten..... 135

Figure 5-25: Transect data for Test Number Ten for the combination of 80° wetted sector angle and 270° side sector angle. 136

Figure 5-26: Transect Test Number Thirteen shows test layout, the combination of wetted sector 137

Figure 5-27: Weather conditions (wind speed and direction) for transect Number Thirteen. 138

Figure 5-28: Transect data for Test Number Thirteen for the combination of 160° wetted sector angle and 290° side sector angle..... 139

Figure 5-29: Transect test layout for curved movement on a 200-metres radius and weather conditions during Test Number Fourteen. 140

Figure 5-30: Weather conditions (wind speed and direction) for transect from curved movement of a 200m radius for Test Number Fourteen. 141

Figure 5-31: Transect data for Test Number Fourteen for curved movement on a 200-metre radius for the combination of a 180° wetted sector angle and a 270° side sector angle. 142

Figure 5-32: Transect test layout for a curved movement on 300 metre radius and weather conditions during Test Number Fifteen. 143

Figure 5-33: Weather condition (wind speed and direction) for transects from the curved movement on a 300 m radius for Test Number Fifteen. 144

Figure 5-34: Transect data for Test Number Fifteen of a curve movement of 300-metre radius testing for a combination of a 180° wetted sector angle and a 270° side sector angle. 145

Figure 5-35: Transect test layout for a curved movement on a 400 metres radius and weather conditions during Test Number Seventeen. 146

Figure 5-36: Weather conditions (wind speed and direction) for a transect from curved movement on 400m radius for Test Number Seventeen..... 147

Figure 5-37: Transect data for test Number Seventeen for a curved movement on a 400 metre radius for the combination of a 180° wetted sector angle and a 270° side sector angle. 148

Figure 5-38: Screenshot from Weatherzone forecast website shows wind toolbar for upcoming seven days, and the solid circle displays the date and the dotted circles display the wind speed and time (Weatherzone, 2015b). 150

Figure 5-39: Synoptic pressure systems that, surround the experimental site (Bureau of Meteorology, 2015a). 151

Figure 5-40: Four screenshots show current wind speed decreasing gradually at that date until it reached zero. The solid circle displays the time and the dotted circle displays wind speed (Weatherzone, 2015b) record two. 152

Figure 5-41: Two screenshot at different times show a period of zero wind for more than hour (Weatherzone, 2015b) record one. 153

Figure 6-1: Measured and predicted radial legs for the combination of 180° wetted sector and 270° side sector angles at quiescent wind speed. 157

Figure 6-2: Measured and predicted radial legs for the combination of 140° wetted sector and 270° side sector angles at quiescent wind speed. 158

Figure 6-3: Measured and predicted radial legs for the combination of 105° wetted sector and 270° side sector angles at quiescent wind speed. 159

Figure 6-4: Measured and predicted radial legs for the combination of 80° wetted sector and 270° side sector angles at quiescent wind speed. 160

Figure 6-5: Measured and predicted radial legs for the combination of 160° wetted sector and 290° side sector angles at quiescent wind speed. 162

Figure 6-6: Comparing the measured transect for the combination of 180° wetted sector and 270° side sector angles for a curve movement of a 200-metre radius with a transect measured with a straight movement. 164

Figure 6-7: Comparing the measured transect for the combination of 180° sector and 270° side sector angles for a curve movement of a 300-metres radius with a transect measured with a straight movement. 165

Figure 6-8: Comparing the measured transect for the combination of 180° wetted sector and 270° side sector angles for a curve movement of a 400-metre radius with a transect measured with a straight movement. 166

Figure 6-9: A comparison between the three curved transects for 200 m, 300 m and 400 m radii for the same wetted sector angle of 180° and a side sector angles of 270° 167

Figure 7-1: Simulated Transect depth for $\theta = 135°$ and $\phi = 67.5°$ and a machine speed of 50 m/h. 175

Figure 7-2: Simulated transect depths for $\theta = 150°$ and $\phi = 60°$ for a machine speed of 50 m/h. 176

Figure 7-3: Simulated transect depth for $\theta = 170°$ and $\phi = 75°$ with a machine speed of 50 m/h. 177

Figure 7-4: Simulated transect depth for $\theta = 180°$ and $\phi = 90°$ with a machine speed of 50 m/h. 178

Figure 7-5: Simulated transect depth for $\theta = 130°$ and $\phi = 60°$ with a machine speed of 50 m/h to obtain optimum performance results. 179

Figure 7-6 Screen shot for TravGUN V3.1 showing how to select the calibration options between travelling guns and end-guns. 180

Figure 7-7: Wind rose for Toowoomba location showing annual averages over five years (WillyWeather (2017). 181

Figure 7-8: Birds-eye view of a centre pivot with an end-gun showing the position of the lateral and end-gun, the starting point at the northerly direction and the clockwise travel direction. 182

Figure 7-9: The effect of wind on the application pattern for an end-gun when the travel direction is directly into the wind. 184

Figure 7-10: Depths of water along the simulated catch-can transect, showing the effect of wind on the transect for an end-gun sector angle of 130° and a side sector angle of 60° when the wind is across the pivot spans, and the machine is moving directly into the wind. 185

Figure 7-11: The effect of wind on the application pattern for an end-gun when the travelling position was between upwind and crosswind with a travel direction of 135°. 186

Figure 7-12: The effect of wind on transect for a sector angle of 130° and a side sector angle of 60° when the position of the transect (the pattern) was between a crosswind and upwind effect, on a travel direction of 135°. 187

Figure 7-13: The effect of wind on the application pattern for an end-gun with an upwind travelling position and a travel direction of 180°. 188

Figure 7-14: The effect of wind on the transect for a sector angle of 130° and a side sector angle of 60° when the position of the pivot was upwind and had a travel direction of 180°. 189

Figure 7-15: The effect of wind on the application pattern for an end-gun when travelling between crosswind and downwind on a travel direction of 225°... 190

Figure 7-16: The effect of wind on the sprinkler transect for a sector angle of 130° and a side sector angle of 60° when the position of the pivot was between crosswind and upwind with a travel direction of 225°. 191

Figure 7-17: The effect of wind on the application pattern for an end-gun when travelling downwind on a travel direction of 270°. 192

Figure 7-18: The effect of wind on a sprinkler transect with a sector angle of 130° and a side sector angle of 60° when the position of the transect is across the wind, and the end-gun travel direction is 270°. 193

Figure 7-19: The effect of wind on the application pattern for an end-gun when the travel position is between downwind and crosswind on a travel direction of 315°. 194

Figure 7-20: The effect of wind on a sprinkler transect with a sector angle of 130° and a side sector angle of 60° when the position of the pivot was between downwind and crosswind, on a travel direction of 315°. 195

Figure 7-21: The effect of wind on the application pattern for an end-gun when the pivot position was downwind, with an end-gun travel direction of 360°..... 196

Figure 7-22: The effect of wind on a sprinkler transect for a sector angle of 130° and a side sector angle of 60°, when the position of the transect was a downwind, and the travel direction was 360°. 197

Figure 7-23: The effect of wind on the application pattern for an end-gun when the travelling direction is between crosswind and unwind, on a travel direction of 45°..... 198

Figure 7-24: The effect of wind on a sprinkler transect for a sector angle of 130°, and a side sector angle of 60°, when the position of the pivot was between a crosswind and upwind, on a travel direction of 45°. 199

Figure 7-25: A diagram shows the differences in the arc length for end-gun patterns with different radii with the same central angle. 201

Figure 7-26: The differences between straight and curve transects for a 250 metre long centre..... 203

Figure 7-27: The differences between straight and curve transects for centre pivot of 400 m radii. 204

Figure 7-28: The differences between straight and curve transects for a centre pivot with 550 metre radius. 205

Figure 7-29: The combined application pattern for the centre pivot and end-gun at zero wind speed. 206

Figure 7-30: The first simulated combined application pattern for a centre pivot and end-gun at a wind speed of 1.5 m/s, with wind direction from East and travel direction of 90°. 208

Figure 7-31: The second simulation results showing the combined application pattern for a centre pivot and end-gun at a wind speed of 1.5 m/s, with wind direction from the East, and a travel direction of 135°. 209

Figure 7-32: The third simulated results for the combined application pattern for a centre pivot and end-gun at a wind speed of 1.5 m/s, with a wind direction from the East, and a travel direction of 180°. 210

Figure 7-33: The fourth simulated results were for the combined application patterns for a centre pivot and an end-gun, at a wind speed of 1.5 m/s, with a wind direction from the East, and a travel direction of 235°. 210

Figure 7-34: The fifth simulated results for the combined application pattern for a centre pivot and end-gun at a wind speed of 1.5 m/s, with a wind direction from the East, and a travel direction of 270°. 211

Figure 7-35: The sixth simulated results showing the combined application pattern for a centre pivot and end-gun at a wind speed of 1.5 m/s, with a wind direction from the East, and a travel direction of 315°. 212

Figure 7-36: The seventh simulated results for the combined application pattern for a centre pivot and end-gun at a wind speed 1.5 m/s, with a wind direction from the East, and a travel direction of 360°. 213

Figure 7-37: The eighth simulation results from the combined application patterns for a centre pivot and end-gun at a wind speed of 1.5 m/s, with a wind direction from the East, and a travel direction of 45°. 213

Figure 7-38: Transect shapes for different wetted sector angles, with constant side sector angle perpendicular to the direction of travel. 215

Figure 7-39: Diagram showing how the positions of X, Y points change as a result of the arced movement. 216

Figure 7-40: A comparison of three transect data sets showing the effect of the arc movement using different approaches including a correction factor. 219

Figure A-1: Radial leg data test one collected from three lines of collectors placed around a stationary sprinkler. 252

Figure A-2: Weather conditions (wind speed and direction) for radial leg test one. 252

Figure A-3: Surface plot for radial leg test one shows the effect of wind on distortion sprinkler pattern. 253

Figure A-4: Radial leg data for test two collected from three lines of collectors placed around a stationary sprinkler. 254

Figure A-5: Weather conditions (wind speed and direction) for radial leg test two.254

Figure A-6: Surface plot for radial leg test two shows the effect of wind on distortion sprinkler pattern. 255

Figure A-7: Radial leg data for test three collected from three lines of collectors placed around a stationary sprinkler. 256

Figure A-8: Weather conditions (wind speed and direction) for radial leg test three. 256

Figure A-9: Surface plot for radial leg test three shows the effect of wind on distortion sprinkler pattern. 257

Figure A-10: Radial leg data for test five collected from three lines of collectors placed around a stationary sprinkler. 258

Figure A-11: Weather conditions (wind speed and direction) for radial leg test five. 258

Figure A-12: Surface plot for radial leg test five shows the effect of wind on distortion sprinkler pattern. 259

Figure B-1: Transect test number eight shows test layout, the combination of sector and side sector angles and other directions relevant to that test. 262

Figure B-2: Weather conditions (wind speed and direction) for transect test number eight. 262

Figure B-3: Transect data for test number eight for the combination of 180° sector angle and 270° side sector angle..... 263

Figure B-4: Transect test number nine shows test layout, the combination of sector and side sector angles and other directions relevant to that test. 264

Figure B-5: Weather conditions (wind speed and direction) for transect test number nine. 264

Figure B-6: Transect data for test number nine for the combination of 180° sector angle and 270° side sector angle. 265

Figure B-7: Transect for test number twelve shows test layout, the combination of sector and side sector angles and other directions relevant to that test. 266

Figure B-8: Weather conditions (wind speed and direction) for Transect test number twelve. 266

Figure B-9: Transect data for test number twelve for the combination of 140° sector angle and 270° side sector angle. 267

Figure B-10: Transect test number five shows test layout, the combination of sector and side sector angles and other directions relevant to that test. 268

Figure B-11: Weather conditions (wind speed and direction) for transect test number five. 268

Figure B-12: Transect data for test number five for the combination of 105° sector angle and 270° side sector angle. 269

Figure B-13: Transect test number six shows test layout, the combination of sector and side sector angles and other directions relevant to that test. 270

Figure B-14: Weather conditions (wind speed and direction) for transect test number six. 270

Figure B-15: Transect data for test number six for the combination of 105° sector angle and 270° side sector angle. 271

Figure B-16: Transect test number one shows test layout, the combination of sector and side sector angles and other directions relevant to that test. 272

Figure B-17: Weather conditions (wind speed and direction) for transect test number one. 272

Figure B-18: Transect data for test number one for the combination of 80° sector angle and 270° side sector angle. 273

Figure B-19: Transect test number two shows test layout, the combination of sector and side sector angles and other directions relevant to that test. 274

Figure B-20: Weather conditions (wind speed and direction) for transect test number two. 274

Figure B-21: Transect data for test number two for the combination of 80° sector angle and 270° side sector angle. 275

Figure B-22: Transect test number three shows test layout, the combination of sector and side sector angles and other directions relevant to that test. 276

Figure B-23: Weather conditions (wind speed and direction) for transect test number three. 276

Figure B-24: Transect data for test number three for the combination of 80° sector angle and 270° side sector angle. 277

Figure B-25: Transect test layout for a curvature movement of 100 metres radius and weather conditions during test number sixteen. 278

Figure B-26: Weather conditions (wind speed and direction) for transect test number sixteen. 279

Figure B-27: Transect data for a curve movement of 100-metre radius and the combination of a 180° sector angle and 270° side sector angle for test number sixteen. 279

Figure C-1: Synoptic pressure systems surrounding the experimental region (Bureau of Meteorology, 2015) record two. 281

Figure C-2: Four screenshots showing current wind speed decreasing gradually at that date until it reached zero. The solid circle displays the time and the dotted circle displays wind speed (Weatherzone, 2015) record two. 282

Figure C-3: Two screenshots at different times show periods of zero winds of more than one (Weatherzone, 2015) record two. 283

Figure C-4: Synoptic pressure systems surrounding the experimental region (Bureau of Meteorology, 2015) record three. 284

Figure C-5: Four screenshots show that current wind speed decreased gradually at that date until it became zero, (Weatherzone, 2015) record three. 285

Figure C-6: Four screen shots at different times shows the period of zero wind and wind gusts during that time (Weatherzone, 2015) record three. 286

Figure C-7: Synoptic pressure systems that surrounded the experimental region (Bureau of Meteorology, 2015) record four. 287

Figure C-8: Four screenshots showing current wind speed decreased gradually until it became zero, (Weatherzone, 2015) record four. 288

Figure C-9: Four screenshots at different times, showing the period of zero wind and wind gusts during that time (Weatherzone, 2015) record four. 289

Figure C-10: Two screenshots at different times, showing the period of zero wind as 120 minutes (Weatherzone, 2015) record four. 290

Figure C-11: Synoptic pressure systems that surrounded the experimental region (Bureau of Meteorology, 2015) record five. 291

Figure C-12: Four screenshots showing current wind speed decreasing gradually until reaching zero, (Weatherzone, 2015) record five. 292

Figure C-13: Two screenshots at different times show the period of zero wind was 90 minutes (Weatherzone, 2015) record five. 293

Figure C-14: Synoptic pressure systems that surrounded the experimental region (Bureau of Meteorology, 2015) record six. 294

Figure C-15: Four screenshots show current wind speed decreasing gradually at that date until reaching zero, (Weatherzone, 2015) record six. 295

Figure C-16: Four screen shots at different times show wind speed fluctuated at different times on that date (Weatherzone, 2015) record six. 296

Figure C-17: Four screen shots show current wind speed fluctuated and dropped to zero on that date (Weatherzone, 2015) record six. 297

List of Tables

Table 3-1 A diagonal matrix of ($K\alpha ijand\ K\beta ij$) values used as indicators in the algorithms 67

Table 5-1 Summary for all radial leg tests and wind conditions that used as a criteria to present these tests either in this chapter or in the Appendix A..... 106

Table 5-2: Summary for all Transect tests and wind conditions that used as a criteria to present these tests either in this chapter or in the Appendix B..... 124

Table 7-1: Simulating and measured results (information) for the variety of selected sector and side sector angles from the literature and industry..... 174

List of Abbreviations

AE	Application efficiency
ASAE	American Society of Agricultural Engineer
BOM	Bureau of Meteorology
CP	Centre Pivot irrigation machine
CU_{HH}	Heermann and Hein Coefficient of Uniformity for centre pivot irrigation system
CU	Coefficient of Uniformity
DU	Distribution Uniformity
kPa	Kilo Pascal
m	Metre
m/s	Metre per second
MSLP	Mean Sea Level Pressure
RMSE	Root Mean Square Error

1 CHAPTER ONE

Introduction

1.1 Background

Wind impacts the irrigation performance of all sprinkler systems, particularly those sprinklers that throw into higher elevations above the ground and crop surface. Two sprinkler irrigation systems that are most prone to being impacted by wind are travelling big gun irrigation machines and end-guns on centre pivot machines. An end-gun is commonly attached to the end of centre pivot irrigation machines to extend the irrigated radius by up to 50m and/or allow the machine to water the corners of a square field. The irrigated area under an end-gun can equal up to one quarter of the total area irrigated by a centre pivot system. Therefore, the performance of end-guns in wind have a big impact on the uniformity of the total area irrigated by centre pivot systems.

Richards and Weatherhead (1993) developed a semi-empirical model for predicting the distortion of the wetted patterns in windy conditions using re-analysed data (Musa, 1988), which can be calibrated using limited experimental data. Al-Naeem (1993) modified the (Richards & Weatherhead, 1993) model to include the effect of variable trajectory angles, sector angles and sector positions for different big gun types. Smith et al. (2008) developed the TravGUN model, which has the capacity to calibrate from three catch can transects perpendicular to a big gun's travel direction and to simulate the wind effect for any wind speed and direction.

Travelling big-gun sprinklers and end-guns on centre pivot systems have many common characteristics but some specific differences, notably, the magnitude of the

wetted sector angle and its orientation (side sector) relative to the travel direction. A preliminary investigation of TravGUN simulating end-gun performance in wind, highlighted an error during simulation due to end-gun patterns that were generally oriented perpendicular to the direction of travel. A total number of 288 simulation tests were performed in this investigation for a range of wetted sector angles for 5° intervals from 360° of full circle with range of side sector angle of 45°, 90°, 180, and 270°, respectively. In addition, the original TravGUN software could not be calibrated from transect data that was measured on one side of the sprinkler with a side sector angle perpendicular and asymmetrical to the direction of travel. In summary this model could not be used in its current form to simulate, and improve end-gun performance.

Therefore, the overall aim of this dissertation is to develop a set of methods and tools (software) that provide the capacity to determine the irrigation performance (uniformity) of end-guns on centre pivot machines operating under windy conditions.

1.2 The Hypothesis

End-gun irrigation performance can be measured, simulated and optimised under different wind conditions.

1.3 TravGun limitations

Although big gun travelling machines and end-guns on centre pivots have some common characteristics, there are limitations to using existing software to simulate end-gun performance under different wind conditions. The first difference is, that while software like TravGUN is built to simulate the performance of large sprinklers in wind, the calibration process of the model is from transect data measured from sector angles greater than 180° and side sector angles always symmetrical and parallel to the

direction of travel. End-guns operate with sector angles of greater or less than 180° asymmetrical and perpendicular to the direction of travel. The second challenge is that big guns travel along straight paths, while end-guns travel along curved paths.

Further development and modification of the TravGUN model would be required to simulate the irrigation performance of end-guns on centre pivots, due to the differences between the operations of these two types of large sprinklers. Therefore, the following objectives are necessary to achieve this goal.

1.4 Objectives

The overall aim of this project is to investigate the performance (Application uniformity) of end-guns on centre pivot irrigation systems, and develop a new methodology to simulate the effect of wind on wetted distribution pattern of end-guns on centre pivots, using TravGUN software, by achieving the following specific research objectives:

1. Develop a new numerical sub-model to generate radial leg data from catch can transects for any combination of wetted sector and side sector angles.
2. Develop a new method to predict the appropriate wind speed for field data collection of catch-can transects in an open field.
3. Identify the appropriateness of the TravGUN model to simulate end-gun performance for all combinations of wetted sector and side sector angles.
4. Validate the proposed field measurement technique for end-gun field tests to capture data for TravGUN calibration.
5. Validate the modified TravGUN model containing the new sub-model to simulate the irrigation performance of end-guns on centre pivot systems.

6. Simulate end-gun water application patterns for typical settings on centre pivots in windy conditions under a full irrigation rotation.
7. Investigate the effect of the curved movement of centre pivot end-guns on applied water depths.

1.5 Thesis Structure

The thesis consists of nine chapters as follows:

Chapter 1 includes an introduction and the objectives of the thesis and outlines the dissertation structure.

Chapter 2 is a literature review of the previous models developed to predict the wetted distribution patterns of big gun sprinklers under windy conditions. It reviews the previous work which evaluates the performance of end-guns on centre pivots. It addresses all the similarities and the differences between the characteristics of end-guns on centre pivots and travelling big-gun sprinklers (large impact sprinkler). It also reviews the main factors which affect the performance (application uniformity) of big-gun sprinklers (large impact sprinklers).

Chapter 3 includes theoretical and mathematical processes, using a series of algorithms (for MATLAB script) in a new sub-model for the TravGUN model to produce an end-gun radial leg from catch can transects, for any combination of wetted sector and side sector angles.

Chapter 4 presents the characteristics of the test site and field work methodology, describing: the method of measurement; the equipment used to collect the data; a methodology to determine the appropriate weather conditions in terms of quiescent wind speed; the method of measuring radial leg data; and the method of measuring catch can transect data for straight and curved movement.

Chapter 5 includes the field measurement results including, the most accurate radial leg data; the most accurate catch can transect data for different combinations of sector and side sector angles for both straight and curved movements; and weather data, including wind speed and direction during the tests.

Chapter 6 includes the validation of the new TraGUN sub-model for different combinations of wetted sector and side sector angles travelling on straight and curved paths by comparing measured data with simulation results from the new sub-model, using graphs and statistical methods.

Chapter 7 presents the optimum sector and side sector angles for end-guns on centre pivots in no wind, and the simulation results for end-gun patterns in windy conditions. Different approaches to calculation are presented and the applied water depth is corrected according to the degree of curvature of the end-gun travel path. The combined simulated patterns for both centre pivot and end-gun sprinklers in windy conditions are presented with irrigation performance results.

Chapter 8 presents the discussion of all of the results included in this dissertation.

Chapter 9 presents the conclusions and suggestions for future work.

2 CHAPTER TWO

Literature Review

2.1 Introduction

This chapter will address the similarities and differences between the characteristics of end-guns on centre pivots and travelling big-gun sprinklers (large impact sprinklers) It reviews the main factors which affect performance (application uniformity), the previous models developed to predict the wetted distribution patterns under windy conditions, and the previous work evaluating the performance of end-guns on centre pivots.

2.2 The similarities and the differences between end-guns and travelling big-gun sprinklers

The end-gun on a centre pivot is a single big sprinkler similar to a travelling big-gun and has similar general characteristics, such as large nozzles greater than 25 mm in diameter, high operating pressures (400 to 700 kPa) and high discharge which leads to large sprinkler wetted radii up to 50 metres (Nelson Irrigation, 2018) as shown in Figure 2-1.

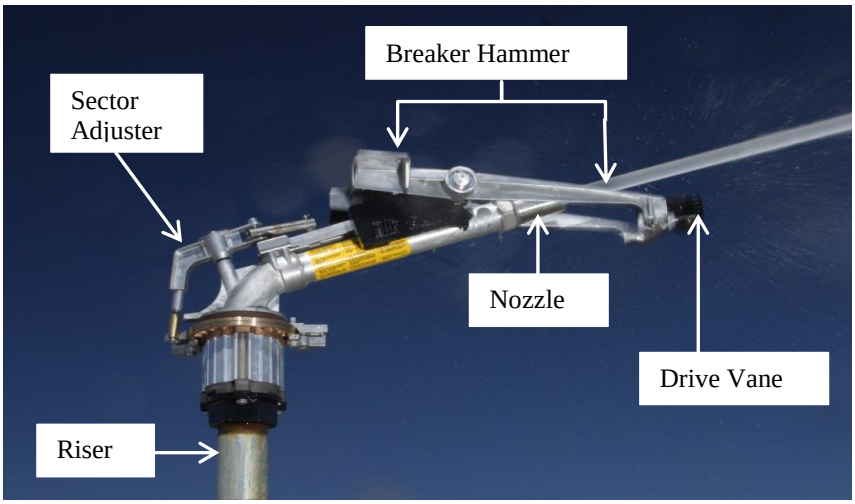

Figure 2-1: Main components of the Nelson SR100 large impact sprinkler, used in travelling big-guns and in end-guns on centre pivots (Nelson Irrigation, 2010)

2.2.1 End-gun on centre pivot irrigation systems

Centre pivots consist of a number of spans attached to a fixed centre tower containing a water supply point and power source, around which the other spans and towers rotate, as shown in Figure 2-2 (a) and (b). The spans have a self-supporting frame which commonly ranges in length from 34.2 m to 62.4 m (Foley, 2008). The length of the centre pivot system is dependent on the number of spans and the length of the span itself. They range in total length from 300 m to 580 m (Wigginton et al., 2011).

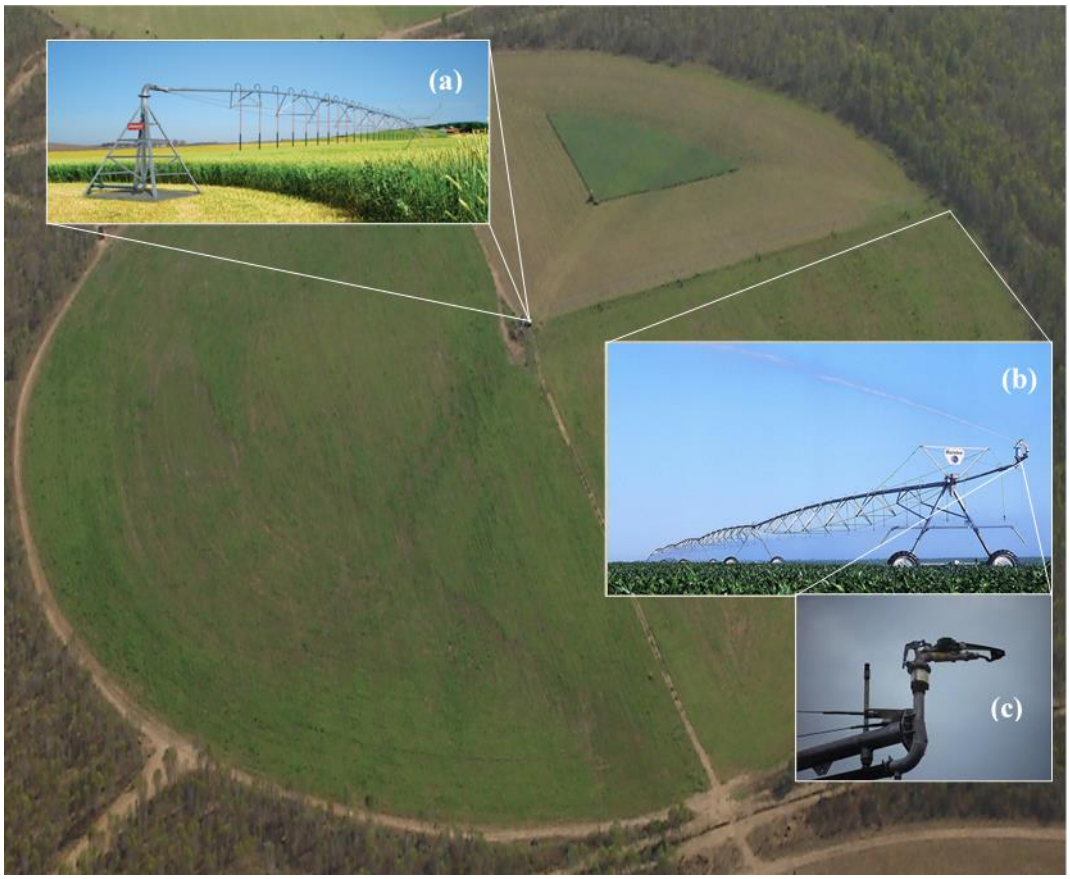

Figure 2-2:The shape of an irrigated field using a centre pivot system with an end-gun attached to the outer end of the pivot, where (a) is the fixed centre tower, (b) number of spans of the centre pivot attached to the end-gun, (c) end-gun on centre pivot system (Centralstation, 2014) (Lindsay Corporation, 2011, 2012) (Google Image, 2014)

The shape of the irrigated area using centre pivot irrigation systems is circular, as a result of the circular movement of centre pivots. Typically, the area of the entire field is square or rectangular in shape. The irrigated area of square fields using centre pivots is approximately 78% (Keller & Bliesner, 1990). One attempt to increase the irrigated area in the corners includes attaching an end-gun at the outer end of the last span of the centre pivot, which can be switched on when the machine approaches the corner. In other situations, the end-gun may remain switched on the entire time, as shown in Figure 2-2 (c). The end-gun adds 25 to 40 metres (Keller & Bliesner, 1990) to the radius of centre pivot irrigated fields, as shown in Figure 2-3. Therefore, the end-gun irrigation contributes an additional 15% to 20% for the entire irrigated field. Newell et al. (2002) stated that Nelson SR100 guns are commonly used as centre pivot end-guns.

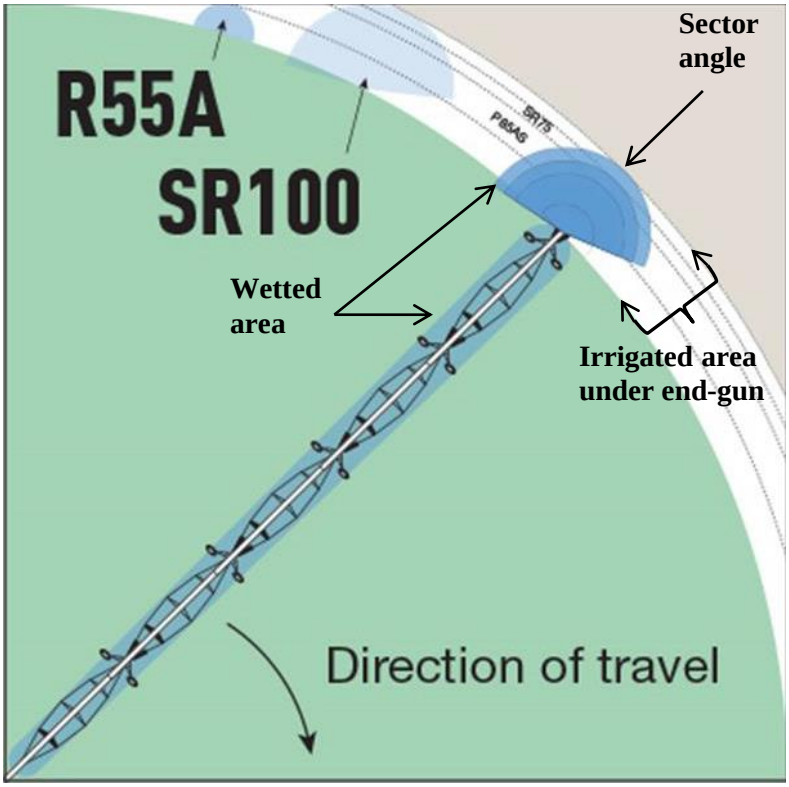

Figure 2-3: Diagram of the end-gun on centre pivot shows wetted sector and travel path (Nelson Irrigation, 2018)

2.2.2 Travelling big-gun sprinkler

The travelling big-gun sprinkler consists of a big-gun which is mounted on a cart and connected with a flexible, high-density, polyethylene hose to the pressurised water supply. The hose is coiled on a large reel which is supplied with water from the central pressurised supply pipe, as shown in Figure 2-4.

Figure 2-4: A travelling big gun sprinkler machine consists of a big gun on a cart wheel (1), distribution hose (2) and self-propelled stationary hose reel (3) and central pressurised supply water pipe (4) (Google Image, 2015) (Wade Rain, 2018)

To operate the system, the hose reel is placed on the headland of a field and the big-gun is pulled to the opposite end of the field. Typically, the length of the travel path is from 200 to 500 m (Southorn, 1998). When, the big-gun is operating, the water is thrown in a high-pressure jet, with the breaker hammer and drive vane making the big-gun rotate. The big-gun on the cart is pulled cross the area which is slowly irrigated from the winding of the hose onto the reel or the winding of a steel wire onto the reel on the cart itself in a straight-line travel path. This leads to irrigation of a strip between 40m and 100m wide. The process is repeated across the field and overlapped to ensure adequate wetting (Lacey, 2006), as shown in Figure 2-5.

The differences between travelling big-gun sprinklers and end-guns on centre pivots are that big-guns operate with wetted sector angles from 220° to 360° (Newell et al., 2002) and the travel direction is generally parallel to the central axis of the wetted pattern, as shown in Figure 2-5. However, big-guns could operate at any sector angle,

using a wetted sector angle less than 360° with a side sector parallel to the direction of travel reducing tracking problems when the cart is moving on a dry path.

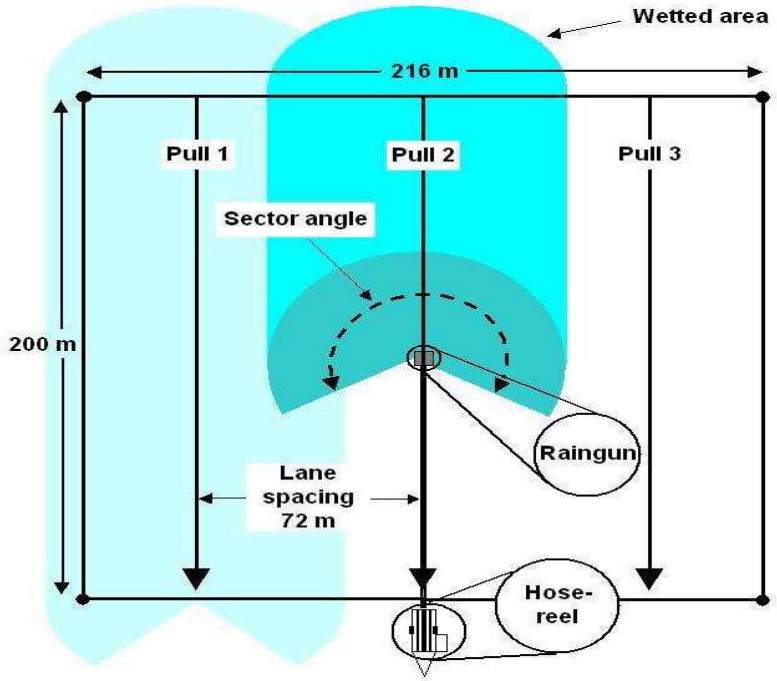

Figure 2-5: Diagram of travelling big-gun showing wetted sector and travel path (Lacey, 2006)

Generally, end-guns operate with wetted sector angles from 150° to 210° and their travel direction is generally perpendicular to the central axis of the wetted distribution pattern. However, Keller & Bliesner (1990) and Nelson Irrigation (2017a) explain that the side sector should deviate from the central axis of the wetted distribution pattern by approximately 5° to 25° from the vertical axis to the direction of travel in order to achieve better overlapping between the end-gun and the rest of the sprinklers on the outer span. The motion direction for wetted distribution pattern in end-guns on centre pivots is similar to a curved line, depending on the radius of the centre pivot, as shown in Figure 2-3, whereas the motion direction for the wetted distribution pattern in a big-gun is on a straight line, as shown in Figure 2-5. Another difference is that the height of an end-gun on a centre pivot varies from 3 to 4 metres (Merkley & Allen, 2004) while the height of a big-gun on travelling carts varies from 1 to 2 metres at maximum elevation (Trailco T200-2, 2018). Finally, an end-gun on a centre pivot operates with

a lower trajectory angle compared with some travelling big-gun sprinkler (Al-Naeem, 1993; Nelson Irrigation, 2017b).

2.3 Sprinkler characteristics

End-guns and big-guns (large impact sprinklers) operate at high pressure and high discharge. The characteristics of travelling big-guns and end-guns on centre pivots are determined by: discharge, wetted diameter or area, application rate, distribution pattern, and radial leg. Typically, they produce a large circular wetted pattern in a full circle or part circle. These patterns can be presented as radial leg or wetted distribution patterns. The radial leg data can be measured from a stationary sprinkler (Richards & Weatherhead, 1993; Oliveira et al., 2013) or can be produced from a travelling machine using a unique (Smith et al., 2008) methodology.

2.3.1 Wetted distribution pattern

The term "wetted distribution pattern" refers to the form in which the specific amount of water is distributed around one single sprinkler, including full or part circular patterns. Depth distribution patterns can be presented as contour maps or colour densograms, as shown in Figure 2-6.

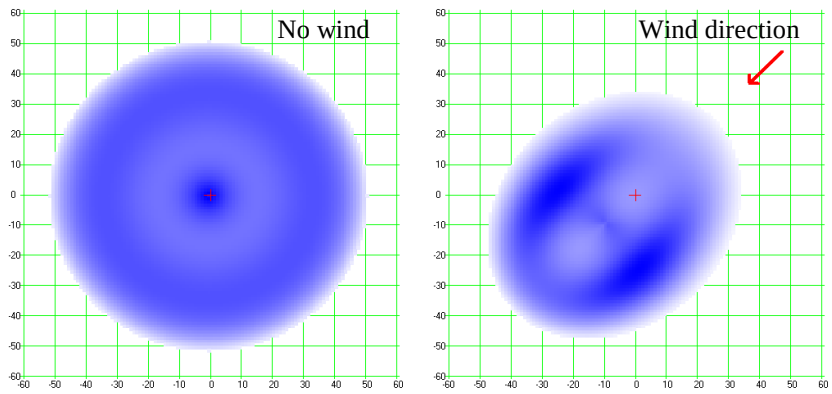

Figure 2-6: Distribution patterns as visual form full circle during (left) calm conditions and (right) wind speed of 4.5 m/s, the dark colour refer to more water depth (Newell, 2003)

2.3.2 Radial leg

The term radial leg is used to characterise specific individual sprinklers under conditions of no wind or under laboratory conditions, to present the application rate against the throw distance from the sprinkler, as shown in Figure 2-7.

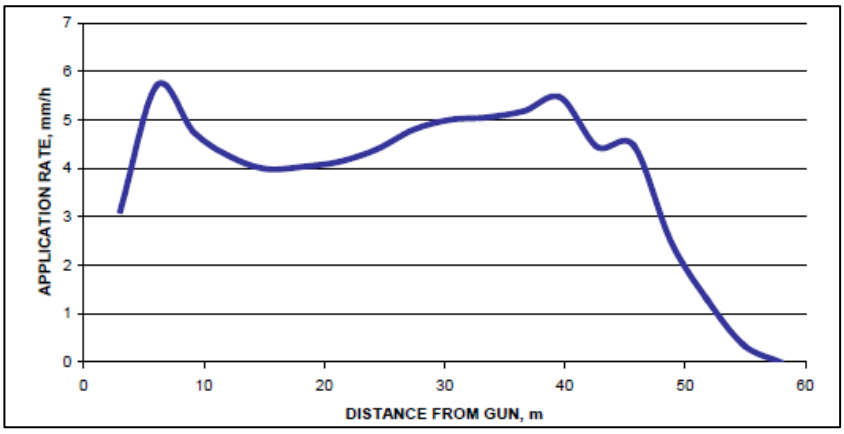

Figure 2-7: A radial leg from stationary gun from Newell et al. (2003)

2.4 Irrigation Performance (Application Uniformity)

Irrigation performance can be reported as application uniformity and application efficiency. Application uniformity is the evenness of an application across the targeted irrigation area (Jensen, 1980). In fields irrigated non-uniformly, some parts will be irrigated to the required depth, while other parts will be either under or over-irrigated. Non-uniformity leads to yield variation across the irrigated field and the problem becomes worse when fertiliser is added to the irrigation water. Generally, any reduction in application uniformity will reduce application efficiency (Gunston & Ali, 2012). There are several factors that contribute to non-uniformity for large nozzled sprinklers, such as, wetted sector and side sector angles, trajectory angle, operating pressure, nozzle height, machine movement and its consistency. The uniformity of travelling big gun sprinklers is measured by placing a line of collectors perpendicular

to the travel direction in order to capture the variations in water depth across the field. The two most common methods of reporting irrigation uniformity for sprinklers are the distribution uniformity (DU) and a Christiansen's coefficient of uniformity (CU). Distribution uniformity is defined by Jensen (1980) as:

$$DU = \frac{D_{LQ}}{\bar{D}} \qquad 2\text{-}1$$

and CU is calculated from (Christiansen, 1942):

$$CU = \left(1 - \frac{\sum_{i=1}^{n} | D_i - \bar{D} |}{n\bar{D}} \right) \qquad 2\text{-}2$$

where, D_{LQ} is the average of the lowest quarter of the applied depth, D_i are individual water application depths, $\bar{D}$ is average application depth, n is number of collectors.

These equations are used for nearly all sprinkler systems. Heermann and Hein (1968) developed a measure of application uniformity that should be used specifically for centre pivot machines to account for the greater annular area that outer sprinklers contribute, by weighting them with their radial distance. The Heermann and Hein (1968) coefficient of uniformity can be written as:

$$CU_{HH} = \left[1.0 - \frac{\sum_{s} S_s | D_s - \bar{D} |}{\sum_{s} D_s S_s} \right] \qquad 2\text{-}3$$

where, D_s the applied water depth for one collector position, $\bar{D}$ is the average applied water depth for all collectors and S_s is the radial distance to equally spaced collectors.

Application efficiency (AE) is the ratio of the net irrigation depth to the gross depth of water applied (Jensen, 1980). Application efficiency is a measure of losses associated with water being applied to a field. However, this study will focus on uniformity.

2.5 The factors that affect the performance (application uniformity)

There are two main factors which affect the performance (application uniformity) of a large impact sprinkler which are the machine operating conditions (machine adjustment) controlled by the operator and the weather conditions (wind speed and direction) (Oliveira et al., 2012). While weather factors are impossible to control, some changes in machine adjustment could overcome the influence of weather conditions.

2.5.1 Sprinkler machine operating adjustments

Sprinkler machine operating adjustment includes, wetted sector angle, side sector angle, trajectory angle, nozzle pressure, nozzle shape, nozzle size, nozzle height and machine movement and its consistency (machine speed).

- **Sector angle**

Sector angle is the wetted arc of rotation of the big sprinkler, as shown in Figure 2-8. In Figure 2-8 (A), the sector angle equals 340° and the side sector angle equals 0°. While in Figure 2-8 (B), the sector angle equals 220° and the side sector angle equals 90°. The value of the sector angle varies from approximately 220° to 360° for a big gun. The optimum operation angles are dependent on the performance objective. For example, a smaller sector angle will give a higher application rate and the optimum sector angle for a travelling big gun is 240° (Al-Naeem, 1993). Reducing the sector

angle increases distribution uniformities and reduces the amount of water being applied beside the travel path (Newell et al., 2002). Using digital simulation results, Prado et al. (2012) found the best uniformity coefficient when the sector angle ranges between 180° and 230°.

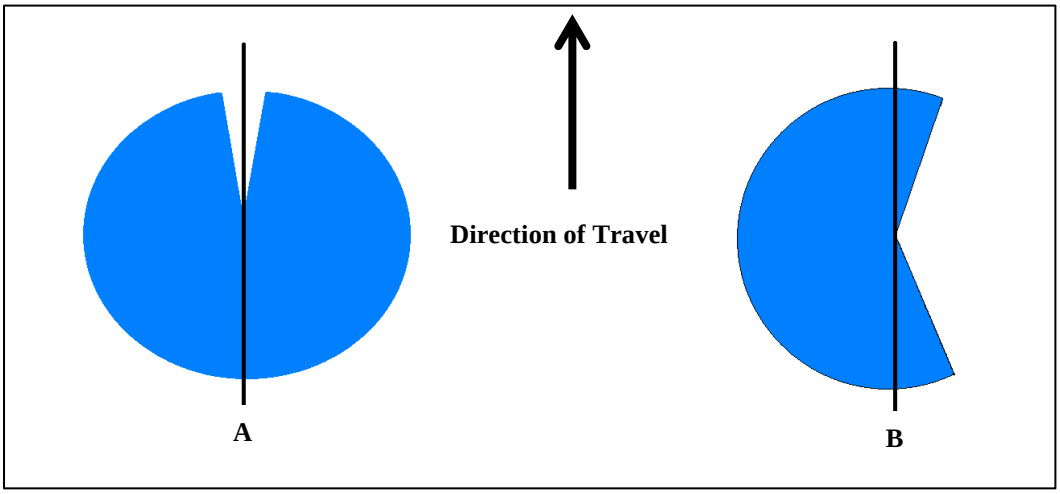

Figure 2-8: Sector and side sector angles. A- Sector angle 340° and Side sector parallel to travel direction. B- Sector angle 220° and Side sector perpendicular to travel direction

- **Side sector angle**

The side sector angle is the angle between the centre of the non-wetted sector and the travel direction, as shown in Figure 2-8. An angle of 0° (Figure 2-8(A)) is commonly used in big-guns, and an angle of 90° (Figure 2-8 (B)) is commonly used on end-guns.

- **Trajectory angle**

The trajectory angle is the angle of the sprinkler jet exiting the nozzle above the horizontal. The trajectory angle can play an important role in application uniformity since it influences the wetted pattern. Von Bernuth (1988) stated that when choosing the appropriate trajectory angle for small sprinklers, consideration should be given to the droplet-size distribution and the wind velocity. The impact of the air resistance is

greater on smaller droplets. The result is that the larger droplets travel further and the smaller droplets tend to land closer to the sprinkler and are more prone to wind drift (Richards & Weatherhead, 1993). Al-Naeem (1993) demonstrated that low trajectory angles produced more uniform application under high wind speed for big guns. Lacey (2006) reported that by using a Komet Vari-angle® big gun sprinkler, high application uniformities could be achieved with a trajectory angle of 15° at high wind speeds and 25° at low wind speeds, as shown in Figure 2-9. Oliveira et al. (2013) reported that when reducing the trajectory angle 3° from 28° the radius of throw was reduced by approximately 3.4 to 4%.

Figure 2-9: Large sprinklers with adjustable trajectory angle (Nelson Irrigation, 2014) (India Mart, 2014)

- **Nozzle pressure**

Nozzle pressure has the largest effect on distribution application pattern. Firstly, as given by the orifice Equation 2-4, when an increase in pressure causes an increase in the discharge, this is usually shown as an increase in the application rate over the wetted area. Secondly, the increase in discharge means an increase in the jet velocity. In the case of rotating sprinklers this should mean an increase in the radius of throw

for all droplet sizes and, hence, an increase in the wetted area. Thirdly, the pressure and velocity increases cause a change in the jet break-up and a change in the droplet size distribution, with a resultant smaller droplet size on the spray pattern. Low pressure will reduce throw distance and result in poor jet break-up and large droplets. As a result, high water deposition tends to occur in a single radius of the wetted pattern, adversely affecting uniformity. Conversely, high water pressure causes excessive jet break-up and fine droplets which are prone to wind-drift. In this case, high water deposition tends to occur near the gun, also resulting in low uniformity.

- **Nozzle shape**

Nozzle shape has a major influence on the manner in which the jet is broken up into streams of individual droplets. Three types of nozzles are used in large impact sprinkler. These being ring, taper-ring, and taper, as shown in Figure 2-10. Ring nozzles interrupt the smooth conical flow and result in greater head losses as the water exits the nozzle, so that the jet stream breaks up more easily as it is released and a lesser throw is obtained, as shown in Figure 2-10 (C) and Figure 2-11 (A). Taper nozzles give the greatest throw distance from the sprinkler, and therefore a greater wetted area, due to the smooth conical internal shape of the nozzle, as shown in Figure 2-10 (A) and Figure 2-11 (B). The taper-ring nozzle (Figure 2-10 (B)) has a similar initial uniform diameter reduction to the taper nozzle, with a sharp diameter reduction nearer to the exit to provide droplet sizes and throw diameters that are midway between those produced from full taper and full ring nozzles (Newell et al., 2002).

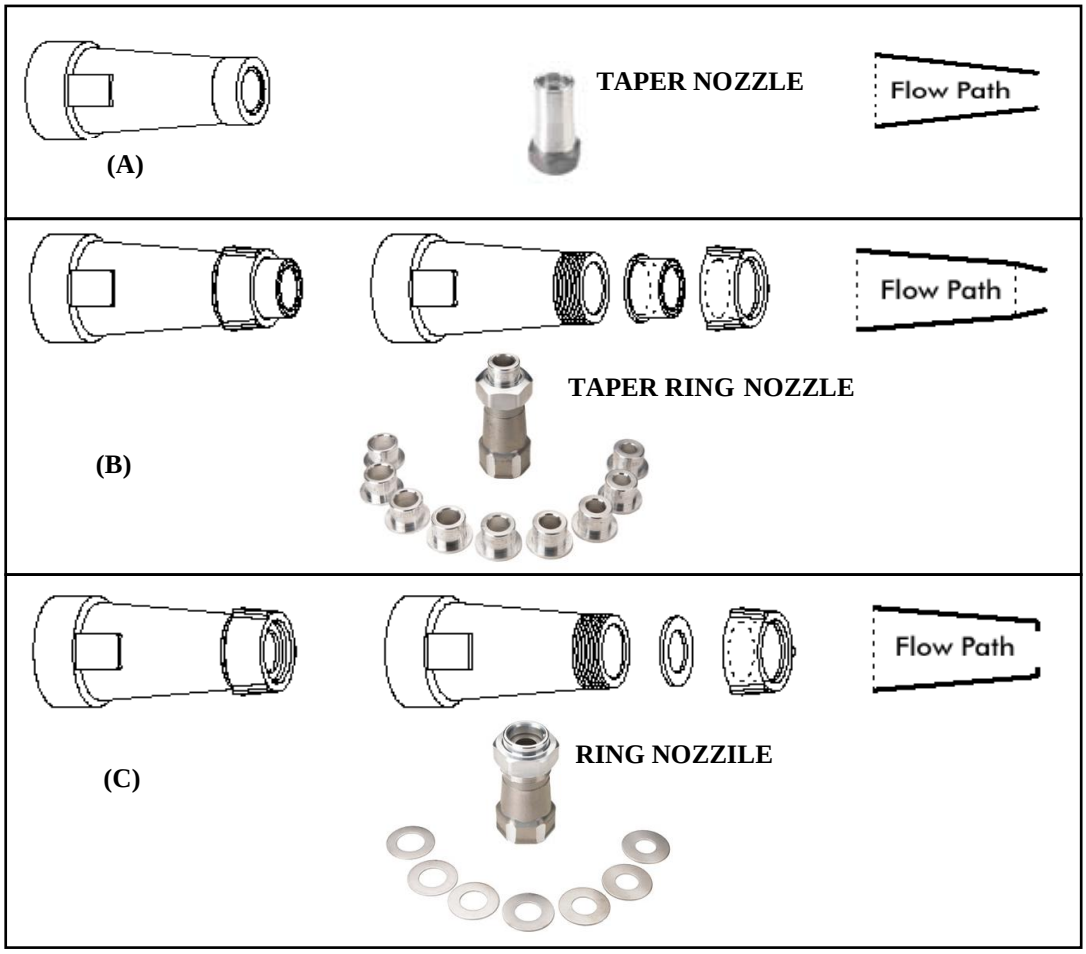

Figure 2-10: Different nozzle types (A) taper nozzle, (B) taper ring nozzle and (C) ring nozzle (Newell et al., 2002) and (Nelson Irrigation Australia, 2016)

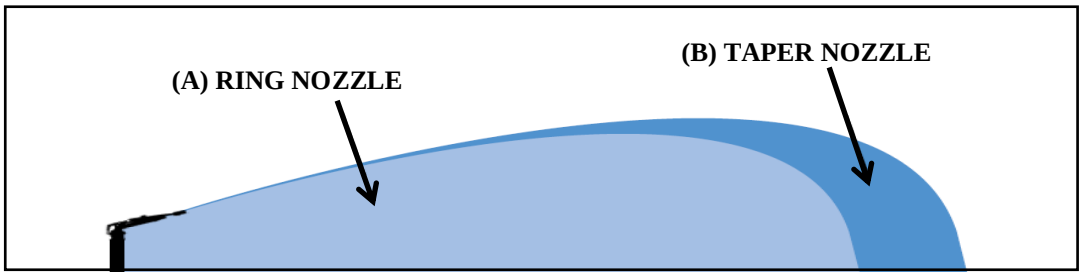

Figure 2-11: The distribution behaviours of droplets from different nozzle shapes (A) Ring nozzle, (B) Taper nozzle (Nelson Irrigation, 2016)

- **Nozzle size**

Nozzles are essentially an orifice and must perform according to the standard orifice equation:

$$Q = CA\sqrt{2gH_P} \qquad 2\text{-}4$$

where Q is the nozzle discharge (m^3/s), C is a coefficient, A is the area of the orifice (m^2) and H_p is the pressure head (m). According to this equation, the nozzle discharge is related to the area when the pressure is constant; as the area increases the discharge should be increased, and vice versa. For large sprinklers and big-guns, the water jet induces the stream of surrounding air mass, reducing air resistance and enhancing throw (Richards & Weatherhead, 1993).

- **Nozzle height**

Limited research has been conducted into the effect of nozzle elevation on sprinkler irrigation performance. Under no wind conditions, the effect of nozzle elevation has no significant effect as a result of free fall due to gravity. Wind speed increases with height above a soil surface and the relationship can be approximated by a logarithmic function of wind speed with height (Al-Naeem, 1993). However, there has been no study conducted to determine the effect of wind on different nozzle heights as a result of increasing the distance of the diversion of distribution of application pattern by wind for the same wind speed.

- **Machine speed**

Newell et al. (2002) reported that machine speed varies throughout traveller runs in both soft hose and hard hose travelling guns. However, a newly designed machine reduces the variation by using sensors for the hose travel velocity and the hose reel pressure. Furthermore, the speed of an end-gun on a centre pivot depends on the machine speed itself and the radius of the centre pivot (machine length) which affects the radial velocity.

- **Lane spacing**

Lane spacing, or the overlapping between two paths on a travelling big-gun, vary between different manufacturers. The lane spacing can have significant effects on the uniformity of an irrigation event (Newell et al., 2002). Increasing lane spacing can reduce applied depths and uniformity. Jensen (1980) recommended lane spacing should be no more than 40% of the wetted diameter for a travelling gun. Lacey (2006) recommended that lane spacing should be reduced when wind speed increases. Miodragović et al. (2012) recommended that for high wind speed, high uniformity could be achieved by reducing the lane spacing and increasing machine speed to maintain the application rate at high uniformity. However, the lane spacing between an end-gun on a centre pivot and the other sprinkler on the outer lateral span or the overhang in a centre pivot machine is determined by the wetted radius of the sprinklers and the distance between the last sprinkler and the position of the end-gun and the sector angle of the end-gun itself.

2.5.2 Weather condition

Weather conditions include wind speed and direction. Sprinkler irrigation systems have a unique problem of distortion of the wetted application pattern by wind. This problem has a large impact on reducing application uniformity. Reducing the uniformity would also have adverse consequences for the efficiency of the system (Pair, 1970). Because weather conditions cannot be controlled, the only way to deal with wind when using sprinkler irrigation is by changing the adjustment of some machine operation factors (sector and side sector angles, trajectory angle, lane spacing and machine speed) which could maintain application uniformity with acceptable values of application uniformity under windy conditions.

Solomon (1987) reported that wind affects the sprinkler wetted distribution pattern according to three parameters. The first two are wind speed and direction which are easily dealt with when wind speed and direction are approximately constant. The third parameter occurs when wind speed and direction are not constant and the problem would be more complex. Therefore, more solutions are required to solve such a complex problem. Blackmore et al. (2006) reported a new conceptual system requirements for machines operating under windy conditions. The design of the autonomous machines should include the ability to have different levels of weather dependence and independence. Weather dependence would exist when the autonomous sprinkler could stop when conditions were too windy and wait until it could start again.

Much research and effort has been conducted to determine the effects of wind on distortion of the wetted application pattern and to maintain the uniformity when using sprinkler irrigation under windy conditions. Shull and Dylla (1976b) reported that the deviation of the measured patterns from the no-wind patterns increased as wind velocity increased. Shull and Dylla (1976a) recommended maintaining the uniformity and applying the same total water depth by increasing machine travel speed and decreasing the lane spacing. Von Bernuth (1988) concluded that wind has a significant effect on the distance of throw of the sprinkler and was more pronounced with smaller drops. Marco et al. (1989) demonstrated that the influence of wind on sprinkler irrigation performance is a major consideration for designers, especially when using agricultural chemicals such as fertilizer, pesticides and fungicides with sprinkler irrigation systems. Vories and Von Bernuth (1986) and Seginer et al. (1991) stated that sprinkler irrigation non-uniformity would affect crop yield.

2.6 Models that predict the distortion in wetted distribution pattern under wind conditions for large sprinklers

Reviewing the literature shows that different approaches have been taken to determine the effect of wind on distortion of the wetted application pattern from sprinkler irrigation for different kinds and sizes of sprinkler nozzles, ranging from small (Fukui et al., 1980; Von Bernuth & Gilley, 1984; Vories & Von Bernuth, 1986; Seginer et al., 1991; Vories et al., 1987; De Lima et al., 2002; Han et al., 1994) to medium-size (Von Bernuth, 1988; FariaBeskow, et al., 2012; FariaColombo, et al., 2012) to large-size nozzles (Shull & Dylla, 1976a; Prado & Colombo, 2013; Prado et al., 2013). This literature review focuses on large impact sprinklers known as big-gun.

There are different approaches to determine the impact of wind in distortion of the wetted application pattern for large impact sprinklers. Grose (1999) classified the models into three types: empirical models, semi-empirical models and deterministic models. Granier et al. (2003) also classified the models into three types: statistical approach, semi-empirical approach and ballistic approaches. Although those two classifications are named differently, they have the similar meanings. The three main models are described below.

2.6.1 Empirical models

This approach requires the recording of large numbers of measurements of wetted application patterns for a range of wind speeds and directions. The relationship between wind speed and direction is determined by using statistical analysis to formulate equations which are used to predict the behaviour of spray in wind (Elliott et al., 1980; Gat & Molle, 2000; Hipperson, 1985; Karmeli, 1978; Musa, 1988; Solomon & Bezdek, 1980).

2.6.2 Semi-empirical models

A group of researchers use a semi-empirical approach to determine the distortion of wetted application patterns of large impact sprinklers in windy conditions. This approach uses existing theoretical models to predict the results using a mathematical calculation to calibrate the model and compare the results with measured data from real field tests to validate the model. This approach reduces field work, effort and cost compared with the empirical approach (Richards & Weatherhead, 1993).

Richards and Weatherhead (1993) developed a semi-empirical model to predict the distortion by wind of wetted application patterns. The model determines the distortion due to the combination of wind drift (WD) and range shortening (RS).

$$WD = \left[A + B(r/R) + C(r/R)^2 \right] W \qquad 2\text{-}5$$

$$RS = \left[D(r/R) + E(r/R)^2 + F(r/R)^3 \right] WS \qquad 2\text{-}6$$

where r radial distance from the sprinkler in wind, metres

R maximum radial distance reached in zero wind, metres

A to *F* are constants to be obtained by calibration,

W wind speed, m/s

$$S = \left(\sin^2(e)\cos^2(\lambda) + \sin^2(\lambda)\right)^{0.5} \qquad 2\text{-}7$$

e is trajectory angle.

λ is the angle between the jet direction and wind direction.

The model was deduced from the observations of Shull and Dylla (1976b) and the results of Dalvand (1986), with the data collected from (Musa, 1988). The shape of the wetted application pattern is squashed and changes from a circular to an oval shape and the extra drag of wind will cause the centre of the wetted pattern to move down-wind. The wetted application pattern will be shortened in both up-wind and cross-wind and lengthened down-wind. The degree of distortion of the sprinkler pattern from an individual nozzle is a function of the wind speed and the droplet size distribution. The effects of wind, as shown in Figure 2-12, come from three direct actions. The droplet flight is lengthened in the downwind direction; it is shortened in the upwind direction; the width of the wetted area in the crosswind direction is reduced for all droplet sizes.

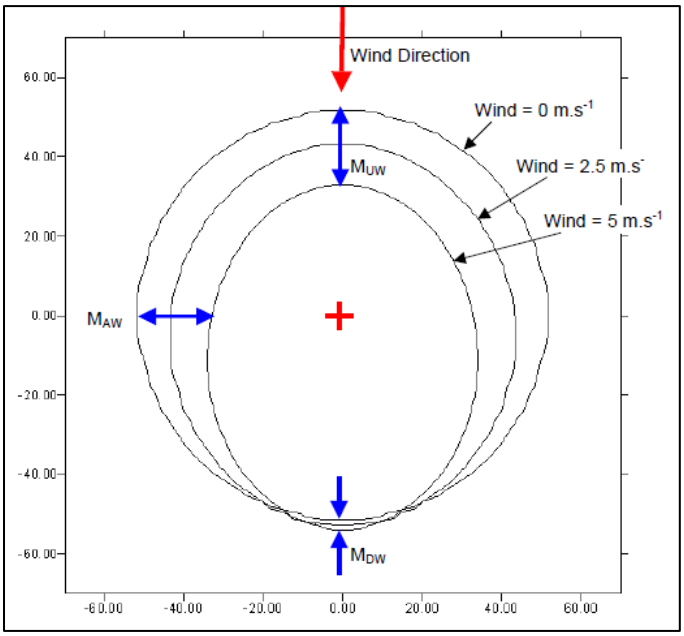

Figure 2-12: Movement of sprinkler patterns due to wind from Newell et al. (2003)

Calibration of the model required finding the value of the six constants from the experimental data. The value of $(r/R = 1)$ is affected by range shortening and the model was deduced as follows:

$$A+B+C=1.9 \qquad 2\text{-}8$$

For wind drift,

$$D+E+F=3.2 \qquad 2\text{-}9$$

For range shortening, the process requires two sets of field data under different wind speeds and one under no wind.

Al-Naeem (1993) further developed the Richards and Weatherhead (1993) semi-empirical equations to include the effects of changing the trajectory angles, sector angles, sector positions, in different wind speed and wind directions. In this study, instead of selecting and rotating a recorded wetting pattern, the pattern is generated directly to evaluate the irrigation performance at different specific sprinkler adjustments.

The model defines the sector angle and side sector angle by determining the values of ω , $\alpha 1$ and $\alpha 2$, as shown in Figure 3-3.

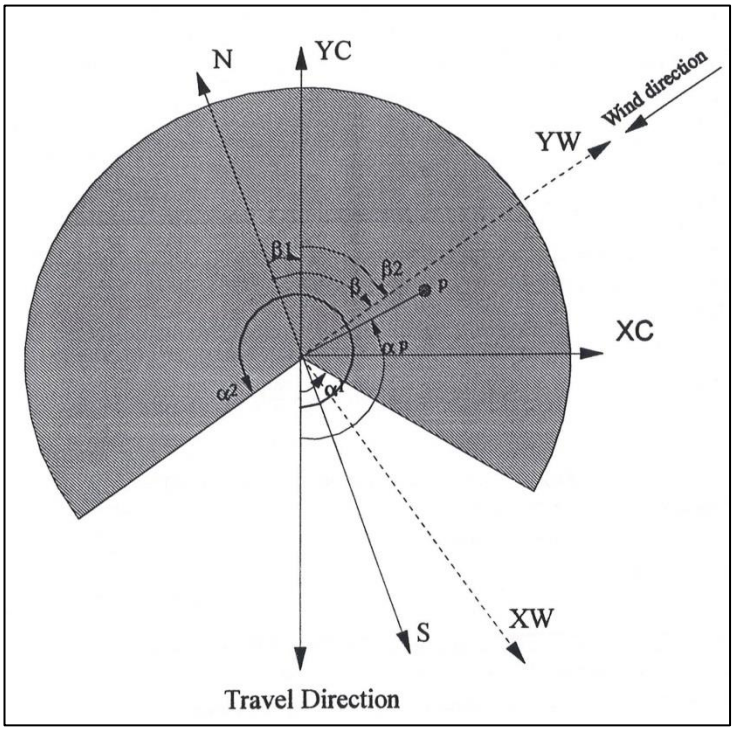

Figure 2-13: The angles used in the model by Al-Naeem (1993)

where ω is the wetted sector angle.

$\alpha 1$ is the angle between travel direction of the machine and the first edge of the wetted sector angle measured anti-clockwise.

$\alpha 2$ is the angle between travel direction and the second edge of the wetted sector angle measured anti-clockwise.

The model introduced three scenarios for the position of the wetted sector angle in relation to machine travel direction and wind direction.

1. For the sector angle set symmetrical to the travel direction, the model calculates the value of $\alpha 1$ using the following expression:

$$\alpha 1 = \left[\frac{360 - \omega}{2} \right] \quad \text{2-10}$$

2. For the sector angle set symmetrical to the wind direction ($\beta 2$ is the angle between wind direction and machine travel direction), the model calculates the value of $\alpha 1$ using the following expression:

$$\alpha 1 = \left[180 - \left(\beta 2 + \frac{\omega}{2} \right) \right] \quad \text{2-11}$$

3. For the sector angle to be set at any position, the user is asked to input the value of $\alpha 1$ as well as ω.

The model also determined the effect of sectoring angle on the application rate by multiplying the application rate with the ratio of $\left(\frac{360}{\omega} \right)$. Finally, the model determined the dry zone area to calculate whether the position of the wetted pattern fell (after the effect of wind shift) in the dry sector or not.

Smith et al. (2008) developed the computer programme TravGUN to simulate the irrigation application pattern of travelling gun machines under different wind conditions. This model enabled the researchers to generate a sprinkler pattern from one line of collectors across the sprinkler movement path to estimate the applied depths under quiescent wind conditions, as shown in Figure 3-14.

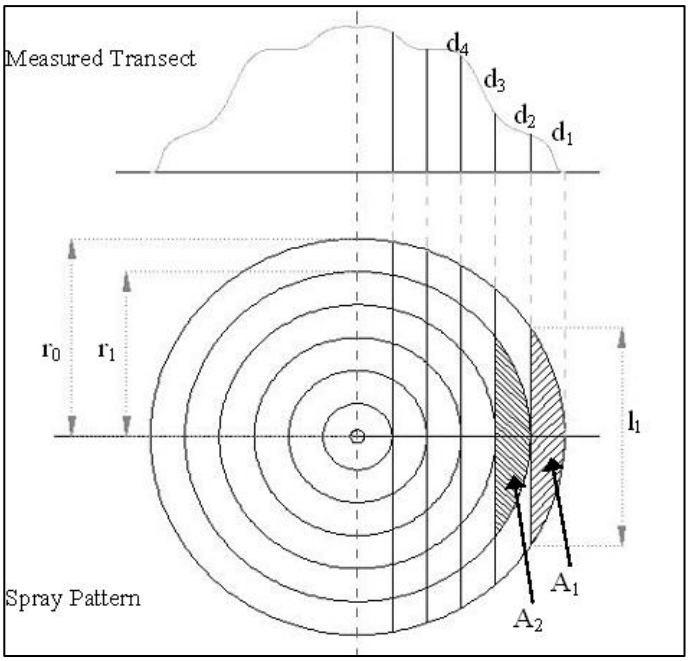

Figure 2-14: Procedure for determining the radial leg pattern from the measured transect (Smith et al., 2008)

The distance travelled by the machine in the time contributing to the water depth d_1 can be estimated by using the equation:

$$l_1 = 2\sqrt{r_0^2 - r_1^2} \qquad 2\text{-}12$$

where l_1 is the length chord of segment area A_1 , r_0 is the outer radius of largest annular area, r_1 is the outer radius of the next annular area, d_1 is the average water depth in area A_1 , and d_2 is the average water depth in area A_2 .

The average application rate for the segment area A_1 can be estimated by using the following equation:

$$\bar{Z}_1 = d_1 V / l_1 \qquad 2\text{-}13$$

where $\bar{Z}_1$ is the application rate for area A_1 and V is the irrigation machine speed.

The application rate for area A_2 then can be calculated by using the following equation:

$$\bar{Z}_2 = \left(d_2 - \frac{2\left(\sqrt{r_0^2 - r_2^2} - \sqrt{r_1^2 - r_2^2}\right)\bar{Z}_1}{V} \right) \frac{V}{2\sqrt{r_1^2 - r_2^2}} \qquad 2\text{-}14$$

The second step is to measure the applied depths along transects perpendicular to the direction of the travelling machine under two windy conditions to calculate the six empirical parameters which are based on the Richards and Weatherhead (1993) model. This approach reduces field work significantly. The most important thing is that wind speed and direction during each test remain relatively constant.

2.6.3 Ballistic models

Another approach uses the deterministic or ballistic model to predict the distortion by wind of the wetted application pattern using the equation of motion for individual droplets within the sprinkler. This new approach requires less effort and work in the field but it requires expensive equipment to conduct the tests.

It is important to note that this approach was developed by Grose (1999) to determine the distribution pattern under different wind conditions. This model development, through use of deterministic ballistic models, is based on an assumption that the wetted pattern could predict the wind effect by solving for the equations of motion for individual droplets within the sprinkler water distribution. The ballistic models are able to predict the motion of different droplet sizes along the radial leg of the sprinkler. Moreover, the approach is achieved through three stages. Firstly, the concept of the transformation of water from a rigid and deformed phase into a mixture of water droplets surrounded by air in a multi-phase form was developed. Equations for this general concept are formulated to define the relationship between the components of the multi-phase mixture, including the equations of motion determined by the system so that the viscous force dissipation becomes small compared to the forces of

dispersion as a result of the drag force. Secondly, reducing the complexity of the model by assuming the multi-phase interior of the sprinkler distribution is in one dimension. Finally, measuring the droplet size distributions at ground level along the sprinkler.

2.7 Measurement methodology

There are three main ways to measure the wetted pattern from sprinklers, namely, transect, full grid, and droplet size distribution. The transect measurement is usually suitable for self-propelled irrigation machines, whereas full grid and droplet size distribution measurements are used with stationary sprinklers.

2.7.1 Transect measurement

To measure the transect, a line of collectors or water collectors are placed perpendicular to the direction of the travelling machine to capture water depths. There are two purposes of this method. Firstly, to evaluate the uniformity of the existing machine in the field; and secondly, for calibration of computer models.

The test methods for uniformity assessment of travelling big-guns is defined within an international standard (ISO, 2003) and uses measurements collected under ideal field conditions. In field tests, the collectors are put in two lines perpendicular to the direction of travel. The interval spacing between the collectors in the line is a maximum of 6 metres and the distance between the lines is 50% of the travel distance.

The test procedure for application uniformity of a centre pivot with an end-gun sprinkler is detailed in ASAE S436.1 (2003) and involves putting two transects of collectors perpendicular to the travel direction. The interval distance between collectors depends on the sprinkler types; a maximum spacing of 3 metres is used for

static sprinkler devices, and 5 metres is used for impact sprinklers. The distance between the two transect lines varies from 3 metres at the pivot centre to 50 metres at the end of the outer span.

Smith et al. (2008) used a transect measurement to generate the radial leg from one transect of collectors placed perpendicular to a travelling big-gun under conditions of no wind and two transects under different wind speeds and directions to calibrate a computer programme called TravGUN. This method is used to predict the uniformity of the travelling machine under different weather conditions by using minimum data measurements.

Lacey (2006) used TravGUN to generate a database of wind effects on application uniformity for typical traveller gun machines by measuring transects of collectors. The study was conducted to evaluate a range of equipment and management strategies for improving irrigation efficiency and to assess the impacts of travelling gun non-uniformity during the season on field scale vegetable production.

Prado and Colombo (2010) compared measured transect data of a irrigation machine with simulated transect data by running their SIMULASOFT software. The distance between each line was 6 m, with a 2 m spacing between the collectors in the same line.

2.7.2 Full grid measurement

The application patterns of a stationary sprinkler operating under windy conditions can be determined by placing a full grid of collectors around the individual sprinkler during the tests to predict the effects of wind on the distortion of the application pattern.

In their work, Richards and Weatherhead (1993) used a full grid of collectors to predict the distortion of full circle application patterns in windy conditions. The test area was

divided into a set up with collectors on an 8m by 8m grid. The applied depth of water at each catch can on the grid was recorded for a specific wind speed and direction.

Al-Naeem (1993) used these full-circle wetted patterns from grids of collectors to further enhance the Richards and Weatherhead (1993) model.

Colombo et al. (2009) measured data from field tests on a square grid of 14 by 14 collectors around the sprinkler to collect the water on a 6m by 6m spacing. A set of 53 field tests were carried out under windy conditions. Field data were compared with 160 distribution patterns using a computer simulation model (Prado & Colombo, 2007; Prado et al., 2008; Prado, 2008) under conditions of no wind to choose the optimum uniformity with particular sector angles and travel lane spacing under different windy conditions.

Oliveira et al. (2013) used a full grid of collectors to collect data from 53 field trials under different wind conditions and combinations of nozzle pressure. The collectors were placed in a grid of total size of 84m by 84m, with 6 metre intervals with the sprinkler nozzle installed in the centre. The study was conducted to compare field measured data with simulated data. The results obtained from this method demonstrated good similarity between simulated data obtained from running their programme and the field measured data.

2.7.3 Drop size distribution measurement method

The proportions of the droplet size distribution along a radial leg can be used in a measurement method to determine the water distribution pattern from a stationary sprinkler which can be utilised in assessing the uniformity of a travelling big-gun sprinkler.

Two optical particle sizing instruments (OAP and SPO) were used by Grose (1999). The measurements of droplet size taken by both of these instruments are based on the obscuration of light directed to fall on a detector. Measurements were taken at 5m intervals starting at 5m from the stationary sprinkler nozzle. The duration of each sampling period was chosen so that, in general, more than 3000 droplets were sampled at each location. Although these methods are significantly less time-consuming than other methods of measurements, they still require expensive measuring devices.

2.8 Review of research conducted on end-gun performance

The general features of sprinkler irrigation are suitable for a wide range of crops. Centre pivots, like other self-propelled sprinklers, are suitable for tall crops (Pair, 1970). In addition, they have the capacity for variable application rates by varying the travel speed (Southorn, 1998). Furthermore, they have ability to apply chemicals as well as water to the plant (Marco et al., 1989; Martin & et.al, 2007; Palacin et al., 2005). Hence, uniformity is an absolute necessity when applying these to crops.

As mentioned in the first part in this chapter, end-guns are commonly attached to a centre pivot to increase the radius of all of the circular irrigated areas or to irrigate the corner area to make the shape of the total irrigated area as square as possible. Researchers have studied the performance of end-guns on a centre pivot system and found a lack of uniformity in end-gun patterns, and these will be discussed here.

2.8.1 Analysing the motion of the wetted distribution pattern of end-guns on a centre pivot systems

Bittinger and Longenbaugh (1962) conducted a theoretical analysis on the distribution of water from a moving irrigation sprinkler for both lateral movement and centre pivot.

They concluded that when the radius of a circular sprinkler motion is greater than five sprinkler pattern radii, the application patterns produced are essentially equivalent to those of linear motion.

Solomon and Kodoma (1978) analysed end-guns on a centre pivot wetted distribution pattern from a stationary sprinkler and generalized the movement of the application rate curves using the Bittinger and Longenbaugh (1962) approach. The study concluded that a sector angle was 135° produces good results and performance according to these criteria and depends not only on the characteristics of the end-guns, but also on the characteristics of the rest of the pivot machine and on how both characteristics are matched.

von Bernuth (1983) proposed a technique for analysing end-gun applications on a centre pivot. The effect of cycling an end-gun on and off was studied in depth for a typical centre pivot condition to select sprinkler nozzles for flow uniformity by using computational techniques and field verification. The analyses demonstrated that with the increased flow and reduced head due to the end-gun being on, the pressure distribution within the system deviates from the original distribution. This deviation can be minimized by decreasing total flow (or increasing pipe size).

Omary and Sumner (2001) introduced a modelling of water distribution for small nozzles mounted on a centre pivot irrigation system. The value of the deviation of water distribution pattern as a result of the circular path of the spray on a centre pivot was assumed to be linear when the sprinkler was located at the outer end of the pivot.

2.8.2 The performance of end-guns in centre pivot systems

In developing a simulation model for the centre pivot system to examine the effect of wind on the uniformity of water distribution pattern, Rapp (1979) excluded the wetted area under the end-gun from uniformity coefficient calculation, implying that end-gun performance would reduce the coefficient of uniformity for all systems.

Regarding wind influence, Kincaid (1996) reported that wind effect on the outer edge of a centre pivot where the end-gun is located is greater than at the pivot point.

Tarjuelo et al. (1999) analysed the uniformity of different sprinkler irrigation systems. The global water distribution was considered for a centre pivot system. The tests demonstrated that the major variability in uniformity was detected at the outer end of the lateral span. Moreover, this zone is more susceptible to wind action. The study suggested using a medium-sized end-gun located at 2m above the ground to overcome the problem.

In a very profound essay, Foley (2008) reported that a variation in depth occurs between the last regular pivot sprinkler on the last span and end-guns, which leads to low uniformity.

Vories et al. (2008) found a slightly lower water flow rate and increased water pressure when end-guns were shut off.

Henggeler and Vories (2009) evaluated the uniformity under end-gun and lateral span separately. They found the ratio of end-gun to lateral span application rate was between 0.5 to 2.0. The unevenness in water applied under both areas can be improved by selecting the proper size of end-gun orifice. They added that the uniformity of the whole machine was increased by 1% when the end-gun data was excluded from the

calculation, which means that the uniformity for machines with end guns are slightly lower than the same machine without the end gun.

Smith and North (2009) reported that the irrigation pattern, application rate and uniformity under end-guns are completely different and that, generally, the uniformity was poorer than for the rest of the machine.

Agriculture Victoria (2017), following Foley (2008), recommended not using end-guns on a centre pivot because the wetted pattern created by end-guns is generally uneven, particularly under windy conditions.

2.9 Summary and the Research Gap

Reviewing the literature demonstrates the existence of debates regarding the performance of end-guns on a centre pivot and there is a lack of research to determine the effect of the arc motion of the wetted distribution pattern of end-guns on a centre pivot. Limited work has been conducted to simulate the application pattern for end-guns on centre pivots. The previous studies analysed the wetted distribution pattern of an end gun on a centre pivot from a stationary sprinkler under conditions of no wind and assumed a linear motion of end-guns on a centre pivot. Big-guns and end-guns have similar characteristics. However, the literature reports some specific differences of end-guns related to operational conditions. Due to the large size and the nature of the movement of an end-gun on a centre pivot in a field, it is difficult to measure the wetted distribution pattern using a full grid of collectors from a stationary sprinkler under laboratory conditions. The TravGUN software (Smith et al., 2008) provides a novel methodology (minimum field data collection) for moving irrigator machines using transects of collectors perpendicular to the travel direction to generate radial leg

data and to simulate the wind distortion of the wetted distribution pattern at different wind speeds and directions.

This review of the literature has identified the following research gaps:

1. Wind speed and direction have the main impact on reducing the coefficient of uniformity for the large gun sprinkler Hipperson (1985).
2. TravGUN (Smith et al., 2008) has the capacity to generate radial leg data for big-gun sprinklers travelling in a straight path with a limited range of combined sector and side sector angles (at least 180° sector angle and a side sector angle parallel to the direction of travel), while end-guns operate with different combinations (less than 180° sector angle and less or more than 90° side sector angle). As a result, these differences between big-guns and end-guns related to some operating characteristics.
3. Following the recommendation of Lacey (2006) for big-gun application uniformity, the application uniformity of end-guns on centre pivots could be improved by changing the trajectory angle, sector angle nozzle shape, and possibly the nozzle pressure.
4. End-guns on centre pivots could be automatically adjusted as the machine moves to maximise uniformity.

In conclusion, the literature review highlighted the poor irrigation performance in the area irrigated by the end-gun. The preliminary investigation of TravGUN highlighted an error during simulation of end gun performance when the side sector angle is perpendicular to the direction of travel, and the TravGUN model cannot be calibrated from transect data measured on one side of the sprinkler. Therefore, TravGUN is not able to simulate the application uniformity for end-guns on centre pivots without

modification of the model, and the method of data collection to characterise the radial leg.

3 CHAPTER THREE

Development of a new TravGUN sub-model

3.1 Introduction

The conclusions from of Chapter 2 have highlighted that the existing TravGUN model cannot generate radial leg data for normal end-gun operation as a result of the different combination of wetted sector and side sector angles between travelling guns and end-guns.

The aim of this chapter is to describe the mathematical development of a new mathematical model to be used as a new TravGUN sub-model. The objective of this development is to enable TravGUN to produce radial leg data from transects of collectors placed perpendicular to the direction of travel for any combination of wetted sector and side sector angles for all large gun sprinklers. The first section introduces the definitions and the concepts that were developed for this purpose, as well as presenting the three geometric shapes that would emerge from all combinations of wetted sector and side sector angles. The second section presents all of the mathematical equations and algorithms that were used to calculate the length of the wetted segment areas, based on three possible geometric shapes. The third section presents a novel approach that was developed to calculate the application rate at each segment area, based on the original TravGUN model ideas, as well as the series of algorithms that were developed using a MATLAB script to achieve this goal in a novel way. Finally, this chapter describes the broader mathematical calculation process, and

how to adjust the result based on the proportion of the wetted sector angle to the full circular pattern.

3.2 Development of a new mathematical model

To enable the development of a mathematical model to generate radial leg data for any combination of wetted sector and side sector angles, two concepts need to be highlighted. Firstly, we must define and link the two edges of the wetted sector and its orientation, with the direction of travel, as shown in Figure 3-1. Secondly, we must identify in which quarters of a circle, the mathematical processes are carried out for the sprinkler pattern calculations. Finally, separate calculations processes in specific individual quarters are needed to identify the impact of asymmetrical side sector angle as a result of the deviation from the direction of travel and then combine the results of the relevant quarters.

The process of the mathematical development includes the use of the original Equations 2-12, 2-13 and 2-14 respectively from the original TravGUN (Smith et al., 2008).

The description of the new sub-model is based on the assumption that the line of forward travel direction is always perpendicular to any catch cans transects, and is the starting radius for all internal angles which are always measured clockwise positive. The variable angles θ, ϕ, ω_1, ω_2 are shown in Figure 3-1 and Figure 3-2 and are defined as follows:

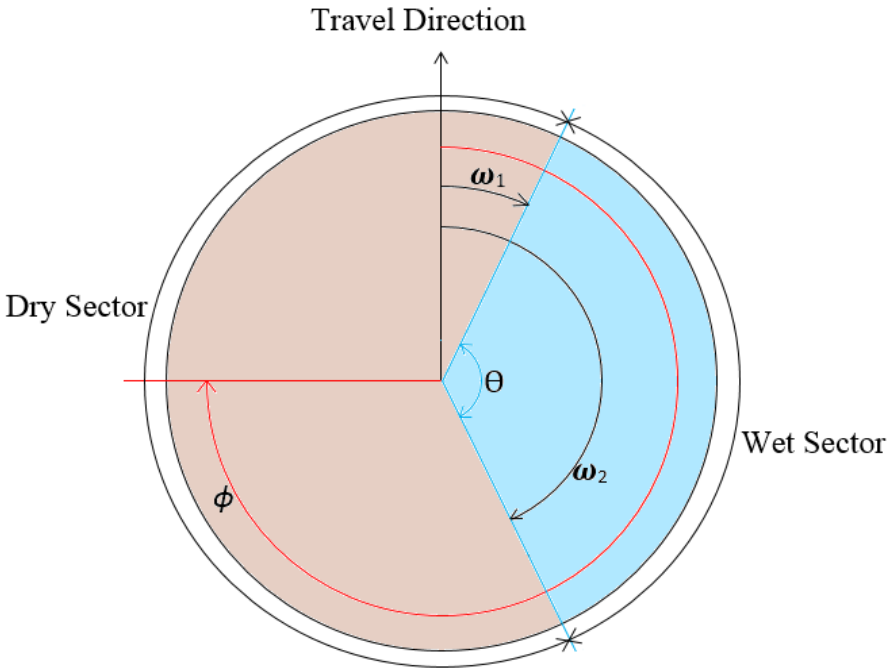

Figure 3-1: Scheme showing the main angles used in developing the TravGUN sub-model.

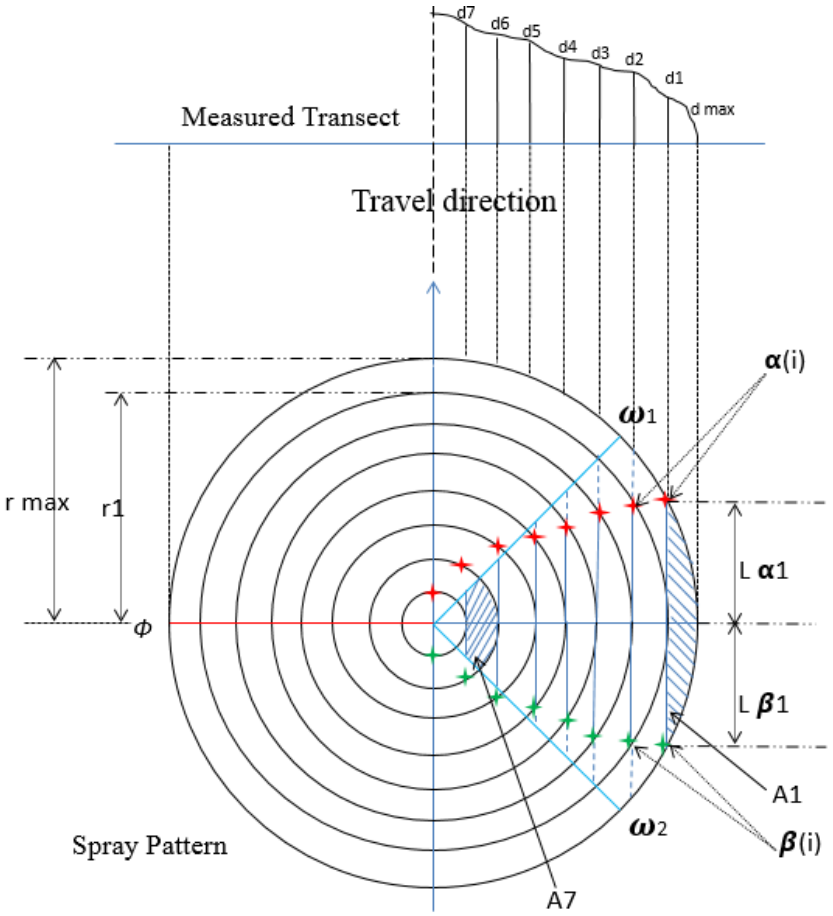

Figure 3-2: Procedure for determining the radial leg pattern from the measured transect for case 1 (when the sector angle is between 0° and 180° and the side sector angle is perpendicular to the direction of travel).

The internal angle of the wetted sector which is part of the full rotation of the large gun sprinkler, is labelled as θ, the wetted sector angle, shown in Figure 3-1.

The angle ϕ is the horizontal clockwise angle from the direction of travel to the centre of the dry sector, and is known as the side sector angle.

This wetted sector is bound by two radii with positions at clockwise angles from the direction of travel, ω_1 and ω_2, so that $\theta = \omega_2 - \omega_1$.

The angles ω_1, ω_2 can be calculated from Equation 3-1 and Equation 3-2 respectively:

$$\omega_1 = \phi - 180 - \left(\frac{\theta}{2}\right) \qquad \text{Equation 3-1}$$

$$\omega_2 = \phi - 180 + \left(\frac{\theta}{2}\right) \qquad \text{Equation 3-2}$$

The angles ω_1 and ω_2 are used to identify in which quarter the calculation process is occurring for three different scenarios. Other mathematical calculations are also based on the values of those two angles, ω_1 and ω_2.

The calculation process in the original TravGUN model used to determine the radial leg from the zero wind transect only used half of the circular sprinkler pattern. The assumption was that the wetted pattern was symmetrical about the travel direction line.

The proposed mathematical model has the ability and the flexibility to generate radial leg data from transects of collectors measured under any combination of wetted sector and side sector angles (symmetrical and asymmetrical side sector angles alike).

The main procedural development on which the new mathematical model is based, is to separate the calculation process into two separate quarters of the circular sprinkler

pattern. The first quarter is always between the direction travel and a radius at an angle of 90° clockwise. The position of the second quarter is always between the angles of 90° and 180°. The mathematical symbol α will refer to all constants and variables which are calculated in Quarter One for Case 1, and all lengths from ω_1 side for Cases 2 and 3 as it will be detailed in the end of this section; and the mathematical symbol β will refer to all constants and variables which are calculated in Quarter Two for Case 1, and all lengths from ω_2 side for Cases 2 and 3. Equations 2-12 to 2-14 from the original TravGUN model (Smith et al., 2008) will be altered, and then determined separately for each quarter before these calculated results will be combined. Figure 3-3 shows how the developed new sub-model and algorithms work. The calculations take place for both α and β sides at the same time and then the total length will be combined from both sides. The indicator i refers to the looping numbers in the algorithm.

The original Equation 2-13 (Smith et al., 2008) used to determine the length of each full segment shaded in Figure 3-2, will be changed to the following:

$$L_{\alpha i} = \sqrt{r_{i-1}{}^2 - r_i^2} \qquad \text{Equation 3-3}$$

$$L_{\beta i} = \sqrt{r_{i-1}{}^2 - r_i^2} \qquad \text{Equation 3-4}$$

The value of the segment length in Equation 2-12 (Smith et al., 2008) and the application rate in Equation 2-13; will be estimated in between the two radii at ω_1 and ω_2 (borders), as shown in Figure 3-2, Figure 3-6, and Figure 3-8. The position of the leading radius ω_1 and the trailing radius ω_2 of the wetted sector angle will determine in which quarter the segment length will reside. Because, the values of the relevant

angles will be counted according to their positions, the mathematical calculations will be slightly different in some cases.

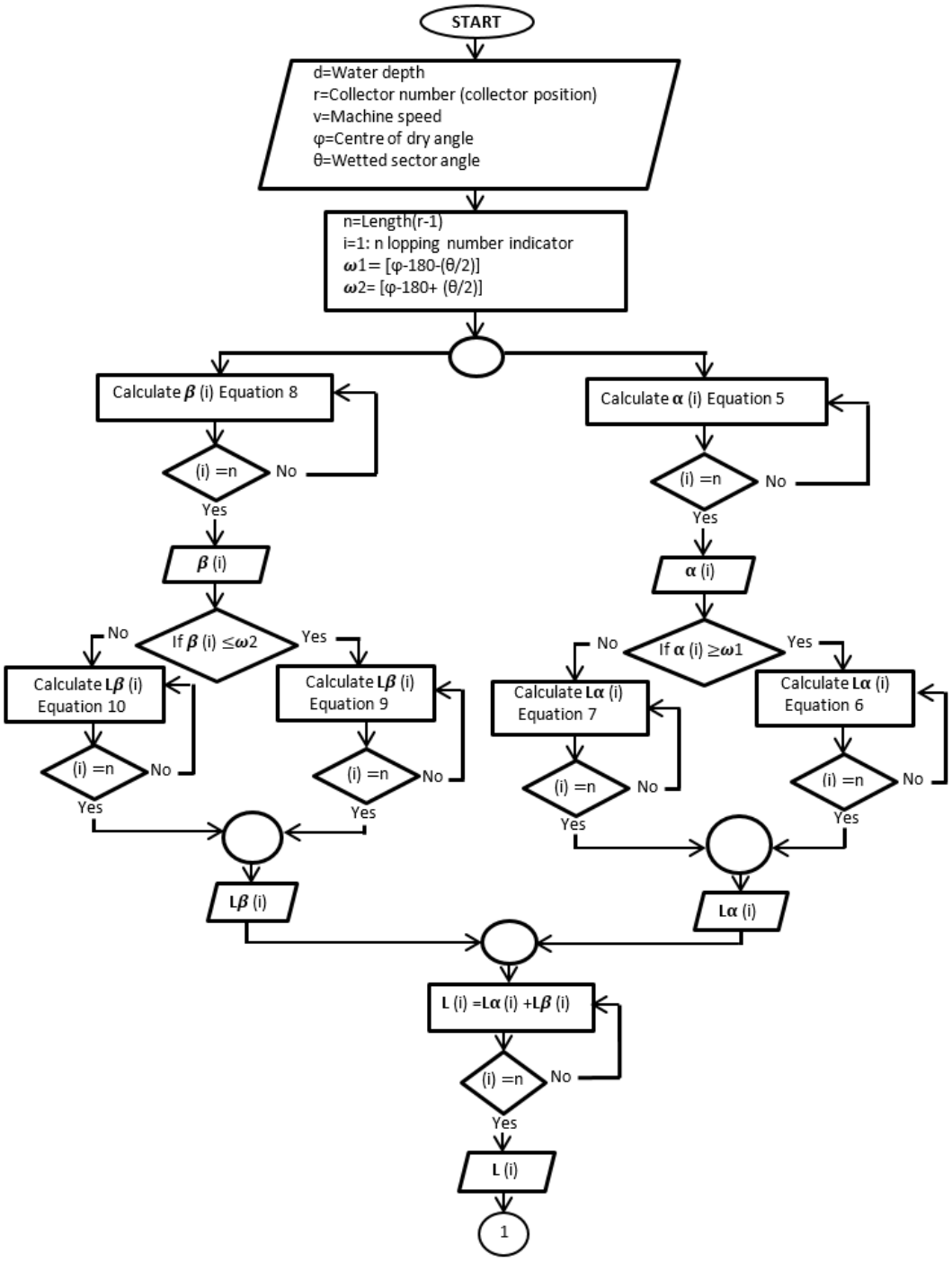

Figure 3-3: Summary of the calculation process for length segment area for two separate quarters (first case).

For all combinations of wetted sector and side sector angles, when compared to the direction of travel, three geometric shapes emerge as follows:

- Case 1 is where the wetted sector angle θ is less than 180° ($\theta < 180°$) and the position of ω_1 is in quarter One, and the values of ω_1 are between 0° and 90°, and the position of ω_2 is in Quarter Two, and the values of ω_2 are between 90° and 180°, as shown in Figure 3-2.
- Case 2 is where the wetted sector angle θ is less than 180° ($\theta < 180°$) and the position of ω_1 is in Quarter Two, and the values of ω_1 are between 90° and 180°. The position of ω_2 is in Quarter Three, and values of ω_2 are between 180° and 270° as shown in Figure 3-6.
- Case 3 is where the wetted sector angle θ is less than 90° ($\theta < 90°$) and both of ω_1 and ω_2 are in the same quarter (either Quarter One or Two). In other words, the difference between ω_2 and ω_1 is greater than 0° and less than 90° (0°> θ >90°), as shown in Figure 3-8.

The model will now be developed to calculate the length of the segment area, L, used to estimate the duration for the application rate for each area segment, for each of the above three cases.

3.3 Calculation of segment lengths for three combinations of sector and side sector angles

The three cases anticipated for combinations of wetted sector angle , θ , and side sector angles , ϕ , will used in separate algorithms to calculate the full and part segment lengths , L , and these are described separately in the following sections.

3.3.1 Case 1: Segment length *L* for 90°< θ <180° and 225°< ϕ <315°

Figure 3-4 shows the values of α_i , for each i (α_1 , α_2 , ... , α_i) defined as the internal angles clockwise from the direction of travel to the leading points of the segment area, which is the internal angle of ABC shown in Figure 3-4. Each value of α is calculated from the two distances r_i and r_{i+1} as:

$$\alpha_i = \sin^{-1}\left(r_{i+1} \big/ r_i\right) \qquad \text{Equation 3-5}$$

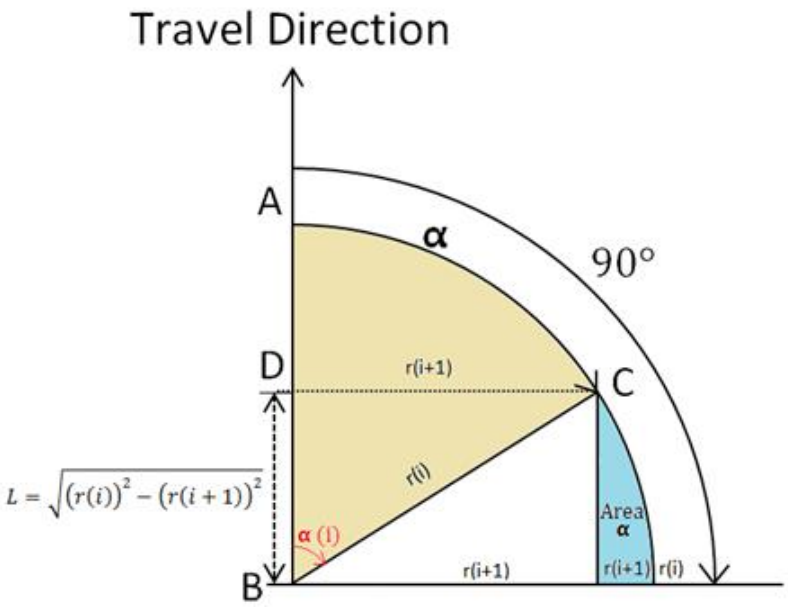

Figure 3-4: Diagram showing the value of the α angle.

The values of α are used to determine the half length of the segment or fragment area in the first quarter, $L\alpha_{(i)}$ as shown in the flowchart in Figure 3-3. If α_i is equal to or greater than ω_1, then the length is calculated by Equation 3-6, as shown in Figure 3-2 and in the flowchart in Figure 3-3.

$$L\alpha_i = \sqrt{r_i^2 - r_{i+1}^2} \qquad \text{Equation 3-6}$$

If the angle α_i is less than the angle of leading edge, ω_1 then the length is calculated by Equation 3-7; as shown in Figure 3-2 length $L\alpha_7$ for area A_7

$$L\alpha_i = r_i \times \tan(90 - \omega_1) \qquad \text{Equation 3-7}$$

Similarly, with regard to the first geometric shape A_1 in Figure 3-2, the values of the β_i angle (β_1 , β_1 , ..., β_i) in quarter two are defined as the angles between the direction of travel clockwise to the trailing point of the half segment area β_i (interior angle of ABC) as shown in Figure 3-2 and Figure 3-5. The values of β_i angles are calculated from Equation 3-8 as:

$$\beta_i = \left[\cos^{-1}(r_{i+1} / r_i)\right] + 90 \qquad \text{Equation 3-8}$$

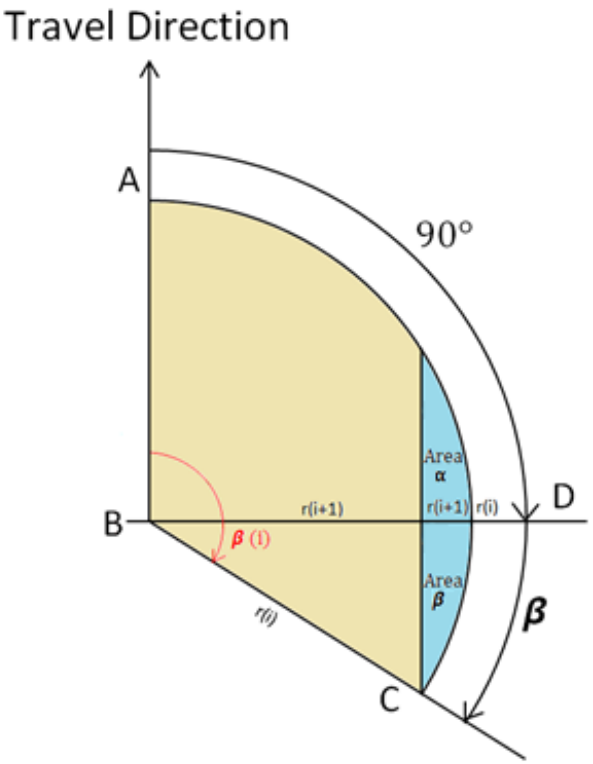

Figure 3-5: Diagram showing the value of the β angle.

If β_i is less than or equal to the angle of the trailing edge ω_2, then the length is calculated by Equation 3-9, as shown in the flowchart in Figure 3-3.

$$L\beta_i = \sqrt{r_i^2 - r_{i+1}^2} \qquad 3\text{-}9$$

If β_i is greater than the angle of the trailing edge ω_2, then the length is calculated by Equation 3-10, as:

$$L\beta_i = r_i \times \tan\left[(\omega_2 - 90)\right] \qquad 3\text{-}10$$

The total lengths of area A_1 or area A_n in Figure 3-2 of two half segment (i) $L\alpha_i$ and $L\beta_i$ will be calculated by finding the summation of $L\alpha_i$ and $L\beta_i$ for the first Case 1, according to the values of wetted sector and side sector angles.

3.3.2 Case 2: Segment length *L* for 90° ≤ θ < 180° and -315° ≤ ϕ < 45°

For the second geometric shape, calculations will proceed, as shown in Figure 3-6, when the value of ω_1 is equal to or greater than 90° and equal to or less than 180°, where ω_1 is located in Quarter Two, and the value of ω_2 is equal to or greater than 180° and equal to or less than 270°, and where ω_2 is located in Quarter Three.

The location of r_i will be shifted to x_i because the maximum water throw will deviate and decrease when ω_1 passes the first quarter and the small segment area A_i will change to a semi triangular shape as shown in Figure 3-6. The number of the collectors in each combination of sector and side sector angles should be the same but the location of the collectors should be recalculated depending on the positions of the leading and trailing edges in relation to which quarter they were in before undertaking the measurement. The new location can be estimated by the multiplication of r_i by $\cos\omega_1$ or ω_2.

The value of $X\alpha_i$ is calculated using Equation 3-11.

$$X\alpha_i = r_i \times \cos(\omega_1 - 90) \qquad 3\text{-}11$$

The length, L, that the sprinkler pattern (machine) travels in the shaded area A_i in Figure 3-6, is what will be used to calculate the application rate, in this area, using the following Equations 3-12, 3-13 and 3-14, respectively. Firstly, we will calculate the length, $Ldryalpha_i$, from the non-irrigated or dry parts of the segments on the α side in Quarter Two, using Equation 3-12. Secondly, we will calculate the total length of the segment on the α side in Quarter Two using Equation 3-13. Finally, the length of

each semi-triangular area will be calculated by subtracting the dry length within the α side from the total length using Equation 3-12. Figure 3-7 summarizes the calculation process and shows how the algorithm is working.

$$Ldry\alpha_i = r_i \times \sin(\omega_1 - 90) \quad 3\text{-}12$$

where $Ldry\alpha_i$ are the partial lengths of the segment area that are dry on the α side in Quarter Two.

$$Lwet\alpha_i = \sqrt{(r_i^2 - X\alpha_{i+1}^2)} \quad 3\text{-}13$$

where $Lwet\alpha_i$ are the wet plus dry total lengths of the segment area on the α side in Quarter Two.

$$Lz\alpha_i = Lwet\alpha_i - Ldry\alpha_{i+1} \quad 3\text{-}14$$

where $Lz\alpha_i$ are the lengths used to estimate the application rate times in each semi triangular area on the α side.

A similar calculation will be followed to calculate the values of $X\beta_i$ as used in the following Equations 3-15, 3-16, 3-17 and 3-18:

$$X\beta_i = r_i \times \cos(270 - \omega_2) \quad 3\text{-}15$$

$$Ldry\beta_i = r_i \times \sin(270 - \omega_2) \quad 3\text{-}16$$

where $Ldray\beta_i$ are the partial lengths of the segment area that are dry on the β side in Quarter Three.

$$Lwet\beta_i = \sqrt{r_i^2 - X\beta_i^2} \quad 3\text{-}17$$

where $Lwet\beta_i$ are the wet plus dry total lengths of the segment area on the β side in Quarter Three.

$$Lz\beta_i = Lwet\beta_i - Ldry\beta_i \quad 3\text{-}18$$

where $Lz\beta_i$ are the lengths used to estimate the application rate times in each semi triangular area on β side.

Figure 3-7 summarizes the calculation process and shows the order of operations for case 2.

Case Two will have two different lengths for the semi-triangular area Ai on sides α and β. One set of length values from side α or β will be used in calculating the application rate in the next step. Therefore, the longest set of lengths will be chosen to determine whether the calculation process will be performed on side α or β.

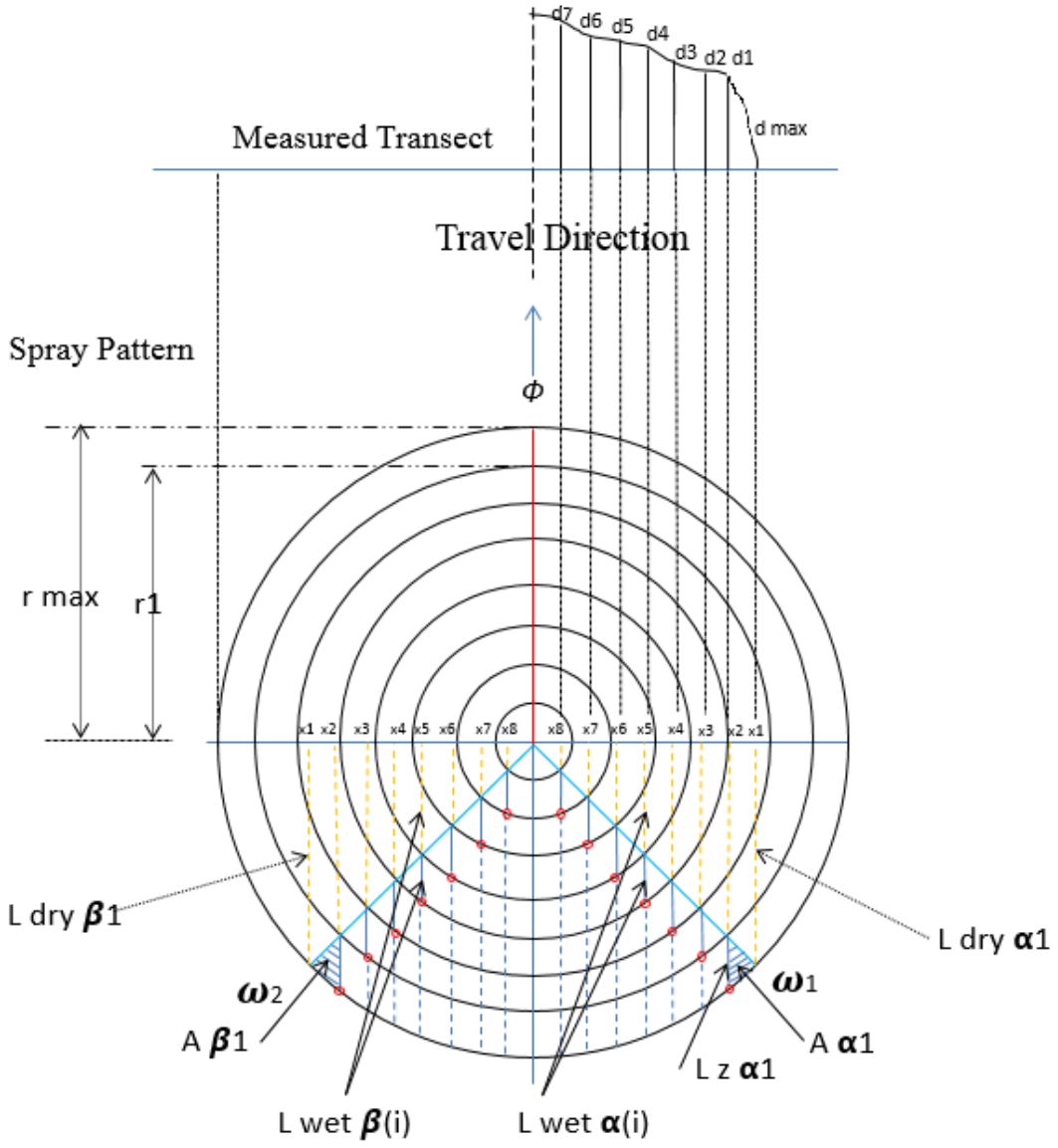

Figure 3-6: Procedure for determining the radial leg pattern from the measured transect for case 2 (when sector angle less than 180° and greater than 0° and side sector angle parallel to the direction of travel)

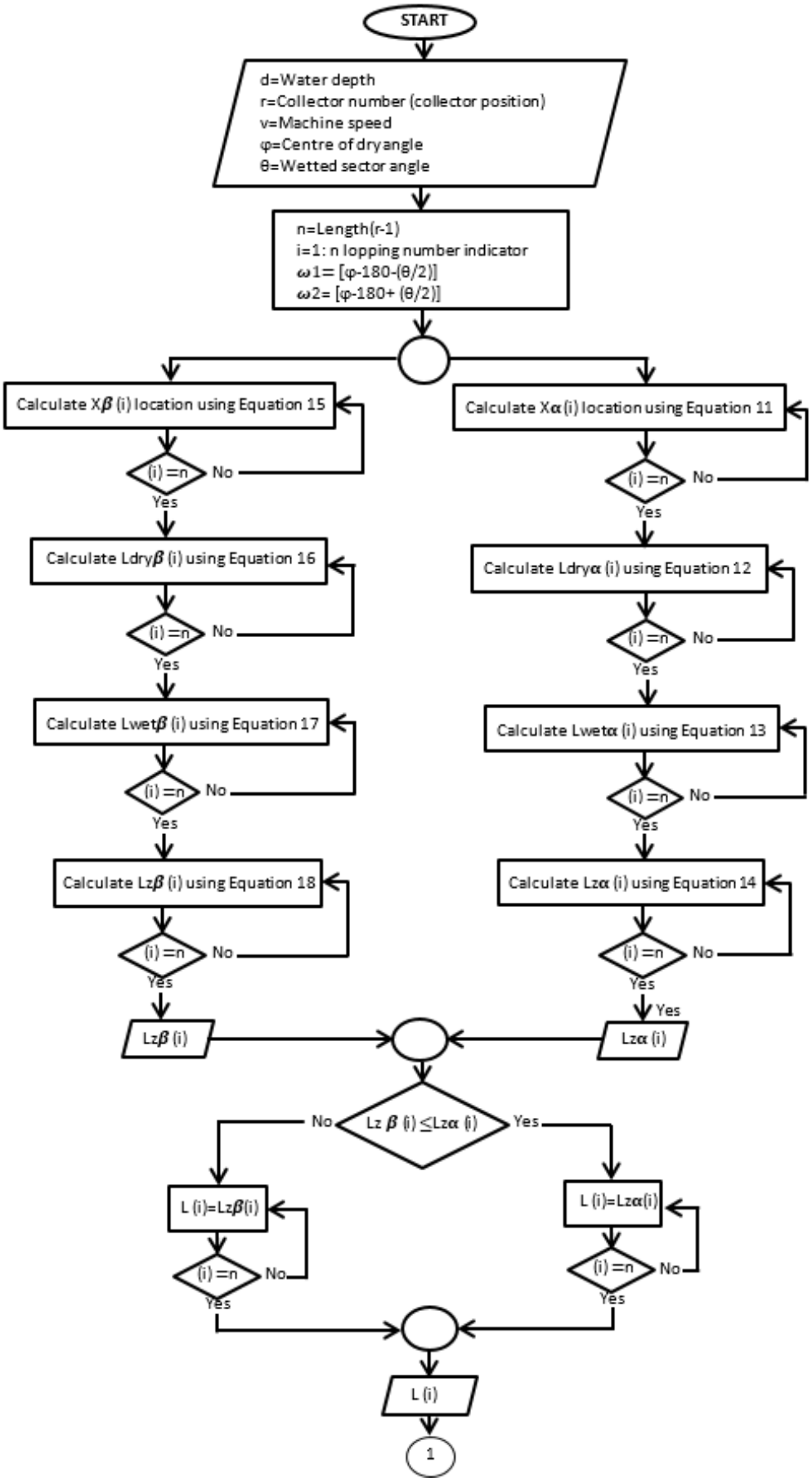

Figure 3-7: Summarisation of the calculation process of length of segment area from two separate quarters (second case).

3.3.3 Case 3: Segment length *L* for 0° < θ < 90° and 180° < ϕ < 270°

For the third wetted sector shape, as shown in Figure 3-8 when the value of ω_1 is greater than 0° and less than 90° and the value of ω_2 is greater than ω_1 and less than 90°, where ω_1 and ω_2 are located in Quarter One, the following calculations are required to complete the analysis.

The location of r_i will be shifted to X_i because the maximum distance water is thrown will decrease as long as ω_2 does not pass the first quarter line, while the wetted segment area A_i will change to a semi-triangular shape. The number of collectors in each combination of sector and side sector angles should be the same but the location of the collectors should be recalculated depending on the positions of the leading and trailing edges, and in which quarter they are positioned, before undertaking the measurement. The new location can be estimated by the multiplication of r_i by $\cos \omega_1$ or ω_2.

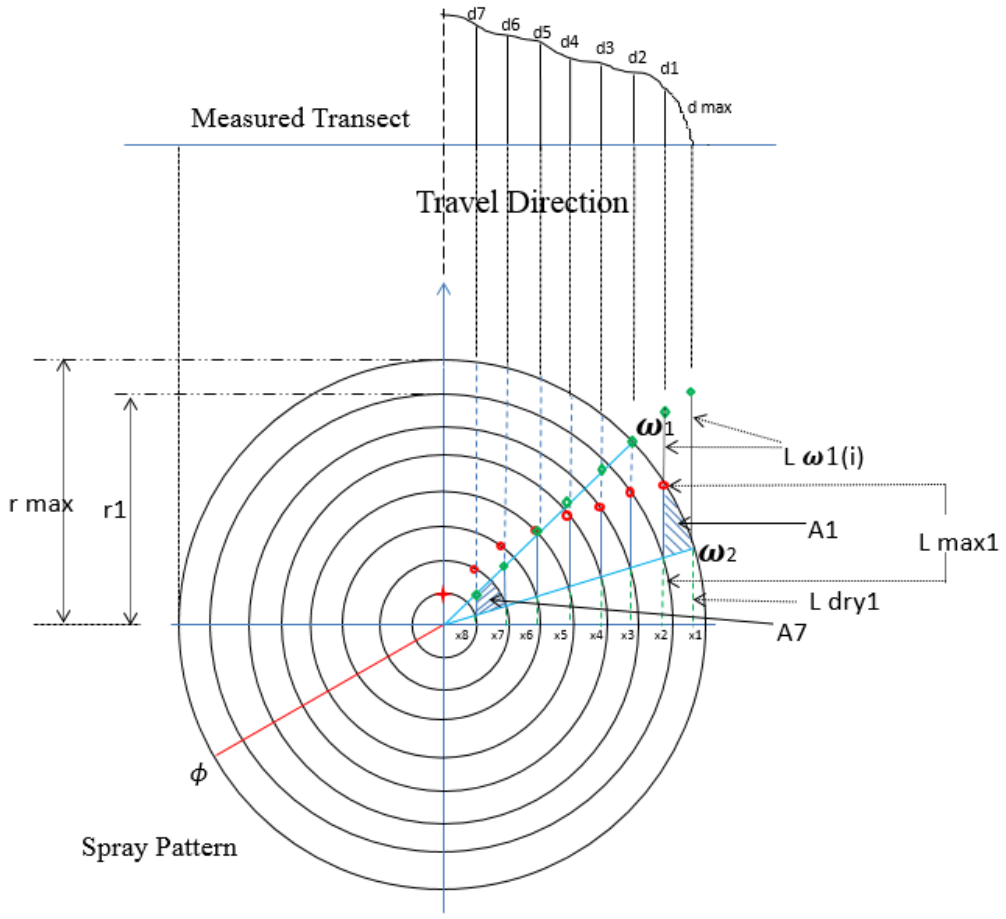

Figure 3-8: Procedure for determining the radial leg pattern from the measured transect for case 3 (when the sector angle less than 90° and greater than 0° and the side sector angle changes from 180° to 270° for each quarter to the direction of travel).

The value of $X\beta_i$ is calculated using Equation 3-19.

$$X\beta_i = r_i \times \cos(90 - \omega_2) \qquad 3\text{-}19$$

The distance required to calculate the application rate when the sprinkler pattern (machine) passes the area A_i can be calculated in three steps by using the following Equations: 3-20, 3-21, 3-22, 3-23 and 3-24 respectively. The first step will be to calculate the length from the dry β side (the lengths from the intersection point of ω_2 with the vertical extended lines from points X_i along X axis parallel to the Y axis as shown in Figure 3-8) using Equation 3-20.

$$Ldry\beta_i = r_i \times \sin\left|(90 - \omega_2)\right| \qquad 3\text{-}20$$

where $Ldry\beta_i$ are the lengths of area A_i from dry angles from (β) side.

The second step will be to calculate the lengths from the intersection point of ω_1 with the vertical extended lines from point X_i along the X axis parallel to the Y axis as shown in Figure 3-8 using Equation 3-21.

$$L\omega_{1i} = X\beta_i \times \tan(90 - \omega_1) \qquad 3\text{-}21$$

where $L\omega_{1i}$ are the side lengths of a triangle consisting of $X\beta_i$ and $\omega 1$ from wetted angles in (α) side.

The third step will be to calculate the lengths from the leading points α_i (the intersection point of r_i with vertical extended lines from points X_i along the axis parallel to the Y axis as shown in Figure 3-8) to using Equation 3-22.

$$L\max\alpha\beta_i = \sqrt{r_i^2 - \left|X\beta_{i+1}{}^2\right|} \qquad 3\text{-}22$$

where $L\max\alpha\beta_i$ is the total of both dry and wet lengths on one side of a segment in the same quarter.

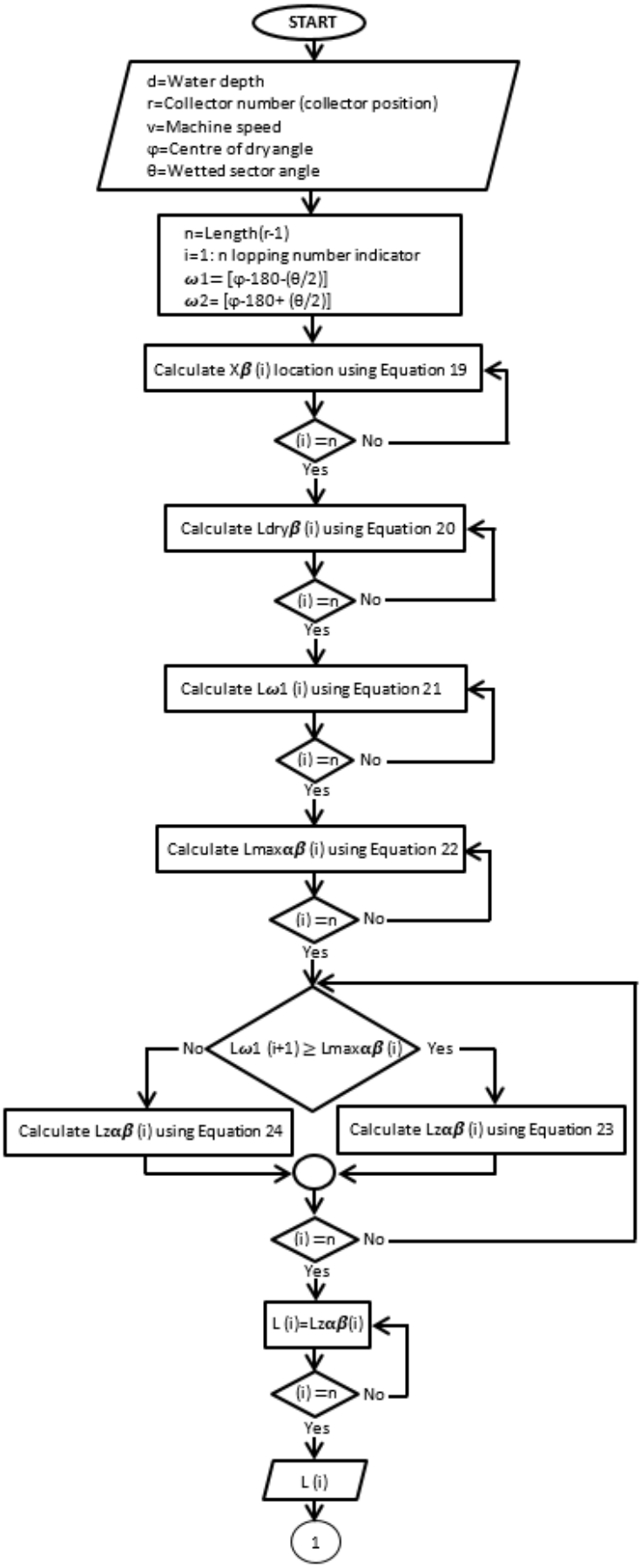

Figure 3-9: Summarisation of the calculation process of length of segment area from two separate quarters (third case).

After calculating those three different set of lengths, the algorithm will calculate the specific lengths which are used to calculate the application rate in each semi-triangular area, using the following two conditions:

- Condition One: if the length between the intersection point ω_1 with the extended lines from X_1 point on the X-axis along Y-axis L_{i+1} is equal to or greater than the length from the leading point α_i to the point X_i on the X-axis vertical along Y-axis, $L\max\alpha\beta_i$, then the length will be estimated using Equation 3-23, as shown in Figure 3-8 and in flowchart in Figure 3-9 that summarizes the calculation process.
- Condition Two: if the length between the intersection point ω_1 with the extended lines from the point X_i on the X-axis along the Y-axis to $L\omega_{1i+1}$ is less than the length from the leading point α_i to the point X_i on X-axis vertical along Y-axis, $L\max\alpha\beta_i$, the length will be estimated using Equation 3-24, as shown in Figure 3-8 and Figure 3-9.

The lengths are used to estimate the time, whereas the machine passing the semi triangular area A_i will be calculated by applying the following condition:

If $L\omega_{1i+1} \geq L\max\alpha\beta_i$

$$Lz\alpha\beta_i = L\max\alpha\beta_i - Ldry\beta_{i+1} \qquad 3\text{-}23$$

Else $L\omega_{1i+1} < L\max\alpha\beta_i$

$$Lz\alpha\beta_i = L\omega_{1i+1} - Ldry\beta_{i+1} \qquad 3\text{-}24$$

From the previous three general cases and by following similar approaches, the new sub-model has the capacity to estimate the length for any combination of sector and side sector angles. In cases, we must take into account which quarter the calculation process will occur within.

For example, in Case 1, it might occur in the first quarter plus second quarter or third quarter plus fourth quarter. In Case 2, it might occur in the second quarter plus third quarter, or fourth quarter and first quarter. In Case 3, it might occur in the first quarter, second quarter, third quarter and fourth quarter. The calculation process is still similar, but the mathematical equations will be slightly different according to each individual case and the values of the leading and trailing edges.

3.4 Calculating the application rate at each segment or fragment of segment

The new approach of splitting the calculation process into two separate quarters will also be applied to calculate the application rate at each part of the segment area to subtract the water depth that is contributed from the outer annular area, onto the inner annular area, as shown in the flowcharts in Figure 3-12 and Figure 3-13. A similar process will be applied to the original Equations 2-13 and 2-14 (Smith et al., 2008) which are used to calculate the application rate at each segment using the following:

$$\bar{z}_{\alpha 1} = d_{\alpha 1} V / L_{\alpha 1} \quad \text{3-25}$$

$$\bar{z}_{\beta 1} = d_{\beta 1} V / L_{\beta 1} \quad \text{3-26}$$

where $\bar{z}_{\alpha 1}$ and $\bar{z}_{\beta 1}$ are the applications rate in segment area 1, V is the machine speed, and $L_{\alpha 1}$ and $L_{\beta 1}$ are the lengths of segment area 1.

Further the application rate at segment area 2 can be calculated using the following equations:

$$\overline{z}_{\alpha 2} = \left(d_{\alpha 2} - \frac{\left(\sqrt{r_0^2 - r_2^2} - \sqrt{r_1^2 - r_2^2} \right) \overline{z}_{\alpha 1}}{V} \right) \frac{V}{\sqrt{r_1^2 - r_2^2}} \qquad 3\text{-}27$$

$$\overline{z}_{\beta 2} = \left(d_{\beta 2} - \frac{\left(\sqrt{r_0^2 - r_2^2} - \sqrt{r_1^2 - r_2^2} \right) \overline{z}_{\beta 1}}{V} \right) \frac{V}{\sqrt{r_1^2 - r_2^2}} \qquad 3\text{-}28$$

This method would be applicable for sector angles greater than or equal to 180° with a side sector angle symmetrical to the direction of travel. Therefore, the process of developing a new TravGUN sub-model to calculate the application rate in each part segment area can be achieved via two stages: firstly, by developing algorithms for sector angles θ less than 180° with a side sector perpendicular to the direction of travel, ($\phi = 90°$ or $\phi = 270°$); and, secondly, by developing algorithms for sector angles θ less than 180° with a side sector asymmetrical to the direction of travel ($\phi \neq 270°$ or $\phi \neq 90°$).

3.4.1 Calculating the application rate for a sector angle of less than 180° with side sector angle symmetrical to the direction of travel

The TravGUN model was based on the assumption that "The lateral transect of applied depths is simply the integral or summation of the sprinkler pattern in the direction parallel to the travel direction. This consists of depth measurements d_i taken at a series of lateral distances x_i from the travel path starting at the outer extent of the wetted area, and finishing as close as practically possible to the machine". Calculating the radial leg pattern from a transect of applied depths, measured under quiescent conditions from a sector angle, θ, less than 180°, with a side sector angle of $\phi = 90°$ or $\phi = 270°$ to the direction of

travel will result in a negative value in the radial leg near the machine, as a result of subtracting water depths from the collectors near the machine. These collectors began by not receiving as much water from each radial leg pattern (or full sprinkler pattern) as the sector angle decreases and the dry angle increases along the transect, as shown, in Figure 3-10. This figure shows three scenarios for calculating water depths: complete calculation, partial calculation and no calculation. The blue area (segments and fragments of segments) represents the application rate at each area. The full green areas (not intersecting with leading or trailing edges ω_1, ω_2) are counted or used in the calculation process. The green and yellow areas (intersecting with the leading or trailing edges ω_1, ω_2) will be counted or used in the partial calculation process. The full yellow areas (not intersecting with the leading or trailing edges ω_1, ω_2) will not be counted or used in the calculation process. Two new variable are introduced, K_α and K_β to determine the calculation scenario for each area. These variables or indicators give one of three signals. A value of K_α or K_β greater than 1.0 indicates complete calculation, a value between $0 \le K \le 1.0$ indicates partial calculation and a value less than zero indicates no calculation. This new sub-model can be implemented to develop an algorithm using a MATLAB script as shown in flowchart Figure 3-12 and Figure 3-13.

$$\overline{z}_{\alpha 2} = \left(d_{\alpha 2} - \frac{\left(\sqrt{r_0^{\,2} - r_2^{\,2}} - \sqrt{r_1^{\,2} - r_2^{\,2}} \right) \overline{z}_{\alpha 1} \times K_\alpha}{V} \right) \frac{V}{\sqrt{r_1^{\,2} - r_2^{\,2}}} \qquad 3\text{-}29$$

$$\overline{z}_{\beta 2} = \left(d_{\beta 2} - \frac{\left(\sqrt{r_0^{\,2} - r_2^{\,2}} - \sqrt{r_1^{\,2} - r_2^{\,2}} \right) \overline{z}_{\beta 1} \times K_\beta}{V} \right) \frac{V}{\sqrt{r_1^{\,2} - r_2^{\,2}}} \qquad 3\text{-}30$$

where the value of K_α and K_β will be described in the following steps.

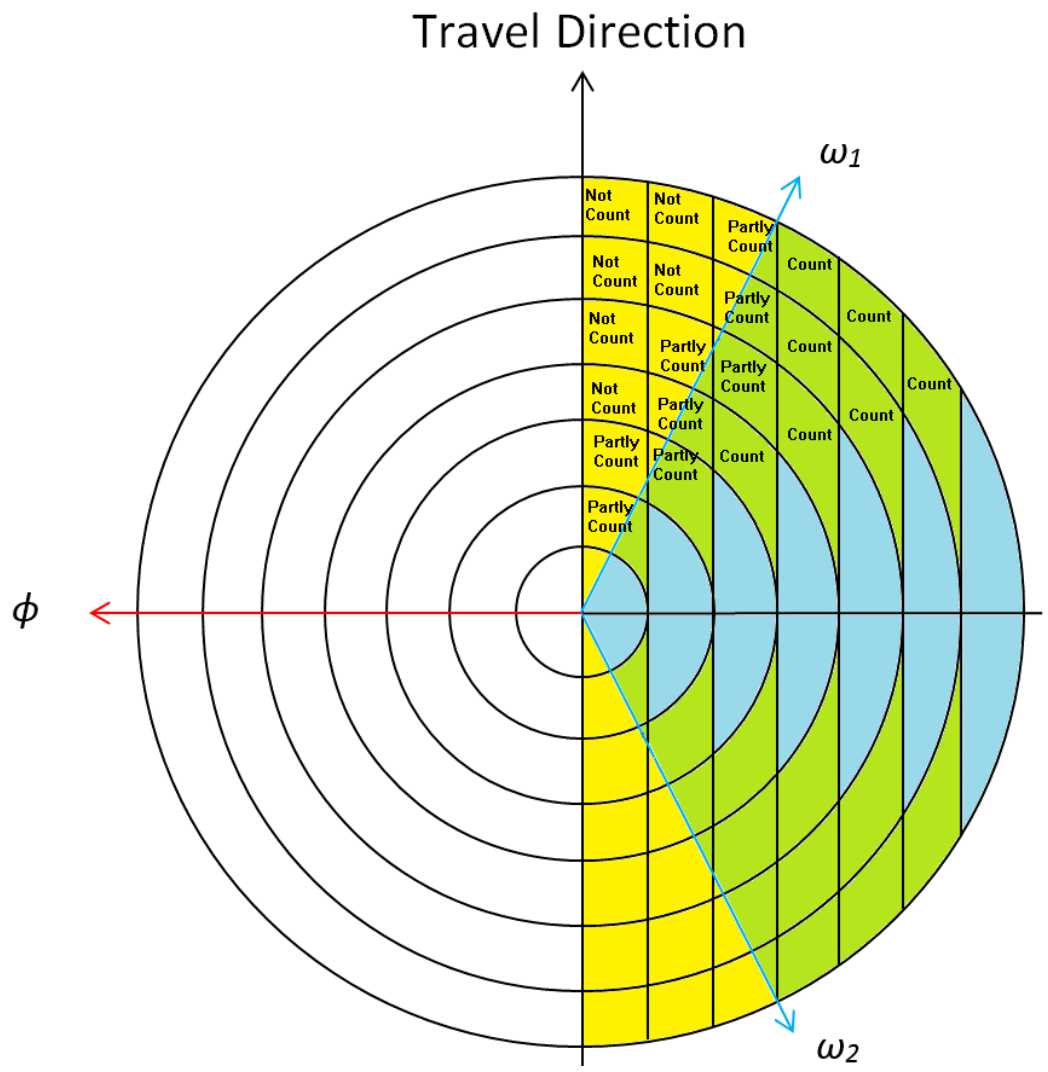

Figure 3-10: An irrigation pattern scheme showing different areas where the mathematical calculations are undertaken to calculate the application rate for sector angles less than 180° with a side sector symmetrical to the direction of travel.

This novel approach is used to identify the point in each annular area which can be used as a balance point as shown by the red stars in Figure 3-11. The outcome of using this point in the mathematical formula would be to provide different values greater than one, less than one and greater than zero or less than zero. These values of K can be used as the mathematical indicators and then used in the algorithms during the calculation process using Equation 3-29 and 3-30 as shown in the flowcharts in Figure 3-12 and Figure 3-13. The balance point is the vertical distance along the X axis from the centre of the sprinkler to the intersection point between annular area one

and the leading edge ω_1 from the α side, or trailing edge ω_2 from the β side as shown (the red stars) in Figure 3-11. The value of these points can be calculated using the following equations:

$$LK\omega_{1i} = \cos(90 - \omega_1) \times r_i \quad 3\text{-}31$$

$$LK\omega_{2i} = \cos(\omega_2 - 90) \times r_i \quad 3\text{-}32$$

where $LK\omega_{1i}$ and $LK\omega_{2i}$ are the balance points at each annular in both sides α and β respectively as shown in Figure 3-11.

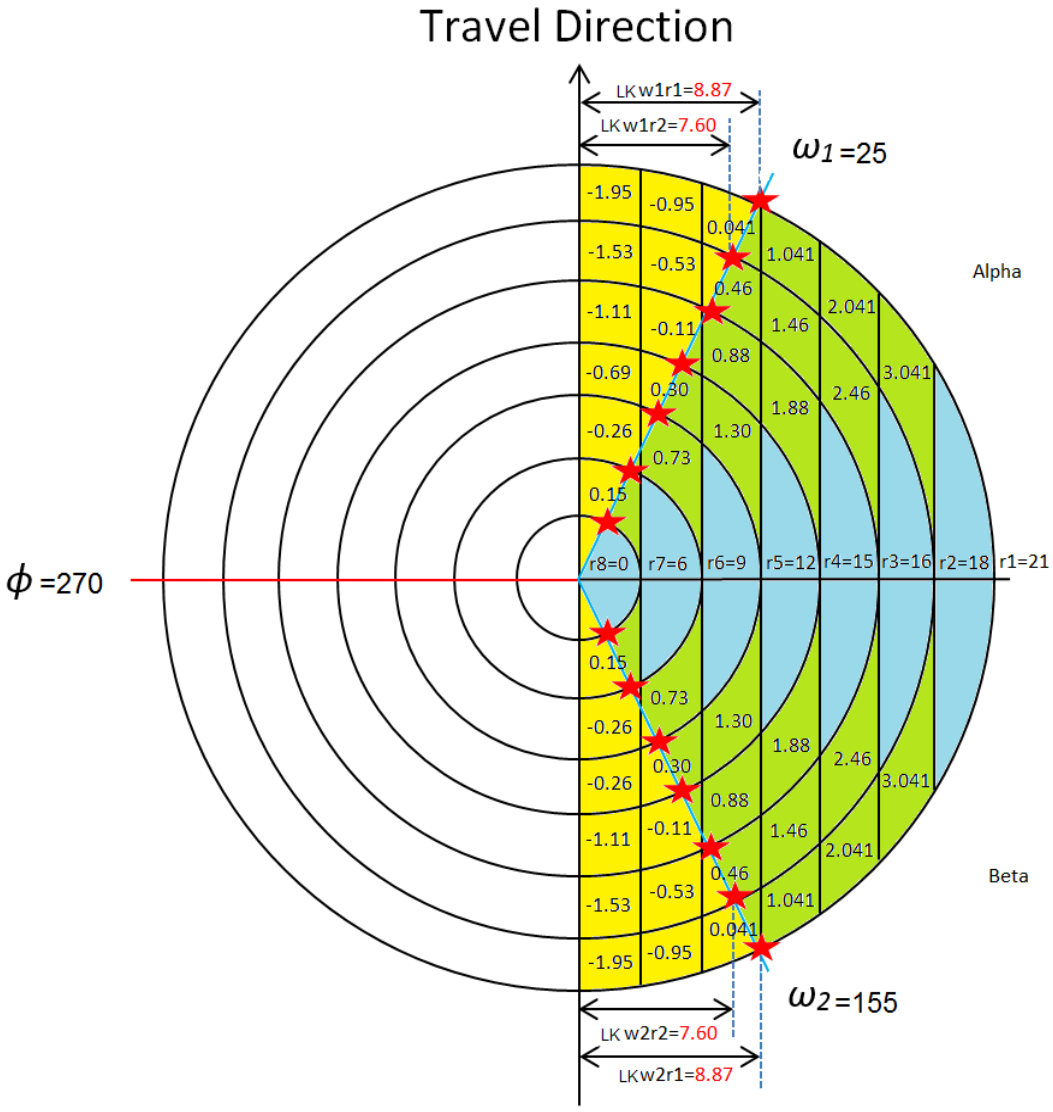

Figure 3-11: Procedure showing the critical points (LKω1 , LKω2) and a spatial distribution of the indicators ($K\alpha_{ij}$ and $K\beta_{ij}$) for sector angles less than 180° with side sector symmetrical to the direction of travel.

Equations 3-31 and 3-32 are applied to determine the distances along the X axis at each annular from both α and β sides respectively.

The values of K_α and K_β are determined for each i by applying Equation 3-31 and 3-32 followed by Equation 3-33 and 3-34.

$$K\alpha_{ij} = \left[\frac{\left(r_i - LK\omega_{1i}\right)}{\left(r_i - r_{i+1}\right)} \right] \quad 3\text{-}33$$

$$K\beta_{ij} = \left[\frac{\left(r_i - LK\omega_{2i}\right)}{\left(r_i - r_{i+1}\right)} \right] \quad 3\text{-}34$$

The computer program will start calculating the value at the first annular area, then loop to the second annular area, third, fourth and so on until the last annular area near the sprinkler, as shown in the flowchart in Figure 3-12 and Figure 3-13. The result will be a square matrix consisting of row (i) and column (j). The symbol (i) refers to the row number and the symbol (j) refers to the column number. These values will be used diagonally as shown in Table 3-1 and Figure 3-13. The program will start subtracting water depth values at segment area (2) from the water depth in collector (3) using Equation 3-35. We will start using the value of $K\alpha_{(1,2)}$ at the top left-hand side of the first loop. The net water depth at each segment area or fragment segment area (i) will be calculated using Equation 3-36 on the α side. Then the calculation process will see the second loop starting at the value of $K\alpha_{(3,1)}$. The program will run two loops. The second loop will repeat the water depth subtraction and add one additional row after each loop. The first loop will calculate the application rate at each annular area and then proceed to the next column. Therefore, the program will finish

its calculation at indicator values $K\alpha_{(7,6)}$ at the bottom right-hand side. In other words, the program will use mathematical matrix indicators diagonally as shown in Table 3-1.

Table 3-1 A diagonal matrix of ($K\alpha(ij) and\ K\beta(ij)$) values used as indicators in the algorithms

	1	2	3	4	5	6	7
1	4.0417	3.0417	2.0417	1.0417	0.0417	-0.9583	-1.9583
2	4.4643	3.4643	2.4643	1.4643	0.4643	-0.5357	-1.5357
3	4.8869	3.8869	2.8869	1.8869	0.8869	-0.1131	-1.1131
4	5.3095	4.3095	3.3095	2.3095	1.3095	0.3095	-0.6905
5	5.7321	4.7321	3.7321	2.7321	1.7321	0.7321	-0.2679
6	6.1548	5.1548	4.1548	3.1548	2.1548	1.1548	0.1548
7	6.5774	5.5774	4.5774	3.5774	2.5774	1.5774	0.5774
8	7	6	5	4	3	2	1

The algorithm will proceed as follows:

- If the value of ($K\alpha_{ij}$ or $K\beta_{ij}$) is equal to or more than one then, let the value of ($K\alpha_{ij}$ or $K\beta_{ij}$) be equal to one when subtracting water depth from the green area.
- If the value of ($K\alpha_{ij}$ or $K\beta_{ij}$) is less than one and more than zero, then let the value of ($K\alpha_{ij}$ or $K\beta_{ij}$) be equal to ($K\alpha_{ij}$ or $K\beta_{ij}$) when subtracting water depth from both green and yellow areas.
- Finally, if the value of ($K\alpha_{ij}$ or $K\beta_{ij}$) is equal to or less than zero, then let the value of ($K\alpha_{ij}$ or $K\beta_{ij}$) be equal to zero when subtracting water depth from the yellow areas as shown in Figure 3-12 and Figure 3-13.

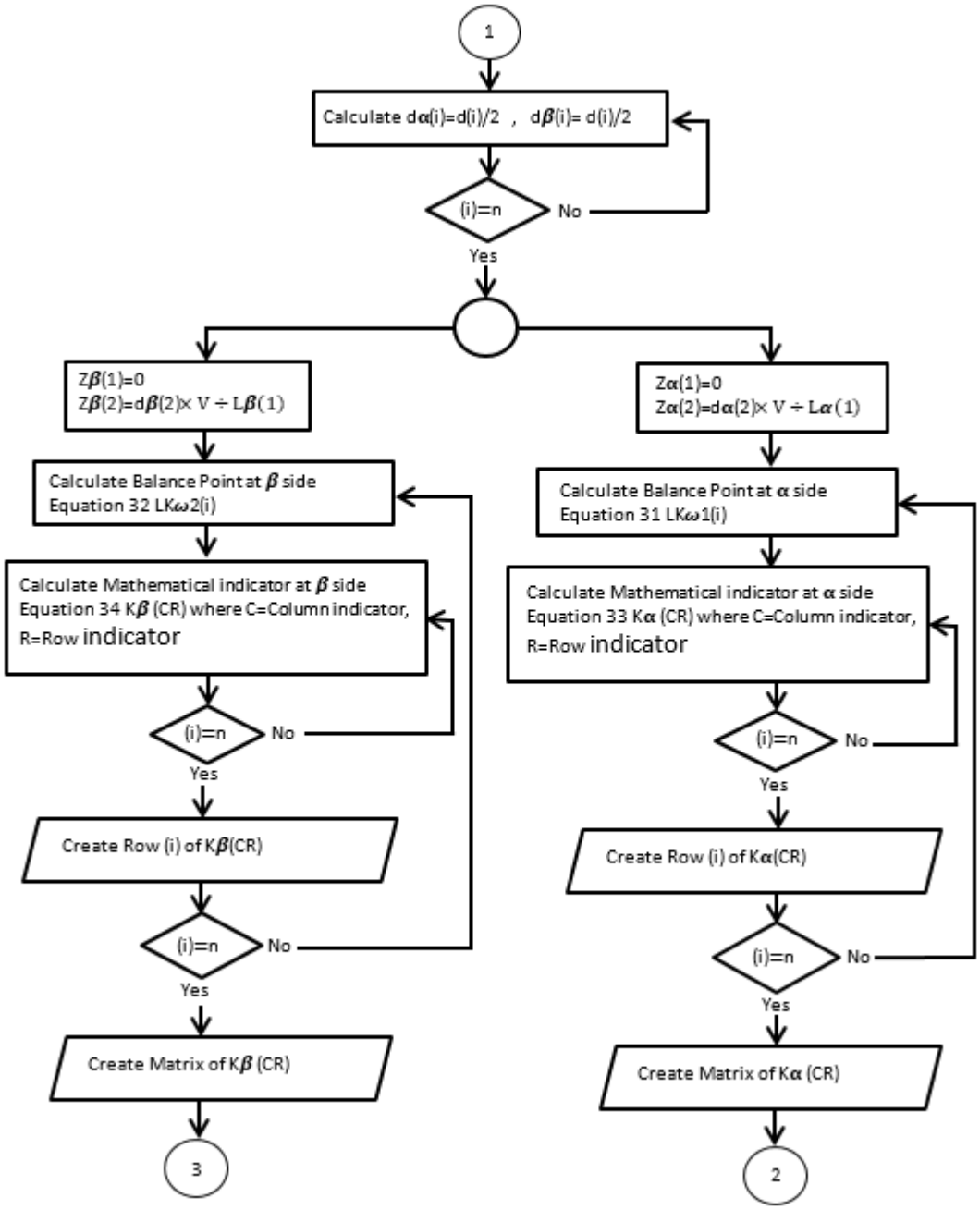

Figure 3-12: Summarisation of the calculation process of application rates at each segment area from two separate quarters

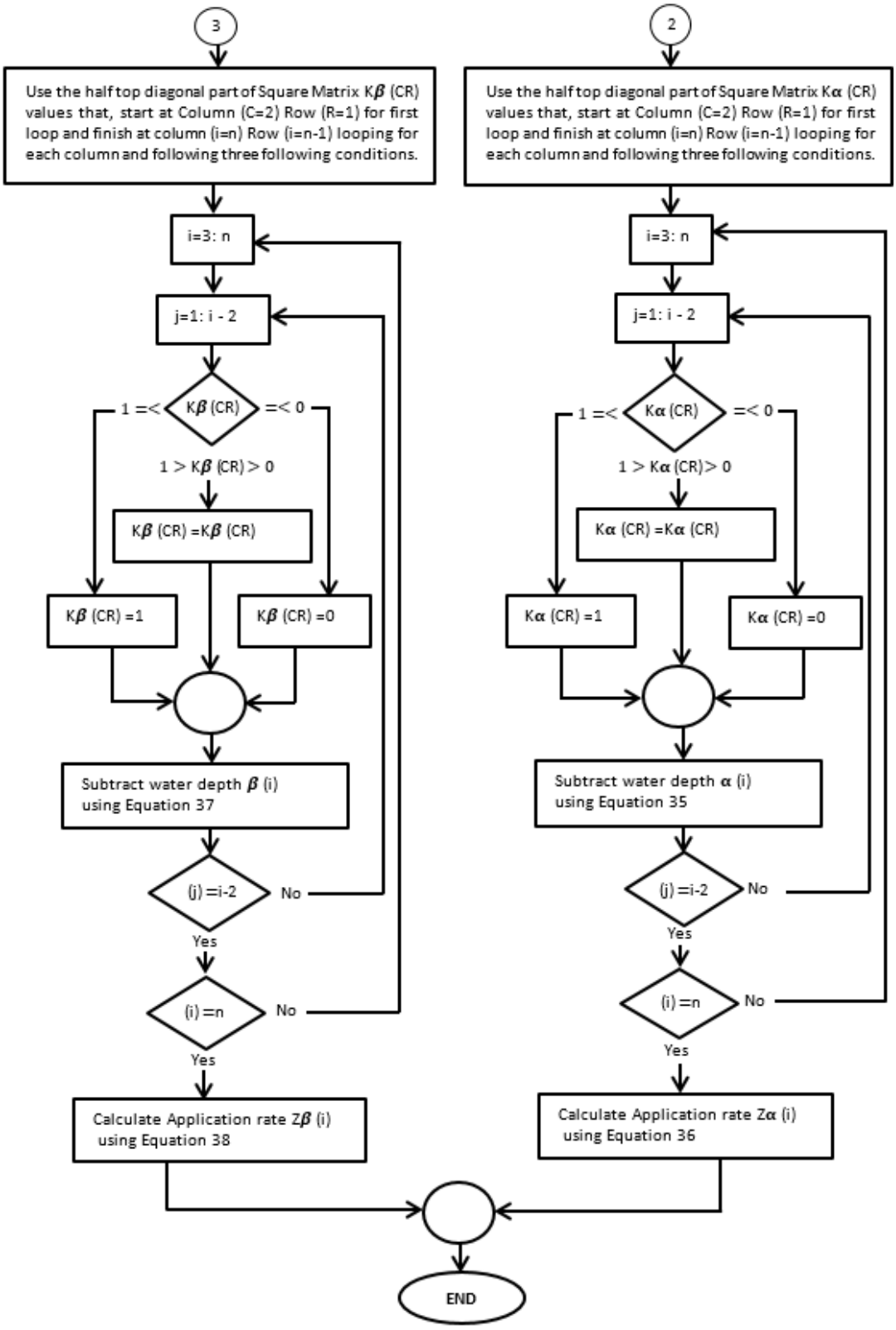

Figure 3-13: Summarisation of the calculation process of application rates at each segment area from two separate quarters

The original Equation 2-14 (Smith et al., 2008), that was used to subtract the water depth in collector one from the water depth in collector two, then subsequently three, four, five and so on is replaced in the new sub-model using Equations 3-35, 3-36, 3-37 and 3-38:

The Equation 3-35 calculates the net water depth in the collector after subtracting the value of water depth from the previous collectors from α side.

$$d \cdot net_{\alpha(i)} = \left(d_{\alpha(i)} - \frac{\left(\sqrt{r_j^{\,2} - r_i^{\,2}} - \sqrt{r_{j+1}^{2} - r_i^{\,2}} \right) \overline{z}_{\alpha(j+1)} \times K_{\alpha(i-1,\,j)}}{V} \right) \qquad 3\text{-}35$$

where $d \cdot net_{\alpha(i)}$ is the net water depth at half the segment area or fragment area on the α side.

(i) is the annular indicator number starting from the third value and at the same time is refer to first loop and refer to column number.

(j) is the row indicator number starting from the first value on the second loop.

The value of $d \cdot net_{\alpha(i)}$ from Equation 3-35 is then used to calculate the corresponding application rate $\overline{z}_{\alpha(i)}$:

$$\overline{z}_{\alpha(i)} = \left(d \cdot net_{\alpha(i)} \right) \times \frac{V}{L_{\alpha(i-1)}} \qquad 3\text{-}36$$

where $\overline{z}_{\alpha(i)}$ is the application rate at segment or fragment area 2 on the α side.

$L_{\alpha(i-1)}$ is the length of segment or fragment area 2 on the α side.

The Equation 3-37 calculates the net water depth in the collector after subtracting the value of water depth from the previous collectors from β side.

$$d \cdot net_{\beta(i)} = \left(d_{\beta(i)} - \frac{\left(\sqrt{r_j{}^2 - r_i^2} - \sqrt{r_{j+1}^2 - r_i^2} \right) \overline{z}_{\beta(j+1)} \times K_{\beta(i-1,j)}}{V} \right) \qquad 3\text{-}37$$

where $d \cdot net_{\beta(i)}$ is the net water depth at half the segment area or fragment area on the β side.

(i) is the annular indicator number starting from the third value of the first loop and refers to Column number.

(j) is the row indicator number starting from the first value on the second loop.

The value of $d \cdot net_{\beta(i)}$ from Equation 3-37 is then used to calculate the corresponding application rate $\overline{z}_{\beta(i)}$:

$$\overline{z}_{\beta(i)} = \left(d \cdot net_{\beta(i)} \right) \times \frac{V}{L_{\beta(i-1)}} \qquad 3\text{-}38$$

where $\overline{z}_{\beta(i)}$ is the application rate at segment or fragment area 2 on the β side.

$L_{\beta(i-1)}$ is the length of segment or fragment area 2 on the β side.

$d_{\alpha(i)}, d_{\beta(i)}$ are estimated by dividing $\frac{d_{(i)}}{2}$ because the side sector angle is symmetrical.

The application rate for all these half segment areas on each side of the quarter will be equal and will represent the radial leg depth data for the sprinkler.

3.4.2 Calculating the application rate for a sector angle of less than 180° with the side sector asymmetrical to the direction of travel

A side sector angle asymmetrical to the direction of travel leads to differences in water depth d_i between the α side (Quarter One) and the β side (Quarter Two) as shown in Figure 3-14, especially near the sprinkler. When the side sector (the centre of dry area ϕ) is greater than 270°, the water depth d_i will decrease from the α side (Quarter One) and increase on the β side (Quarter Two) and vice versa. The proportion of increasing and decreasing amounts of water depth from side to side can be determined in different areas as shown in Figure 3-14. The first area on the outer side of the sprinkler pattern (in blue) will receive its water depth from the full sprinkler pattern and the water depth will be equal on both sides. The second area (in pink) will receive part of the full sprinkler pattern on the α side and the full sprinkler pattern on the β side. Finally, the brown area nearest to the sprinkler will receive part of sprinkler pattern on both α and β sides.

Calculating the application rates on both α and β sides separately will not be applicable because there are three different proportion areas as shown in Figure 3-14. The best method of calculating the application rate is to develop an algorithm using a similar approach as for the symmetrical case (find the balance points and the two matrixes of mathematical indicators) on both sides α and β. The water depth will not be divided into both sides. The program will calculate the application rate at the first annular area which is equal to zero and then calculate the application rate at segment area one using Equation 2-13 as shown in Figure 3-15 and Figure 3-16. The algorithm will then start to subtract the water depth at the second segment area from

the α and the β sides using Equations 3-35 and 3-37 respectively. Finally, we can calculate the application rates at two halves of the segment area or fragment of segment area using Equation 3-39. The flowchart in Figure 3-15 and Figure 3-16 shows the calculation process in flowchart form.

The value of $d \cdot net_{\alpha\beta(i)}$ from Equations 3-35 and 3-37 is then used to calculate the corresponding application rate $\bar{z}_{(i)}$:

$$\bar{z}_{(i)} = \left(d \cdot net_{\alpha\beta(i)}\right) \times \frac{V}{L_{\alpha\beta(i-1)}} \qquad 3\text{-}39$$

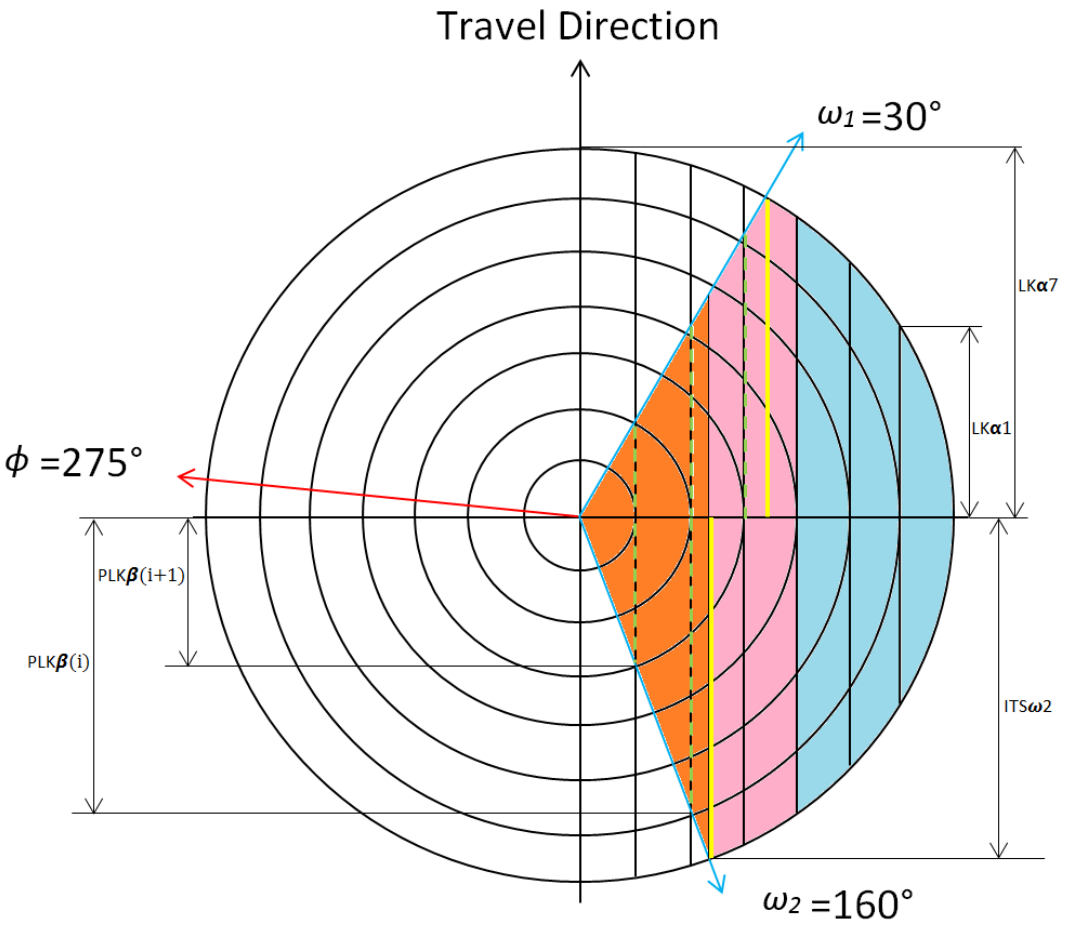

Figure 3-14: A scheme showing three different areas: blue area is equal on both sides, pink area received part pattern from the α side and full pattern from the β side, orange area received part pattern on both the α and β sides.

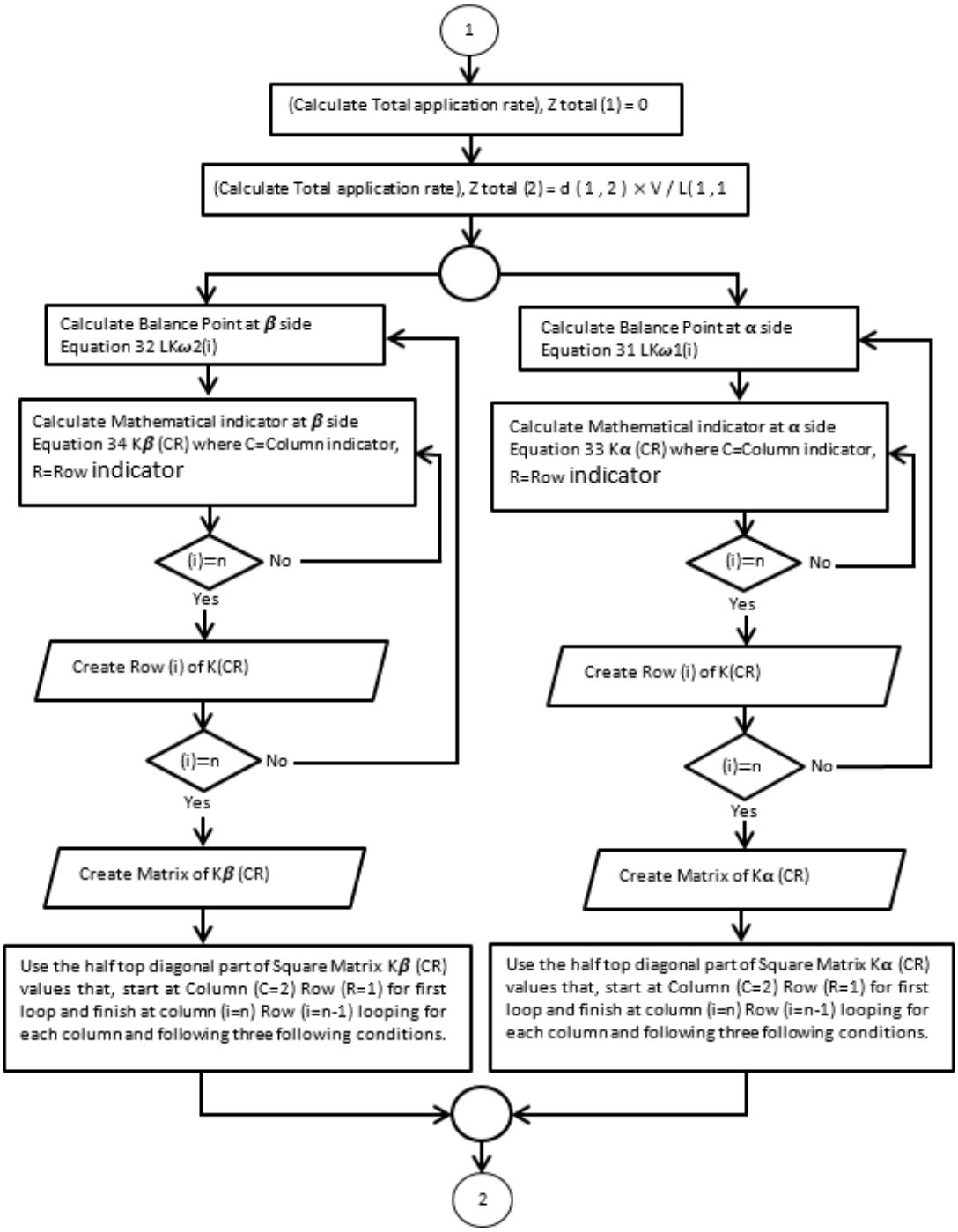

Figure 3-15: Summarisation of the calculation process of application rates at each segment area from two separate quarters.

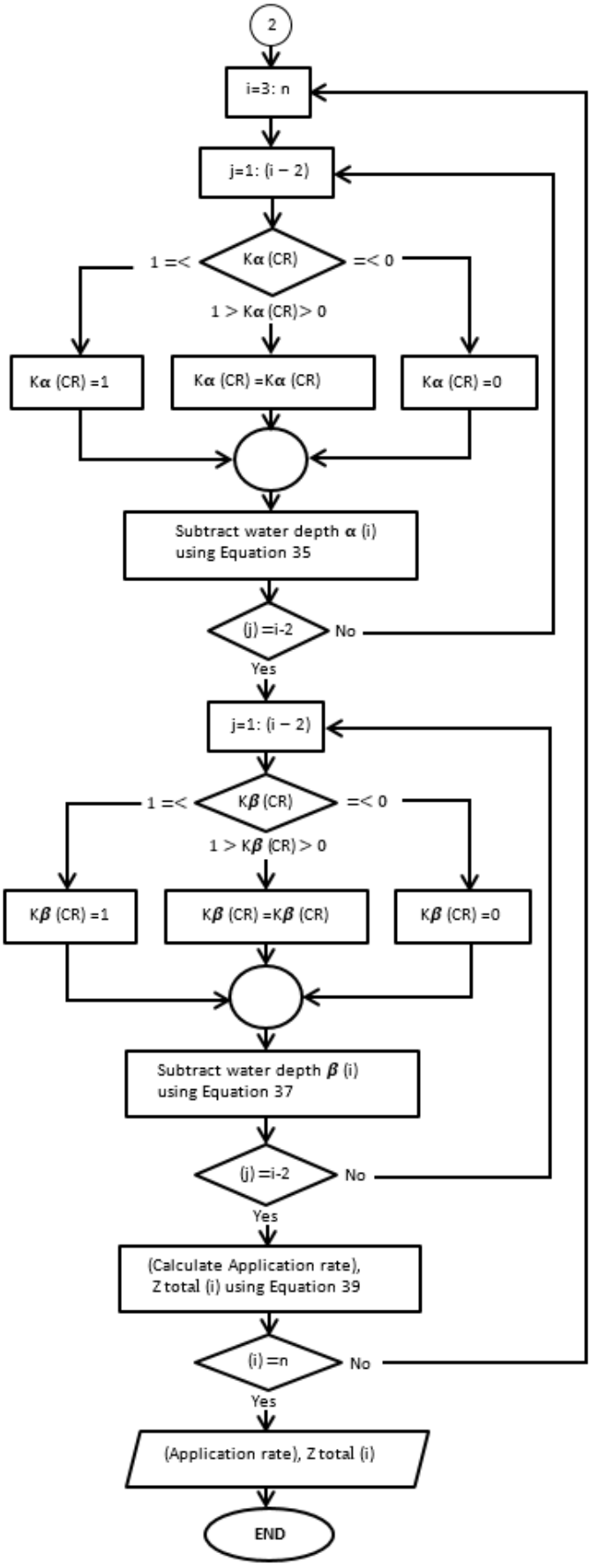

Figure 3-16: Summarisation of the calculation process of application rates at each segment area from two separate quarters.

3.5 Boundaries of sector angles calculation in the model

The current calculation process is only conducted using ω_1 & ω_2 values which are greater than 0° and less than 180°. However, the value of ω_1 could also be less than 0° and the value of ω_2 could be or more than 180°. In other words, ω_1 and ω_2 could either be specifically in the first, second, third and fourth quarter; or both be in one specific quarter as shown in the Figure 3-2, Figure 3-6 and Figure 3-8. However, the current calculation process will be based on the assumption that the value of ω_1 is equal to or greater than 0° and the value of ω_2 is equal to or greater than 180°, even if the value of the wetted sector is greater than 180°. In other words, there is a special case when the value of ω_1 is less than 0° and the value of ω_2 is greater than 180°, as shown in Figure 3-17.

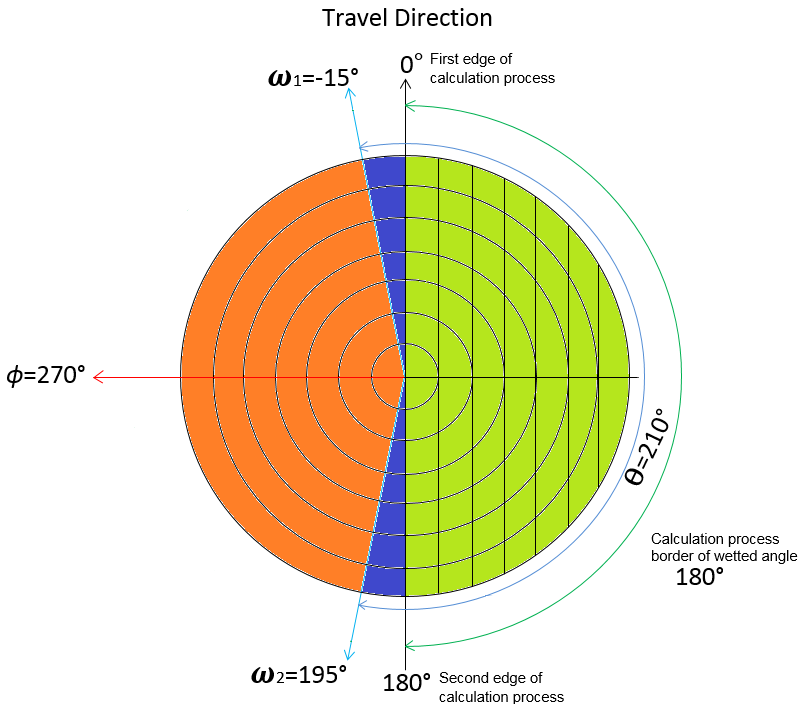

Figure 3-17: Three different areas: orange represents dry angle; the blue area from ω_1 to ω_2 represents wetted sector angle; and green (between 0° to 180°) represents the area where the calculation process takes place.

Figure 3-17, is used to demonstrate the position of the calculation process for this case. The value of the wetted sector angle θ is 210°, the value of the side sector angle, ϕ , is 270°, the value of the leading edge ω_1 is -15°, and the value of the trailing edge ω_2 is 195°. In this combination of sector and side sector angles, the current calculation process considers the value of ω_1 to be 0° as the first edge of the calculation process and the value of ω_2 to be 180° as the second edge of the calculation process.

Figure 3-18 shows another different combination of sector and side sector angles. The value of the wetted sector angle θ is 120°, the value of the side sector angle, ϕ , is 260° which is not symmetrical to the direction of travel, the value of the leading edge ω_1 is 20°, and the value of the trailing edge ω_2 is 140°. In this combination of sector and side sector angles, the current calculation process considers the value of ω_1 to be the same (20°) and the value of ω_2 to be the same (140°).

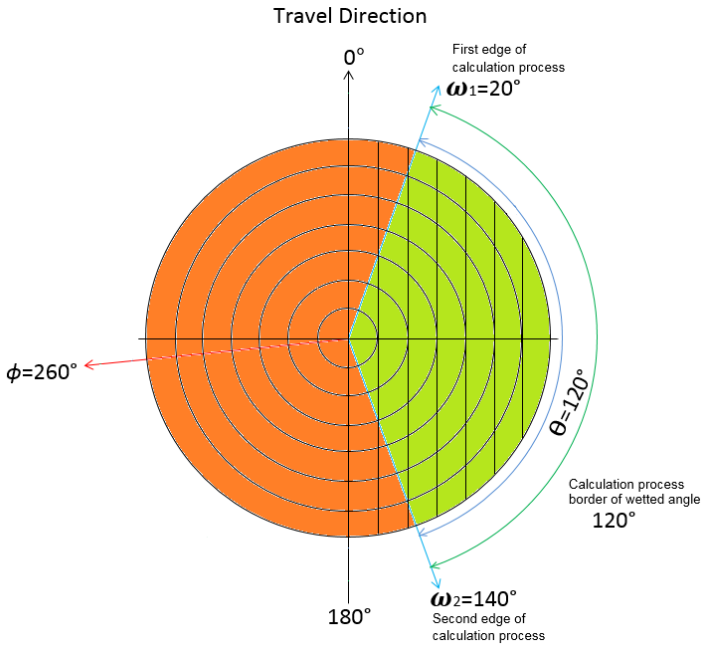

Figure 3-18: Two different areas: the orange area represents dry angle; and the green area between ω_1 and ω_2 represents wetted sector angle corresponding with the first edge of calculation process and the second edge of the calculation process (20° to 140°) respectively.

In this combination of sector and side sector angles (as shown in Figure 3-18), the calculation process will take place between the values of ω_1 and ω_2. In other words, the value of the first edge of the calculation process will correspond with the value of the leading edge ω_1 and the value of the second edge will correspond with the value of the trailing edge ω_2.

Another combination of sector and side sector angles is shown in Figure 3-19. The value of the sector angle, ϕ, is 330°, the value of the wetted sector angle θ is 200°, the value of the leading edge ω_1 is 50° and the value of the trailing edge ω_2 is 250°. In this case, the current calculation process considers the value of ω_1 to be the first edge of the calculation process (50°) and the value of ω_2 to be the second edge of the calculation process (180°).

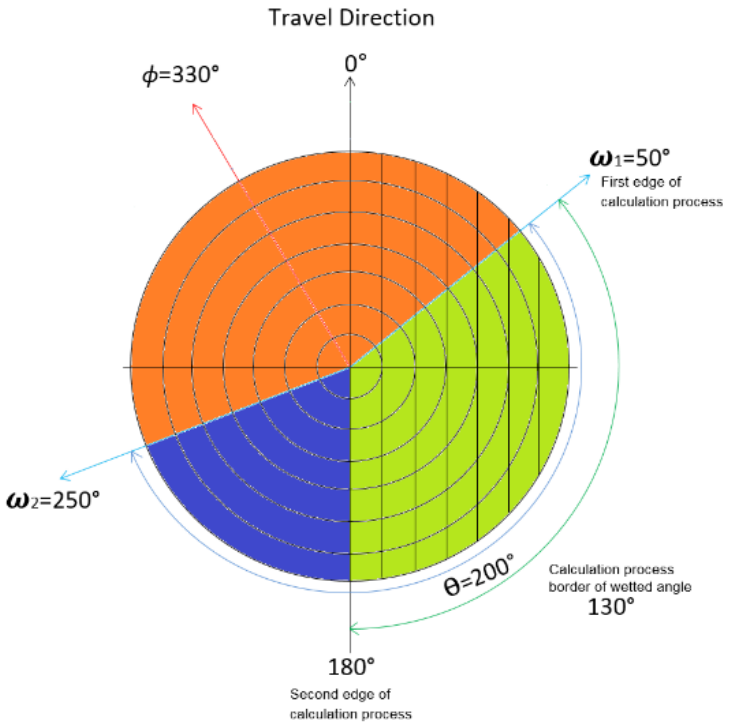

Figure 3-19: Three different areas: orange represents the dry angle; blue area from ω_1 to ω_2 represents wetted sector angle; and green area between ω_1 to 180° represents the area where the calculation process takes place.

Finally, the following combination of sector and side sector angles is shown in Figure 3-20. The value of the side sector angle, ϕ, is 210°, the value of the wetted sector angle θ is 200°, the value of the leading edge ω_1 is -70° and the value of the trailing edge ω_2 is 130°. In this case, the calculation process considers the value of ω_1 to be equal to 0° as the first edge of the calculation process and the value of ω_2 to be 130° as the second edge of the calculation process.

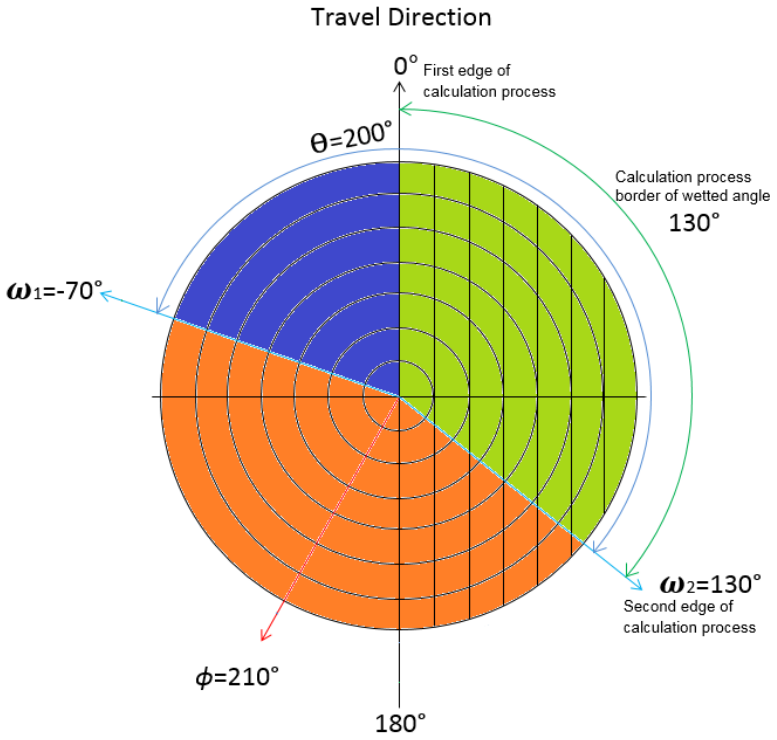

Figure 3-20: Three different areas: orange represents the dry angle; blue area from ω_1 to ω_2 represents wetted sector angle; and green area between 0° to ω_2 represents the area where the calculation process takes place.

However, the ratio of the sector angles to 360° will be considered to apply in all combinations of sector and side sector angles during the calculation process, in order to adjust the water depth when calculating the application rate (radial leg) from transect or transect from radial leg.

3.6 Summary

This chapter presented the process of developing a new mathematical model to be coded into TravGUN as a new sub-model. Firstly, presented the process of calculating the length of the segment area that can be used to estimate the time for the machine to pass this area to calculate the application rate for any combination of wetted sector and side sector angles. Secondly, presented the process of the development of the new sub-model to calculate the application rate for wetted sector angle less than 180° perpendicular and asymmetrical to the direction of travel using novel approach to achieve this aim. Finally, this chapter presented the border of the calculation process and how adjusting the value of the application rate according to the proportion of wetted sector and side sector angle to the full circle pattern. The field tests and the validation for this development will be presented in the following Chapters five and six. This new sub-model provides a useful tool for generating radial leg data and the sprinkler pattern for end-gun on centre pivot and then simulate end-gun pattern for different wind speed and directions in the following stages.

4 CHAPTER FOUR

Material and Methods

4.1. Introduction

The purpose of this chapter is to describe the equipment and methodology used to address the objectives of the study. Firstly, it will describe the characteristic of the testing site and the irrigation equipment, and describe how the system variables were controlled or measured. These included machine speed and consistency, pump pressure, wetted sector and side sector angles, water depth, wind speed, and wind direction. Secondly, it will propose a new method for researchers and farmers to measure radial leg data by using stationary full circle and measured transects of different combination of wetted sector and side sector angles under selected wind conditions. Thirdly, the chapter illustrates the adjustment of the machine movement in a curved path. Finally, this chapter also describes the methodologies used to validate the new TravGUN sub-model, to calibrate and simulate end-gun performance, and to adjust the water depth according to different curved radii.

4.2. Characteristics of Testing Site

The experiment site is located at the University of Southern Queensland in Toowoomba as shown in Figure 4-1. The Toowoomba CBD is located at south eastern corner of Queensland in Australia. The altitude is 691 metres above sea level, at a latitude of 27.58°S and longitude of 151.93°E (Bureau of Meteorology, 2016). The distance between the city of Toowoomba and the Pacific coast is between 106 to 110

km (Time and date, 2016). As a result of this position, the weather of Toowoomba city is windy all year, except for the winter season. The average annual wind speed for Toowoomba city is 21.7 km/h and 21.8 km/h between 9 am and 3 pm (Current Result, 2018). However, there are several nights with quiescent wind conditions when the wind speed slows down to zero for one or more hours. Obtaining quiescent wind conditions requires a lot of experience in weather, reviewing historic weather data and monitoring local weather conditions. A new methodology will presented in this chapter to demonstrate how one can obtain zero wind conditions so as to complete the measurements of radial leg and transect data.

As discussed in section 7.4, the prevailing wind direction in Toowoomba is from the East. The direction of this prevailing wind in relation to the experimental site is shown in Figure **4-1**.

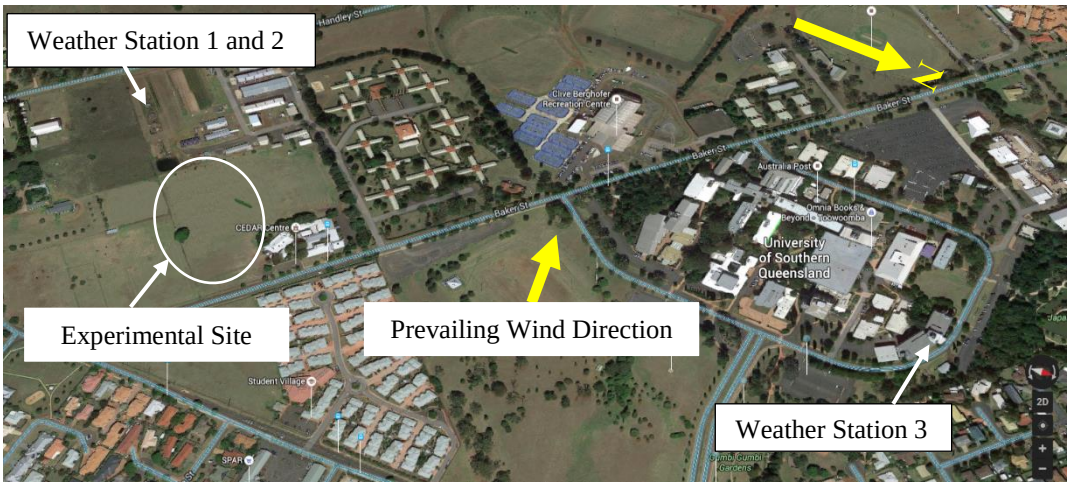

Figure 4-1: Map of experiment site shows the buildings and institutions surrounding the experiment site (Google Maps, 2016).

Figure 4-2 provides an aerial view of the experiment site showing the direction of travel for the moving gun tests. Although this image indicates there are structures and trees surrounding the site which may influence the incoming wind most of these obstacles are relatively low in elevation.

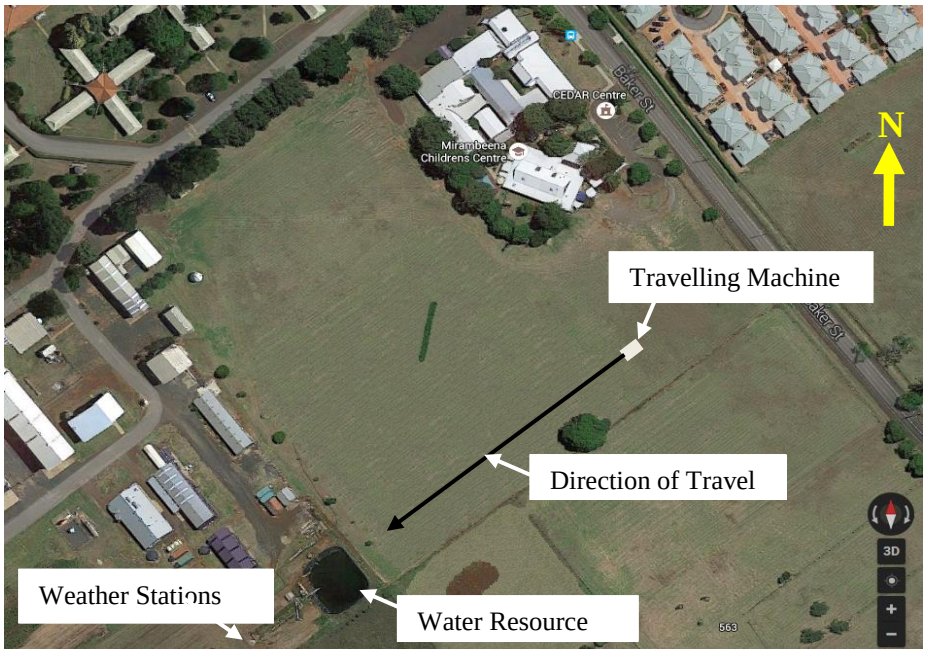

Figure 4-2: Experiment site and location of equipment and all facilities relating to measurement (Google Maps, 2015)

4.3. Machine and Equipment Used and Setup

A travelling gun irrigator was used to perform all tests and collect data to validate the new TravGUN sub-model including both the stationary tests (radial leg data) and moving tests (transect data). Conducting measurements on a centre pivot end gun is difficult, costly, unsafe, and has the complexity of dealing with the overlap from the regular pivot sprinkler patterns of the nozzles on the outer pivot span. Travelling gun sprinkler operation is essentially, identical to end-gun sprinkler operation, with the main difference being the way in which the wetted sector is configured. In addition, the circular movement of centre pivots complicates the collection of irrigation depth data, especially in large open fields. A Trailco Traveller T 200-2 was selected for the trials as shown in Figure 4-3.

The machine was equipped with a Nelson SR100 Big-Gun sprinkler with a 25.4 mm taper/ring nozzle and trajectory angle of 18° (Nelson Irrigation, 2015) as shown in Figure 4-4. The machine was supplied with a high pressure water pump to provide the

sprinkler with sufficient water flowrate and pressure to match the operating conditions suggested by Nelson Irrigation Corporation (2016). This machine was used to perform moving tests on straight and curved paths, and to study the effect of the curved movements of end-guns on centre pivots.

Figure 4-3: Travelling-gun irrigator machine (Trailco T200-2, 2018).

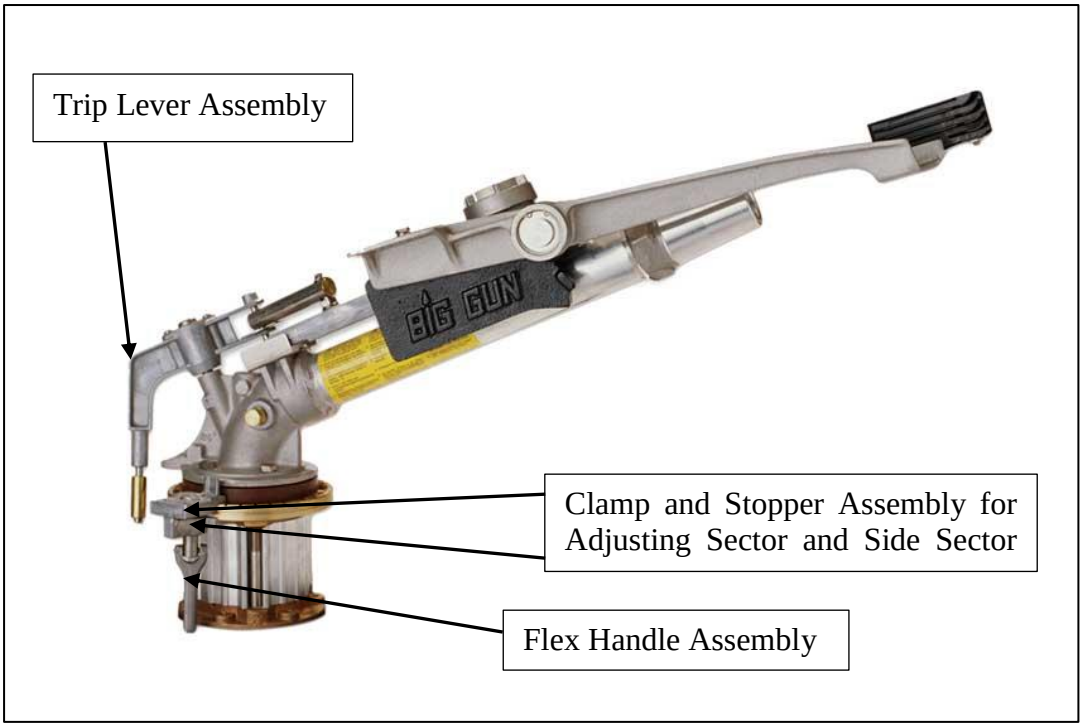

Figure 4-4: Big-gun water sprinkler (Nelson Irrigation, 2015).

4.3.1 Adjusting the pump pressure

A high pressure water pump was installed at the water resource to supply the traveling gun irrigator with appropriate water flow-rate and pressure. The water pressure was monitored and adjusted during all tests. A large diameter, high quality pressure gage was fitted close to the big-gun at the main pipe holding the sprinkler as shown in Figure 4-5. A flowrate control valve was fixed to the main pipe line to control flow-rate. The pressure was fixed at 490 kPa in all stationary testing (radial leg test) and in all travelling tests (transect measurement) as recommended by the manufacture (Nelson Irrigation, 2015). A higher flow and pressure are required at the pump to maintain the constant pressure during the travelling tests as a result of the additional flow-rate is required for the two small nozzles that control machine speed. The sprinkler pattern of the two small nozzles was redirected to the ground in order to

prevent water from falling into the first three collectors near the sprinkler, as shown in Figure 4-5.

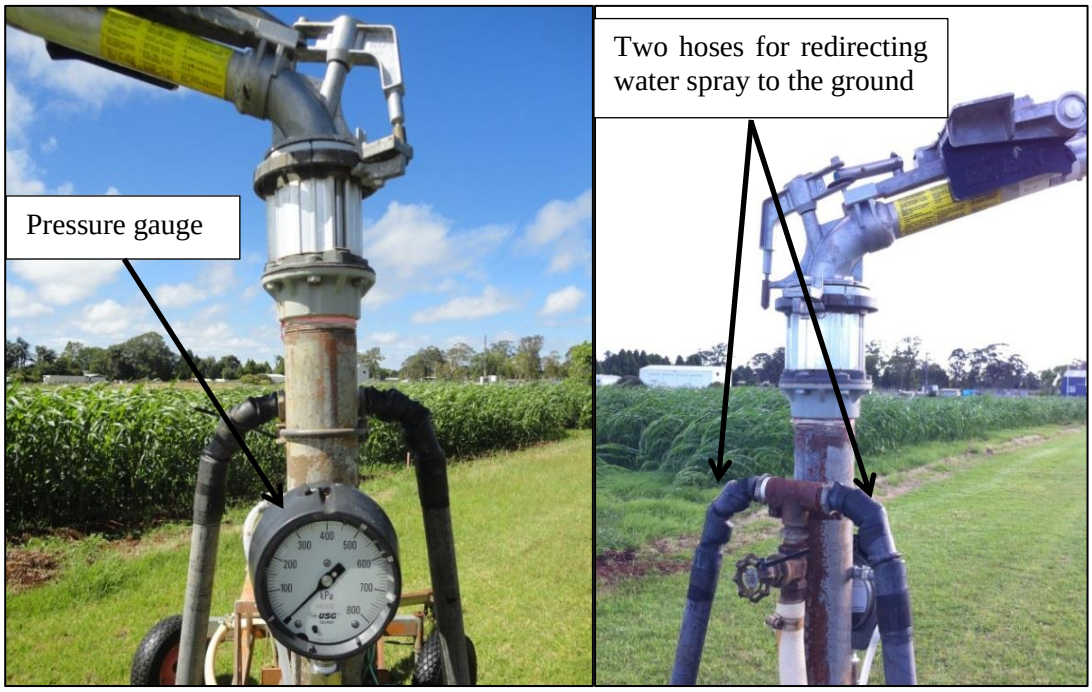

Figure 4-5 : Pressure gauge fixed close to the big gun, and two hoses fixed to redirect the water from the two small speed control nozzles.

4.3.2 Adjusting sector and side sector angles

A 360° protractor was used to inscribe a circle on a white plastic sheet. The dimensions of the sheet were 900 millimetres by 600 millimetres. The centre of the 360° circle on the plastic sheet was put under the centre of the rising pipe that holds the large sprinkler. The nominated sector and side sector angles were determined for each test, before adjusting any angles. A plumb bob was hung from the centre of the nozzle to the corresponding nominated sector angles for each combination as shown in Figure 4-6. The Nelson SR 100 end-gun sprinkler have a trip lever assembly, and two clamps, and a stopper assembly, with either a flex-handle, or a normal screw, as shown in Figure 4-4 (Nelson Irrigation, 2015). These components together have allow control and adjustment of the sector and side sector angles. The nominated sector and side

sector angles (the centre of the dry sector angle ϕ , the wetted sector angle, θ at the leading edge ω_1 and the trailing edge ω_2) are those angles defined and detailed in previous chapters, and were fixed before each measurement by fixing the two clamps, the stopper and the screw assemblies at the located positions as shown in Figure 4-6. These sector and side sector angles were chosen to match with the requirement of the new sub-model development in Chapter Three, and to simulate the performance of an end-gun on a centre pivot.

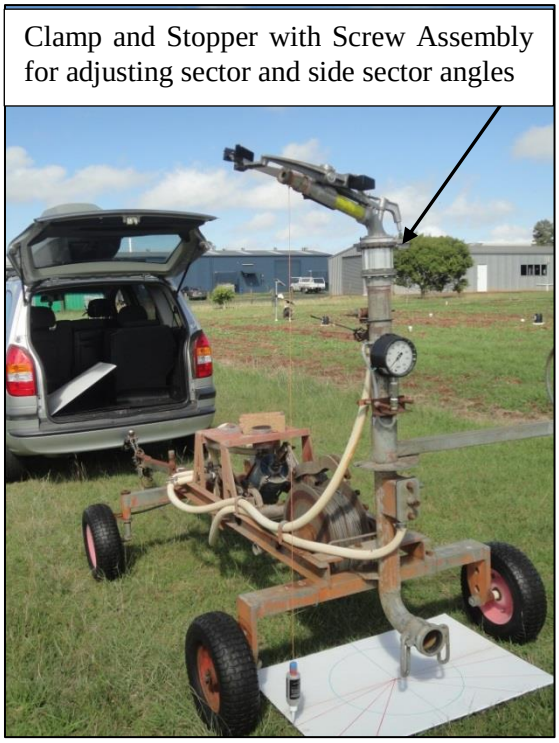

Figure 4-6: Large protractor drawn on plastic sheet to adjust sector and side sector angles.

4.3.3 Adjusting machine speed and consistency

The machine speed was set at the maximum speed to reduce the measurement period and in order to complete the zero wind speed test while minimising the risk of the wind speed changing, or of gusts occur during the test. The maximum travelling speed was 50 m/h for all tests. The speed consistency was monitored during the tests from the

start point, until the end point by installing wooden stakes at 10 metre intervals and recording the time when the axle of the machine's rear tires passed each stake. A fifty metre measurement tape and digital stopwatch were used to set out the stakes and to record the times at each interval. Machine speed was calculated and recorded at each 10 metre interval. Sometimes machine speed varies during the start and end sections of any travel (Newell et al., 2002). These differences can be as a result of the differences in length and weight of the hose required to be towed by the machine at the start and end point of the travel, or as a result of changing cable drum diameters when winding the steel cable in at the beginning and end of the run. Travelling gun irrigators normally have a run length just exceeding 200 metres. The maximum distance in this study was 100 metres. The travel speed did not vary between the beginning and end points due to the short distance of each run and the small pulling load required for this hose.

4.3.4 Measured data and modification

The measured data for both radial leg and transect test (stationary and movable tests) were initially recorded as water volume in millilitres from each collector. Then the data was converted to depths in millimetre by dividing the measured volume by the cross-sectional area of the upper opening of the collectors. The shape of the collectors was a conical cylinder cup. The edge diameter at the top was 110 mm and 95 mm at the bottom with 150 mm height.

4.3.5 Measuring wind speed and direction during tests

Wind speed and direction were monitored and recorded during all tests at one minute interval by the device and then the average for fifteen minute interval were calculated

in order to present the field measurements and data analysis in the following chapter. In addition, the average wind speed and direction during each test were calculated after it was finished. Three sets of weather data were logged at different weather stations (anemometers) at the University of Southern Queensland site as shown in Figure 4-7, which were used to find the average wind speed and direction during the tests. The data from the National Centre of Engineering in Agriculture weather station was chosen, because it is located at the experimental location and provides precise data after review the data from all site.

Figure 4-7: Three weather stations were used to measure wind speed and direction at the experimental site, and two close to the field site are shown here.

4.4. Selecting appropriate local climate condition for open field measurements

The process of predicting and monitoring appropriate local climatic conditions for measurement in the open field requires, three main phases of activity. The first phase is the prediction of a suitable day, when the lowest predicted wind speed could occur during several of the upcoming days from weather forecasts, as shown in Figure 4-8. The second phase is the remote monitoring and recording of the current wind speed and direction, using weather websites, and online (live) during that specific day in which the lowest wind speed will occur, as shown in Figure 4-11. The third phase is to measure and record wind speed, direction and other data at the open field during the test measurements.

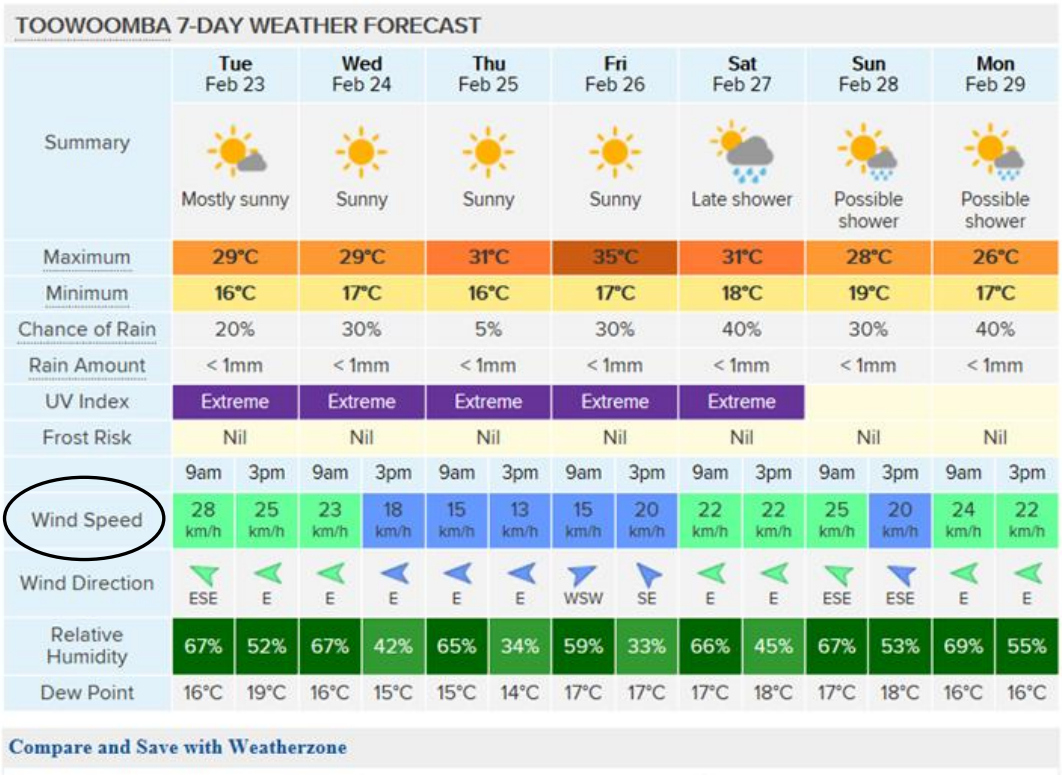

TOOWOOMBA 7-DAY WEATHER FORECAST

	Tue Feb 23		Wed Feb 24		Thu Feb 25		Fri Feb 26		Sat Feb 27		Sun Feb 28		Mon Feb 29	
Summary	Mostly sunny		Sunny		Sunny		Sunny		Late shower		Possible shower		Possible shower	
Maximum	29°C		29°C		31°C		35°C		31°C		28°C		26°C	
Minimum	16°C		17°C		16°C		17°C		18°C		19°C		17°C	
Chance of Rain	20%		30%		5%		30%		40%		30%		40%	
Rain Amount	< 1mm		< 1mm		< 1mm		< 1mm		< 1mm		< 1mm		< 1mm	
UV Index	Extreme		Extreme		Extreme		Extreme		Extreme					
Frost Risk	Nil		Nil		Nil		Nil		Nil		Nil		Nil	
	9am	3pm	9am	3pm	9am	3pm	9am	3pm	9am	3pm	9am	3pm	9am	3pm
Wind Speed	28 km/h	25 km/h	23 km/h	18 km/h	15 km/h	13 km/h	15 km/h	20 km/h	22 km/h	22 km/h	25 km/h	20 km/h	24 km/h	22 km/h
Wind Direction	ESE	E	E	E	E	E	WSW	SE	E	E	ESE	ESE	E	E
Relative Humidity	67%	52%	67%	42%	65%	34%	59%	33%	66%	45%	67%	53%	69%	55%
Dew Point	16°C	19°C	16°C	15°C	15°C	14°C	17°C	17°C	17°C	18°C	17°C	18°C	16°C	16°C

Compare and Save with Weatherzone

Figure 4-8: Photo of Weather Zone forecasts toolbars show minimum wind speed and wind direction change at same time (Weatherzone, 2015b).

There are many sites on the internet that are specialists in predicting local weather conditions for several days in advance. Usually, wind speeds change as a result of the differences in atmospheric pressure. Therefore, monitoring the mean sea level pressure (MSLP) map is the best method to determine the appropriate wind conditions, in which to perform the measurements in zero wind. The Bureau of Meteorology (BOM), Australia's official weather forecaster (www.bom.gov.au) provides reliable online information of MSLP maps in the form shown in Figure 4-9. The general rule is that the winds are the strongest where the isobars are closest together, while winds are normally lightest near high pressure systems where the isobars are widely spaced. Wind directions depend on the location of the high pressure system. In the southern hemisphere, the earth's rotation causes air to flow clockwise around low pressure systems and anticlockwise around high pressure systems (Bureau of Meteorology, 2015b).

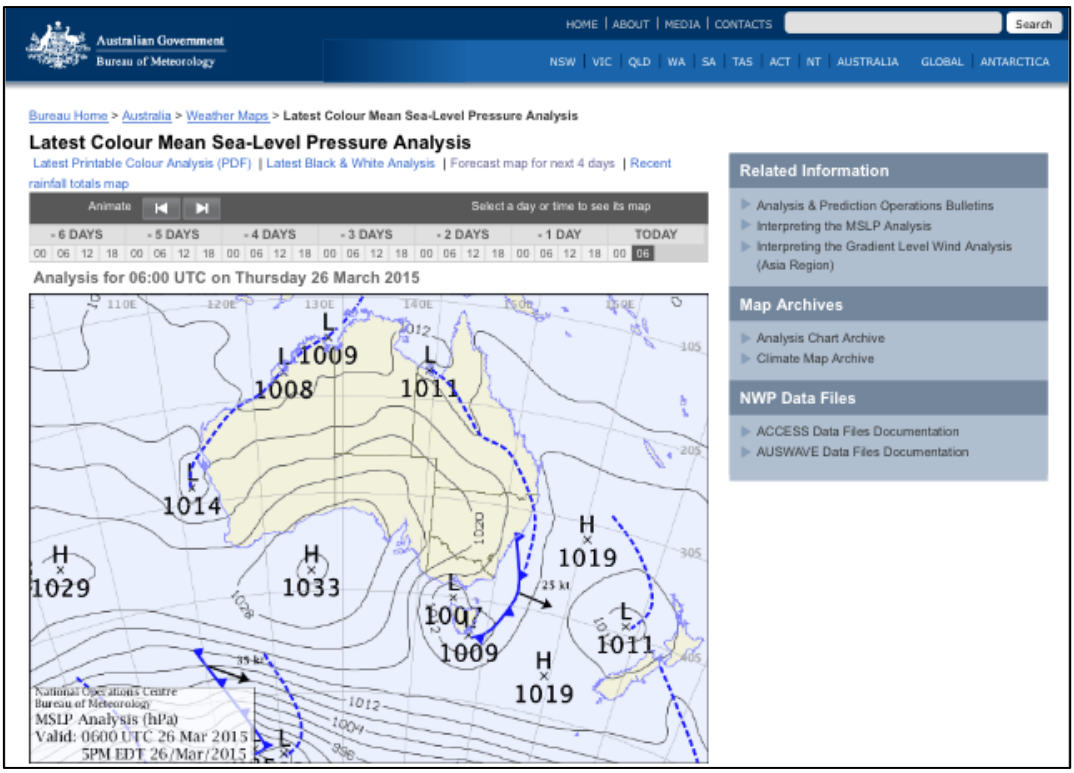

Figure 4-9: Shot-screen (snapshot) from smartphone for Mean Sea Level Pressure map (Bureau of Meteorology, 2015a).

Local wind conditions were observed for eight months from both weather forecast sites, and from open field measurements at the agriculture plot at the University of Southern Queensland from January 2015 until August 2015. The best time for performing the measurement can be predicted by analysing synoptic maps online and through the following steps. The first step is to determine the region of the experiment site on the map as it shown in Figure 4-10. The letter T refers to the location of experiment site. When this region comes under the influences of neutral atmospheric pressures, i.e. where it is surrounded by three or more different atmospheric pressures and the region is not part of, or affected by any, of these specific atmospheric pressures, the conditions will be more favourable.

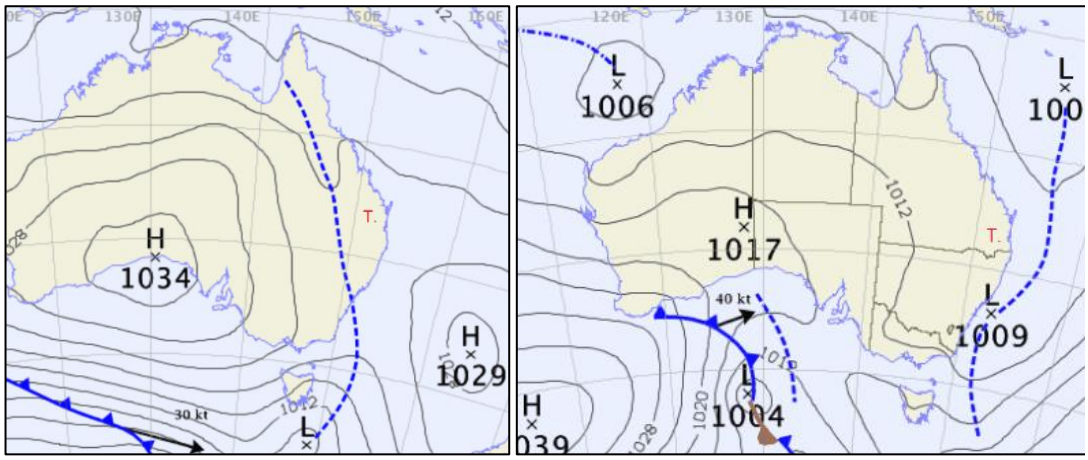

Figure 4-10 : Two different atmosphere pressure maps, letter (T) refer to experimental region influence under neutral pressure, letter (H) centre of high pressure zone and letter (L) centre of low pressure zone (Bureau of Meteorology, 2015a).

The second step is the remote monitoring of current wind speed online through one of the available web sites. Weather Zone is one of these sites (www.weatherzone.com.au) which can be easily accessed by computer or smartphone and updates current wind speed on a 10 minute frequency. The Weather Zone website also provides forecasts for the next seven days. Different toolbars of weather indicators are displayed on this website, as shown in Figure 4-8.

Wind speed and direction are the most important indicators for this project. This website provides predictions of wind conditions at 9am and 3pm each day. This figure shows that during these times between Thursday and Friday for example, the minimum wind speed will occur from Thursday afternoon until Friday morning. Wind directions show there is a change in wind directions during the same period from East to West South West. When both of these weather forecasts sites indicate that the region near the experiment field is subject to favourable conditions during the same time period, the opportunity for zero wind will have a high probability of occurring on that specific night. The process of obtaining a period for zero wind can be summarized using the following procedure. The behaviour of wind speed can be predicted or understood by monitoring this site and recording current wind speeds between different times. This wind information gives an indicator of the wind behaviour slowing down or speeding up. The wind speed starts to slow down after sunset and gradually decreases until it becomes zero, as shown in Figure 4-11.

The period of zero wind could occur at any time during the 24 hours in a day. However, the longest period occurs at night when the atmospheric pressure is high. This will be discussed in more detail in the following chapter (field measurements).

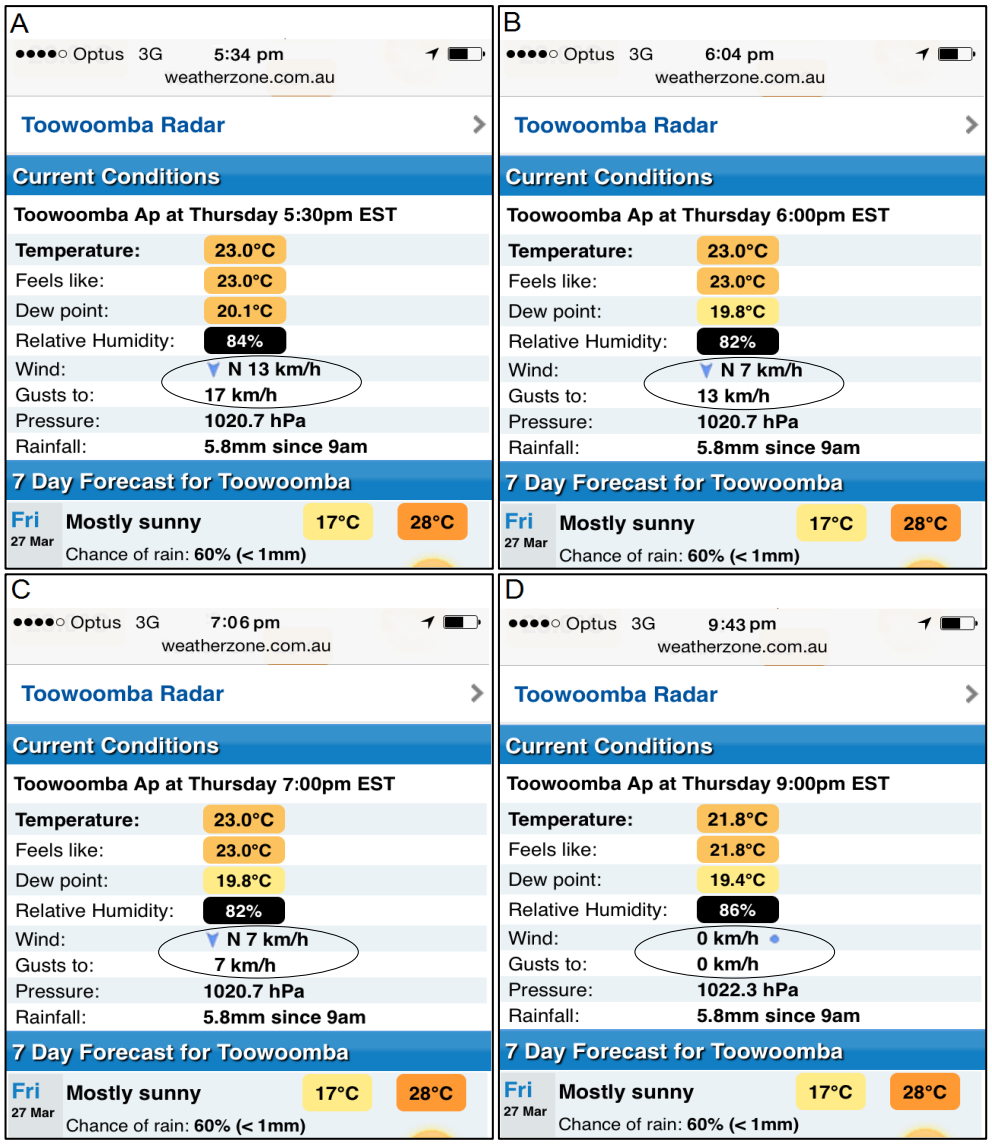

Figure 4-11 : Snapshot (shot-screen) from smartphone for online current weather condition at different times in the same day (Weatherzone, 2015a).

4.5. Measuring radial leg and transect data in the field

The radial leg data is the most important factor in the process of simulating wind effects on the irrigation pattern for all types of big-gun sprinkler. As defined in Chapter Two previously, the radial leg data represents the characteristic for a specific nozzle type, operating pressure, and nozzle size combination (Newell, 2003). Therefore, it is necessary to measure the radial leg data from a stationary test in zero wind conditions before doing any other measurements, or performing any other tests. There are

different methods to measure radial leg data under no wind condition. Firstly, researchers can measure radial leg data under laboratory conditions (Prado, 2008). Secondly, radial leg data can be measured under open field conditions (Liu et al., 2012).

The large size of centre pivot irrigation machines with end-guns makes the measurement of radial leg or transects data impossible in a laboratory. One of the three transects of data is required in quiescent wind, and the other two are measured in different wind speeds and directions, as Smith et al. (2008) recommended for calibration of the TravGUN model. Hence, there is a need to measure transect data from end guns on centre pivots under open field conditions. Therefore, having a good knowledge of the appropriate local weather conditions, such as wind speed and direction is very important.

4.6. Measuring radial leg data from stationary full circle

Radial leg data is measured from a stationary test. The machine was installed in a grassed area near the agriculture plot at the University of Southern Queensland. The movement lever valve was set in a neutral position in order to stop the machine at the centre of the intersection of the lines of collectors as shown in the photo of the field test Figure 4-12. Water pump pressure was adjusted to 490 kPa at the sprinkler for all tests. The sprinkler stoppers were adjusted to rotate through a full circle.

Two different test configurations were used to collect radial leg data from the stationary sprinkler. The first set of data was collected using three lines of collectors, as shown in Figure 4-13. Three lines of collectors were placed radially from the centre of the sprinkler on straight lines with 120° between each line, as shown in the simple

diagram in Figure 4-13. Line One was placed at 15° clockwise from the north direction. Line Two was placed at 135° from the north direction. Line Three was placed at 255° from the north direction. The second series of test data was collected from four lines of collectors as shown in Figure 4-14. Four lines of collectors were placed radially from the centre of the sprinkler at 90° intervals between each line, as shown in the simple diagram, Figure 4-14. Line One was placed at 15° clockwise from the north direction. Line Two was placed at 105° from the north direction. Line Three was placed at 195° from the north direction. Line Four was placed at 285° from the north direction. The distance between each collector in each line for both sets of test was 3 metres. The reason for using four lines of collectors was to increase the accuracy by using more replicates and to understand the effects of wind gusts (low breeze) on the irrigation pattern during the test, even when wind speed is very near to zero. A series of tests were performed with this experimental setup machine adjustment and collector positions. The most accurate data was selected and used in validation stages of this research.

Figure 4-12: A photo of the irrigation machine and the four lines of collectors, setup for stationary tests.

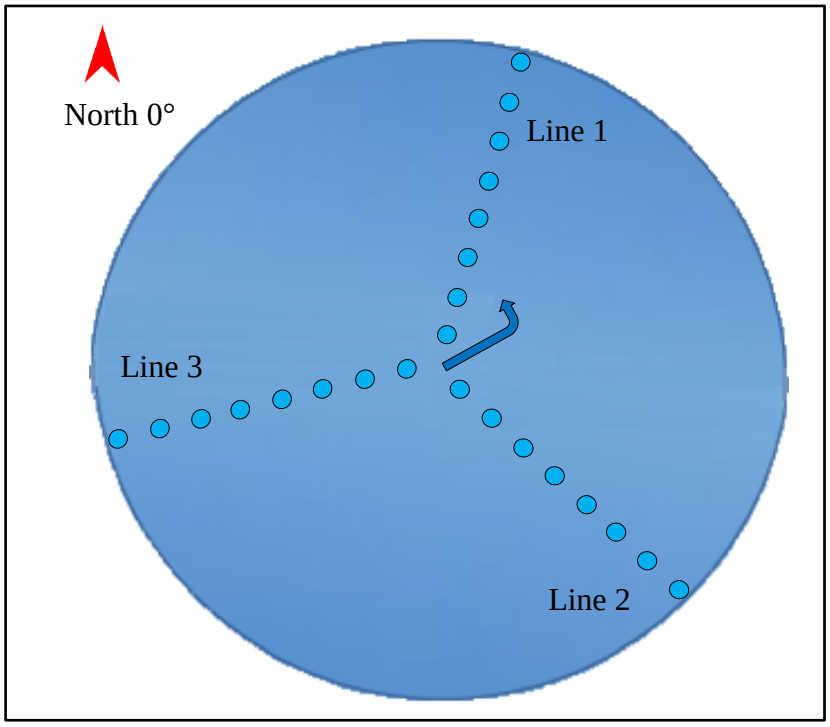

Figure 4-13: Experimental layout for stationary tests; three lines of collectors were placed radially from the centre of the sprinkler 120° intervals.

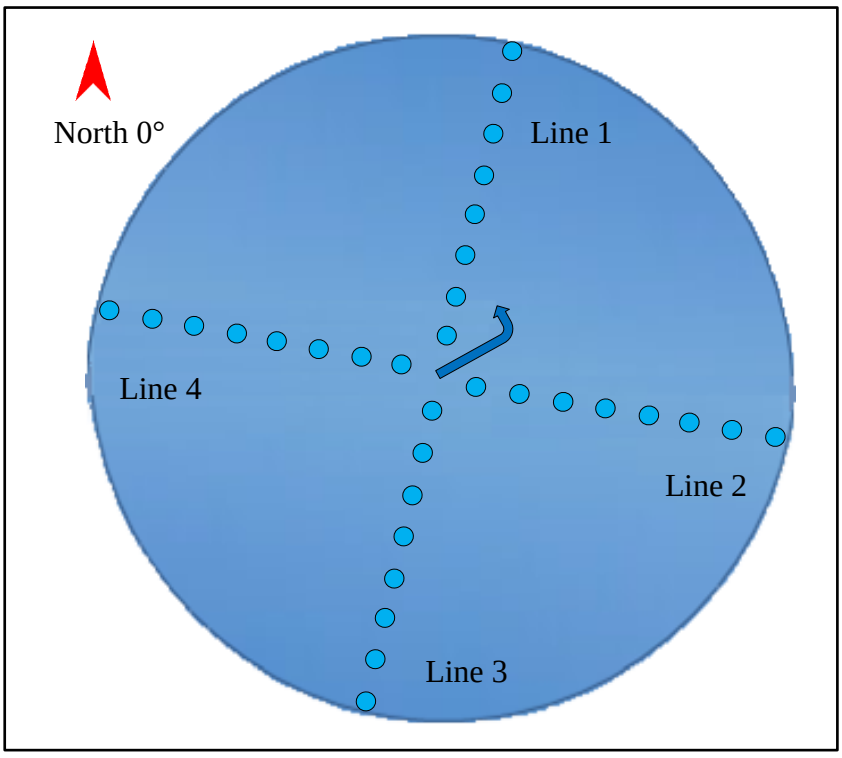

Figure 4-14: The second experimental layout for stationary tests with four lines of collectors placed radially from the centre of sprinkler 90° intervals.

4.7. Measuring transects of different wetted sector and side sector angles

The transect measurement tests occurred with a travelling irrigation machine working with a specific combination of wetted sector and side sector angles. The TravGun model has the ability to generate radial leg data from three transect data sets. The combinations of wetted sector and side sector angles were chosen according to the purpose of this study and in order to validate the new mathematical sub-model. The tests were performed in two groupings. Both of these groups had three parallel lines of collectors positioned on one side of the travel lane, aligned perpendicular to the direction of travel, as shown in Figure 4-15. The data were measured from each of the three lines of collectors for replication purposes. The distance between the parallel lines of collectors was set to 2 metres, so as to decrease any varied depth between lines through a reduction in the travel time across all three them. The distances between each collector along the transect was 3 metres which is the same interval spacing used in the calculation process relation to the plotting and validation stage. The first grouping of transect measurements were performed for sector angles ranging from 90° to 180° and a side sector angle perpendicular to travel direction at 270° (symmetrical to travel direction), as shown in the simple scheme Figure 4-15 and in the photo of the test field in Figure 4-16.

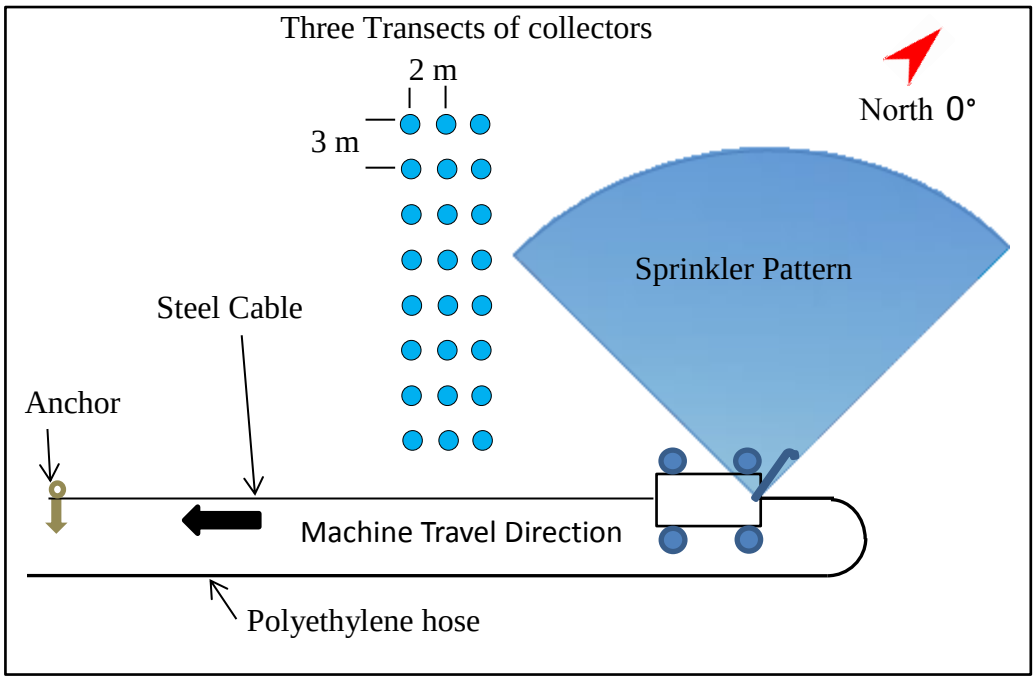

Figure 4-15: Experimental layout for testing where three lines of collectors were placed perpendicular to the machine travel direction, with a sector angle less than 180°, and with a side sector of 270° to the travel direction.

Figure 4-16 : Photo of the experimental field is shown with three lines of collectors placed perpendicular to the travel direction from one side of irrigated area by travelling machine.

The second grouping of transect measurements were performed for sector angles less than 180°, and side sector angles not perpendicular to the direction of travel (greater and less than 270° to the direction of travel), as shown in Figure 4-17.

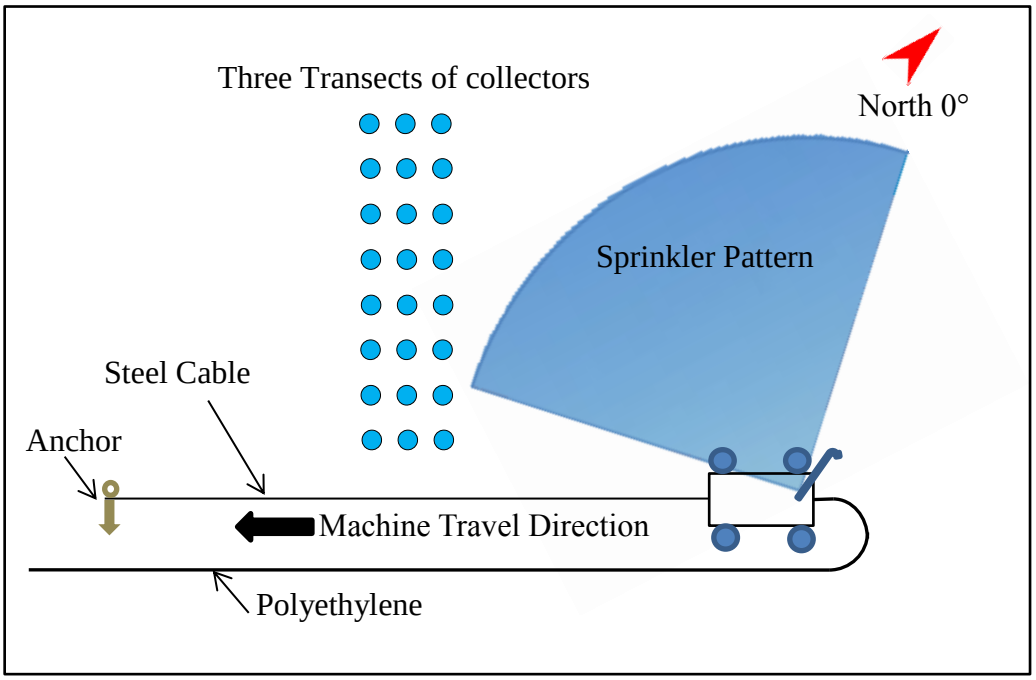

Figure 4-17: Experimental layout showing three lines of collectors which were placed perpendicular to the machine's travel direction, with sector angles less than 180°, and side sector angle not perpendicular ($\phi \neq 270°$) to the travel direction.

4.8. Measuring transects in curve movement

The curved movement tests were performed to simulate the curved movement of end-guns on centre pivots. The purpose of these tests were to find the effect of the curved movement on the transect data. The curved movement of the end-gun can be predicted by calculating the size of the arced path, and driving the travelling gun to follow this arc. Most centre pivot sprinkler irrigation systems have a radius of between 200m to 400m. Therefore, three curves were estimated and pegged out in the field to perform three different tests, to find the effect of the curved movement of the end gun on the centre pivot. The first curve was estimated and pegged out as a 400 m radius of a centre pivot; the second curved path had a 300 m radius; and the third curved had a 200 m radius.

The wetted sector angle was adjusted to 180° with a side sector angle equal to 270° (perpendicular to the direction of travel). The values of the measured transects in

quiescent winds from the different curved path will be compared with a calculated transect for the same wetted sector and side sector angles to discover the differences.

The process of implementing curved path tests can be summarised by the following steps. The first step is to calculate the curved movement of the centre pivot for a specific radius and plot this curve out on a small scale on a sheet of paper. The second step is to estimate the distance required from the sprinkler pattern to pass over the collectors transect on the curved. The third step is to peg out the estimated curved distance on a full scale on the ground at the experimental field. The fourth step is to install strong pegs into the ground on the curved path in the experimental field at a five metre intervals. Finally, the steel winch cable used to move the machine is placed over the top of the curved path, as shown in Figure 4-18 so, that the machine follows the curved path determined by the pegs. Figure 4-18 and Figure 4-19 detail the field configuration to allow the curved sprinkler pattern motion to be measured.

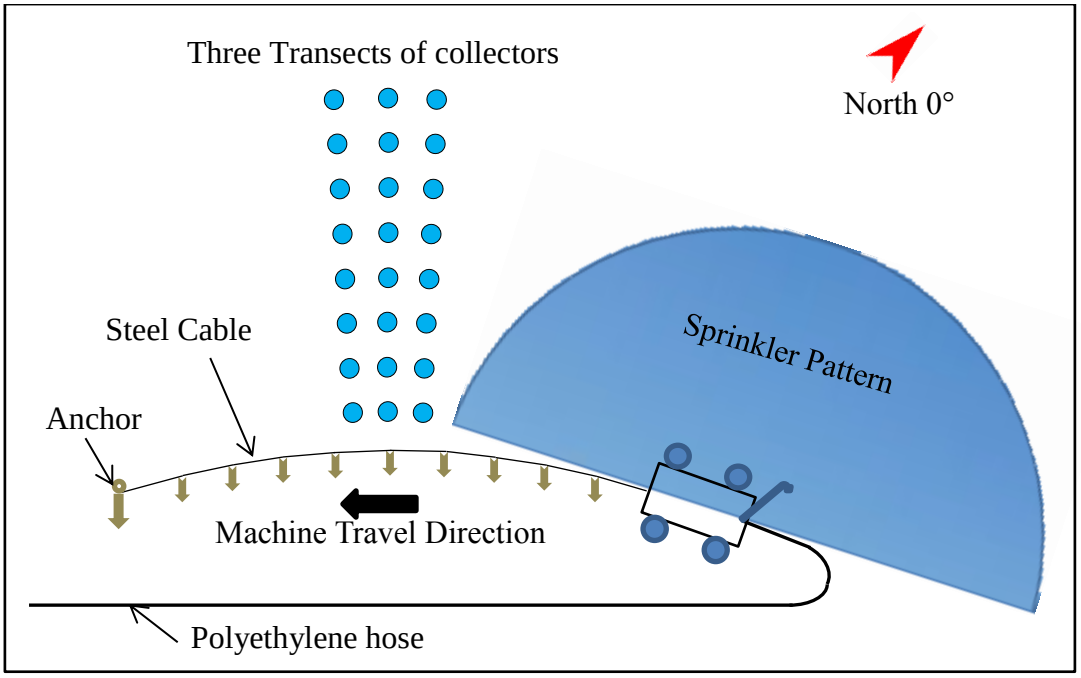

Figure 4-18 : Experimental layout, where three lines of collectors were placed perpendicular to the machine travel direction, and a sector angle of 180°, and a side sector angle perpendicular and asymmetrical to the travel direction was used for a sprinkler travelling on a curved path.

Figure 4-19: Photo of real experimental layout, while three lines of collectors were placed perpendicular to machine travel direction, using a sector angle of 180°, and a side sector angle perpendicular to the travel direction, while the machine is traveling in curved movement.

4.9. Methodologies for validation, and simulation of end-gun patterns in wind using new sub-model

The new mathematical model will add capacity of TravGUN to allow it to generate radial leg data from transect data from both travelling guns and end-guns operating with a wetted sector angle perpendicular and asymmetrical to the direction of travel. The radial leg predicted using the TravGUN sub-model from the measured transects in zero wind for different wetted sector and side sector angles will be compared with the measured radial leg in quiescent wind, so as to validate the new sub-model.

The new mathematical model will be coded in MATLAB script and merged with the TravGUN V2.0 code to develop a new version of TravGUN V3.1 following the validation process. The new version of TravGUN will have the same capability for calibration of the six wind parameters, allowing it to simulate the sprinkler pattern in different wind conditions, in the same way as TravGUN V2.0. However, the mathematical algorithms for calibrating and simulating the end-gun will be modified

to accommodate all possible sector angle configurations for centre pivot end guns. The effect of the curved movement of end-guns on centre pivots will be further developed in more detail in Chapter Seven.

4.10 Summary

This chapter has presented the materials and the methodology that were used in this study. Firstly, the characteristics of testing site were presented, along with the machine and equipment used and install. Secondly, a methodology to predict the appropriate local wind conditions to perform the measurement in an open field were presented. Thirdly, the methodologies that were used to measure radial leg data from full circular patterns, and transect data sets for straight and curved movement were presented. Finally, the next chapter, Chapter 5 will present the field measurements including the results of the radial leg data test, as well as the transect data from different wetted sector and side sector angles, and the transect data from different curved paths and weather condition records encountered during the tests.

5 CHAPTER FIVE

Field measurement and data analysis

5.1 Introduction

This chapter includes the results from the field experimental work performed to measure radial leg data under open field conditions, measuring transects for different combinations of wetted sector and side sector angles and measuring transects when the travelling gun moves on a curved path similar to end-guns on a centre pivots. This chapter also present some examples of weather data from different weather forecast sites, supporting a new methodology reported in the previous chapter, that predicts when the minimum wind speed will occur in order to perform the measurements during no-wind (ideal weather conditions) under open field conditions.

5.2 Measuring radial leg data from a stationary full circle

Two groupings of radial leg data were measured from stationary tests, as mentioned in Chapter Four. The first grouping of data was from three lines of collectors, while the second grouping was from four lines of collectors. The most accurate radial leg data sets in this chapter will be for the lowest wind speeds with the most consistent wind direction. The remaining tests that were performed during higher wind speeds and variable wind directions will be presented in Appendix A. These tests are named according to the sequence in which each was conducted, with some tests described in this chapter and the remainder being provided in Appendix A. The results of Tests One, Two, Three and Five will be presented in Appendix A, because the average wind

speed was higher than 3.5 m/s, and the wind direction changed more than 3 times during the test. Table 5-1 summaries the tests wind conditions and the criteria that are used to present each test in this chapter or in the Appendix A. The results of Tests Four, Six, Seven and Eight will be presented below.

Table 5-1 Summary for all radial leg tests and wind conditions that used as a criteria to present these tests either in this chapter or in the Appendix A.

Test Number	Date	Average Wind Speed	Changes in Wind Direction	Place of Presented
1	15/3/2015	3.7 m/s	Change 4 time	Appendix A
2	18/3/2015	2.5 m/s	Change 5 time	Appendix A
3	18/3/2015	2.2 m/s	Change 4 time	Appendix A
4	18/3/2015	3.4 m/s	Change 2 time	Chapter 5
5	18/3/2015	5.2 m/s	Change 5 time	Appendix A
6	19/3/2015	2.1 m/s	Change 3 time	Chapter 5
7	4/5/2015	0.1 m/s	Change 2 time	Chapter 5
8	4/5/2015	0.0 m/s	Change 0 time	Chapter 5

5.2.1 Measured radial leg data in Test Four

The test was performed on Wednesday 18 March 2015 from 8:10 pm to 9:10 pm. The data were collected from three lines of collectors. The experimental layout is described in Figure 4-13 and Section 4.6. The data from this test is plotted in Figure 5-1. The average value of application rate from the three lines was calculated and plotted as a solid line as shown in this figure. The shape of the average of the three lines appears to be a normal radial leg. However, the data from individual lines are very different because higher wind speeds and the influence of the wind direction are highly different for each line because of their position. It can be seen that there is a variation in the water depth near the sprinkler comparing to that at a distance further from the sprinkler.

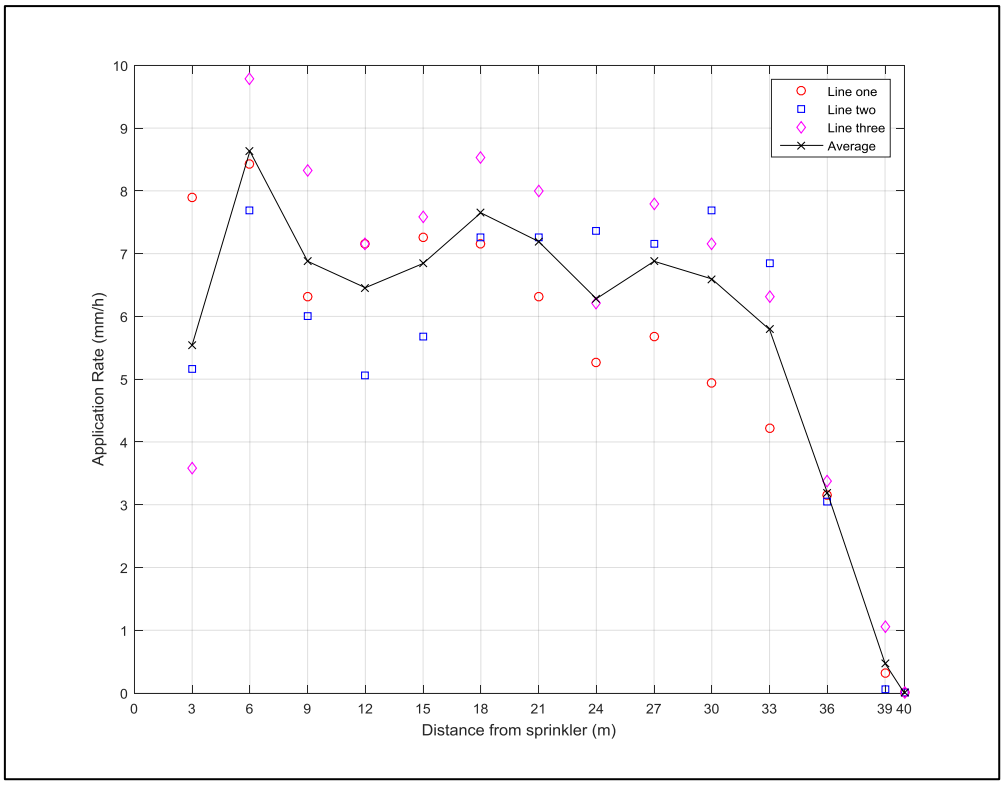

Figure 5-1: Radial leg data Test Four, collected from three lines of collectors placed around a stationary sprinkler.

Weather data was recorded during the test at 15-minute intervals. The resulting wind speed and direction is plotted in Figure 5-2. The X-axis at the bottom represents the time in minutes. The data from the fifteen minute intervals before the test started and after the test ended are included in this figure. The two vertical solid lines define the start and end points of the actual test period. The direction of the arrows cross the top of plot refer to the wind direction at each 15-minute interval. The secondary y-axis on the right refers to the value of the of wind direction angle from 0° to 360°. The left hand side of y-axis represents the wind speed (m/s). The solid line refers to the wind speed, and the dotted line refers to the wind direction. These wind speed and directions plots are used for all of the separate field tests presented in this chapter, and in Appendix A and B.

Figure 5-2 shows that the wind speed was high and changed during the test, while wind direction changed slightly during the test. Average wind speed and direction were calculated and were found to be 3.27 m/s and 39° (North-East) respectively.

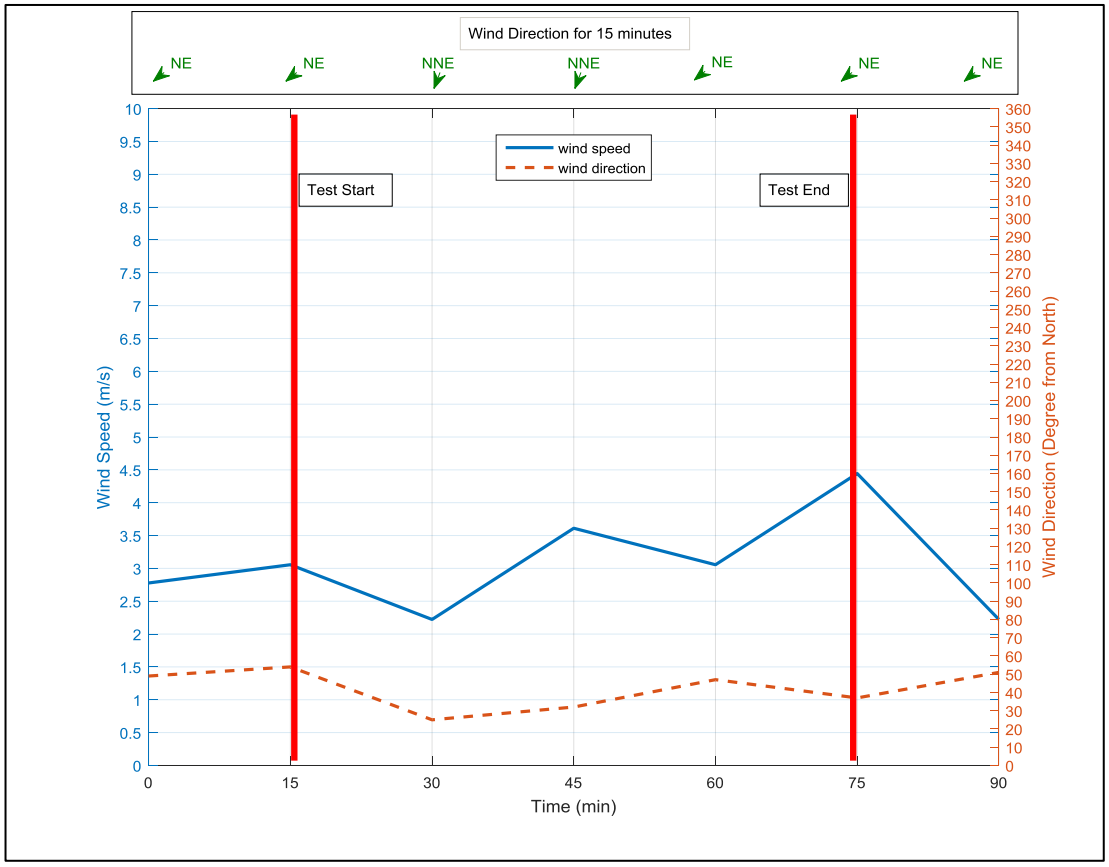

Figure 5-2: Weather conditions (wind speed and direction) for radial leg test four.

In order to analyse and understand the wind effect on the distortion of the sprinkler pattern and justify the variation between the three lines, a series of interpolations were performed from the data of the three lines at each radial distance from the centre of the sprinkler to generate the application rate over a full circular pattern. The interpolated data for the full circular pattern is plotted in Figure 5-3. This figure includes the orientation of the test layout in relation to the northerly direction, the grid of data for full circle sprinkler application rate, and the average wind direction for each 15-minute interval across the top of the plot as a duplicate of the wind directions given in Figure 5-2.

The field test layout in Figure 5-3 shows that the first line was placed at 15° clockwise from a northerly direction, the second line was placed at 135° from a northerly direction and the third line was placed at 255° from a northerly direction. The direction of each radial leg test line starts from the centre of the sprinkler towards the furthest outer point from the sprinkler. Wind speed and direction affect each line in different ways depending on the position of each line. The first line was upwind, according to the average wind direction during the test, as shown in Figure 5-3. So, the application rate decreased in the collector 39 metres from the sprinkler as a result of wind influence. Line two was placed at an oblique angle downwind to the average wind speed and direction. So, the application rate decreased in the collector at a distance of 39 metres as a result of wind range shortening. The third line was situated downwind. Therefore, the application rate in the far distance from the sprinkler at 39 metres increased as a result of the effect of wind influence. The sprinkler pattern shifted with the average wind direction. This result is consistent with that of Richards and Weatherhead (1993).

The application rate in the collectors in the centre and in the middle distances from the sprinklers differed between the lines for two reasons. The first is the interferences between the lines. The interference increases wherever the distances between the collectors in adjacent lines become shorter when they are closer to the sprinkler. The second reason is due to droplet size distributions. Typically, smaller droplet sizes occur near to and in the middle distance from the sprinkler, while large droplet sizes occur at the furthest distances from the sprinkler. Wind has more impact on smaller droplet sizes. Therefore, the variations in application rate occurred more in the centre and middle distance of the sprinkler pattern than at the outer distance, as shown in Figure 5-1 and Figure 5-3. As well, the combined impact of wind influence on the

upwind line compared with the downwind line magnified the differences in the application rate near the centre of the sprinkler.

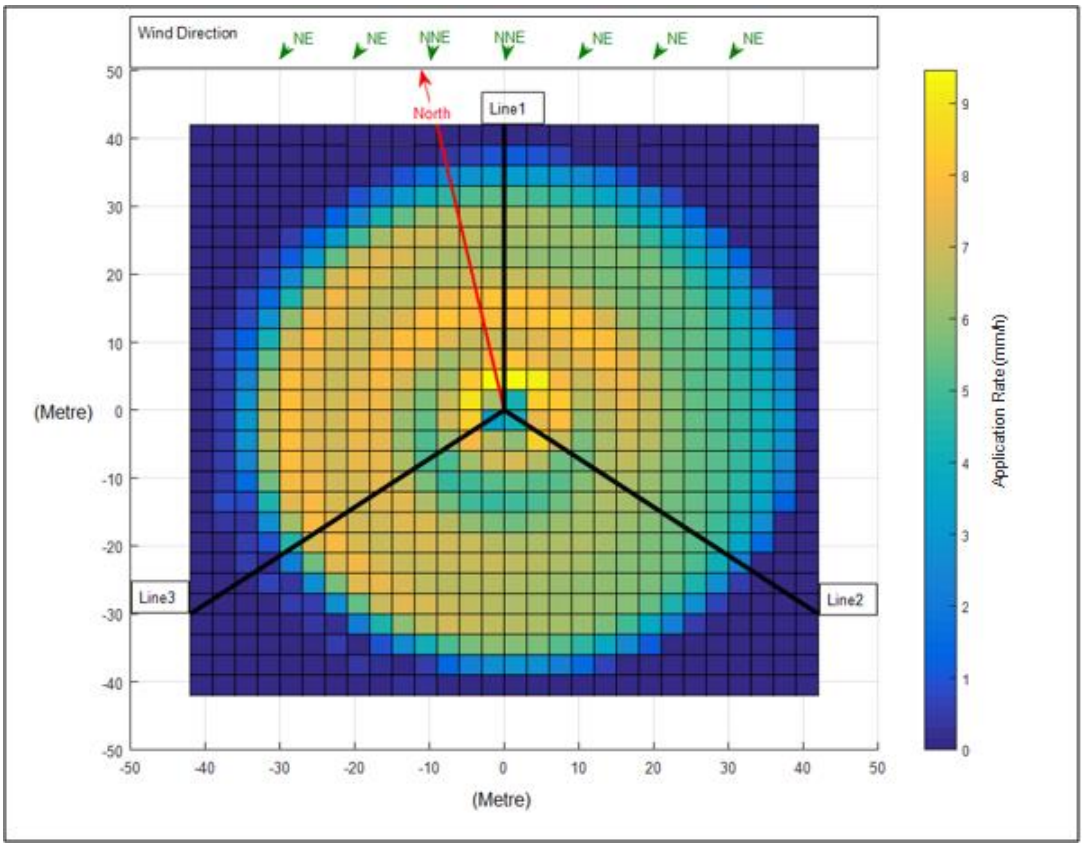

Figure 5-3: Surface plot for radial leg Test Four shows the effect of wind on sprinkler distortion pattern.

Figure 5-3 shows that the application pattern shifted under the effect of wind from the North-East side to the South-West side.

We can conclude that the variation in the radial leg application rates with throw direction was high as result of the high wind speed during the test and the variation close to the sprinkler was larger than the variation at the greatest distance from the sprinkler.

The results of Test Four here could be considered as an initial result in ascertaining the radial leg pattern of the big sprinkler with a taper ring nozzle used in this study. The effect of wind on the distortion of the application pattern could be considered as

normal, however, the wind speed was too high. Therefore, Test Four could not be used in this study to validate the new sub-model.

5.2.2 Measured radial leg data from Test Six

Test Six was performed on Thursday 19 March 2015 from 5:45 pm to 6:45 pm. The test layout was similar to that of the previous test discussed above (Test Four). The average data from the three lines look more representative of a normal radial leg. However, a similar pattern can be seen in the variation between the data for the individual lines of collectors. A plot of the measured catch can data is shown in Figure 5-4.

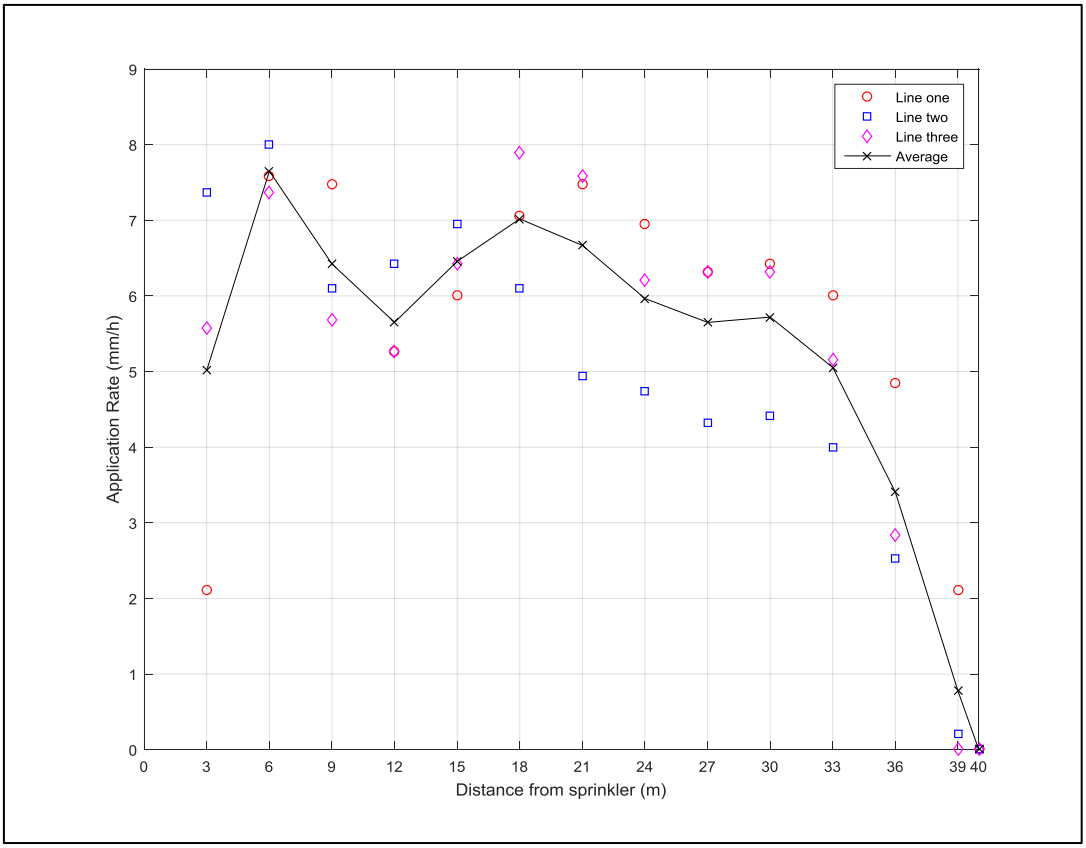

Figure 5-4: Radial leg data from Test Six collected from three lines of collectors placed around a stationary sprinkler.

Weather data was recorded and is plotted in Figure 5-5. The figure shows wind speed at the beginning of the test was low. However, wind speed increased gradually during

the second part of the test. The average wind speed during the test was 2.05 m/s. Wind directions changed gradually during the test, from South-West at the beginning of test to South at the middle of test and to the South-South-East at the end of the test. Average wind direction was 174.4°.

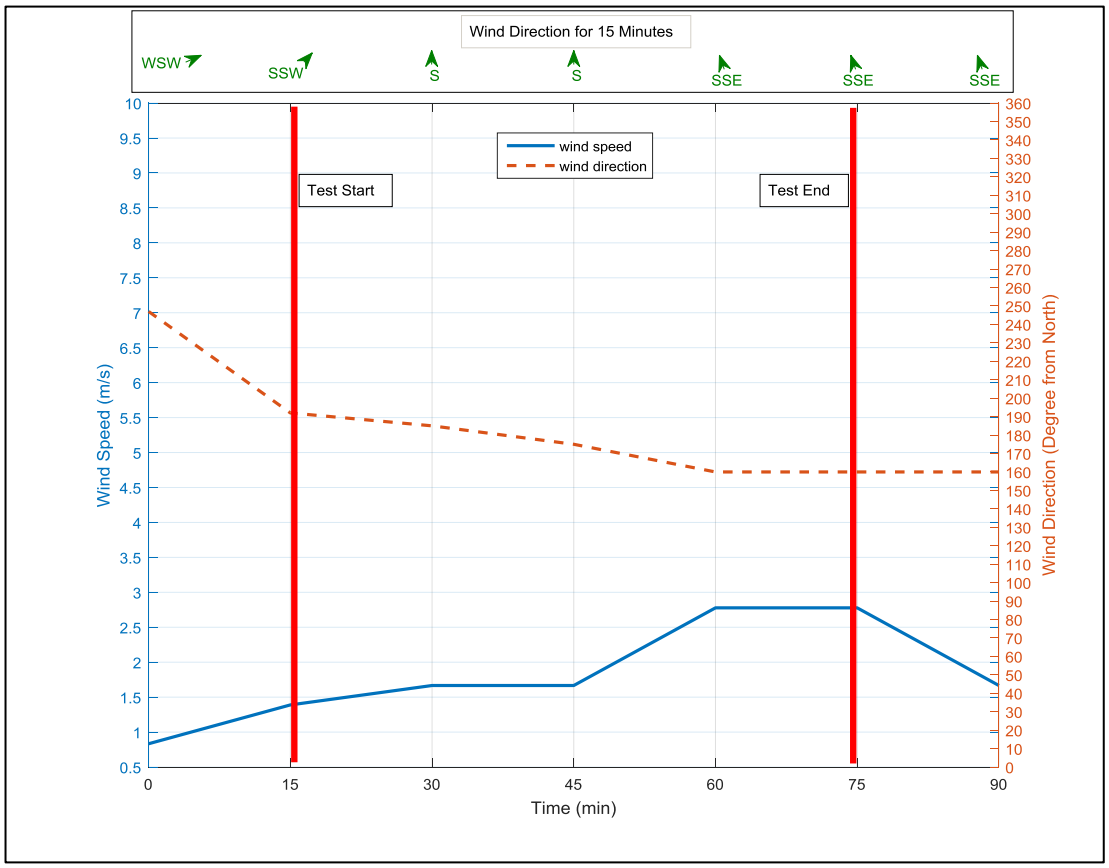

Figure 5-5: Weather conditions (wind speed and direction) for radial leg Test six.

The radial leg data from the three lines were interpolated and plotted in Figure 5-6 in a similar way to those in the previous test discussed above. Figure 5-6 shows clearly that the sprinkler pattern drifted from South to North.

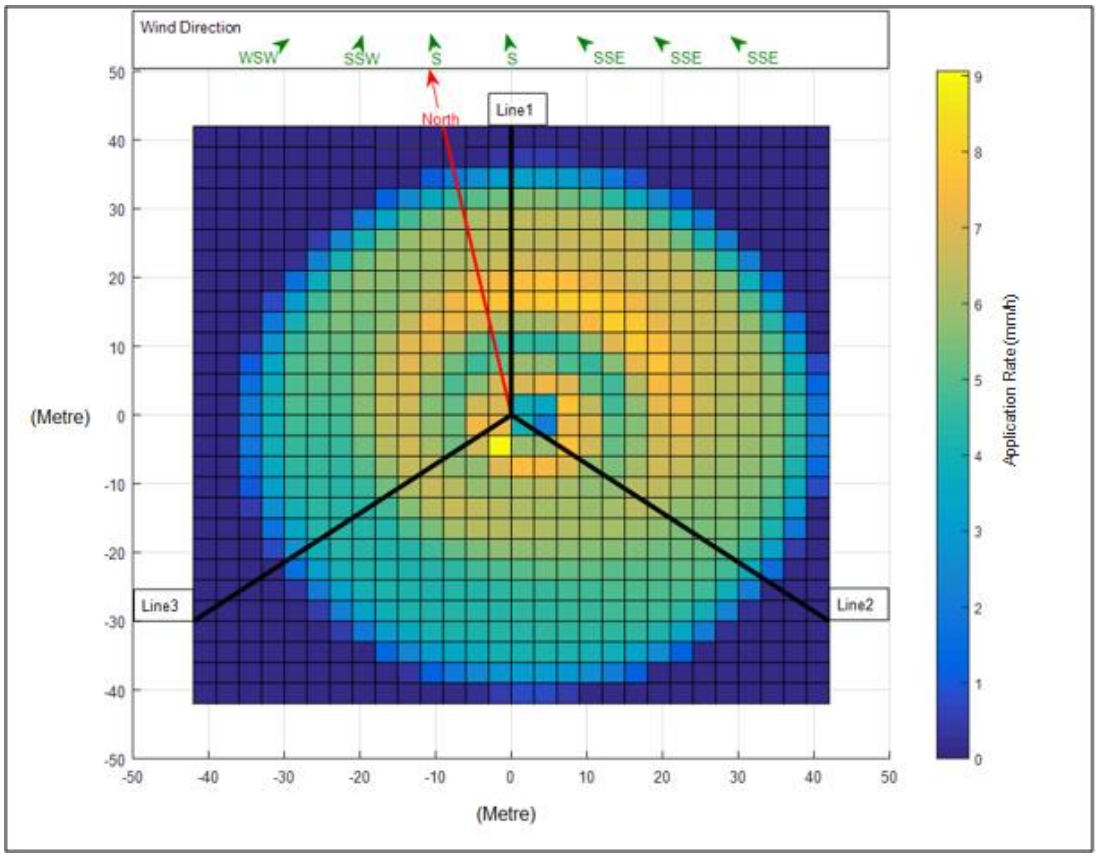

Figure 5-6: Interpolated full circle applied depth plot for radial leg Test Six shows the effect of wind direction on the sprinkler pattern.

5.2.3 Measured radial leg data from Test Seven

The seventh test was performed on Monday 4 May 2015 from 12:15 am to 1:15 am. The data were collected from four lines of collectors. The experimental layout was described in Figure 4.14, Section 4.6. The data from the four lines were plotted as shown in Figure 5-7. The variations between the four lines were less when compared with the previous tests discussed above. However, the variation close to the sprinkler was greater than the variation at furthest distance from the sprinkler.

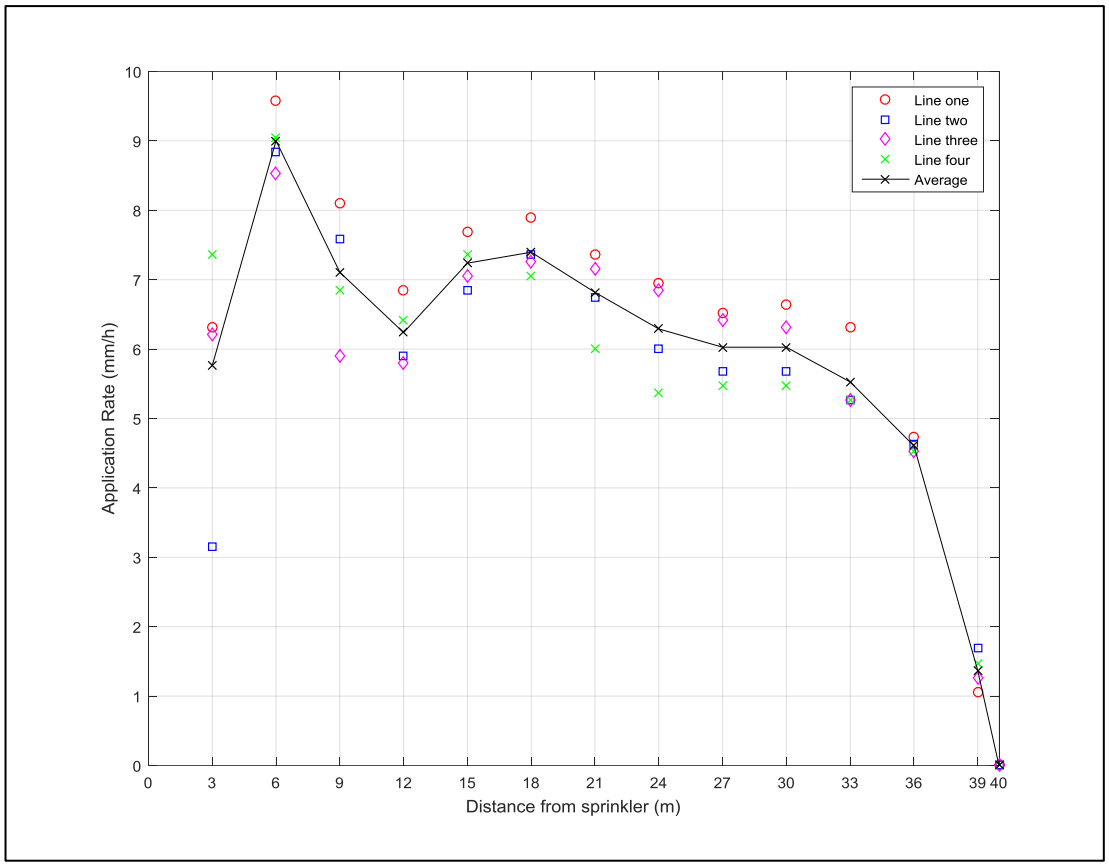

Figure 5-7: Radial leg data from Test Seven collected from four lines of collectors placed around the stationary sprinkler.

Weather data during the test was recorded and is plotted in Figure 5-8. Wind speed was very low during the entire test period. It decreased to zero at the beginning of the test, then increased slightly during the second half of the test. Average wind speed during the test was found to be a low 0.07m/s. Average wind direction was found to be 231° (South-West).

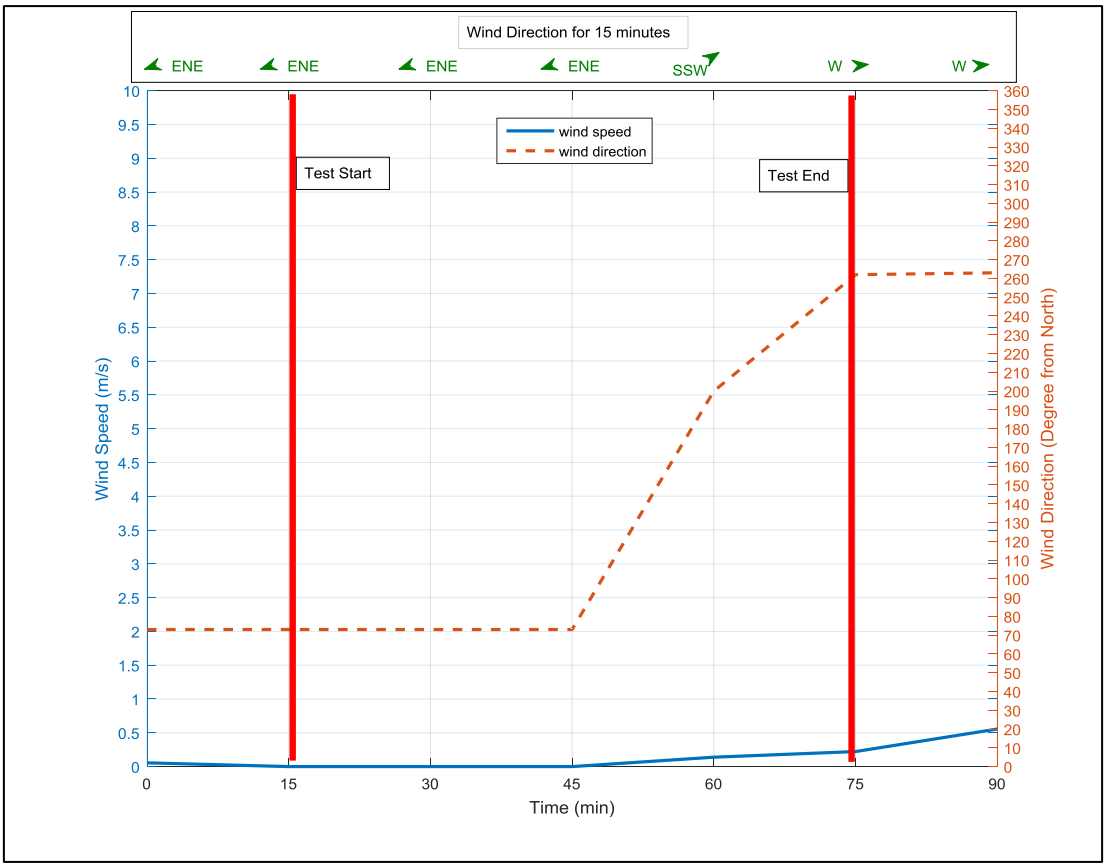

Figure 5-8: Weather condition (wind speed and direction) for radial leg collection in the Test Seven.

The test layout in Figure 5-9 shows Line One placed at 15° clockwise from a northerly direction, Line Two was placed at 105° from a northerly direction and Line Three was placed at 195° from a northerly direction Line Four was placed at 285° from a northerly direction. Wind speed and direction affected each line in a different way, depending on the position of each line and the actual effect of wind speed and direction.

In this case of low wind speed, wind direction has no significant impact on the sprinkler pattern. Figure 5-8 summarises wind speed and direction during the test. The wind speed was zero for 30 minutes during the first half of the test. Therefore, the wind direction will be neglected from this part of the test when calculating the average wind direction or analysing the effect of wind speed and direction. The most important wind direction is that which occurs at the same time as the highest wind speed. So, the

general effect of wind speed and direction during this test will be considered as being from the South-West.

Lines One and Three of Test Seven were cross-wind according to the active wind speed and direction during the test, as shown in Figure 5-8 and Figure 5-9. So, the application rate at the collectors furthest from the sprinkler in Lines One and Three decreased slightly, as shown in Figure 5-7, because Lines One and Three experienced a cross-wind effect. This result is consistent with the reported from Richards and Weatherhead (1993). The application rate at Line Two in the collector furthest from the sprinkler increased slightly as a result of wind influence, because Line Two was placed downwind, as shown in Figure 5-7. The application rate at Line Four in the collector furthest from the sprinkler decreased slightly as a result of wind drift, because Line Four was up-wind, as shown in Figure 5-7. The results of all application rates in the collectors furthest from the sprinkler in all four lines are consistent with Richards and Weatherhead (1993) findings.

The effect of wind speed and direction on the application rate in the first collectors near the sprinkler in all lines were found to be inconsistent in this test. The application rate in the first collector near the sprinkler in Lines One, Three and Four increased slightly as a result of wind drift from the area along the arc from Line Three clockwise to Line Four and Line One. The application rate in the first collector near the sprinkler in Line Two decreased as a result of wind drift from this area to the downwind direction. It is assumed that a minimum or zero application rate occurs in the centre of the sprinkler. Therefore, no additional application rate will result from downwind drift from the centre of the sprinkler. Consequently, wind influence at the first collection point near the sprinkler in Line Two will reduce the application rate and not add to anything from the central area.

There was a variable application rate in the other collectors along all four lines from the middle to distance from the centre of the sprinkler. The variations resulted from wind drift interference between the areas surrounding these collectors.

From further analysis of the variation in the application rate between the four lines at each radius distance, the application rate between each of the four lines was interpolated and plotted in Figure 5-9. The figure is plotted as a surface plot with the positions of the four lines, the northerly direction and wind direction indicated in this figure.

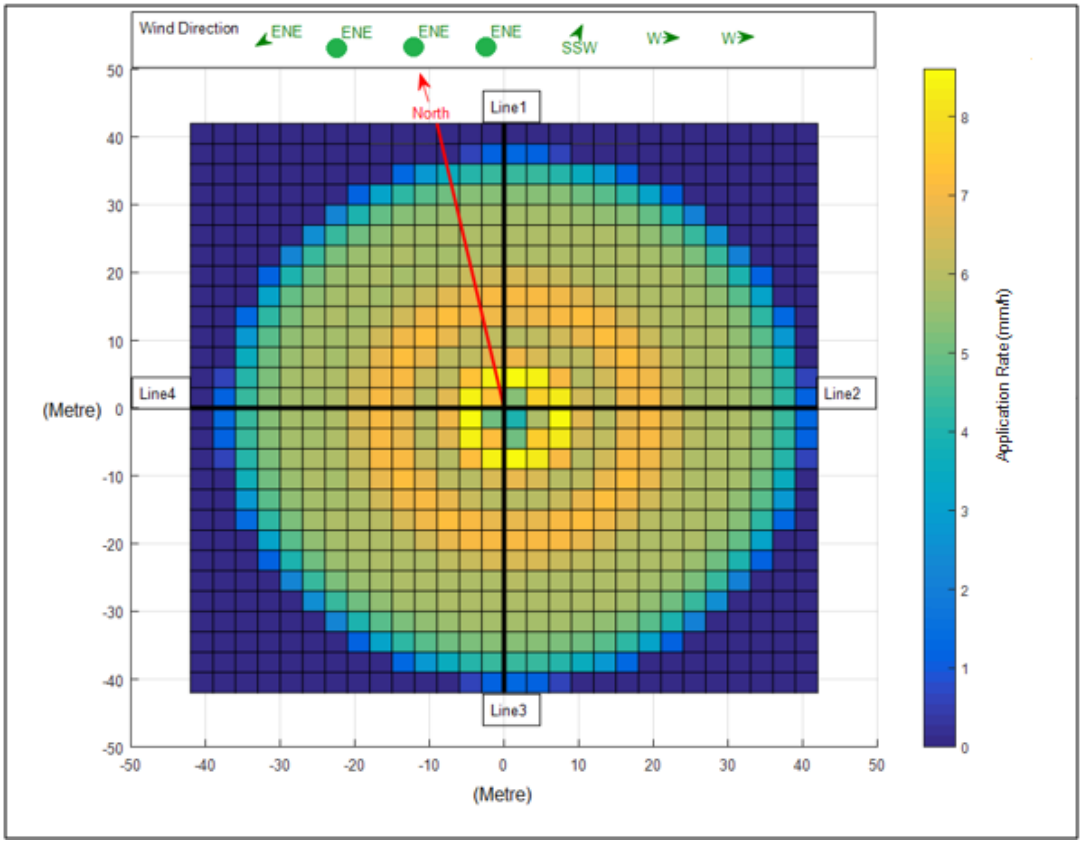

Figure 5-9: Surface interpolation plot of applied depths for radial leg Test Seven shows the effect of wind distortion on the sprinkler pattern.

Figure 5-9 shows a more uniform application pattern compared with previous tests. The centre of this figure shows high variation in the application rate between each line as a result of wind influence of the small water droplet size in the centre of the sprinkler pattern.

Based on the above results and analysis we can use the average of the four lines as the actual data to represent the radial leg of the sprinkler, nozzle and pressure previously described in Chapter Four.

5.2.4 Measured radial leg data from Test Eight

Test Eight was performed for further confirmation of the result of Test Seven. It was performed on Monday 4 May 2015 from 9:45 pm to 10:45 pm. The data was collected from four lines of collectors in a similar fashion to Test Seven. All test conditions in relation to machine set up, collectors position and experiment layout were the same as Test Seven except for the weather conditions which were different. The weather data is plotted in Figure 5-10. The average value of application rate from the four lines was calculated and plotted as a solid line, as shown in Figure 5-10. The shape of the radial leg looks very similar to the seventh radial leg test. However, the data for the individual radial leg lines are different as a result of the differences in wind speed and direction cross the two tests.

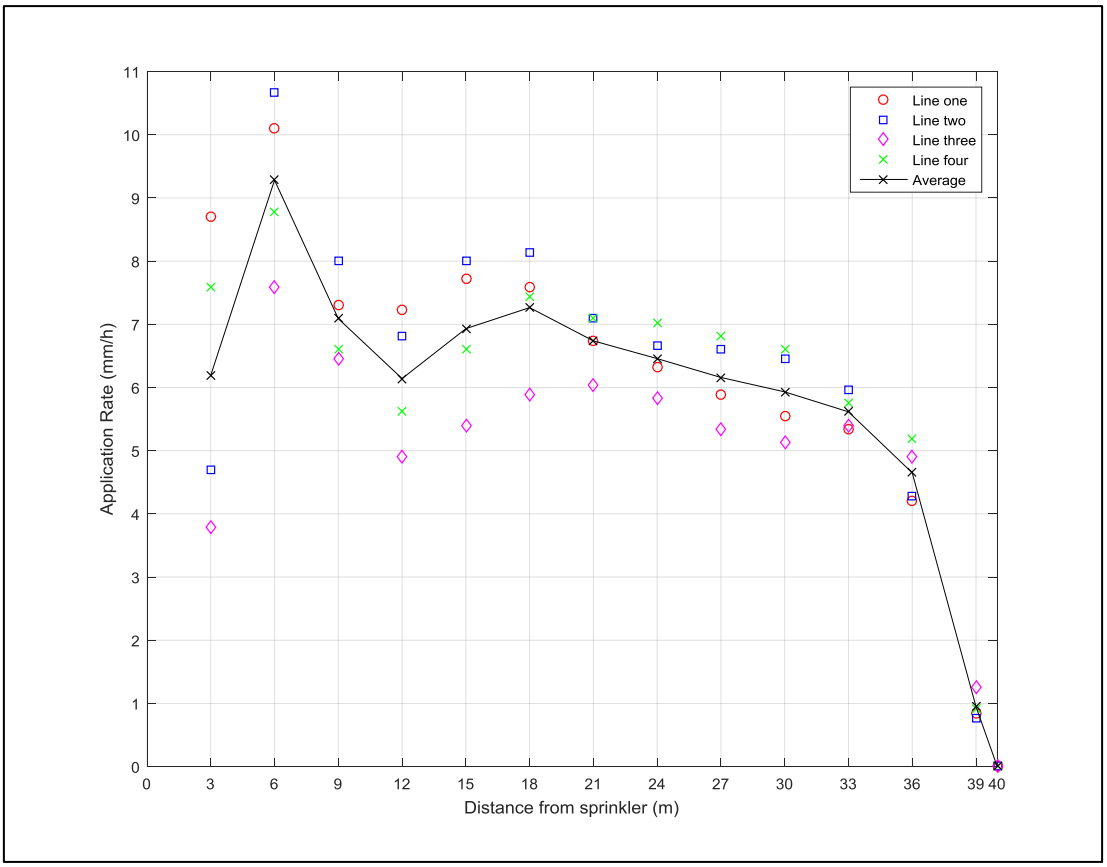

Figure 5-10: Radial leg data from Test Eight collected from four lines of collectors placed around a stationary sprinkler.

Weather data was recorded and plotted during the test, as shown in Figure 5-11. Wind speed was very low during the test and the maximum wind speed during the test was about 0.05 m/s. It was zero m/s before starting the test and increased during the second half of the test. The wind direction was consistent at 332° (North-North-West) during the entire test. Average wind speed was calculated and found to be 0.022 m/s for the entire test period.

The radial leg data in Figure 5-10 shows low variation in the application rate in the collectors furthest from the sprinkler and a higher variation in the collectors near the sprinkler despite the wind being very low during the test. This high variation is a result of using a taper ring nozzle. This type of nozzle produces a small droplet size near the sprinkler and in the middle distance of the radial leg pattern. Smaller droplets are more highly prone to wind influence than large droplets, and it is the larger droplets that reach the maximum throw distance from the sprinkler. Therefore, the application rate

at the furthest distances from the sprinkler varied less than at the middle distance and nearest to the sprinkler.

The weather data in Figure 5-11 shows that the wind speed was zero for 30 minutes during the first half of the test, similar to Test Seven. Therefore, wind direction will be neglected during this period of zero wind when analysing the effect of wind speed and direction during the test. When analysing the results, the combination of the highest and longest wind speed and the wind direction will produce the greatest effect. Therefore, a wind direction of North-North-West will be considered the key factor for this test.

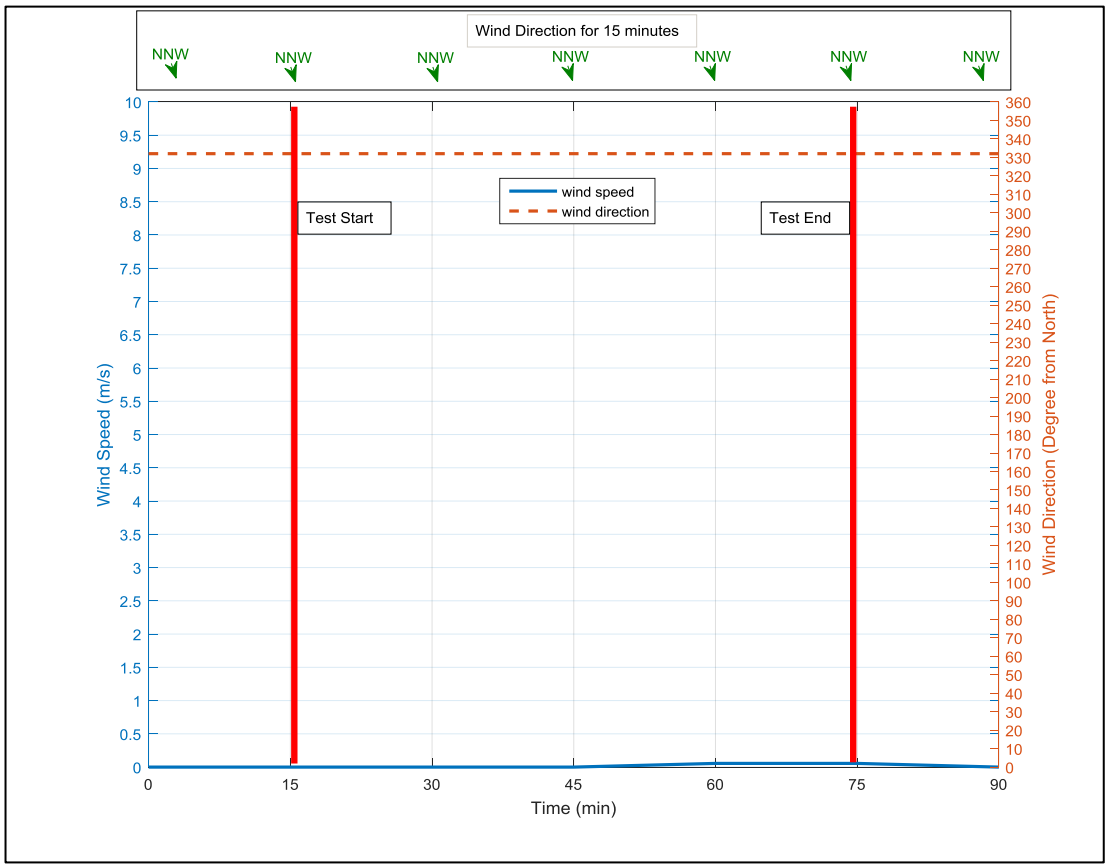

Figure 5-11: Weather conditions (wind speed and direction) for radial leg Test Eight.

The analysis of these effects on the sprinkler pattern is as follows. As shown in Figure 5-12, Line One was between upwind and crosswind according to the active wind speed and direction during the test. Therefore, the application rate at the collectors far from the sprinkler for Line One at 39 metres was slightly reduced

compared to Line Three because of the combined upwind and crosswind effect. This result is consistent with Richards and Weatherhead (1993). The application rate at Line Two in the collector at 39 metres from the sprinkler was slightly reduced as a result of sprinkler throw range shortening due to Line Two being placed perpendicular to the active wind speed and direction. The application rate at Line Three in the collector furthest from the sprinkler was slightly higher than the other lines as a result of wind drift because Line Three was downwind. The application rate at Line Four in the collector at 39 metres from the sprinkler was reduced in a similar way to Line Two as a result of range shortening because Line Four was placed perpendicular to the active wind speed and direction. The results of all application rates in the collectors furthest from the sprinkler in all Four Lines is consistent with Richards and Weatherhead (1993).

The effect of wind speed and direction on the application rate in the collectors near the centre of the sprinkler in all lines were found to be in the opposite effect similar to Test Seven. The application rate in the first collector near the sprinkler in Lines One and Four increased slightly as a result of wind drift from the area along the arc from Line Four clockwise to Line One. The increase of the application rate results from the small size of the water droplets that drifted from the area downwind along Lines One and Four.

The application rate in the first collector near the sprinkler in Lines Two and Three decreased as a result of wind drift in a downwind direction. Assuming zero or a minimum application rate would occur in the centre of the sprinkler, no additional application rate will shift downwind from the centre of the sprinkler to the first collector near the sprinkler in Lines Two and Three.

Figure 5-12 was plotted in a similar way to Test Seven. The figure shows the sprinkler pattern is more uniform than compared with other tests.

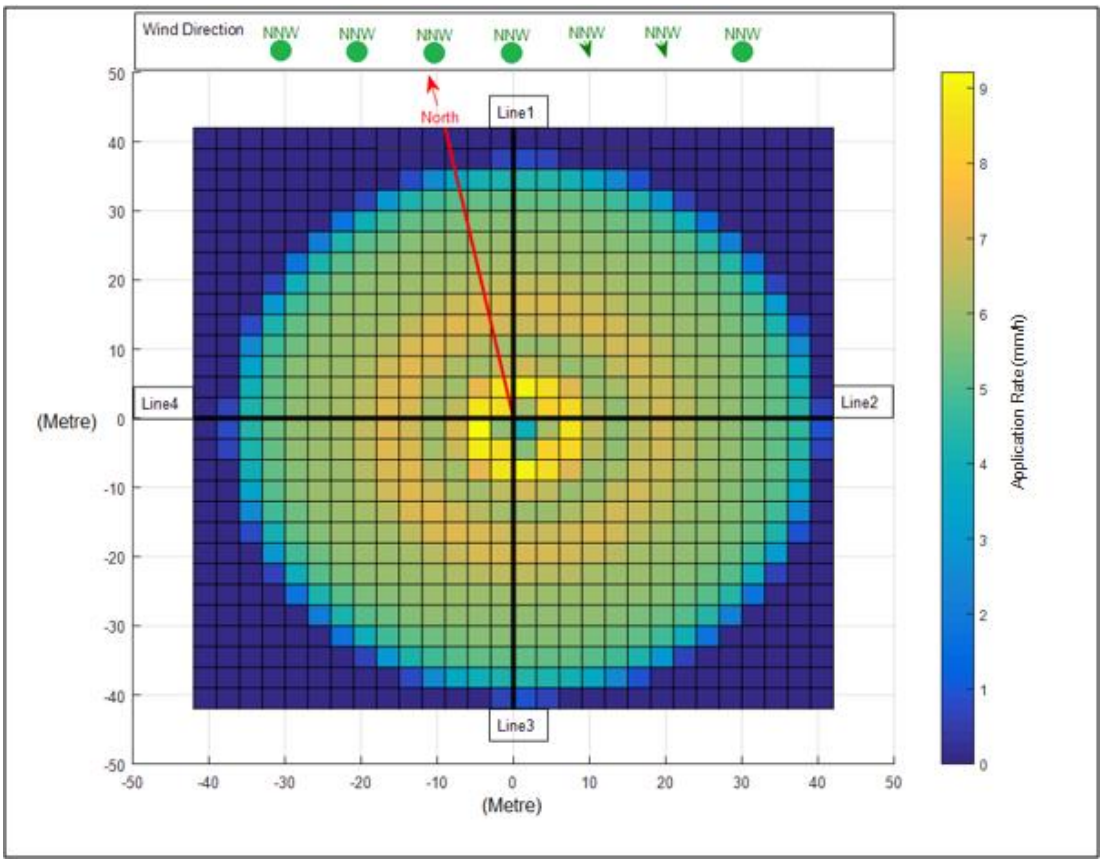

Figure 5-12: Surface interpolation plot for radial leg data Test Eight showing the effect of wind distortion on the sprinkler pattern.

Depending on the above result and analysis we can use the average of the four lines to represent the radial leg of the sprinkler for this combination of nozzle and pressure.

5.2.5 Identifying the radial leg for validation processes

To make the final decision on which data to include in the estimation of the radial leg that will be used for validation purposes, a comparison between the average radial leg data for Tests Seven and Eight is shown in Figure 5-13. This figure shows high agreement between the radial leg data of Tests Seven and eight. There is a similarity between the radial legs of Tests Three and Four as a result of using the same machine set up and experimental layout. In addition, wind speeds were very low during both

tests. However, there were slight variations in the value of the application rate at each radial distance from the sprinkler for both average tests. These variations result from the nature of the experimental differences of wind direction during both tests. The root mean square error was calculated between the average of Tests Seven and Eight and it was found to be 0.2. However, weather conditions during Test Eight were more quiescent. Therefore, the average data from those Tests Seven and Eight will be used in the validation stage of this study in the following chapter.

In conclusion, the radial leg tests using a taper ring nozzle in this study resulted in high variation in the application rate near the sprinkler as a result the production of high amounts of small droplets. Using one or two lines around the sprinkler is not enough to measure radial leg data because low wind speed has an impact on small water droplets. Therefore, using three or four lines at least around the sprinkler reduces the experimental error.

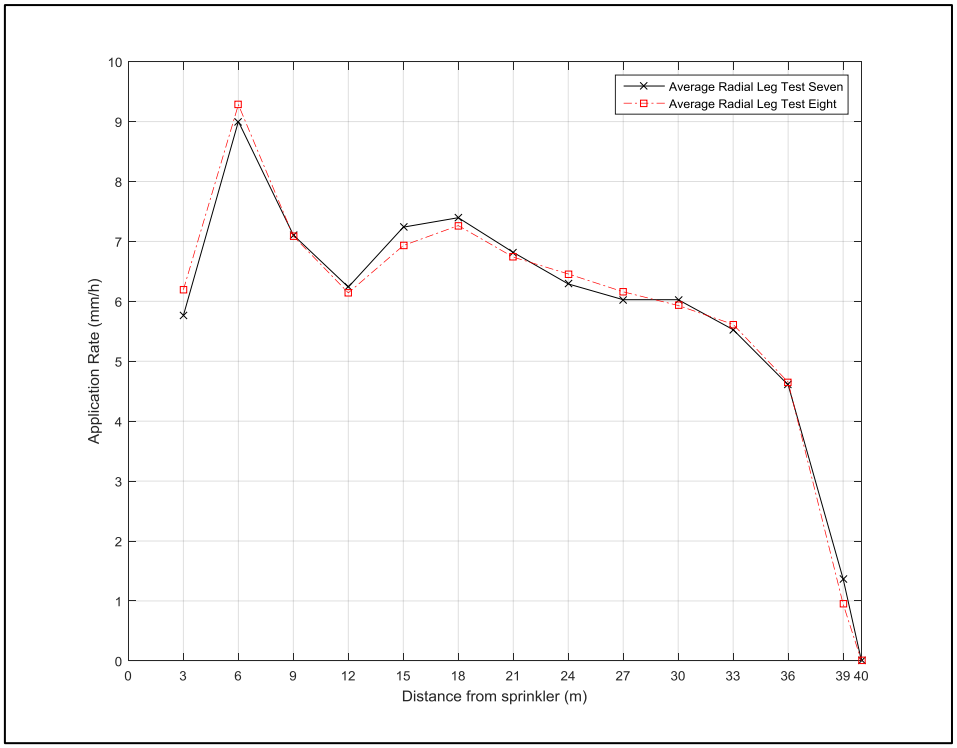

Figure 5-13: Radial water distribution profile of Nelson SR 100 Big Gun sprinkler operating at 490 kPa with a 25.4 mm taper ring nozzle on an 18° trajectory angle as determined on tests Seven and Eight.

5.3 Measured transect data

Two groupings of transects were measured in this study. The first grouping measured different combinations of wetted sector and side sector angles travelling on a straight path. The wetted sector angles for the first group were equal to or less than 180° combined with side sector angles perpendicular and non-perpendicular to the direction of travel. The second collection measured a wetted sector angle equal to 180° combined with side sector angles 270° perpendicular to the direction of travel and travelling on different curved paths. The most accurate transect will be for the lowest wind speed and will be shown in this chapter. The other tests that were performed during higher wind speeds will be shown in Appendix B using similar criteria that was used to present radial leg tests either in chapter five or in the Appendix A. The tests are numbered according to the order in which they were conducted. Table 5-2 summaries all tests wind conditions and places of presented.

Table 5-2: Summary for all Transect tests and wind conditions that used as a criteria to present these tests either in this chapter or in the Appendix B.

Test Number	Date	Average Wind Speed	Changes in Wind Direction	Place of Presented
1	19/3/2015	3.4 m/s	Change 6 time	Appendix B
2	25/3/2015	0.8 m/s	Change 6 time	Appendix B
3	26/3/2015	1.7 m/s	Change 6 time	Appendix B
4	26/3/2015	0.4 m/s	Change 3 time	Chapter 5
5	23/4/2015	0.9 m/s	Change 8 time	Appendix B
6	23/4/2015	0.6 m/s	Change 7 time	Appendix B
7	24/4/2015	1.3 m/s	Change 3 time	Chapter 5
8	27/4/2015	2.1 m/s	Change 8 time	Appendix B
9	3/5/2015	0.3 m/s	Change 8 time	Appendix B
10	5/5/2015	0.0 m/s	Change 0 time	Chapter 5
11	5/5/2015	0.1 m/s	Change 2 time	Chapter 5
12	6/5/2015	0.8 m/s	Change 4 time	Appendix B
13	20/5/2015	0.1 m/s	Change 3 time	Chapter 5
14	28/5/2015	0.3 m/s	Change 3 time	Chapter 5
15	4/6/2015	0.0 m/s	Change 3 time	Chapter 5
16	9/6/2015	0.9 m/s	Change 9 time	Appendix B
17	9/6/2015	0.2 m/s	Change 3 time	Chapter 5

5.4 Measured transects for straight travel

The following results show different combinations of wetted sector and side sector angles used with the machine travelling in a straight path.

5.4.1 Measuring transect Test Number Four

Test Number Four was performed on Thursday 26 March 2015 from 9:00 pm to 11:30 pm. The wetted sector angle was 180° and the side sector angle was 270°. Figure 5-14 demonstrates the test set up including the machine travel direction in relation to the wetted sector and side sector angles, northerly direction, periodic wind direction and average active wind direction. The machine travel direction during the test was from North-East (52°) towards the South-West (232°).

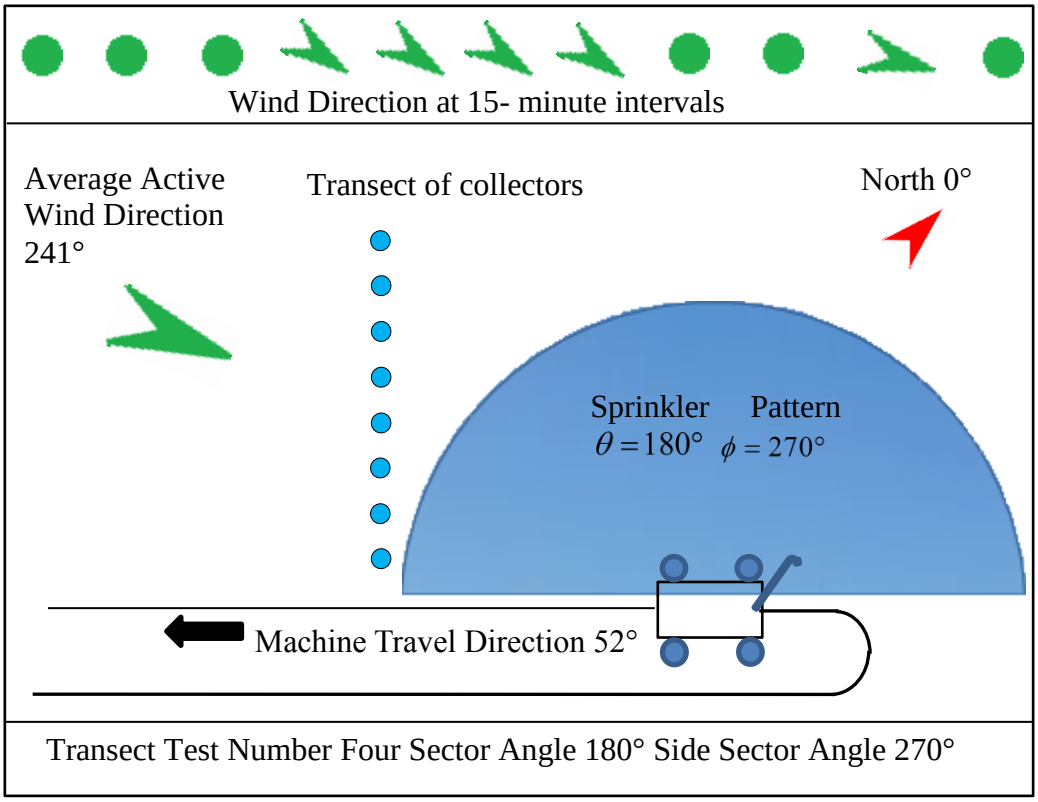

Figure 5-14: Transect Test Number Four shows test layout, the combination of wetted sector and side sector angles and other directions relevant to that test.

The red arrow on the right side refers to a northerly direction. The green arrows and green circles at the top of the figure refer to the active wind direction at fifteen- minute intervals. The green circles refer to inactive wind directions when wind speed is zero and the green arrows refer to active wind direction when the wind speed is more than zero. The large green arrow on the left side of the figure refers to the average active wind speed and direction. The directions of all these arrows are approximate, but the actual wind speed and direction are presented in Figure 5-15.

The average wind speed was calculated to be 0.328 m/s. Average active wind direction was 241° (WSW).

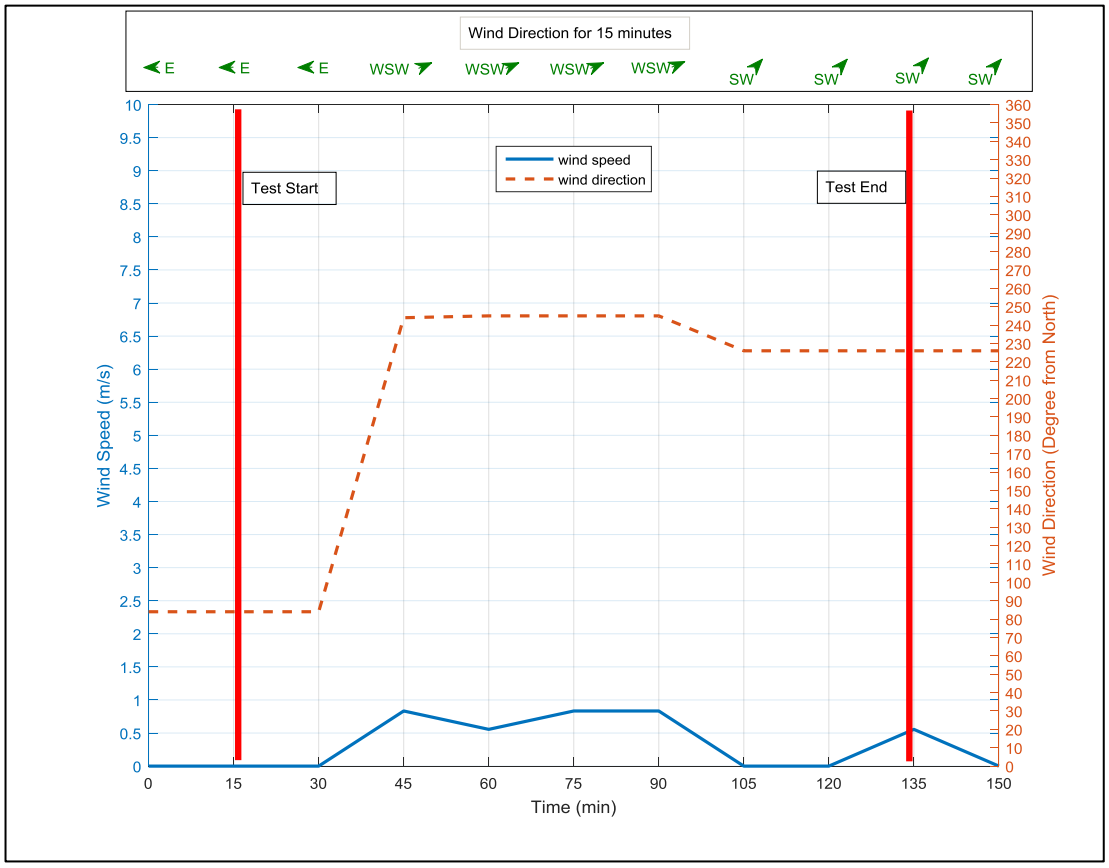

Figure 5-15: Weather conditions (wind speed and direction) for transect Test Number Four.

The average water depth from three lines of collectors were calculated and plotted as shown in Figure 5-16.

The transect data shows that the highest water depth occurred in the first collector near the sprinkler as a result of receiving the application rate from all components of the radial leg pattern. The lowest water depth occurred at the furthest distance from the sprinkler. The figure shows water depth dropped sharply at a distance of 39 metres from the sprinkler. In order to understand the impact of wind speed and direction on the sprinkler pattern, the X and Y axes should be defined according to transect direction and travel direction. The sprinkler pattern for this test is a semi-circle. Assuming the Y axis for this pattern starts from the centre of the sprinkler pattern and extends to the far distance at the end of the transect, and the X axis is the cross distance between the start and the end points of the direction of travel, the mid-point of the pattern along the X axis is the middle distance. The average active wind direction along the transect was between upwind and crosswind on the application pattern, as shown in Figure 5-14.

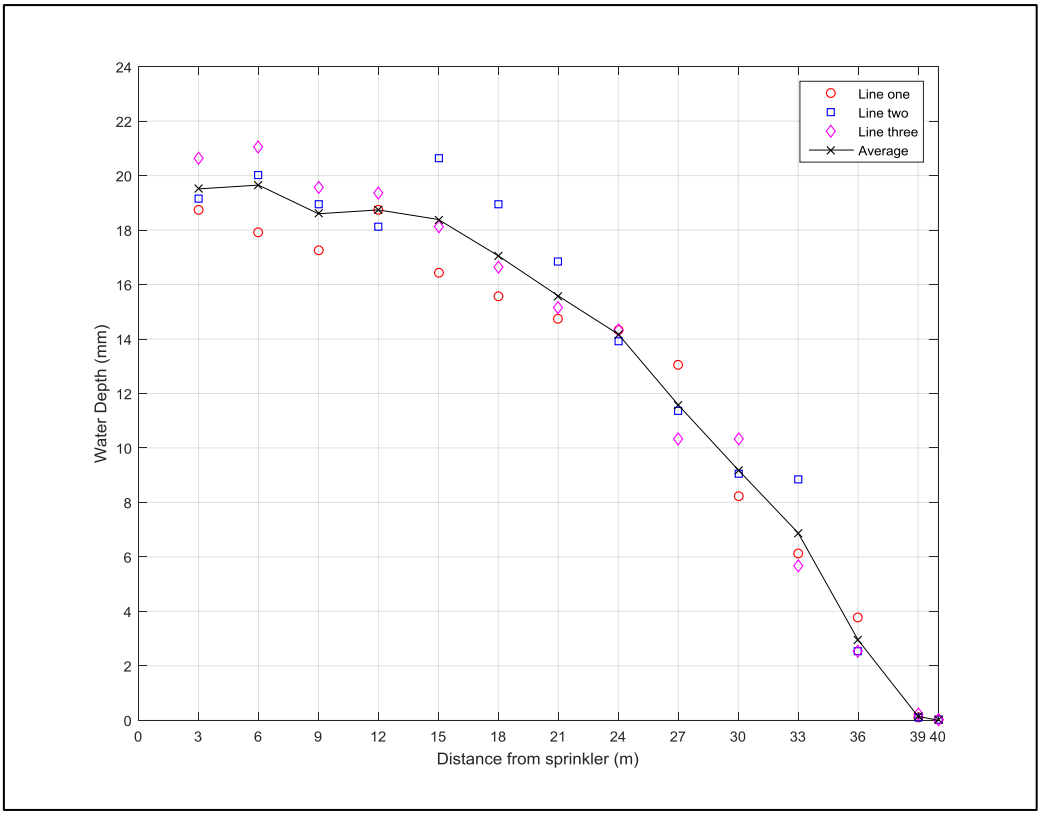

Figure 5-16: Transect data for Test Number Four for the combination of 180° wetted sector angle and 270° side sector angle.

Tests Number Eight and Nine were performed using same sector and side sector angles. However, wind speed during these tests was high. Therefore, the sprinkler patterns were squashed and the shapes of the water depth transects were different. The transect data, test layouts and weather conditions for both tests are shown in Appendix B.

5.4.2 Measured transect data Test Number Seven

Test Number Seven was performed on Friday 24 April 2015 from 6:30 pm to 8:30 pm. The wetted sector angle was 140° and the side sector angle was 270°. The test set up was similar to transect Test Number Four in relation to travel direction, northerly direction and average active wind speed and direction, as shown in Figure 5-17.

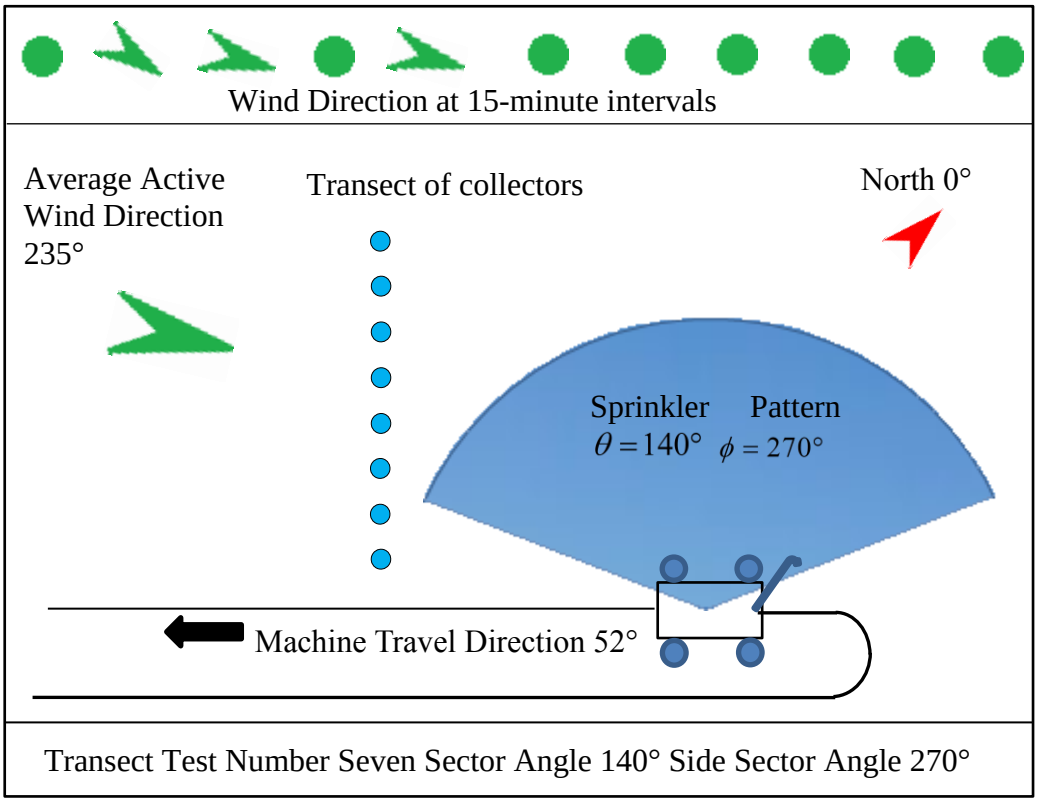

Figure 5-17: Transect Test Number Seven shows test layout, the combination of wetted sector and side sector angles and other directions relevant to the test.

The figure shows that the wetted sector angle, wind speed and wind direction are different from the previous transect for Test Number Four.

Weather conditions were recorded during the test and plotted as shown in Figure 5-18. The average wind speed was calculated and found to be 0.303 m/s. Average active wind direction was 235° (South-West).

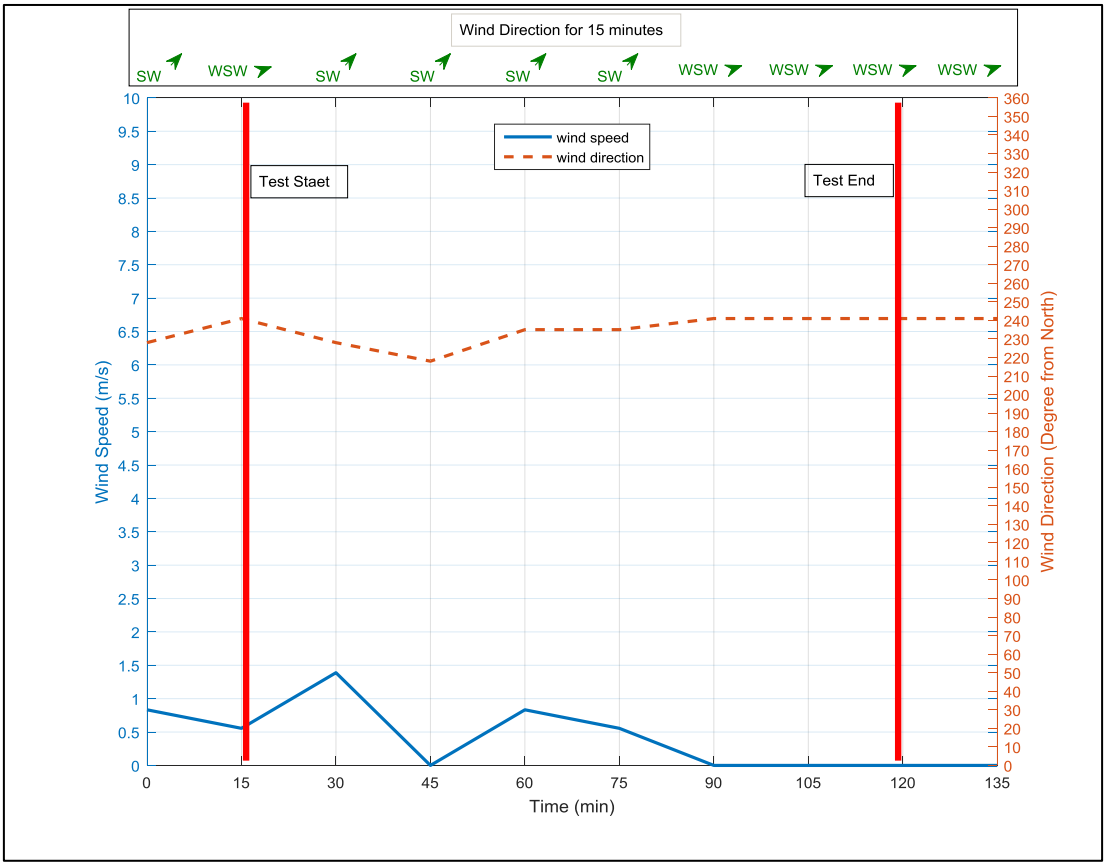

Figure 5-18: Weather conditions (wind speed and direction) for transect Test Number Seven.

The average water depth from three lines of collectors were calculated and plotted as shown in Figure 5-19.

The transect data shows that higher water depth occurred in collector Number Five at a distance of 15 metres from the centre of the sprinkler. Collector Five coincides with the longest dimension of the wetted sector in the direction of travel.

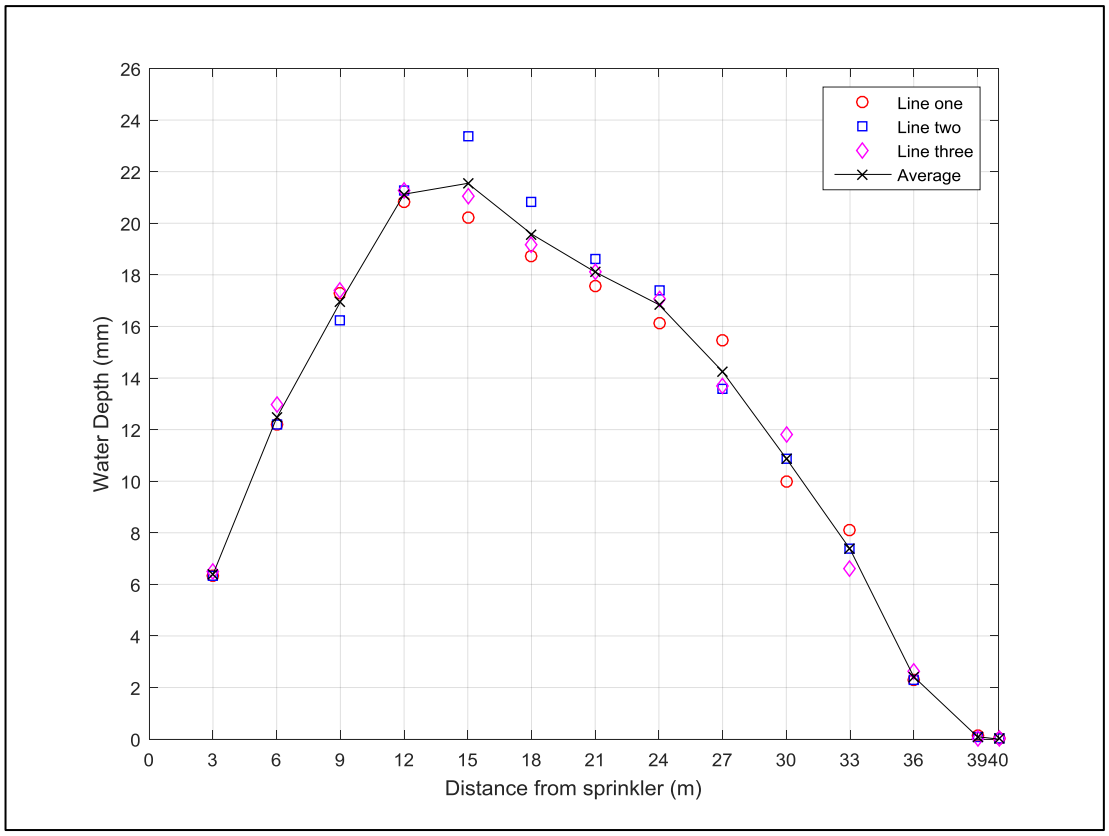

Figure 5-19: Transect data for Test Number Seven for the combination of 140° wetted sector angle and 270° side sector angle.

Test Number Twelve was performed using the same wetted sector and side sector angles, but the wind speed during this test was high. Test layout, weather conditions in relation to wind speed and direction and transect data for this test are shown in Appendix B.

5.4.3 Measured transect data from Test Number Eleven

Test Number Eleven was performed on Tuesday 5 May 2015 from 10:24 pm to 11:50 pm. The wetted sector angle was 105° and the side sector angle was 270°. The test set up in Figure 5-20 shows that the wetted sector angle and weather conditions were different from previous tests.

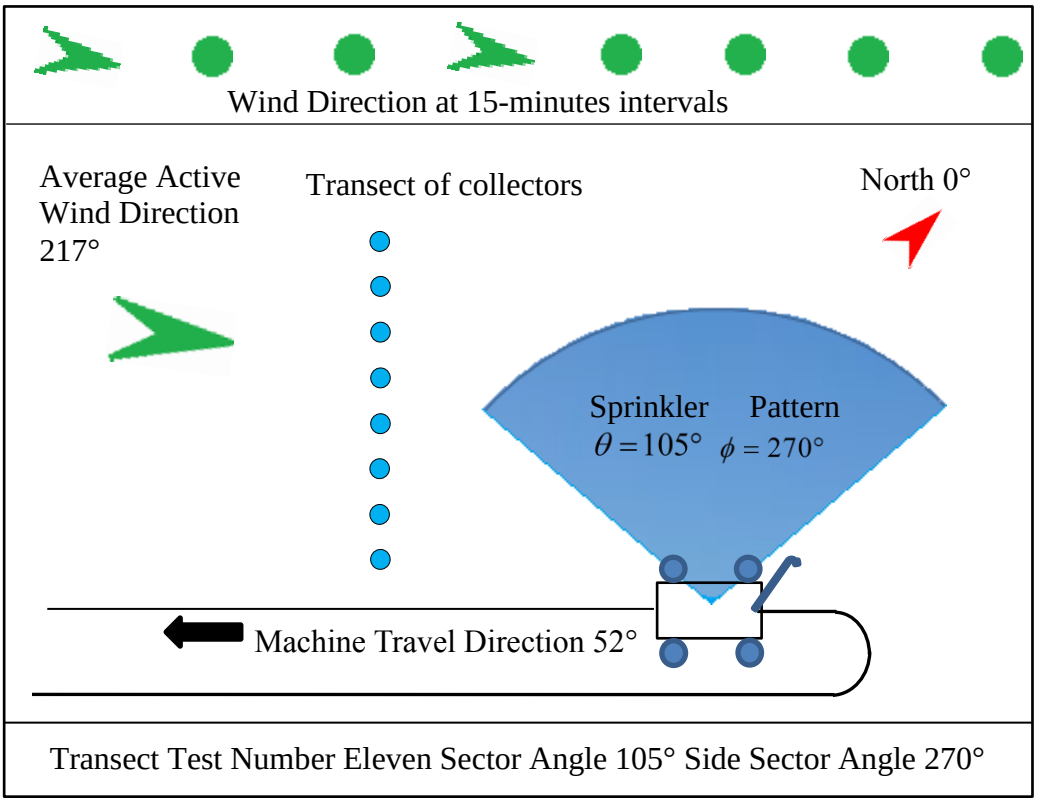

Figure 5-20: Transect Test Number Eleven shows test layout, the combination of wetted sector and side sector angle and other directions relevant to the test.

Weather conditions were recorded during the test and plotted as shown in Figure 5-21. The average wind speed was calculated and found to be 0.174 m/s. Average active wind direction was 217.5° (South-West). The figure shows that wind direction was consistent and changed only slightly during the test and that wind speed was very low.

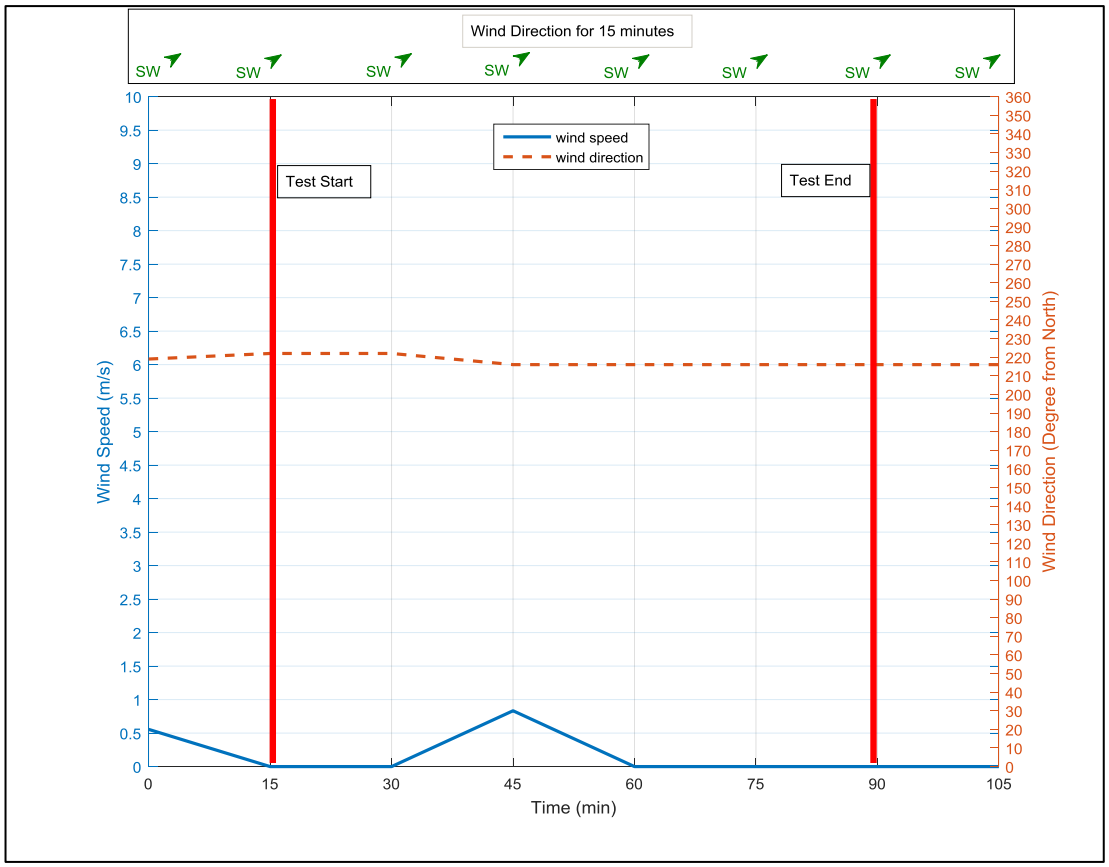

Figure 5-21: Weather conditions (wind speed and direction) for transect Test Number Eleven.

The average water depth from three lines of collectors were calculated and plotted as shown in Figure 5-22.

The transect data shows that the highest water depth occurred in collector Number Eight, at a distance of 24 metres from the centre of the sprinkler. The wind effects along the transect were in-between a crosswind and upwind on the application pattern.

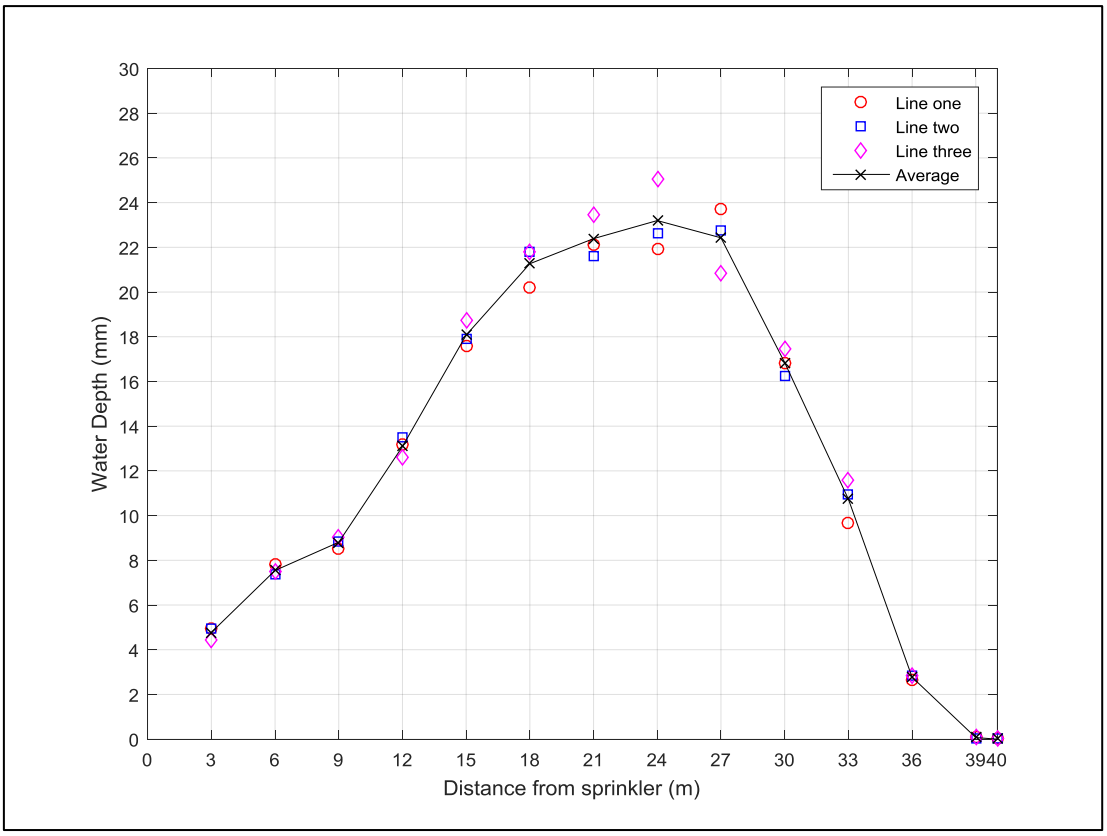

Figure 5-22: Transect data for Test Number Eleven for the combination of 105° wetted sector angle and 270° side sector angle.

Tests Number Five and Six were performed using the same wetted sector and side sector angles as for Test Eleven. Wind speeds were high during the tests. Therefore, the data for these tests are shown in Appendix B.

5.4.4 Measured transect data from Test Number Ten

The transect Test Number Ten was performed on Tuesday 5 May 2015 from 1:18 pm to 2:30 pm. The wetted sector angle was 80° and the side sector angle was 270°. The test layout in relation to wetted sector and side sector angle, travel direction, wind speed and active wind direction are shown in Figure 5-23.

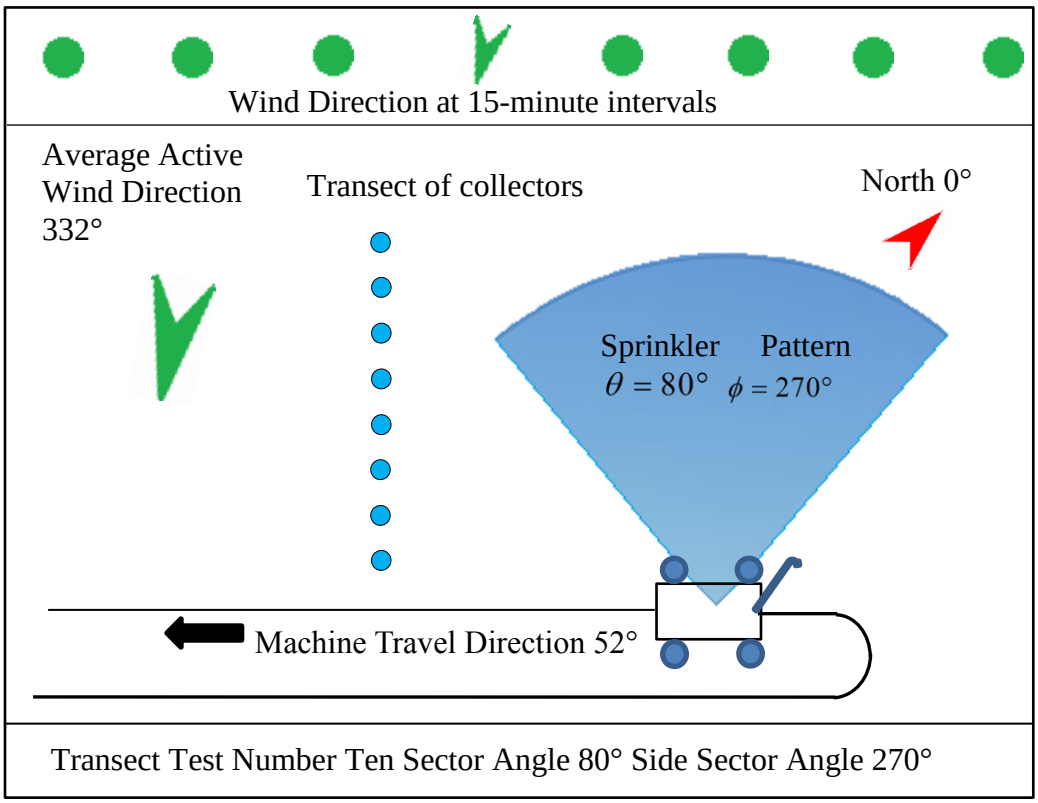

Figure 5-23: Transect Test Number Ten shows test layout, the combination of wetted sector and side sector angle and other directions relevant to the test.

Weather conditions were recorded during the test and plotted as shown in Figure 5-24. Wind speed during the test was very low. The average wind speed was calculated as 0.023 m/s. Average active wind direction was 332° (North-North-West). The figure shows wind direction was consistent during the test and the wind speed was zero.

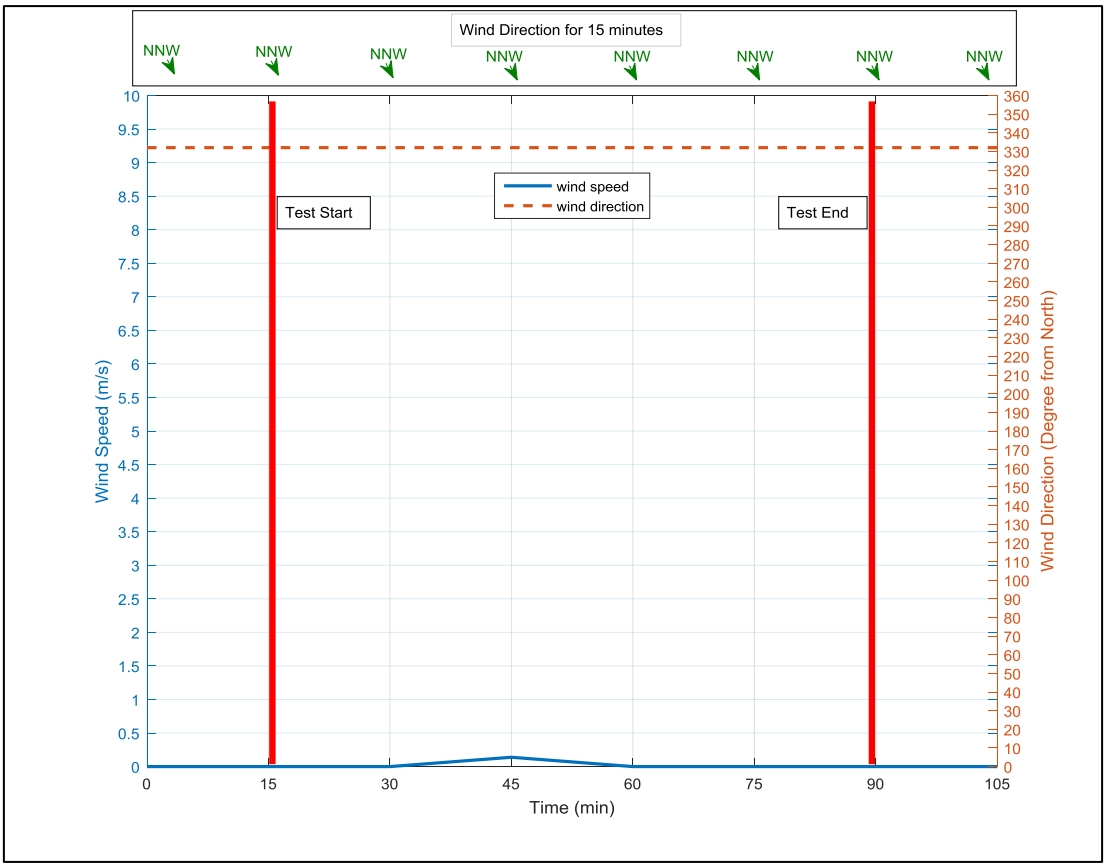

Figure 5-24: Weather conditions (wind speed and direction) for transect Test Number ten.

The average water depth from three lines of collectors were calculated and plotted as shown in Figure 5-25.

The transect data shows that the highest water depth occurred in collector Number Ten from the centre of the sprinkler at a distance of 30 metres.

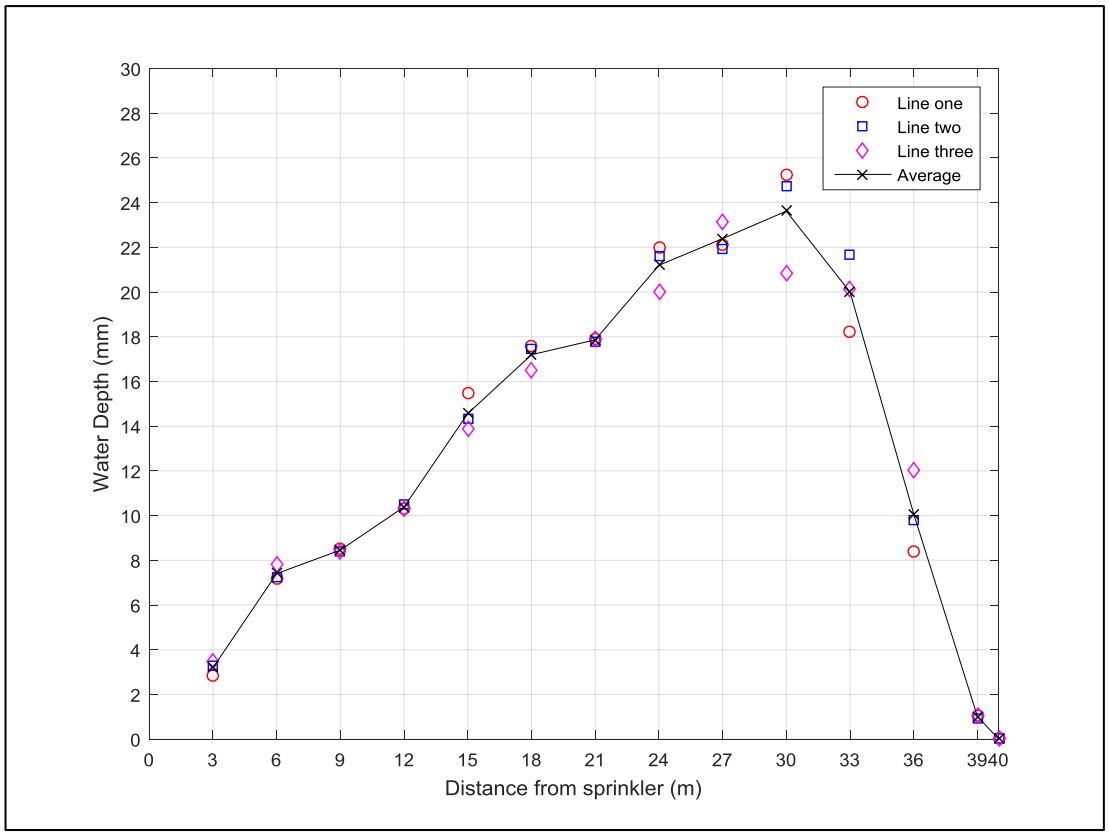

Figure 5-25: Transect data for Test Number Ten for the combination of 80° wetted sector angle and 270° side sector angle.

Tests Number One, Two and Three were performed during high wind speeds using the same wetted sector angles as for Test Number Ten. The transect data for these tests, test layout and weather conditions are shown in Appendix B.

5.4.5 Measured transect data for Test Number Thirteen

Transect Number Thirteen was performed on Wednesday 20 May 2015 from 5:30 am to 7:15 am with a wetted sector angle of 160° and a side sector angle of 290°. The main differences in this test compared with the previous test are that the side sector angle was not perpendicular to the travel direction. All other test conditions are similar to other previous tests in relation to travel direction and northerly direction as shown in Figure 5-26. However, wind speed and direction depended on weather conditions during the test and are indicated as shown in that figure.

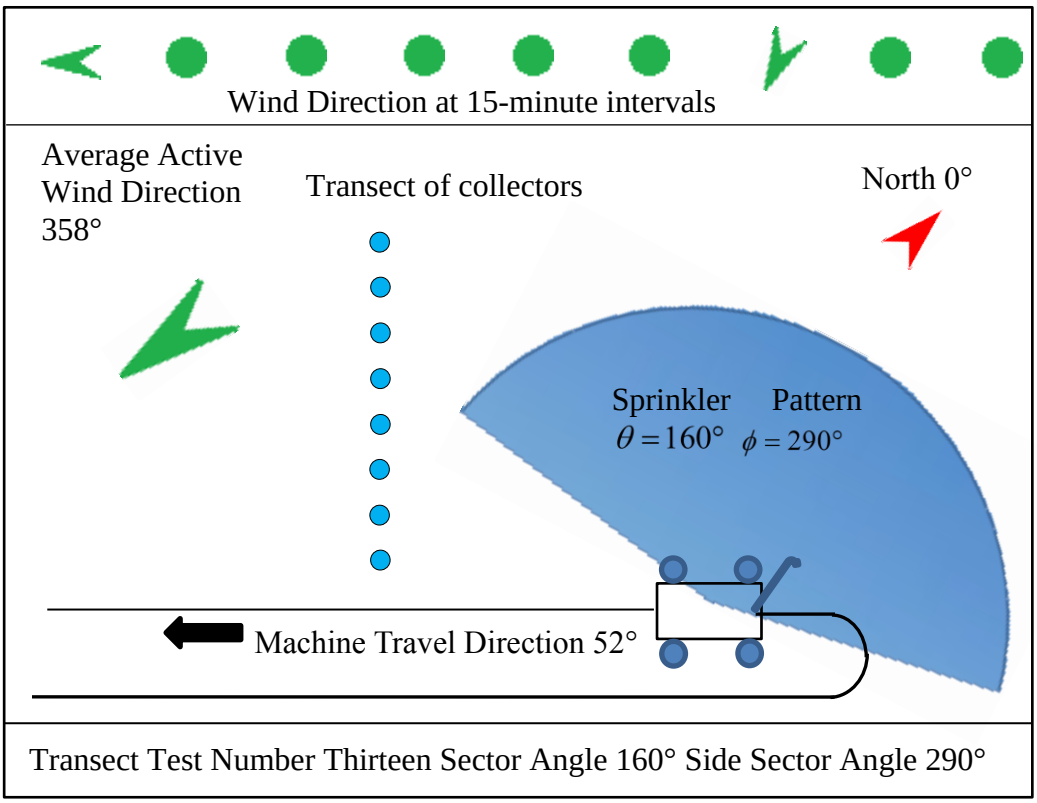

Figure 5-26: Transect Test Number Thirteen shows test layout, the combination of wetted sector and side sector angle and other directions relevant to the test.

Weather conditions were recorded during the test and are plotted in Figure 5-27. The average wind speed was calculated and founded to be 0.104 m/s. The average active wind direction was 358° (North). The figure shows wind direction changed during the test and wind speed was very low.

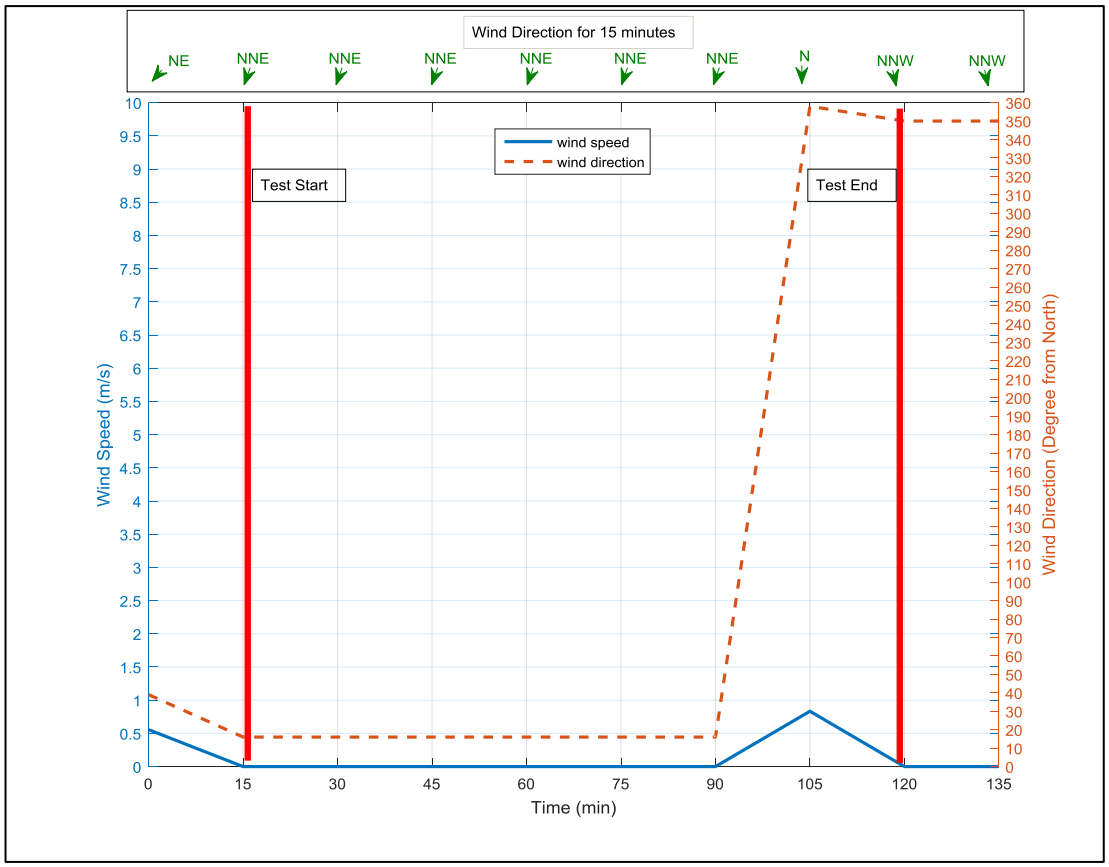

Figure 5-27: Weather conditions (wind speed and direction) for transect Number Thirteen.

The average water depth from three lines of collectors were calculated and plotted as shown in Figure 5-28.

The transect data shows that the highest water depth occurred in collector Number Six at a distance of 18 metres from the centre of the sprinkler.

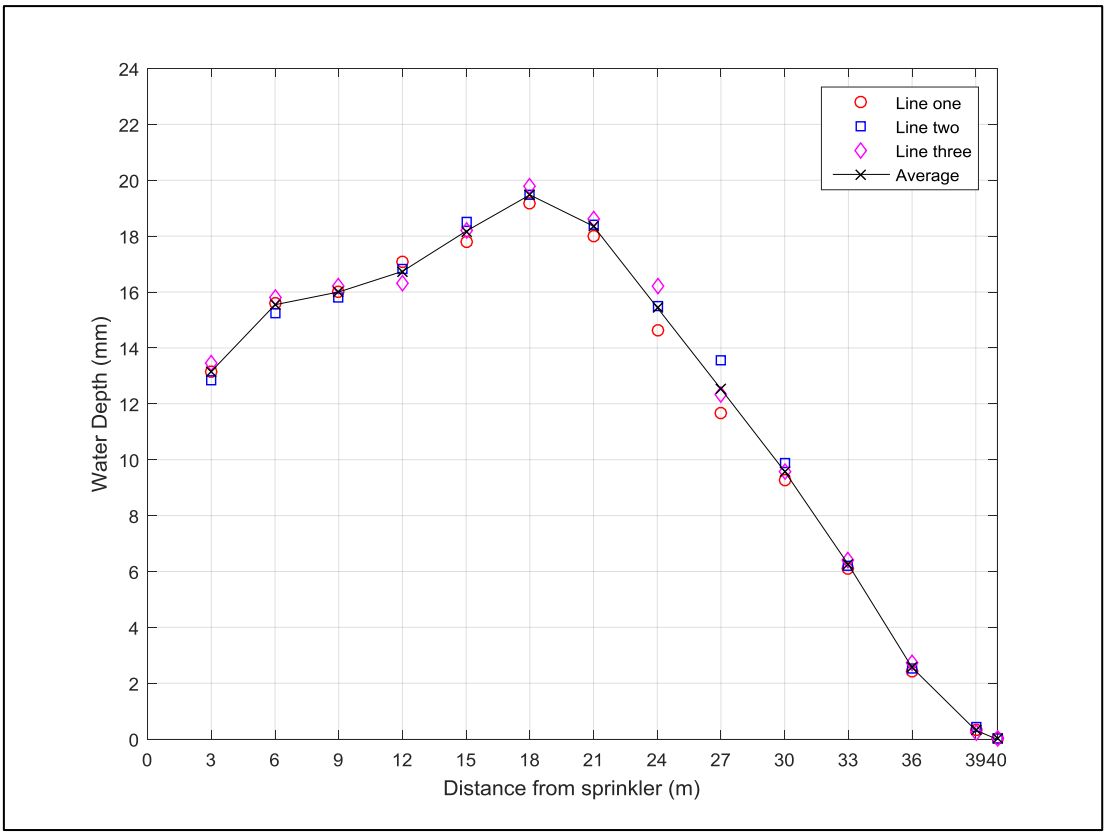

Figure 5-28: Transect data for Test Number Thirteen for the combination of 160° wetted sector angle and 290° side sector angle.

5.5 Measured transects on curved paths

Three tests were performed to examine the effect of the curved path movement of the end gun, on the captured transect data. The wetted sector and side sector were adjusted to 180° and 270° for the three tests. The only differences between the three tests were the curved paths and weather conditions during the tests. The results of these tests are shown below.

5.5.1 Measured transect from Test Number Fourteen

Transect Test Number Fourteen was performed on Thursday 28 May 2015 from 9:00 pm to 10:40 pm with a wetted sector angle of 180° and a side sector angle of 270°. The curved path had a radius of 200 metres. The test layout in relation to travel direction,

northerly direction and average active wind speed and direction are shown in Figure 5-30.

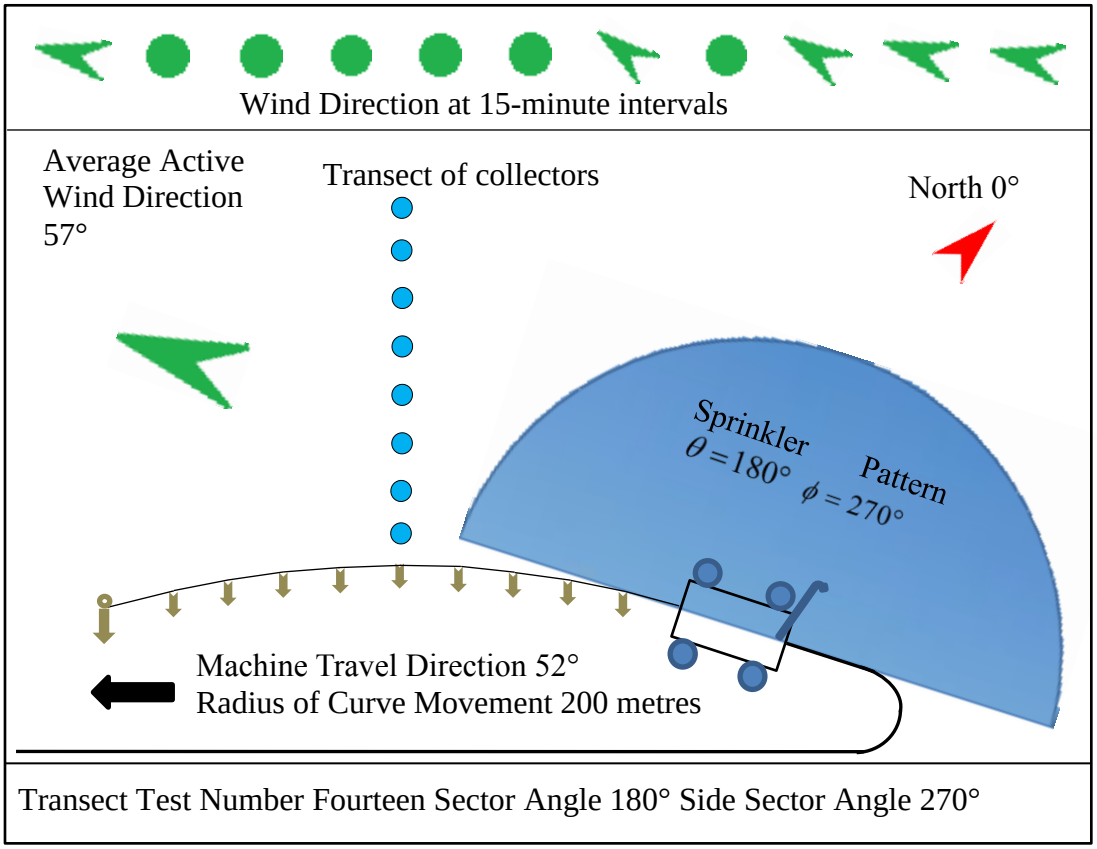

Figure 5-29: Transect test layout for curved movement on a 200-metres radius and weather conditions during Test Number Fourteen.

Weather conditions were recorded during the test and are plotted as shown in Figure 5-31. The figure shows that the wind speed was very low during the test. However, wind speed increased slightly at the end of the test. The average wind speed was calculated and found to be 0.34 m/s. Average active wind direction was 57° (North-East).

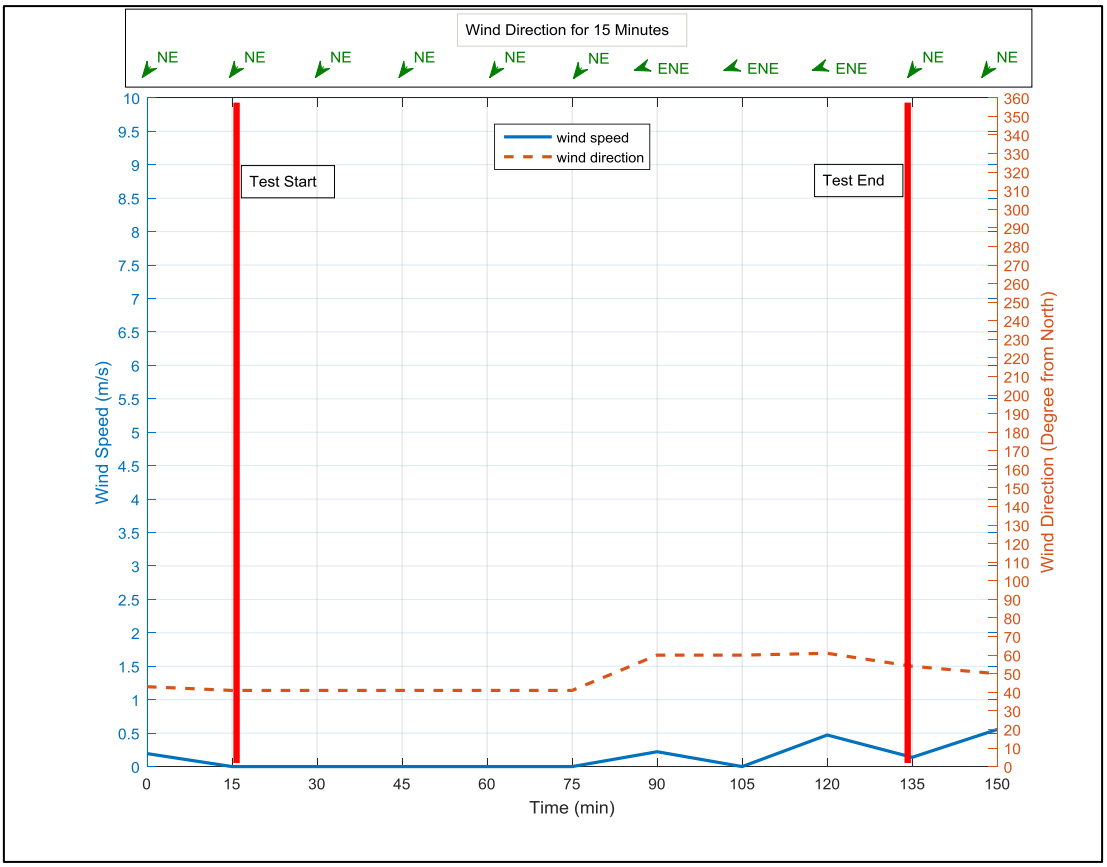

Figure 5-30: Weather conditions (wind speed and direction) for transect from curved movement of a 200m radius for Test Number Fourteen.

The average water depth from the three lines of collectors were calculated and plotted as shown in Figure 5-32. The transect data shows that the water depth decreased slightly at collector Number One near the sprinkler compared with transect Test Number Four for the same wetted sector and side sector angles as a result of the deviation of the leading and trailing edges of the sprinkler pattern (the tangent of the sprinkler pattern travel path) from the point of intersection with the direction of travel during the movement of the sprinkler pattern reaching the first collector from the leading edge and leaving it from the trailing edge. However, the water depth in the transect from curved movement looks similar to the transect for straight movement, except for the first collector.

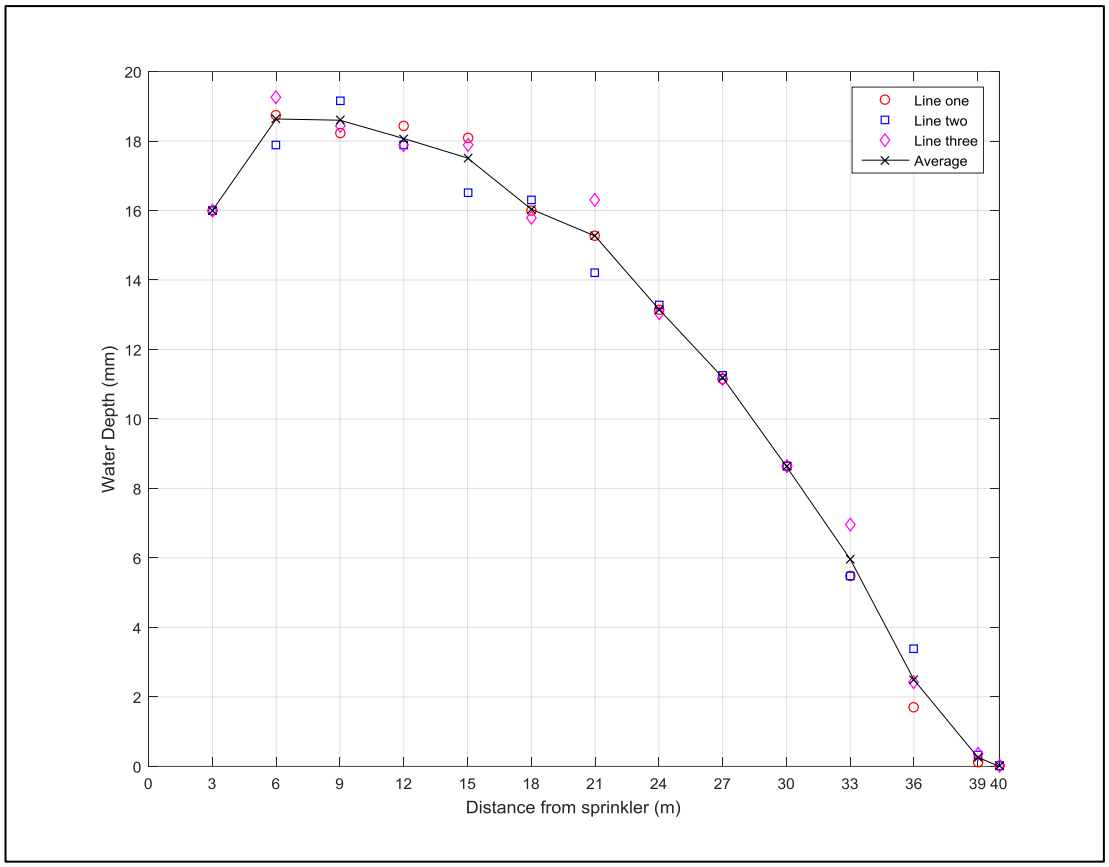

Figure 5-31: Transect data for Test Number Fourteen for curved movement on a 200-metre radius for the combination of a 180° wetted sector angle and a 270° side sector angle.

5.5.2 Measured transect data Test Number Fifteen

Transect Test Number Fifteen was performed on Thursday 4 June 2015 from 4:00 am to 6:00 am with a wetted sector angle of 180° and a side sector angle of 270°. The curved movement had a 300-metre radius. Figure 5-33 shows the test layout in relation to travel direction, northerly direction and average active wind speed and direction, similar to the previous test, except the radius of curvature was different. Weather conditions were also different.

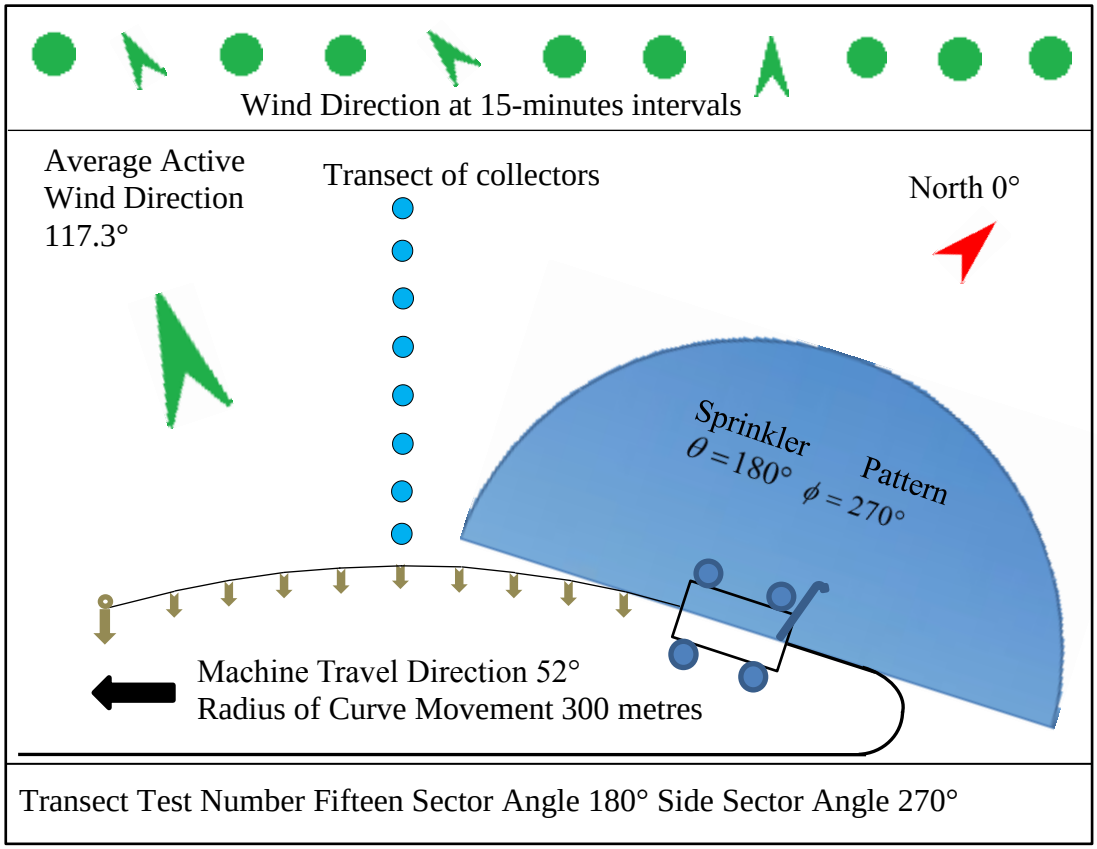

Figure 5-32: Transect test layout for a curved movement on 300 metre radius and weather conditions during Test Number Fifteen.

Weather conditions were recorded during the test and plotted as shown in Figure 5-34. The figure shows wind speed was very low during the test. However, wind speed and direction changed slightly during the test. Average wind speed was 0.025 m/s. Average active wind speed and direction was 117.3° (East-North-East).

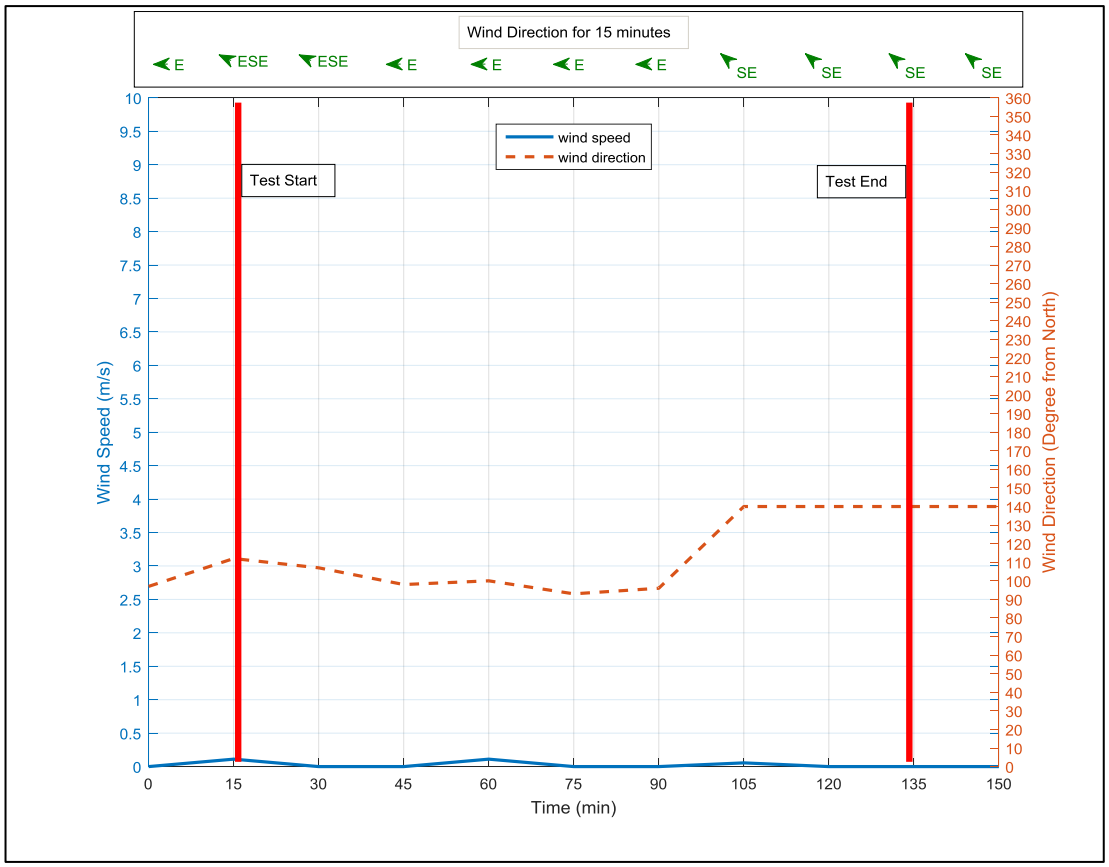

Figure 5-33: Weather condition (wind speed and direction) for transects from the curved movement on a 300 m radius for Test Number Fifteen.

The average water depth from the three lines of collectors were calculated and plotted as shown in Figure 5-34. The transect data shows that the water depth decreased slightly at collector Number One near the sprinkler, similar to the previous test with a curved radius of 200 metres. The water depth in the collectors furthest from the sprinkler were slightly higher than Test Number Fourteen as a result of wind influence, because the sprinkler pattern was between downwind and crosswind.

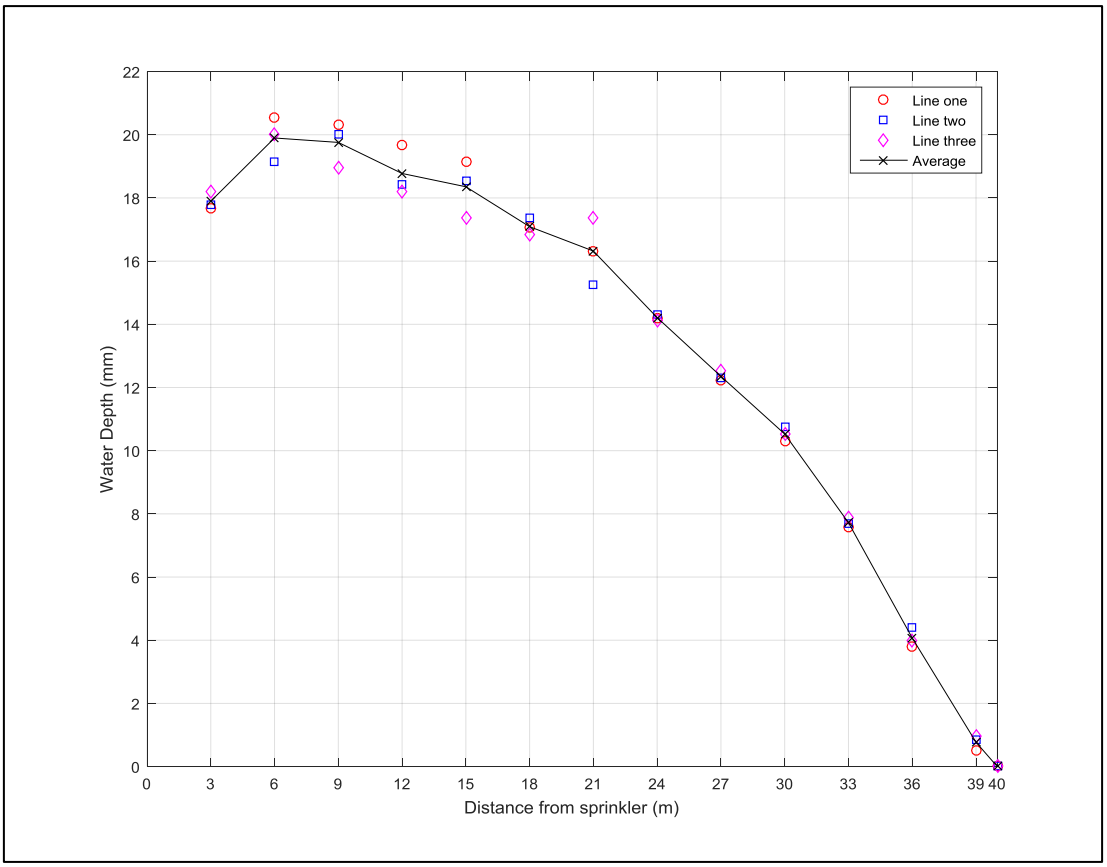

Figure 5-34: Transect data for Test Number Fifteen of a curve movement of 300-metre radius testing for a combination of a 180° wetted sector angle and a 270° side sector angle.

5.5.3 Measured transect data from Test Number Seventeen

Transect Test Number Seventeen was performed on Tuesday 9 June 2015 from 5:00 pm to 6:45 pm with a wetted sector angle of 180° and a side sector angle of 270°. The curved movement was on a 400 metre radius. The test layout in relation to travel direction, northerly direction and average active wind speed and direction are shown in Figure 5-36.

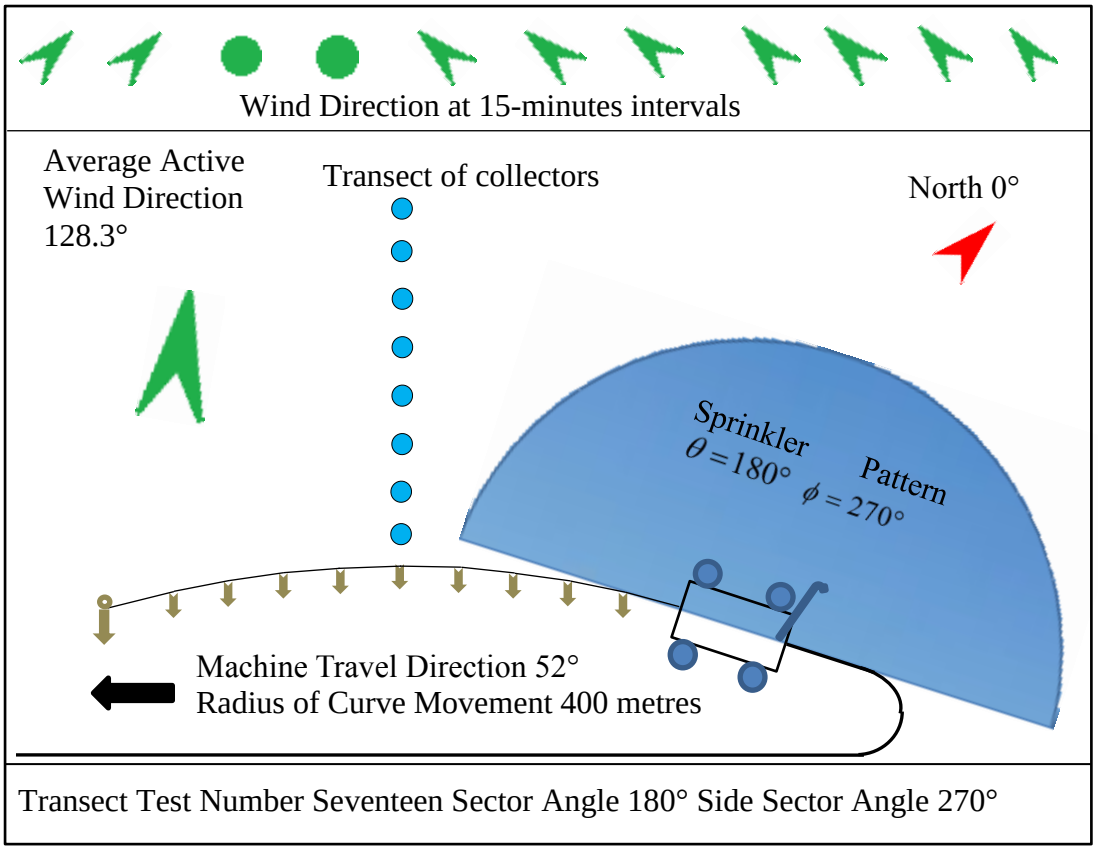

Figure 5-35: Transect test layout for a curved movement on a 400 metres radius and weather conditions during Test Number Seventeen.

Weather conditions were recorded during the test and plotted as shown in Figure 5-37. The figure shows wind speed was low during the test. However, wind speed changed slightly during the test. Wind direction changed widely between South, East, East-South-East and West. Average wind speed was 0.194 m/s. Average active wind speed and direction was 128.3° (South-East).

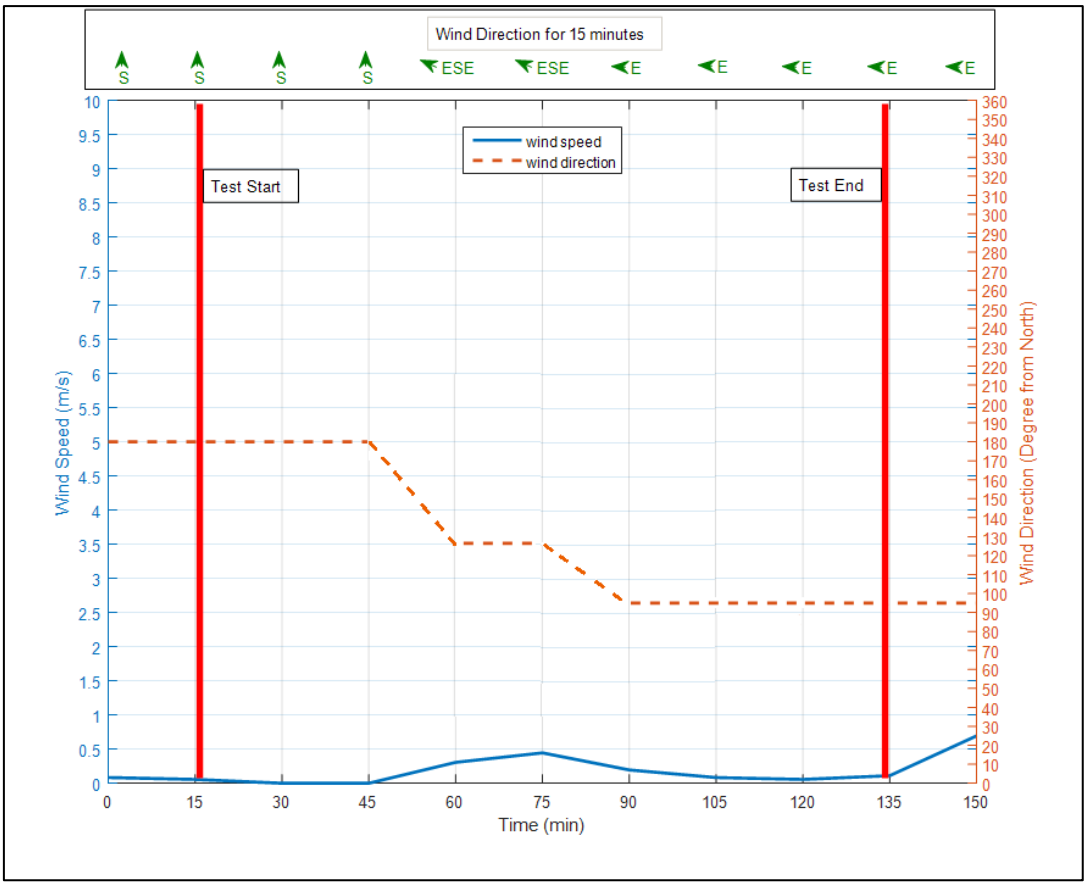

Figure 5-36: Weather conditions (wind speed and direction) for a transect from curved movement on 400m radius for Test Number Seventeen.

The average water depth from the three lines of collectors were calculated and plotted as shown in Figure 5-38. The transect data shows that the water depth decreased slightly at collector Number One nearest the sprinkler, similar to the curve movement in the previous tests. Water depth at the collectors furthest from the sprinkler were lower as a result of range shortening because the sprinkler pattern was between crosswind and upwind in relation to the travel direction with the wind speed influence from the East and West. Average active wind direction (South-East) could not be considered to justify the lower water depth in the collectors furthest from the sprinkler because the wind direction changed widely from South to East and then from East to West.

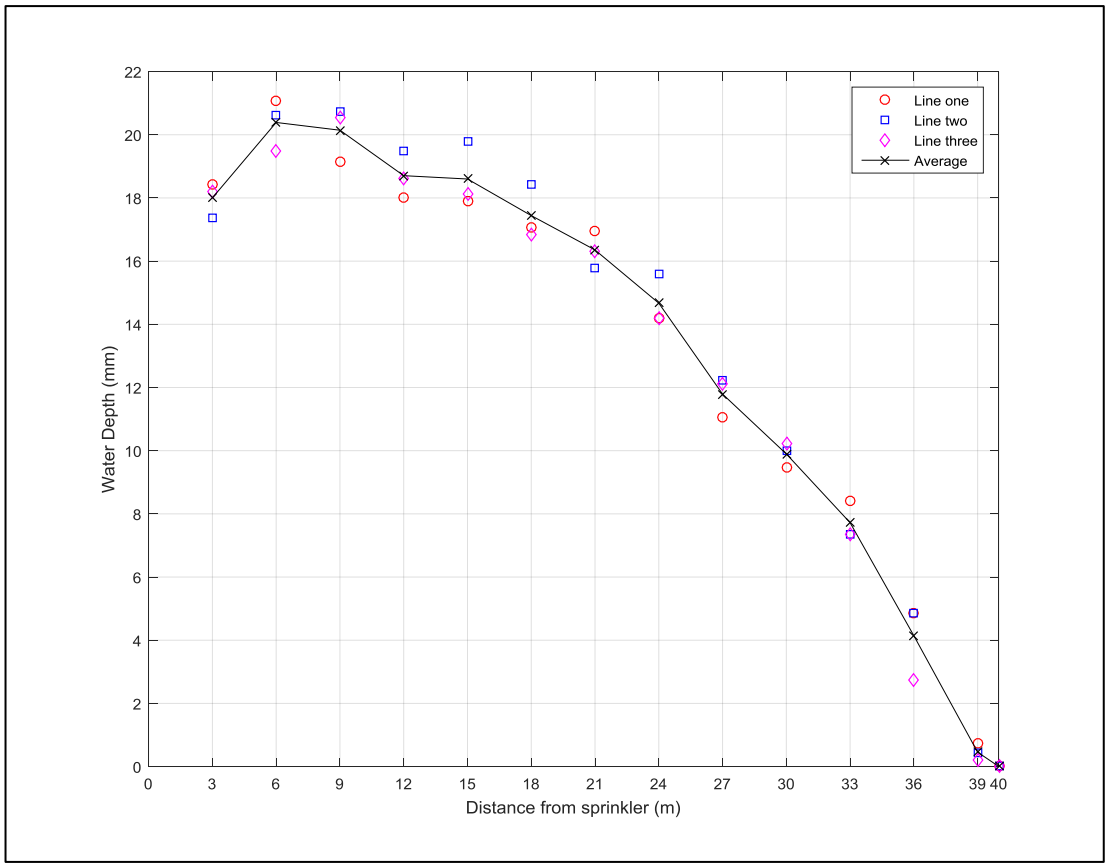

Figure 5-37: Transect data for test Number Seventeen for a curved movement on a 400 metre radius for the combination of a 180° wetted sector angle and a 270° side sector angle.

The three results of the curved movement show there is no significant effect of curved movement on water depth along the transect except in collectors near the sprinkler when compared with transects of the same combination of a wetted sector angle of 180° and a side sector angle of 270° when the machine travelled in a straight line. These results are consistent with those of Bittinger & Longenbaugh (1962). They concluded that when the radius of a circular sprinkler motion is greater than five sprinkler pattern radii, the application pattern as consider as a linear motion.

Tests Number Sixteen was performed during conditions of high wind speed. The result of this test is shown in Appendix B.

5.6 Recording zero wind speed during the measurements

It is very important for researchers to predict when quiescent wind (zero wind) will occur to allow them to perform the measurements to determine the zero wind radial leg. The following section documents the process used in this study to identify or predict when these ideal conditions will occur. The information in the images presented below demonstrate the new methodology that was introduced in Chapter Four to monitor weather forecasts. The images had been recorded online from a smartphone during this study using a screenshot technique. The results include three types of images of weather indicators from two weather forecast websites. The first indicator is an image from www.weatherzone.com.au that includes a toolbar of wind speed and direction for the future seven days for the region containing the experimental field. The second indicator is an image of a synoptic weather chart, namely, the mean sea level pressure (MSLP) map from the Bureau of Meteorology (www.bom.gov.au), Australia's official weather forecaster, for all the regions that surround the region of the experimental field when the minimum wind speed occurs. The third indicator is a screenshot of current weather conditions that includes the indicators of current wind speed and direction from www.weatherzone.com.au.

The record of zero wind will be organized by date and time. The first period of zero wind will be shown in this chapter and the other records of zero wind will be shown in Appendix C.

5.6.1 First Record of zero wind speed

The first documented record of zero wind happened on Thursday 26 March 2015. Figure 5-38 was captured on Wednesday 25 March 2015. The image shows that

forecasted wind speed in the toolbar is different during the next seven days. The lowest wind speed was expected to occur on Thursday 26 March 2015 after 3pm. The wind direction toolbar indicates that the wind direction will change from East-North-East at 9 am to West at 3 pm.

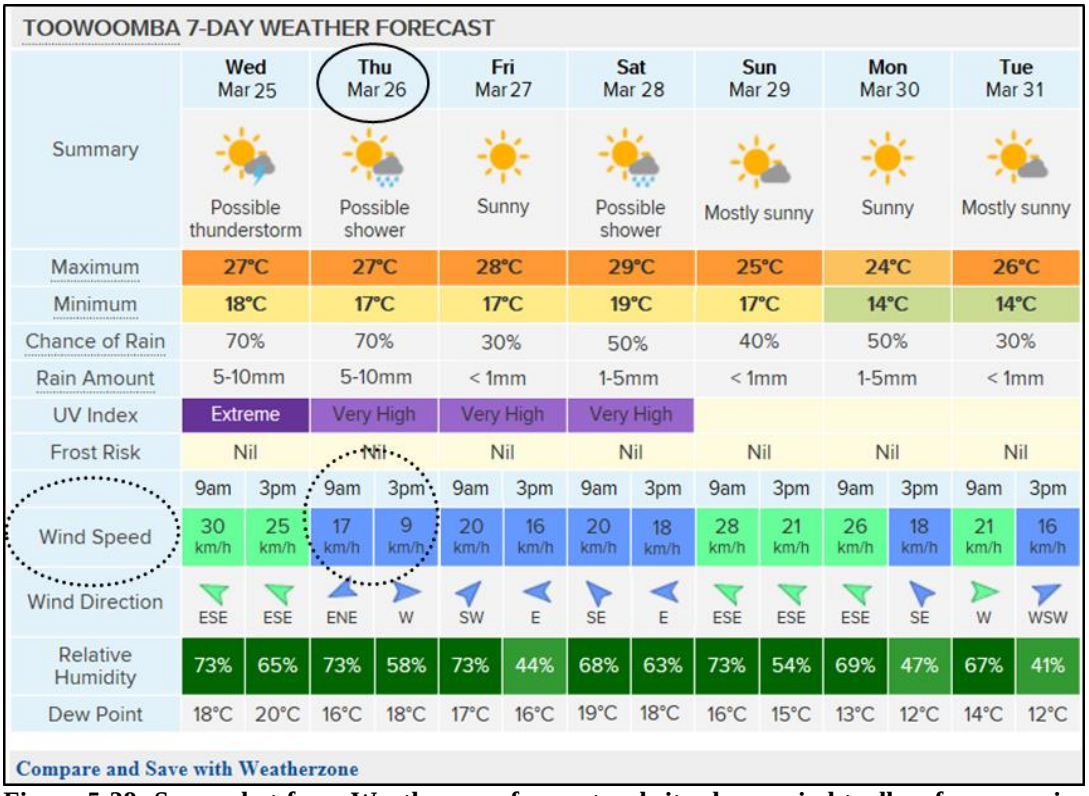

TOOWOOMBA 7-DAY WEATHER FORECAST

	Wed Mar 25	Thu Mar 26	Fri Mar 27	Sat Mar 28	Sun Mar 29	Mon Mar 30	Tue Mar 31
Summary	Possible thunderstorm	Possible shower	Sunny	Possible shower	Mostly sunny	Sunny	Mostly sunny
Maximum	27°C	27°C	28°C	29°C	25°C	24°C	26°C
Minimum	18°C	17°C	17°C	19°C	17°C	14°C	14°C
Chance of Rain	70%	70%	30%	50%	40%	50%	30%
Rain Amount	5-10mm	5-10mm	< 1mm	1-5mm	< 1mm	1-5mm	< 1mm
UV Index	Extreme	Very High	Very High	Very High			
Frost Risk	Nil	Nil	Nil	Nil	Nil	Nil	Nil

	9am	3pm	9am	3pm	9am	3pm	9am	3pm	9am	3pm	9am	3pm	9am	3pm
Wind Speed	30 km/h	25 km/h	17 km/h	9 km/h	20 km/h	16 km/h	20 km/h	18 km/h	28 km/h	21 km/h	26 km/h	18 km/h	21 km/h	16 km/h
Wind Direction	ESE	ESE	ENE	W	SW	E	SE	E	ESE	ESE	ESE	SE	W	WSW
Relative Humidity	73%	65%	73%	58%	73%	44%	68%	63%	73%	54%	69%	47%	67%	41%
Dew Point	18°C	20°C	16°C	18°C	17°C	16°C	19°C	18°C	16°C	15°C	13°C	12°C	14°C	12°C

Compare and Save with Weatherzone

Figure 5-38: Screenshot from Weatherzone forecast website shows wind toolbar for upcoming seven days, and the solid circle displays the date and the dotted circles display the wind speed and time (Weatherzone, 2015b).

Next, the image of the MSLP map at 5 pm on Thursday 26 March 2015 (Figure 5-39) shows the region at the experimental site (letter T in the centre of the five-point star) is not part of the influence of any of the different curving patterns of mean sea level pressure isobars (lines of equal atmospheric pressure) that are situated near the region of the experimental site.

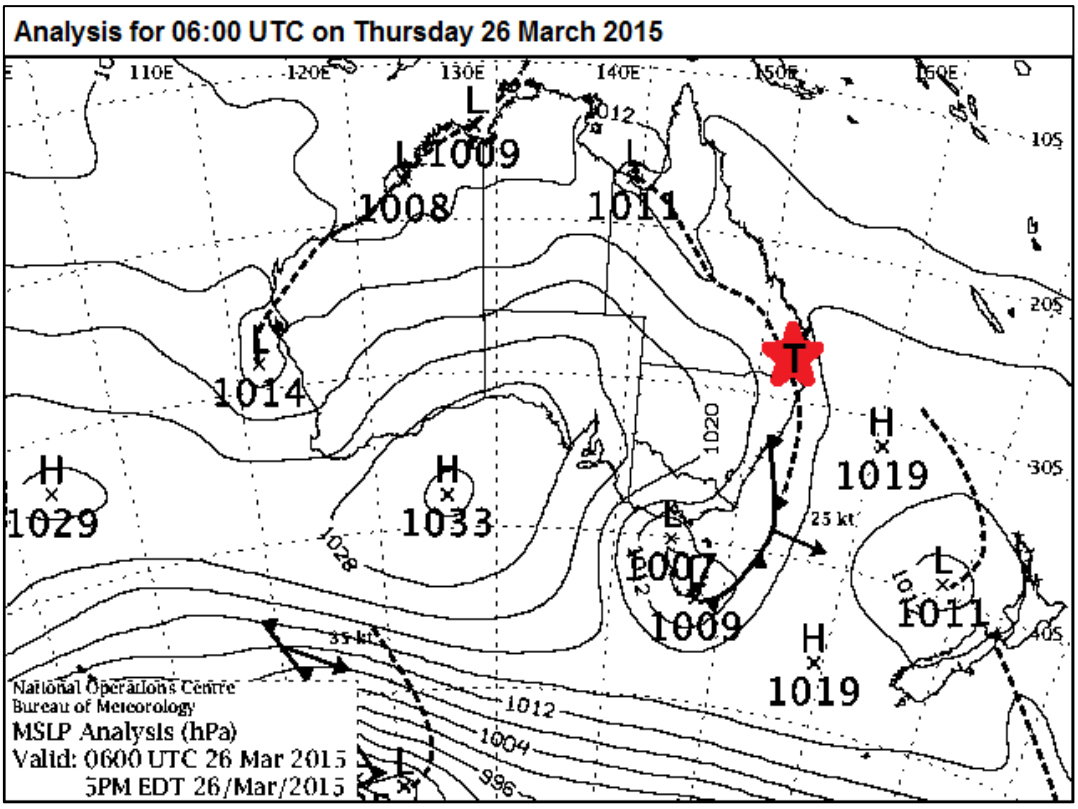

Figure 5-39: Synoptic pressure systems that, surround the experimental site (Bureau of Meteorology, 2015a).

The pressure map analysis at that date shows there is a good chance of zero wind on this night. Figure 5-40 shows four different pressure systems situated around the region of the experimental site (letter T in the centre of the five point star). The extended isobars of the two high pressure systems at the West and East are not far from the region of the experimental site. The extensions of the two low pressure systems at the North-West and South-West are far from the region of the experimental site. The centres of these pressure systems are far from the region of experimental site except for the centre of the high-pressure system to the East of the region of the experimental site. The next stage is to remotely monitor and record current wind speed periodically, in order to understand the behaviour of wind speed, either increasing or decreasing. The following images for current wind speed in Figure 5-40 show four stages of gradually decreasing wind speed after sunset, from quiescent wind speed until it reached zero on Thursday 26 March 2015.

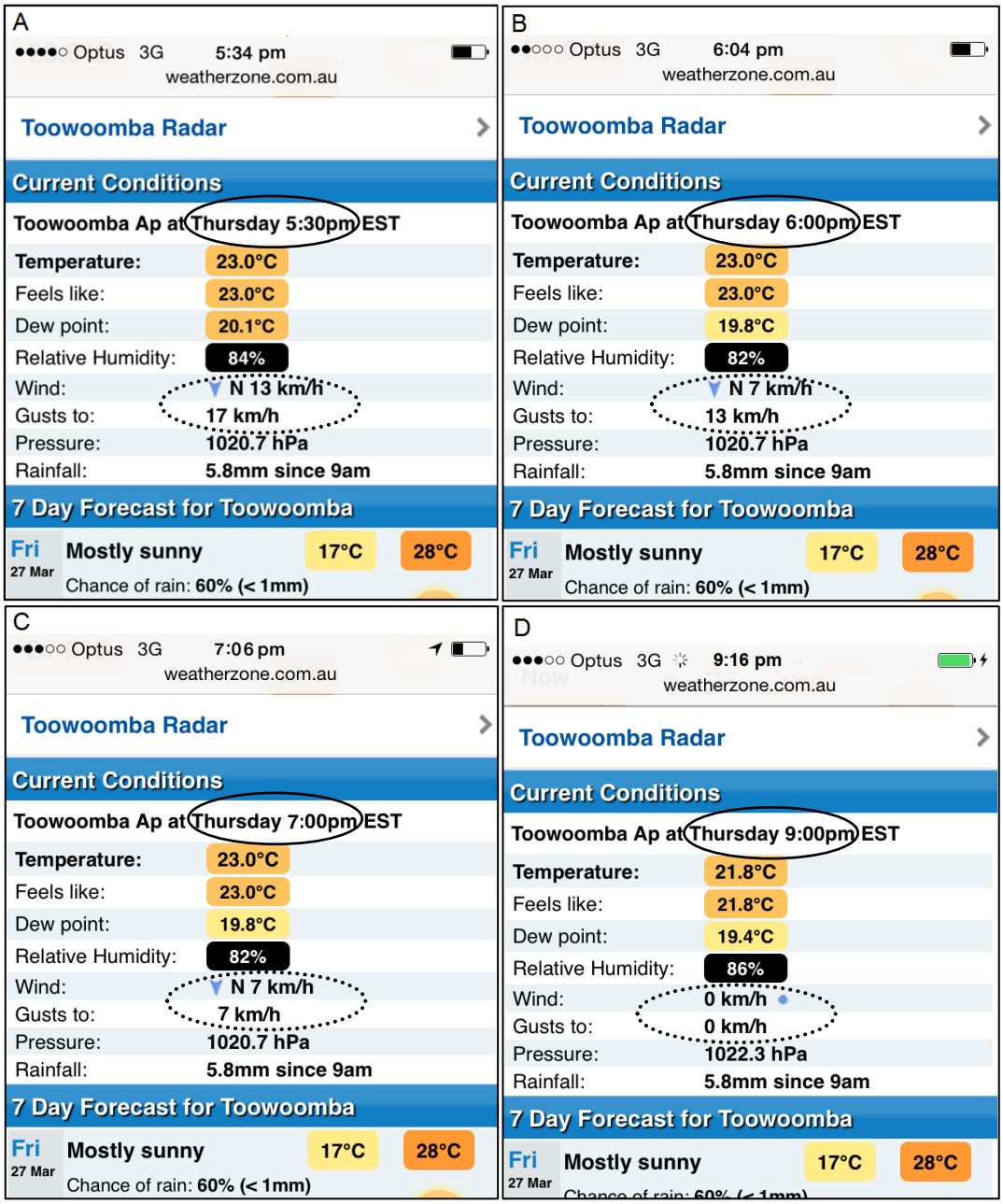

Figure 5-40: Four screenshots show current wind speed decreasing gradually at that date until it reached zero. The solid circle displays the time and the dotted circle displays wind speed (Weatherzone, 2015b) record two.

The first image (A) shows current wind speed was 13 km/h with wind gusts to 17 km/h at 5:30 pm. The second image (B) shows current wind speed was 7 km/h with wind gusts to 13 km/h at 6:00 pm. The third image (C) shows wind speed was 7 km/h with similar wind gusts at 7:00 pm. Finally, image (D) shows wind speed reached zero at 9:00 pm.

The period of zero wind speed was recorded for more than 90 minutes. Zero wind started at 9:00 pm, as shown in image (D) Figure 5-40. The images in Figure 5-41. show wind speed remaining at zero at 9:30 pm in image (A) until 10:30pm in image (B).

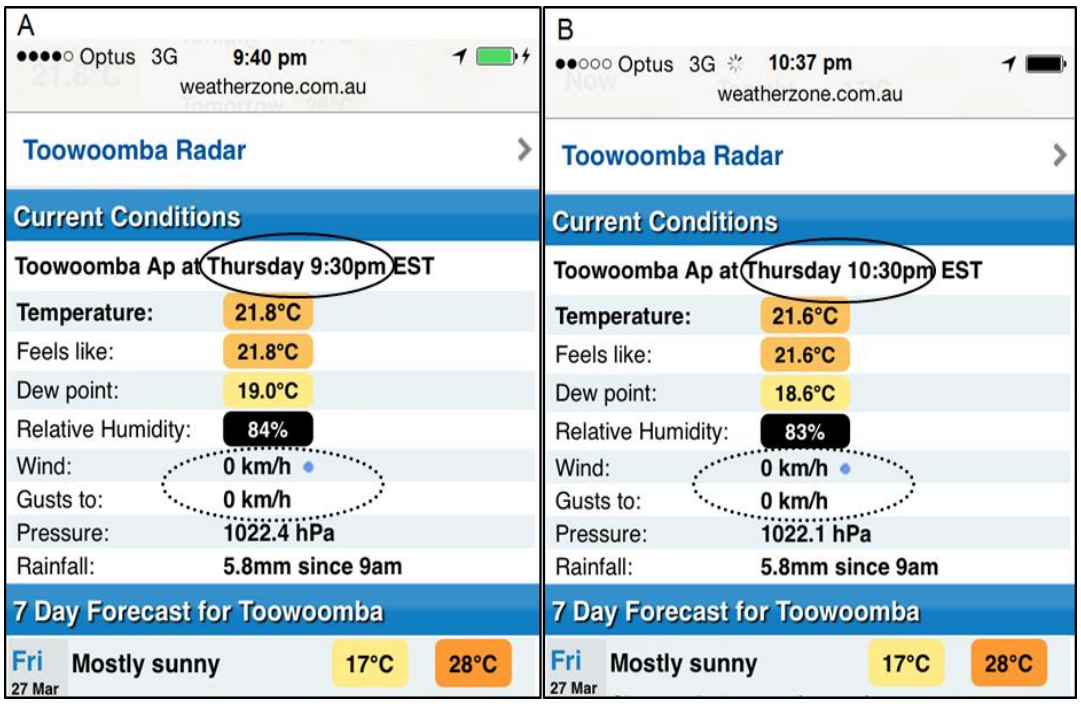

Figure 5-41: Two screenshot at different times show a period of zero wind for more than hour (Weatherzone, 2015b) record one.

Records of zero wind shown in this chapter and in Appendix C for the specific conditions of the experimental site at the University of Southern Queensland (Toowoomba City) in relation to altitude, longitude and latitude, as described in Chapter Four, were analysed and produced the following results: firstly, wind speed decreases to zero, as shown in records one to six, when the region of the experimental site is not part of the influence of any different pressure systems and the isobars do not intersect with the region of the experimental site; secondly, zero wind speed may occur at any time during the year, but is most likely to occur in winter; thirdly, the period of zero wind is longest during winter compared to other seasons; and finally, zero wind is more likely to happen during the night time rather than during the day time.

5.7 Summary

This chapter has presented the results of the many field measurements. The first section presented measuring radial leg data from three and four lines of collectors placed radially around the sprinkler from a full circle of sprinkler rotation in open field. The first section also presented the analysis of wind conditions during the measurement time and the effect of the wind on the radial leg data. Two dimensional spray patterns were generated from the radial legs using MATLAB to interpolate the application rate between the measured lines of collectors. The analysis showed that using taper ring nozzles results in a high variation in the application depth near the sprinkler as a result of producing small droplet sizes near the sprinkler centre, and using the average of three and four lines of collectors around the sprinkler can reduce this variation and the experimental error. The second section presented the measurement of transect data for different combinations of wetted sector and side sector angles perpendicular symmetrical and asymmetrical to the direction of travel, and presented the weather conditions during each tests. The overall results of the transect tests shows that the density of applied water depth moves from the centre of the sprinkler toward the outer end whenever wetted sector angle decrease. In addition, the second section presented transect data for travelling machines on straight and curved paths to explore the effect of the curved movement of end-guns on centre pivots. The results of the curved movement tests did not determine the actual effect of the curved movement, except for decreasing the water depth in the first collector. Finally, this chapter presents an example of the process to identify periods of zero wind speed.

6 CHAPTER SIX

Validation of the new sub-model to estimate the sprinkler radial leg

6.1 Introduction

Chapter 3 introduced a new mathematical model which was capable of determining the sprinkler radial leg from a wider range of sector angles and side sector angles than was previously possible. Subsequently this model was incorporated into a revised version of TravGUN, named TravGUN Version 3.1. This chapter focuses on the validation of this new TravGUN sub-model by comparing the measured and predicted radial legs of different combinations of wetted sector and side sector angles. The measured radial leg used in this chapter refer to the average of the stationary gun field measurement tests at the lowest wind speed, i.e. Tests Number Seven and Eight, presented in Chapter 5. The predicted radial leg was produced using TravGUN V3.1 from the measurements of the catch can transects at different combinations of wetted sector and side sector angles. Graphs and statistical methods are used to compare the measured radial leg and the predicted radial leg. This validation is best performed under quiescent wind conditions so that the fit of the model is not impacted by wind distortion. For this reason only those tests where the wind speed is less than 1 m/s have been included in this chapter. The validation presented in this chapter demonstrates the ability of the model to account for side sector angles perpendicular to the direction of travel, and those not perpendicular to the direction of travel. This chapter also

investigates the impact of the curved end-gun travel movement on the measured catch can transect for a typical wetted sector angle and side sector angle.

6.2 Validation of the predicted radial leg for combinations of different wetted sector angles perpendicular to travel direction

This section will describe the comparisons performed to validate simulated results from the new sub-model with measured data with the side sector angle, ϕ, perpendicular to the travel direction. The validation includes tests performed for the combinations of wetted sector angles, θ = 180°, 140°, 105° and 80° with a ϕ of 270°.

6.2.1 Validation of predicted radial leg from transect of wetted sector angle $\theta =$ 180° and side sector, $\phi =$ 270°

Several field tests were performed with the end-gun sprinkler configured with a $\theta = 180^{o}$ and $\phi =$ 270°. The measured transects collected with the lowest wind speeds were selected as the input data for TravGUN V3.1 to predict the radial leg. The measured radial leg is from the stationary gun test as described above. The measured and predicted radial legs are plotted in Figure 6-1 for the combination of $\theta =$ 180° and $\phi =$ 270°. This figure of sprinkler application rate versus radial distance shows strong agreement between the shapes of the measured and predicted radial legs over most of the radial distance. However, the predicted radial leg deviates from the measured data over the first third (closest to the nozzle) which is especially noticeable for the first point. Between 15m and 40m the predicted and measured radial legs are almost

identical. As described in Chapter 3 the calculations for the predicted radial leg commence at the outermost radius and proceed towards the gun. This means that any small errors will accumulate and be greatest at the smaller radii. Fortunately, the variation in the first third of the pattern near the sprinkler can be considered as having a small impact on applied depths, because like all radial spray patterns the outer radius of the sprinkler has a greater contribution to the applied depths. The root mean square error (RMSE) between the measured and predicted radial leg was 0.85 which is very low.

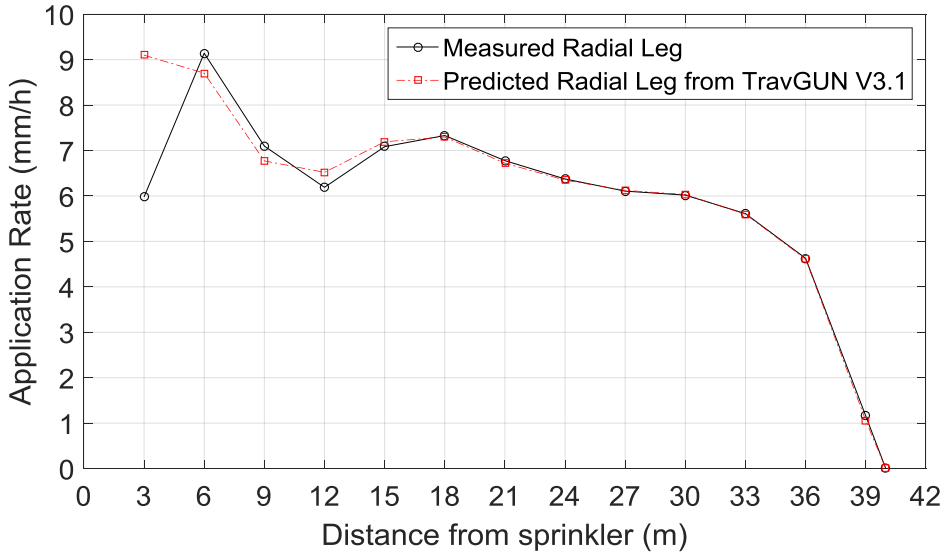

Figure 6-1: Measured and predicted radial legs for the combination of 180° wetted sector and 270° side sector angles at quiescent wind speed.

The maximum difference, apart from the first point, is roughly 0.35 mm/h at 6 and 12 metre radial distancesTravGUN provides a good prediction of the radial leg, however there is a large difference in the application rate at the first point near the sprinkler. This same difference is also present in the other transects below. There are two possible explanations for this, firstly that the model assumes that the radial leg between a radius of zero and the first catch can is equal to the nearest value and secondly that the volume in the transect catch cans from this part of the radial leg is very small relative to the

total volume and is therefore sensitive to any errors in the rest of the predicted radial leg.

6.2.2 Validation of predicted radial leg from transect of wetted sector angle 140° and side sector 270°

The same analysis was completed for a measured transect collected when the sprinkler was operating with a 140° wetted sector angle and a 270° side sector angle and simulated radial leg from TravGUN V3.1. The resulting comparison in Figure 6-2 between the two radial legs shows good agreement.

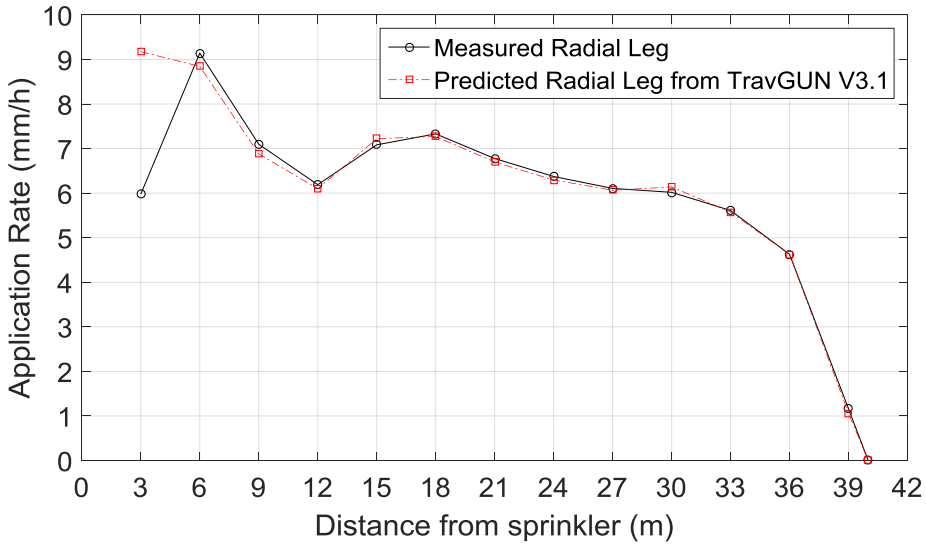

Figure 6-2: Measured and predicted radial legs for the combination of 140° wetted sector and 270° side sector angles at quiescent wind speed.

The result looks similar to the previous test result presented in Section 6.2.1 and Figure 6-1, with the predicted radial leg deviating slightly at small radial distances from the nozzle. The root mean square error was found to be 0.86, which is also very low. The maximum difference in application rate was roughly 0.2 mm/h at 6 metres distance, for those values beyond the 3 metre radius.

6.2.3 Validation of predicted radial leg from transect of wetted sector angle 105° and side sector 270°

The predicted radial leg from TravGUN V3.1 was compared with the transect measured under a combination of a wetted sector angle of 105° and a side sector angle of 270°, shows good agreement (Figure 6-3). The predicted radial leg shape looks similar to the validation tests number in Section 6.2.1 and 6.2.2 for different combinations of wetted sector and side sector angles. However, there are a minor variations between the predicted and measured radial legs for individual points. The root mean square error between the predicted and measured points is 0.85 for this comparison. Noticeable differences in application rate between simulated and measure data, occurred at radial distances of 6, 9, 15 and 24 metre radial distances, for those beyond the first collector.

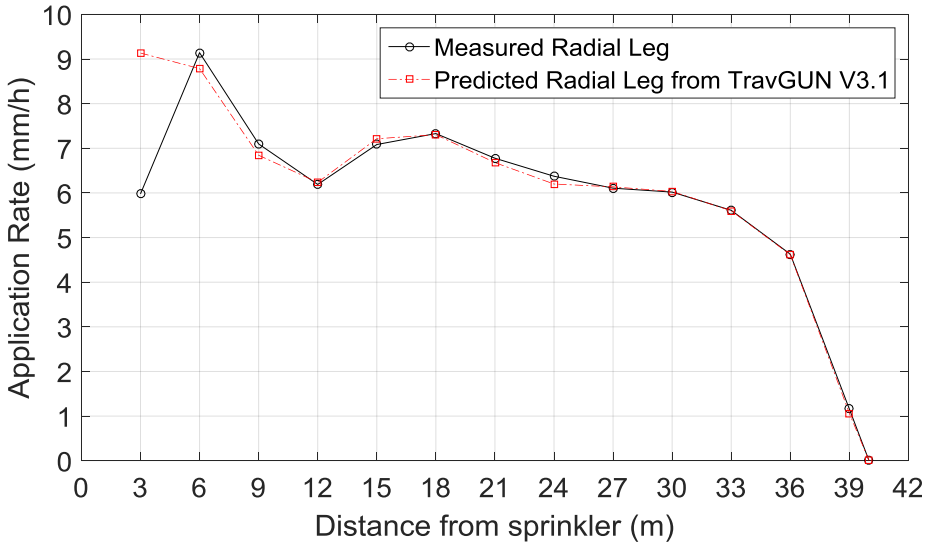

Figure 6-3: Measured and predicted radial legs for the combination of 105° wetted sector and 270° side sector angles at quiescent wind speed.

6.2.4 Validation of predicted radial leg from transect of wetted sector angle 80° and side sector 270°

In a similar manner to the previous sections, the transect corresponding to the lowest wind speed for a sector angle of 80°, and a 270° side sector angle was generated by TravGUN V3.1 to produce a predicted radial leg. This predicted radial leg is plotted with the measured radial leg from the stationary test in Figure 6-4. As observed in the previous tests the predicted line shows a high degree of consistency for the outer two thirds of the sprinkler throw. However, the variation between the two radial legs in the first three points near the sprinkler were considerably higher than in previous comparisons, as shown in Figure 6-4. However, the root mean square error between the results is still a low 0.68.

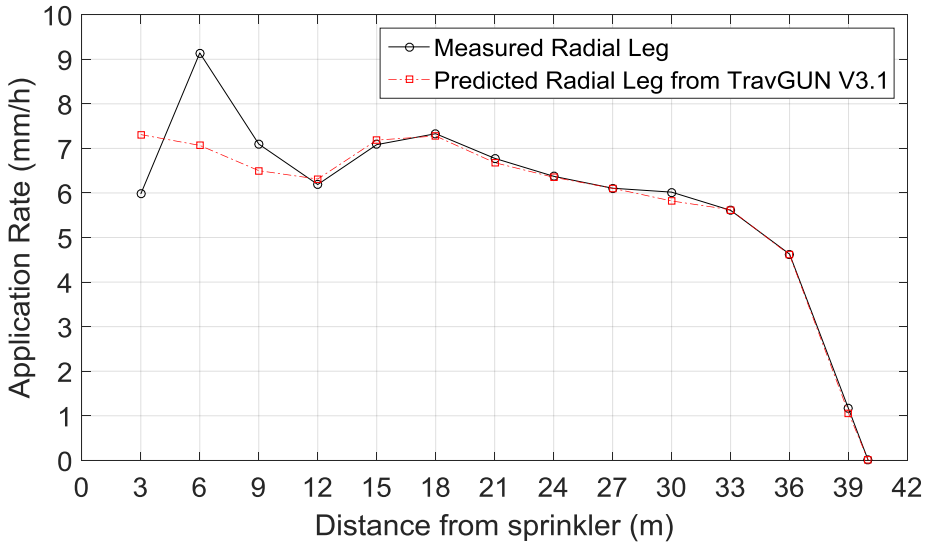

Figure 6-4: Measured and predicted radial legs for the combination of 80° wetted sector and 270° side sector angles at quiescent wind speed.

6.3 Validation of the combination of wetted sector angles not perpendicular to travel direction

The four comparison results above are examples where the orientation of the wetted sector is exactly perpendicular to the path of the travelling gun. A further test was conducted to demonstrate that the new model would also function correctly for scenarios where orientation of the wetted sector angle is not perpendicular to the travel direction, with side sector angles other than 270°.

One of the field test results was conducted using a wetted sector angle of 160° and a side sector angle of 290° in low wind conditions, and is used as an example data set for non-perpendicular sector orientation. The data was analysed in the same manner as for the previous comparative tests, using transect data as processed by TravGUN V3.1 to predict the sprinkler radial leg. The resulting predicted and measured radial legs are shown in Figure 6-5.

Here there is a high degree of consistency between the predicted radial leg and the measured radial leg as shown in Figure 6-5. As for the perpendicular tests the two lines deviate from each other in the first third points near the sprinkler. The root mean square error was 0.87 which is the highest compared to previous comparison in Sections 6.2.1 through 6.2.4. However RMSE is only slightly higher than for the previous tests meaning that no conclusions can be made that the model is working in a less favourable manner in this comparison when compared to the perpendicular wetted sector tests.

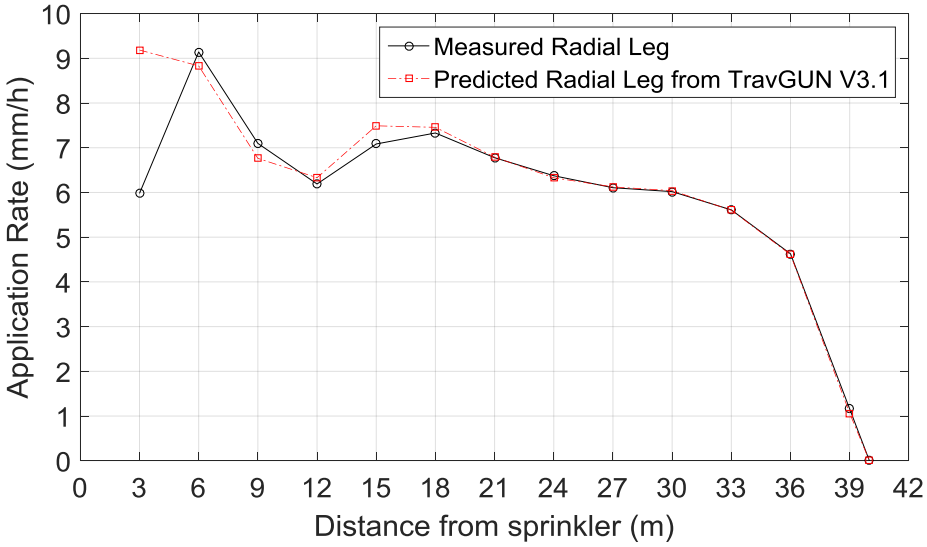

Figure 6-5: Measured and predicted radial legs for the combination of 160° wetted sector and 290° side sector angles at quiescent wind speed.

6.4 The comparison of different curved movement for wetted sector angle of 180° and a side sector angle of 270°

This part of the chapter will investigate the impact of the curved movement of the gun on the applied field depths through measurement of catch can transects. The machine was configured with a wetted sector angle of a 180° and side sector angle of 270°.The methodology for these tests is described in Section 4.8 and the preliminary field measurements are presented in Section 5.5. The standard transect of 180° wetted sector angle and a 270° side sector angle for straight travel movement will be compared with the same angle configuration for curved movement on radii of 200 metres, 300 metres and 400 metres, respectively, to ascertain the effect of different curve movements on the end gun transect data sets.

6.4.1 Comparison of transect from curved and straight movement at a 200-metre radius

In this test the sprinkler was configured as described above while the travel direction followed a curved path to simulate the movement of an end gun on a 200 metre long centre pivot. Figure 6-6 shows a comparison between the catch can transect measured as a result of this curved movement and the corresponding results of the same sprinkler with a straight travel path. The results show that both transects have a similar shape but that the data from the curved transect test is consistently lower than that of the straight test. In addition, the decrease was higher at the first two collectors near the sprinkler compared with the rest. The root mean square error between the two tests was 1.92. There are two factors, which might possibly explain the difference between the two transects. The first of these is the weather conditions. The wind speed and direction for the 200m curved test in Figure 5-30 shows that wind speed was slightly active and increasing at the end of the test up to 0.5 m/s. The average active wind direction was 57° and the pattern travelling direction was 52°. So, the average active wind direction was cross wind as shown in Figure 5-29. These wind conditions would cause the length of the pattern to shorten and become slightly compressed.

The second potential source of the difference is the curve movement. The effect of curve movement is the result of two actions. The first is the dynamic change in travel direction. This dynamic change affects the sector angle when it intersects with the transect at different points of the curved movement. In addition, the curved travel movement for this test is not smooth similar to end-gun on centre pivot. Because, the tangent angle changes sharply at each 5 metres intervals. The second is the difference in time for which a particular catch can is within the wetted sector angle of the gun.

The end result is that the same application rate from the sprinkler is spread over a larger area and therefore the applied depths should be lower than for the equivalent gun operating with a straight travel lane. The results in Figure 6-6 appear to confirm this expected behaviour as the applied depths measured by the collectors in the curved test are consistently lower than for the straight test.

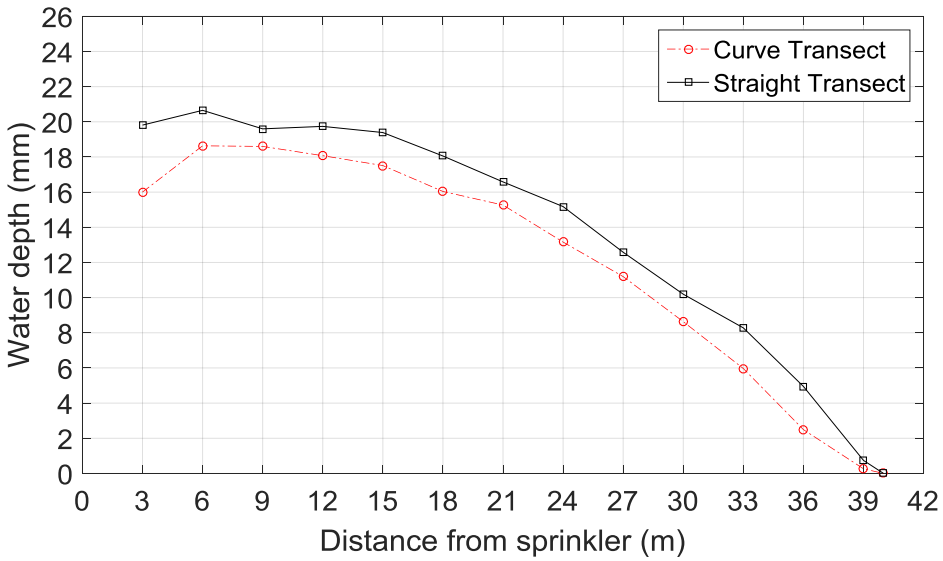

Figure 6-6: Comparing the measured transect for the combination of 180° wetted sector and 270° side sector angles for a curve movement of a 200-metre radius with a transect measured with a straight movement.

6.4.2 Comparison of transect from curved and straight movement at a 300-metre radius

The same methodology was repeated with a curved movement of radius equal to 300 metres. The curved and straight travel transects in this test show a high degree of consistency in the trends of water depth over distance, as shown in Figure 6-7. The differences in water depth between the two transects is lower than in the previous test because wind speed during this test was very low, albeit with some wind action on three short occasions, as shown in Figure 5-32 and Figure 5-33. The root mean square error was 0.94.

The variation in water depth in the collectors near the sprinkler was higher than at the collectors far from the sprinkler. The reason for this variation was not only the result of the curve movement. Wind direction also resulted in the small water droplets near the sprinkler pattern moving slightly away from the centre of the sprinkler in a downwind direction, as shown in Figure 5-32 and Figure 5-33. Therefore, the wind effect was downwind with regard to the X and Y axes of the sprinkler pattern direction. Therefore, if we disregard the little wind effect from this test, we can conclude that curved movement does not have a significant effect on the transect shape, it only alters the water depth.

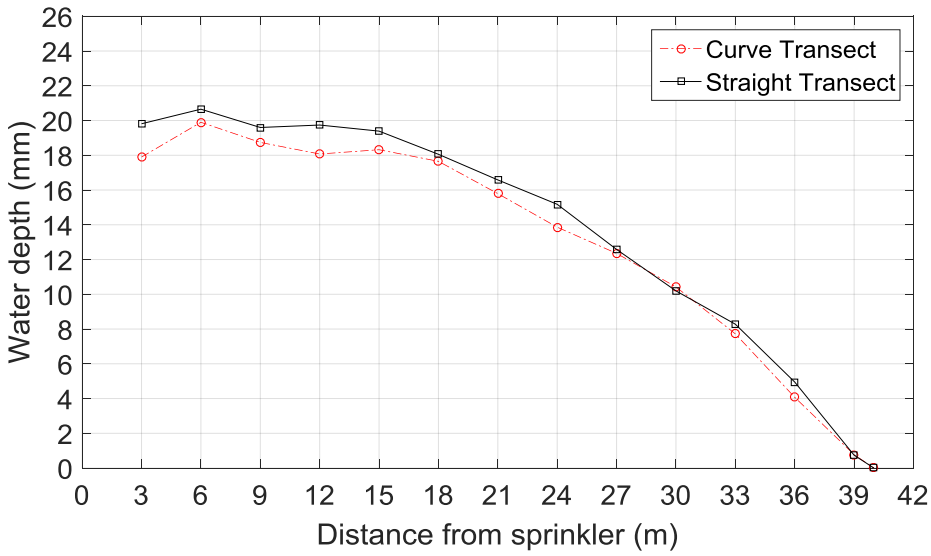

Figure 6-7: Comparing the measured transect for the combination of 180° sector and 270° side sector angles for a curve movement of a 300-metres radius with a transect measured with a straight movement.

6.4.3 Comparison of transect from curved and straight movement at a 400-metre radius

The methodology was repeated again to simulate the movement of an end gun on the outer radius of a 400m centre pivot, with the resulting measured transects shown in Figure 6-4. In this test there is a large variation in water depth at the first collector

between the curved and straight transects. The two transects are very simular for the rest of the collectors. In a similar manner to the 200m radius test, the curved path test will differ from the straight test due to both wind conditions and the curved path itself. The record of weather conditions during the test in Figure 5-35 and 5-36 shows that wind speed was higher than the previous tests and wind direction was also highly variable during the test. Figure 5-35 shows that the average active wind direction had a downwind effect according to the X and Y axes directions for the sprinkler pattern. This wind effect made the sprinkler pattern shift from the first collectors downwind along the transect. This movement in very small water droplets resulted in highly reduced water depth at the first collector and an increased water depth at the collectors in the middle distance of the transect. The statistical analysis for this test shows higher value of 2.40 for RMSE, compared to the curved movement for 200 m and 300 m radii respectively, but this is not likely due solely to the large difference in depth measured at the closest collector to the end-gun. According to this result in relation to wind speed and direction, it is not possible to find and justify the effect of curved movement for this test.

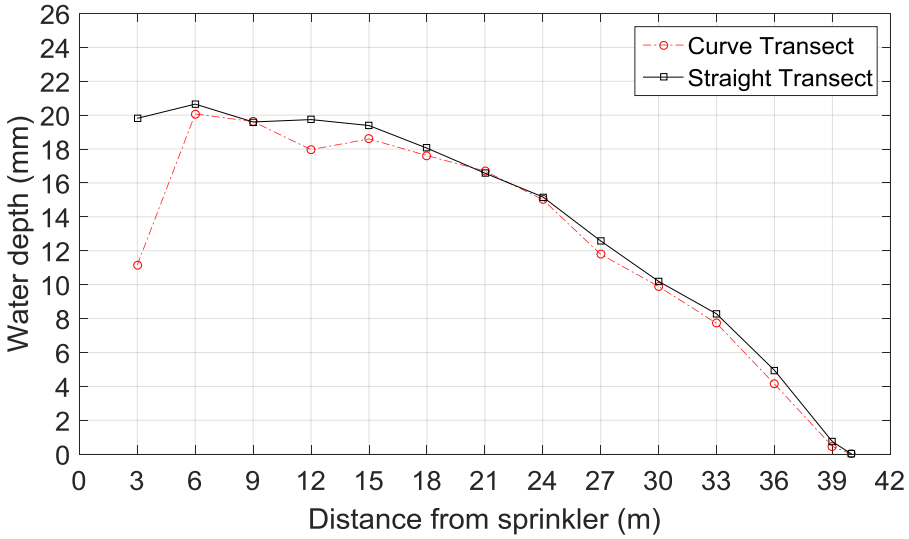

Figure 6-8: Comparing the measured transect for the combination of 180° wetted sector and 270° side sector angles for a curve movement of a 400-metre radius with a transect measured with a straight movement.

6.4.4 Comparison of three curved transects

The comparison between the three curved transects of 200 m, 300 m and 400 m radius for the same wetted sector angle of 180° and a side sector angle of 270° in Figure 6-9 shows that there is a decrease in water depth in the curved transect of 200 m radius compared to other curved transects of 300m and 400 m. The comparison also shows, there is a slight variation in the shapes of the three transects. It is difficult to make any conclusions on the impact of the curved movement on the transects based on these tests, because of the different wind conditions during these tests. It is likely that the impact of the curved movement will be small and in this case it might be difficult to separate this from other sources of variation such as wind speed, wind direction and inaccuracy in configuring the sector angle or machine speed. Therefore, the effect of curved movement will be investigated instead using separate modelling in the following chapter to avoid these other possible factors.

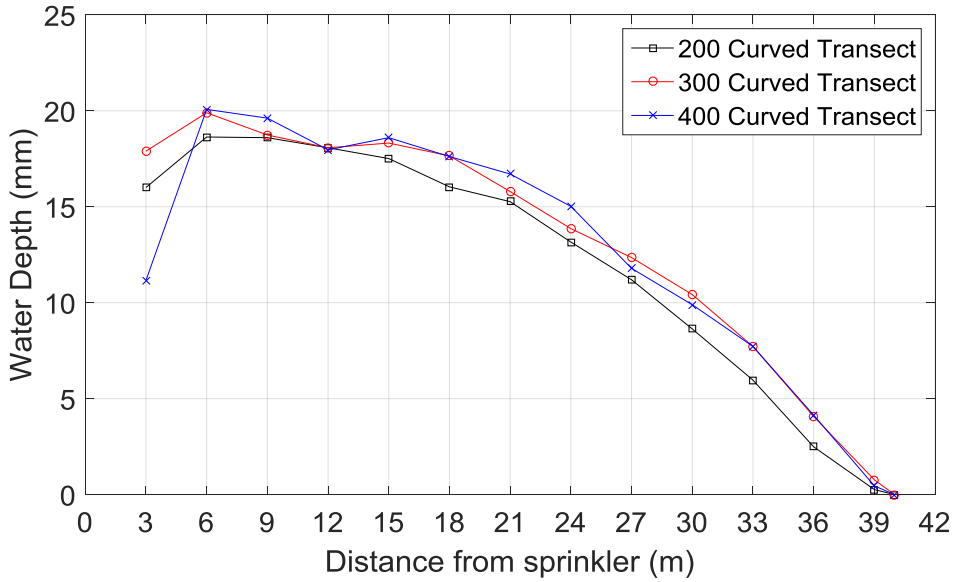

Figure 6-9: A comparison between the three curved transects for 200 m, 300 m and 400 m radii for the same wetted sector angle of 180° and a side sector angles of 270°

6.5 Discussion and conclusions

6.5.1 Validation of the new sub-model in TravGUN

The new mathematical model that was developed in Chapter 3 was written using MATLAB script, and then the algorithms were incorporated into TravGUN resulting in the new Version 3.1. The predicted radial legs, using TravGUN V3.1 for a range of different combination of wetted sector and side sector angles perpendicular and non-perpendicular to the direction of travel, have been compared against the measured radial legs. The graphical comparisons show clearly that the predicted radial legs have similar shapes and trends to the measured transects. The statistical analyses show low value of RMSE for all tests. These validation results have proved that both the algorithms coded in the MATLAB script and TravGUN V3.1 are working correctly and perfectly for different combinations of wetted sector and side sector angles. The predicted transect from the side sector angle perpendicular to the direction of travel with the greatest wetted sector angle, shows closest match between predicted and measured radial legs, when compared to those simulated results from the smallest wetted sector angle, especially in the application rate nearest the sprinkler. Further, the predicted transects from side sector angles that were not perpendicular to the direction of travel, show the highest RMSE values of any comparison.

6.5.2 Impact of the curved movement of the end-gun

The comparisons of the effect of curved movement against straight movement on transect of water depth, for the same wetted sector and side sector angles show that there are minimal differences in transect shape for the combination of a sector angle of 180° and a side sector angle of 270°, for a curved movement of 300 metres radius at slow wind speeds. The result for this test agrees with the findings of Bittinger &

Longenbaugh (1962) who concluided there is little effect where the ratio for the radius of the rotation to the sprinkler pattern radius was greater than 5 for all the testsThey assume for practical purposes that the circular movement produces transect and applied depth results very similar to the linear movement. The recorded wind speeds for the other tests show that there was active wind (gust) during the test periods. Therefore, the results of these tests could not be used to determine the effect of curved movements.

7 CHAPTER SEVEN

Optimising End-Gun Performance under Windy Conditions

7.1 Introduction

This chapter identifies the optimum combinations of wetted sector and side sector angles for an end-gun on a centre pivot under conditions of no-wind, and from simulated performance under different wind conditions, utilizing the new sub-model integrated with TravGUN to simulate the sprinkler patterns.

Firstly, with regard to the uniformity of applied water depths, this chapter includes the optimum wetted sector and side sector angles under conditions of no-wind, maximizing the effective radial distance that receives sufficient water depth when overlapped with the pattern of the outermost sprinklers on the pivot. Secondly, this chapter includes simulation results for the optimum wetted sector and side sector angles under prevailing wind speeds and directions for Toowoomba city, as an example, to discover the effects of wind on the irrigation performance from a full centre pivot rotation. Then, the effect of the curved movement on the applied water depth for a simulated end-gun pattern are estimated, using different approaches to validate the results. Finally, we present the results of the combined sprinkler pattern for a centre pivot irrigation machine with an end-gun, for both zero wind speed, and a prevailing wind at eight positions of a centre pivot, to represent the impact under a full rotation of the machine.

7.2 Optimizing wetted sector and side sector angles under no-wind conditions

The main differences between a travelling gun and an end-gun on a centre pivot have been described in Chapter Two. There is another difference between both in relation to the optimisation process. Optimisation of a travelling gun aims for the most uniform pattern of water depth using the best combination of wetted sector angle, side sector angle, trajectory angle and lane spacing. According to Al-Naeem (1993), the process of optimizing uniformity depends on selecting the best combination of these factors while maintaining the overlap between two or more runs of the sprinkler pattern. However, optimising the uniformity of an end-gun irrigated area from a centre pivot is entirely different from the travelling gun situation, because an end-gun combines and overlaps different sprinkler patterns at the distal end of the pivot, and it has only one pass to complete a uniform irrigation in that area. Hence, the best uniformity of water depth under an end-gun must be achieved with one pass using the best combination of wetted sector and side sector angles.

Wetted sector and side sector angles were initially selected from the ore reviewed literature, from Nelson Irrigation Corporation equipment information, and from local grower practice. Solomon and Kodoma (1978) concluded that for a single large end-gun sprinkler a properly oriented 135° sector angle and 67.5° side sector angle generally gives good results for end gun sprinklers uses with 12.7 to 20.3 mm diameter nozzles operating at 345 kPa. Keller and Bliesner (1990) recommended, a wetted sector angle of 150° with side sector angle 60° to operate continuously with a 15° inside segment to fill in water depth near the edge of the base circular pattern. Nelson Irrigation Corporation (2017a) specified a side sector angle of 75° with side sector

angle of 170° for the SR100 end-gun with 10° behind the machine to effectively match the target depth and maximise the uniformity. Local grower practice was a wetted sector angle of 180° and a side sector angle on 90° for an end-gun on a centre pivot.

The side sector angle is defined in Chapter Three as the angle from the direction of travel clockwise to the centre of the dry sector as per Section 3-2 and Figure 3-1.

Two factors are used in order to optimize the uniformity application of water. The first is maintaining the overlap between the sprinkler patterns of the end-gun and the last regular sprinklers at the distal end of the pivot.

The second factor is to make sure that the effective irrigated radius (75% of the maximum end-gun throw) is receiving the same water depth as the centre pivot average water depth (Keller & Bliesner, 1990). ASAE S436.1 (2003) defines the effective radius of a centre pivot, for the standard calculation of the distribution uniformity, as the distance from the pivot point to the outermost sprinkler on the pipeline, plus 75% of the wetted radius of the outermost water application device (end-gun).

The inner boundary for calculating the Heermann and Hein (1968) coefficient of uniformity chosen here for an end-gun on a centre pivot, will not include the first two collectors in the end-gun pattern, as shown in Figure 7-1. This avoids the water application overlap with the outermost regular pivot sprinklers at the distal end of the pivot point. On the outer side of the wetted radius, the last 10 metres will not be included in the calculation of the coefficient of uniformity, as only the inner 75 % of the effective wetted radius of the end-gun is to be included, according to (ASAE S436.1, 2003). The effective irrigated radius is 30 metres, based on an average end-gun throw of 40 metres found in this study.

As recommended by Nelson Irrigation (2008), a machine speed of 50 m/h at the last tower for a pivot length of 400 metres, with an end-gun radius of 40 metres, was selected for simulating of the combination of end-gun settings.

The results shown in Table 7-1 are for the different combinations of sector and side sector angles based on the literature, the manufacturers' documentation, and local grower, practice for the angles of operation of the end-gun on a centre pivot. These results include the average applied depth, the effective irrigated radius, the length of the overlap with the pattern of the last sprinkler device at the distal distance of the pivot, and the Heermann and Hein (1968) coefficient of uniformity under conditions of no-wind.

These results were obtained by simulating the end-gun transect and calculating its performance using TravGUN V3.1 containing the new sub-model. These radial leg and transect data are for the Nelson SR 100 end-gun with 490 kPa nozzle pressure, a trajectory angle of 18°, a taper/ring nozzle of 25.4 mm diameter (Nelson Irrigation Corporation standard as described in Chapter Four) and a machine speed 50m/h for all tests in this Chapter.

Table 7-1: Simulating and measured results (information) for the variety of selected sector and side sector angles from the literature and industry.

End-gun settings / Results	Sector angle (θ) and Side Sector Angle (ϕ)			
	$\theta = 135°$ $\phi = 67.5°$ Solomon & Codoma (1978)	$\theta = 150°$ $\phi = 60°$ Keller & Bliesner (1990)	$\theta = 170°$ $\phi = 75°$ Nelson Irrigation (2017a)	$\theta = 180°$ $\phi = 90°$ Local grower practice
Average applied water depth	17.7 mm	15.9 mm	17.08 mm	16.5mm
Heermann and Hein uniformity coefficient for effective radius (%)	94.5	94.5	86.7	85.4
Effective irrigated radius	30 m	30 m	27 m	24 m
Overlap	0°	15°	10°	0°

The simulation results for the first combination of $\theta = 135°$ and $\phi = 67.5°$ as shown in Figure 7-1 (A) a plan view of centre pivot end-gun pattern and (B) water depth mm, show high applied water depth equal to 16.5 mm, a high uniformity coefficient of 94.5%, and a long effective irrigated radius of 30 m. However, as the overlap value is zero, a very low applied water depth will occur between the pattern of the last regular sprinkler on the pivot and the end-gun pattern.

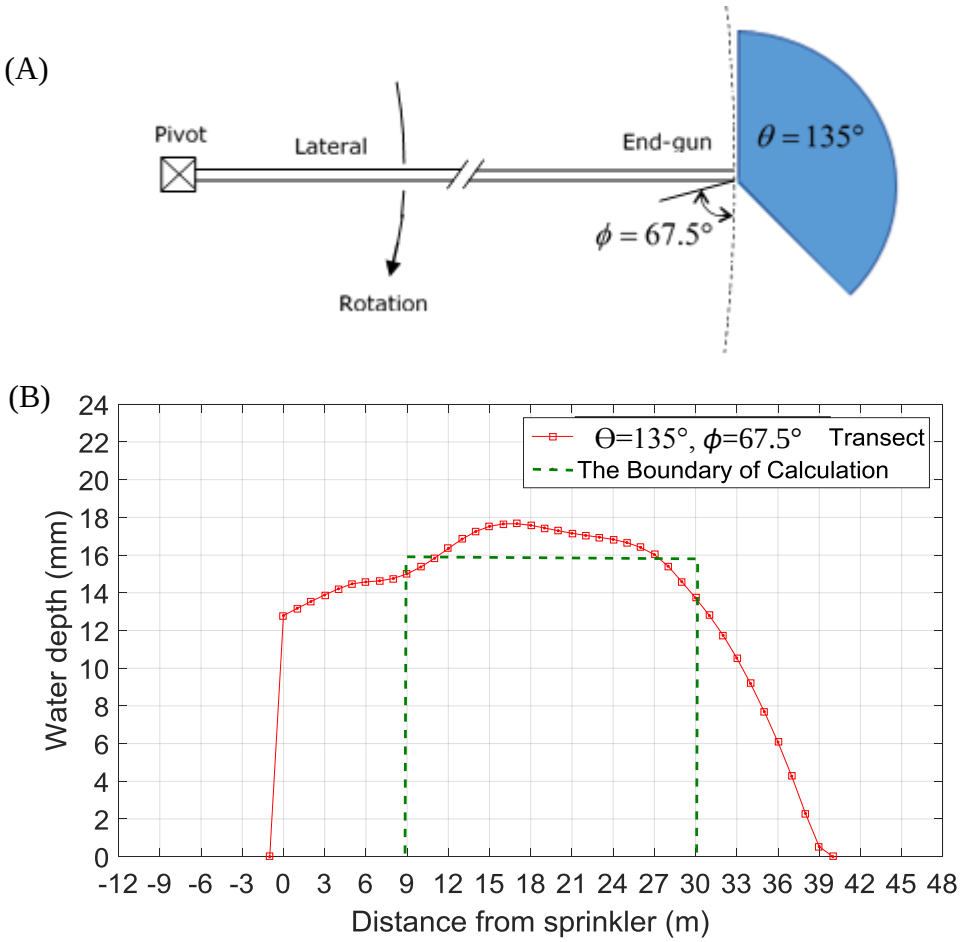

Figure 7-1: Simulated Transect depth for $\theta = 135°$ and $\phi = 67.5°$ and a machine speed of 50 m/h.

The simulation results for the second combination of $\theta = 150°$ and $\phi = 60°$ as shown in Figure 7-2 show an average applied water depth equal to 15.1 mm, a high uniformity coefficient of 94.5% and a large effective irrigated radius of 30 m. However, this configuration has the highest overlap value of 15°.

(A)

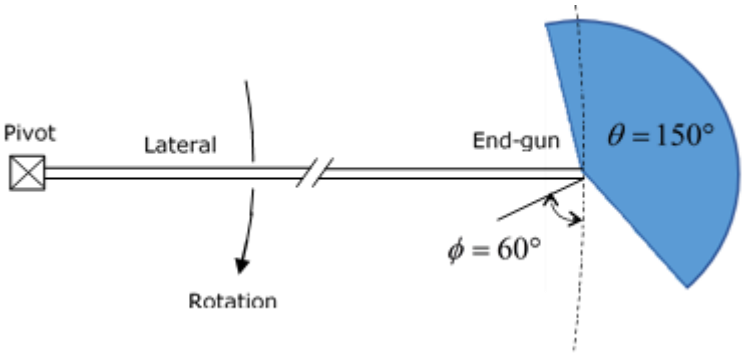

(B)

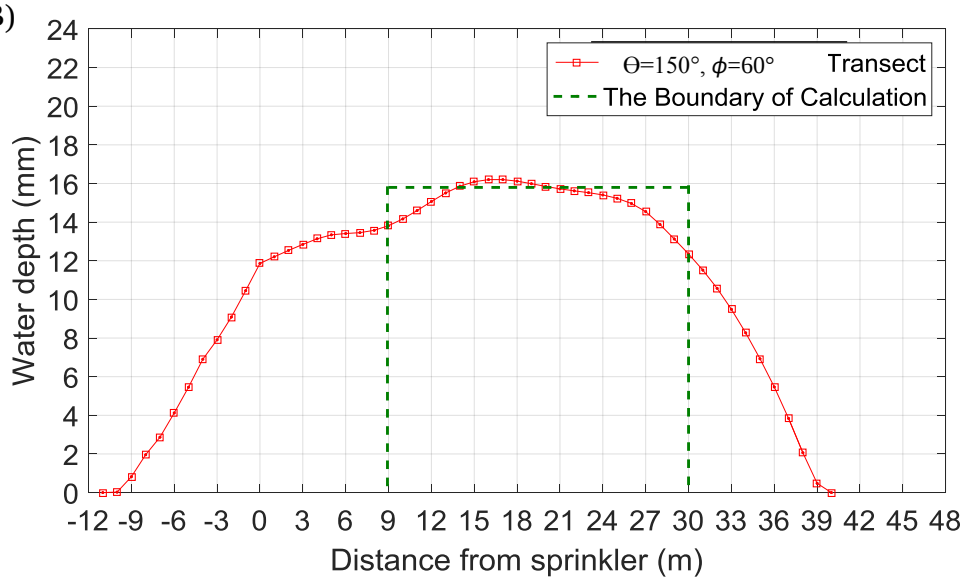

Figure 7-2: Simulated transect depths for $\theta =$ 150° and $\phi =$ 60° for a machine speed of 50 m/h.

The simulation results for the third combination of $\theta = 170°$ and $\phi = 75°$ as shown in Figure 7-3 show a high average applied water depth of 15.9 mm, a high value for overlap of 10°. However, the uniformity coefficient decreased to 86.7% and the effective irrigated radius decreased to 27 m.

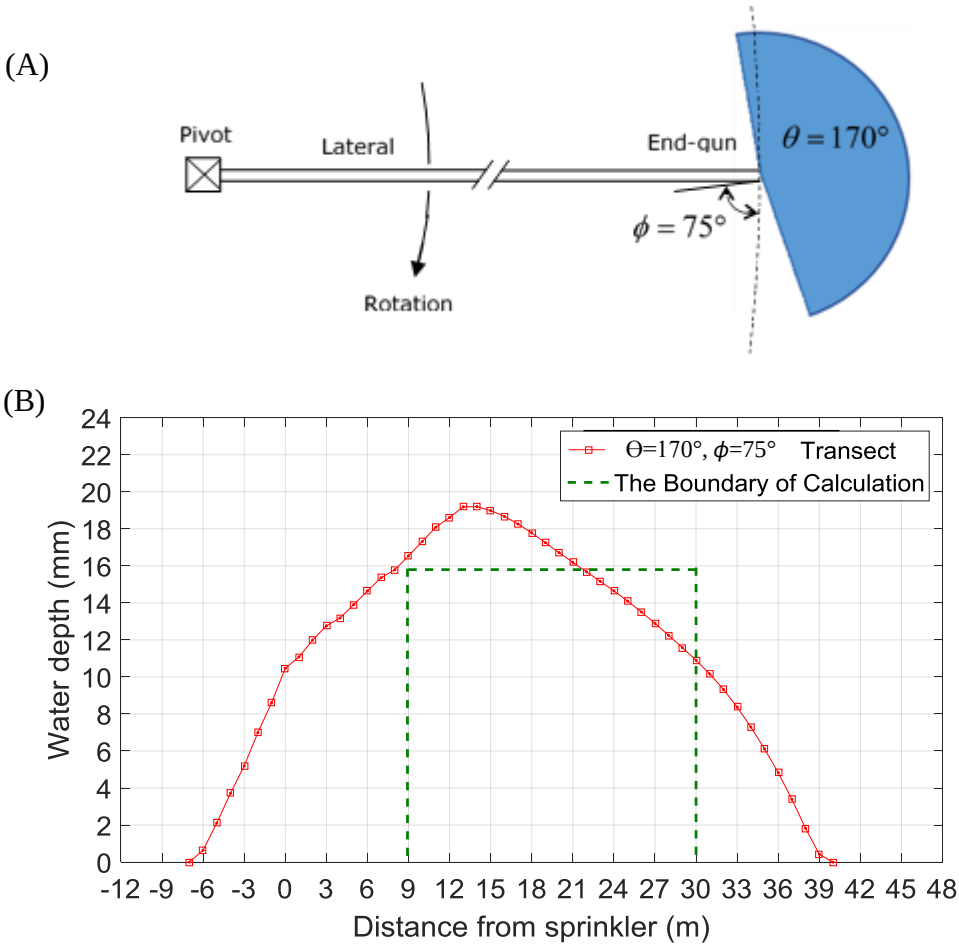

Figure 7-3: Simulated transect depth for $\theta =$ 170° and $\phi =$ 75° with a machine speed of 50 m/h.

The simulation results for the fourth combination, of $\theta = 180°$ and $\phi = 90°$ as shown in Figure 7-4 show a low average applied water depth of 14.4 mm, a low uniformity coefficient of 85.4%, a short effective irrigated radius of 24 m and a low overlap value of 0°.

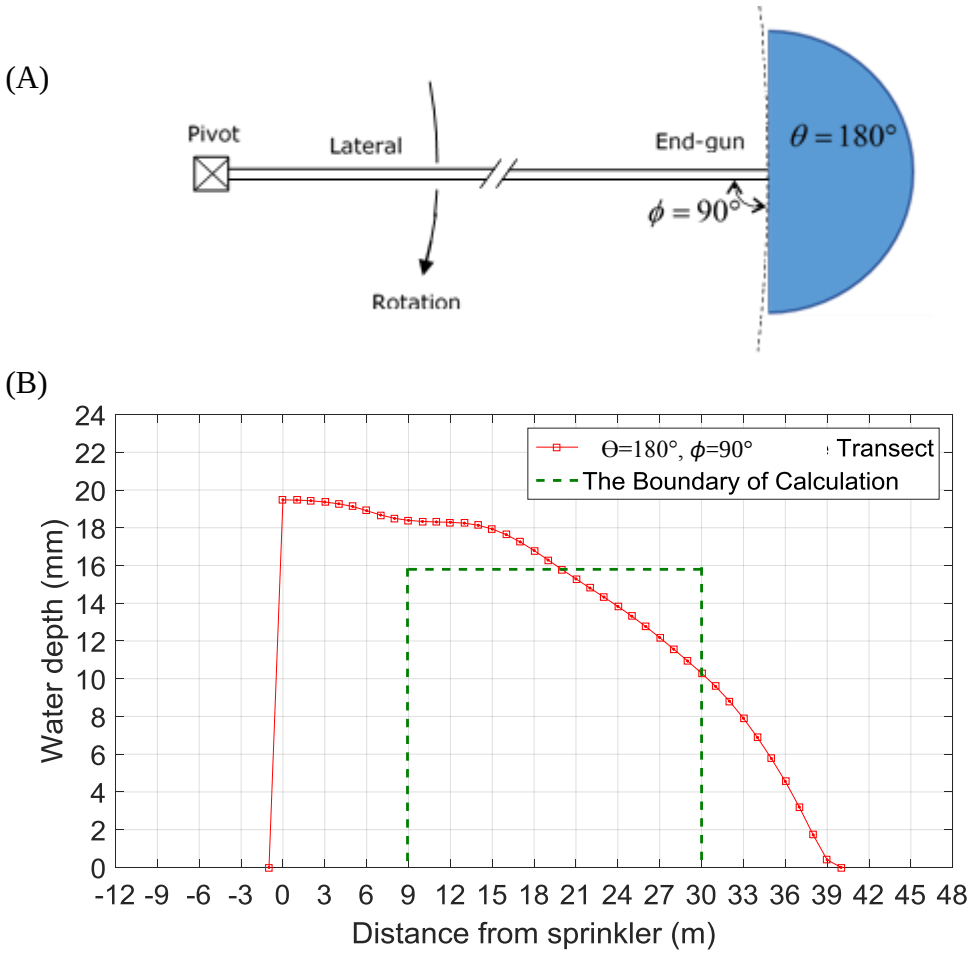

Figure 7-4: Simulated transect depth for $\theta =$ 180° and $\phi =$ 90° with a machine speed of 50 m/h.

The simulation results have shown that these combinations do not provide optimal results in relation to the uniformity coefficient and the overlap of the end-gun and the last regular sprinkler. Therefore, a series of simulation tests for a different combination of sector and side sector angles using the new TravGUN sub-model were conducted to explore the best combination of sector and side sector angles. These simulation results reveal that a wetted sector angle of 130° and a side sector angle of 60° produced the best values for overlap, uniformity coefficient and maximum effective irrigated radius, as detailed in the following.

7.3 Simulated end-gun transect of θ = 130° and ϕ = 60° in no-wind for a machine speed of 50 m/h

The simulation results in no-wind using the new TravGUN sub-model are given in Figure 7-5 and reveal that the combination of wetted sector and side sector angles of 130° and 60°, respectively, provide the optimum transect for achieving the highest CU_{HH} of 95.7% for the bounded area with 5° overlap with the last regular sprinkler on the pivot. The average applied water depth for this area was 15.7 mm. The effective irrigated radius was 30 metres. These results were for the same end-gun configuration and machine speed as used in previous simulations.

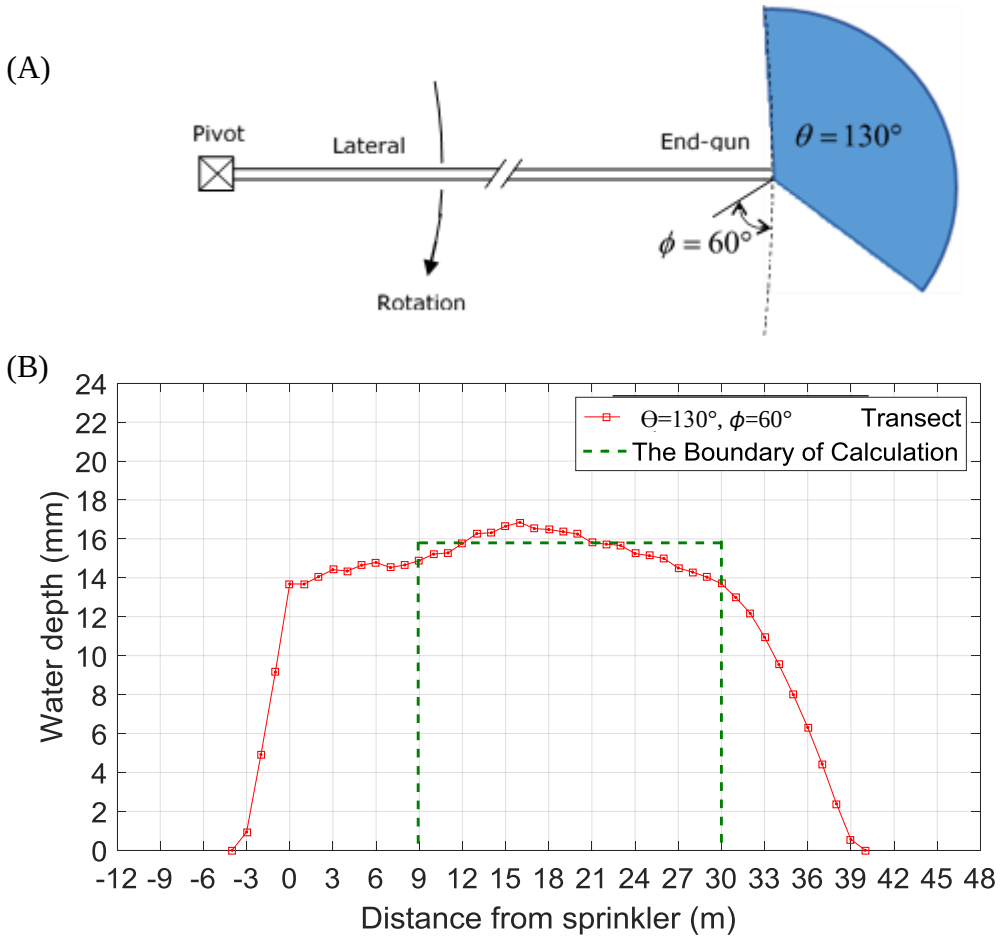

Figure 7-5: Simulated transect depth for θ = 130° and ϕ = 60° with a machine speed of 50 m/h to obtain optimum performance results.

7.4 Simulating the optimum sector and side sector angles under windy conditions

The optimum wetted sector and side sector angles for zero wind speed (using $\theta = 130°$ and $\phi = 60°$) were simulated under windy conditions utilising the TravGUN simulation model combined with the new-sub model for an end-gun on a centre pivot in TravGUN V3.1. The calibration procedures for TravGUN V3.1 are similar to the previous version in the selection of three sets of transect data. One of these transects is measured at zero wind speed, and the other two at different wind speeds and directions (Smith et al., 2008). However, there are some differences to be identified during this process. The first is a switch to alter the programme either to Travelling Gun or end-gun in the system bar in the Big Gun Information page of the Import Wizard, as shown in Figure 7-6.

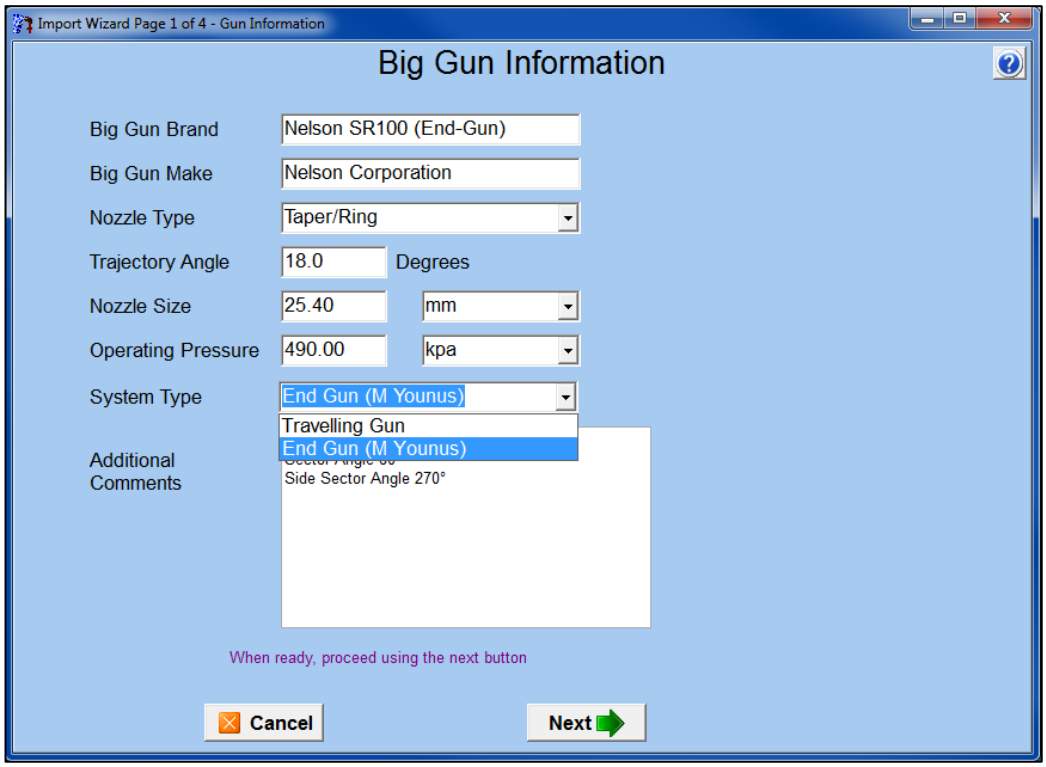

Figure 7-6 Screen shot for TravGUN V3.1 showing how to select the calibration options between travelling guns and end-guns.

The second difference is that all transects data should be measured, and then loaded into TravGUN V3.1 on one side of the end-gun, whereas transect data for travelling guns would be loaded into TravGUN V3.1 on both the negative and positive sides entry panels of the big gun data entry page.

The six wind-effect parameters in TravGUN are computed and then automatically saved in the Input file, enabling the user to simulate the wind effect on transects and the application pattern for different wind speeds, wind directions, travel direction, travel speed and different combinations of wetted sector and side sector angles.

The following results were achieved by simulating transects of a 130° wetted sector and a 60° side sector angle for the same end-gun and standard machine configuration, as previously mentioned for windy condition cases. The wind direction was chosen according to the dominant wind direction from the wind rose for the Toowoomba location. The wind rose shows the prevailing wind direction is from the East for the annual average over five years, as shown in Figure 7-7 (WillyWeather, 2017). A wind speed of 1.5 m/s was chosen for all simulations as it was the average annual wind speed.

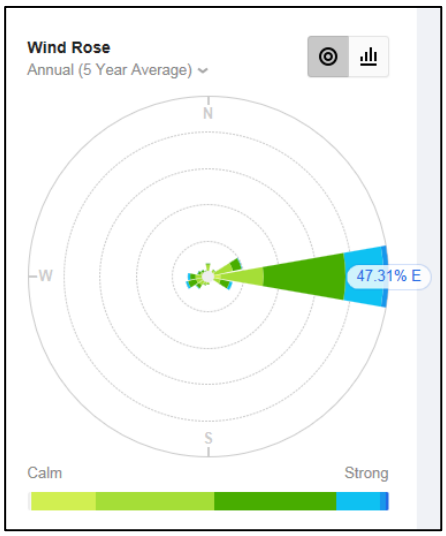

Figure 7-7: Wind rose for Toowoomba location showing annual averages over five years (WillyWeather (2017).

The end-gun setup has the same values for all the simulations, except for the direction of travel. The different directions of travel for the end-gun simulations were chosen due to the nature of the circular movement of the centre pivot irrigation system. It was assumed that the rotation of the centre pivot was clockwise, that the end-gun was attached on the distal end of the last span of the centre pivot, and the first position of the centre pivot had the spans aligned to a northerly direction, as shown in Figure 7-8.

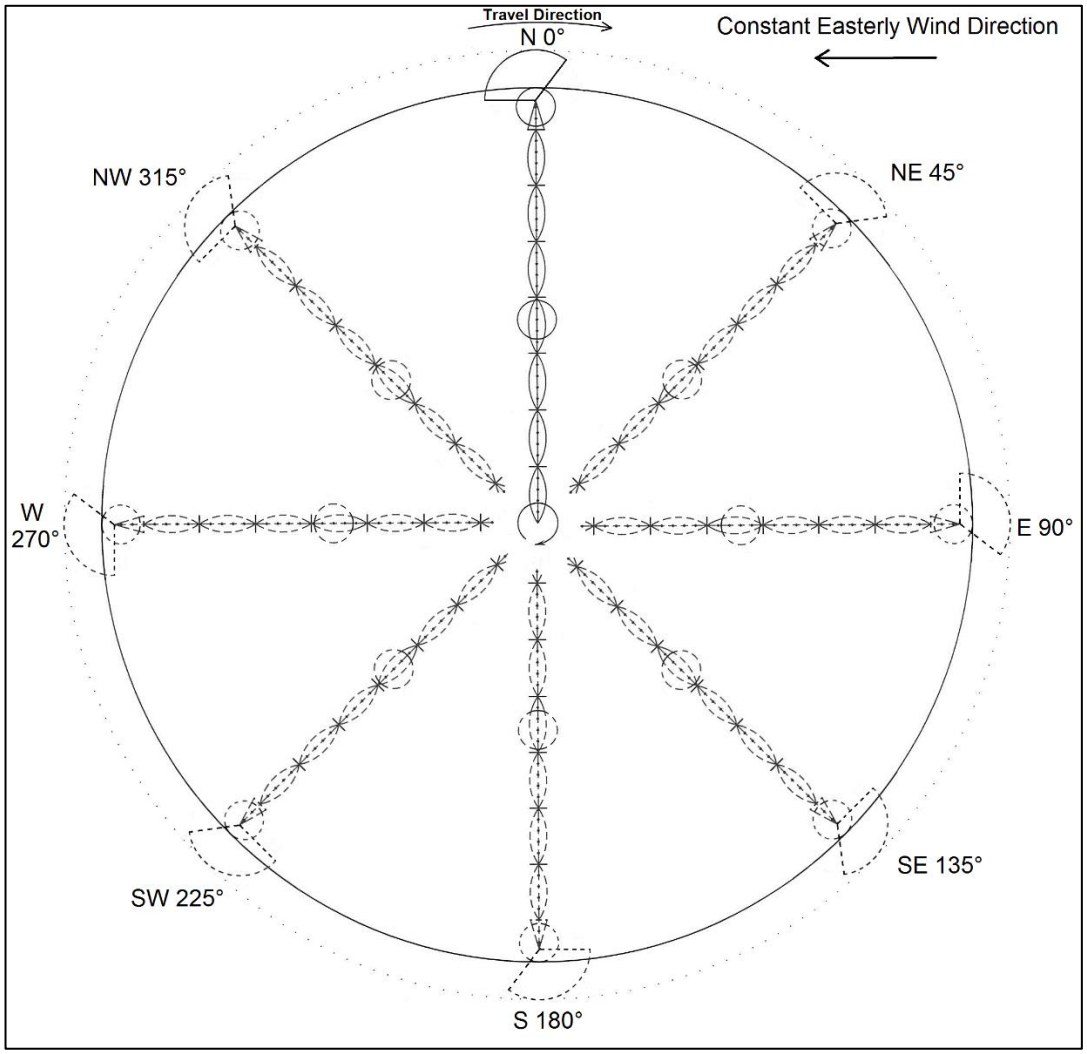

Figure 7-8: Birds-eye view of a centre pivot with an end-gun showing the position of the lateral and end-gun, the starting point at the northerly direction and the clockwise travel direction.

According to the previous assumption, the centre pivot position will be in a northerly direction, and the direction of travel for the end-gun will be from West to East, with a constant wind speed and direction of 1.5 m/s from the East. Eight cardinal points of

the compass (90°, 135°, 180°, 225°, 270°, 315°, 360° and 45°) were chosen as the centre pivot, so as to simulate the clockwise movement in 45° intervals the wind impact on the application pattern through the full circular rotation of the pivot.

7.4.1 Simulation results for an end-gun travelling directly into the wind

The first simulation result in Figure 7-9 shows the wind effect on the application pattern when the end of the pivot was moving from West to East, and the wind direction was from the East. The figure shows that the pattern was slightly distorted and moved toward the West. For this case, the resulting end-gun transect is directly across the wind. Therefore, the pattern has shortened on the northern side due to reduced sprinkler throw, and lengthened toward the West as a result of wind influence on the pattern (Richards & Weatherhead, 1993).

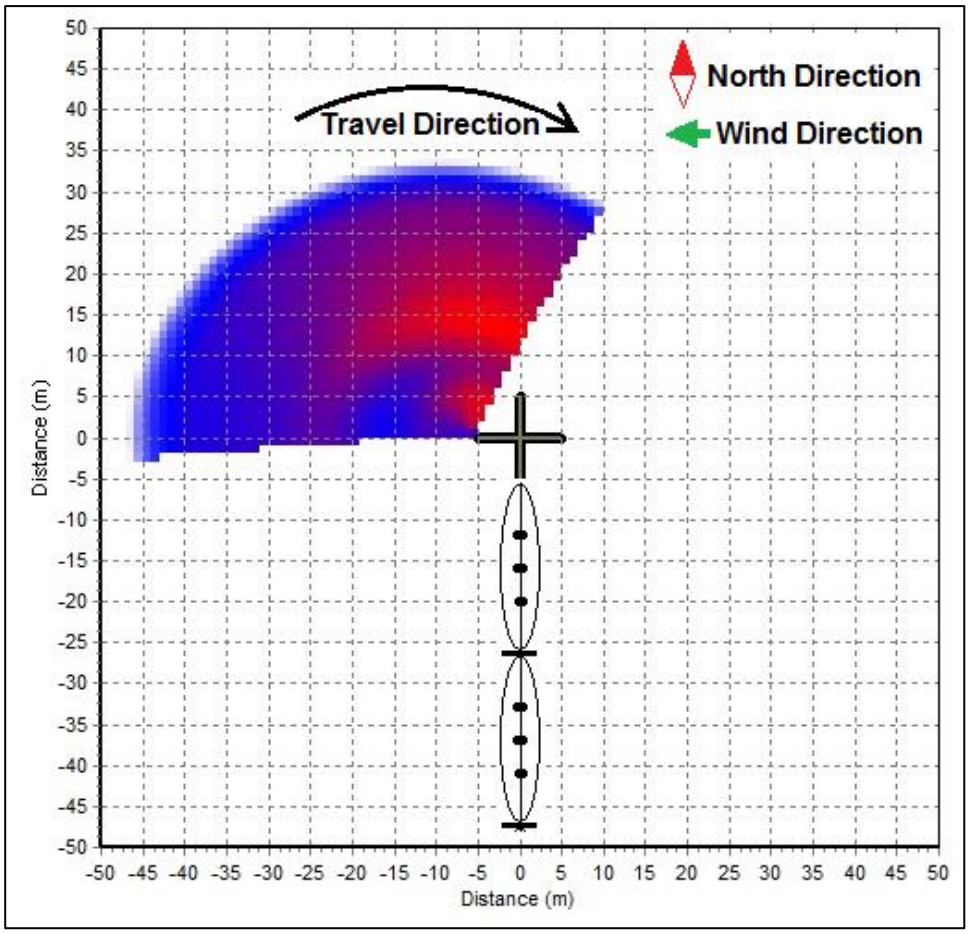

Figure 7-9: The effect of wind on the application pattern for an end-gun when the travel direction is directly into the wind.

The transect data in Figure 7-10 shows the length of the transect and maximum throw decreased from 40 metres at zero wind speed shown in Figure 7-5, to 34 metres with a wind speed was 1.5 m/s as a result of range shortening. In addition, the simulation results show the effective irrigated radius decreased from 30 metres to 27 metres, also as a result of range shortening. The coefficient of uniformity, CU_{HH} decreased from 95.7 to 84.9%, while the average water depth increased from 16.5 mm to 17.1 mm.

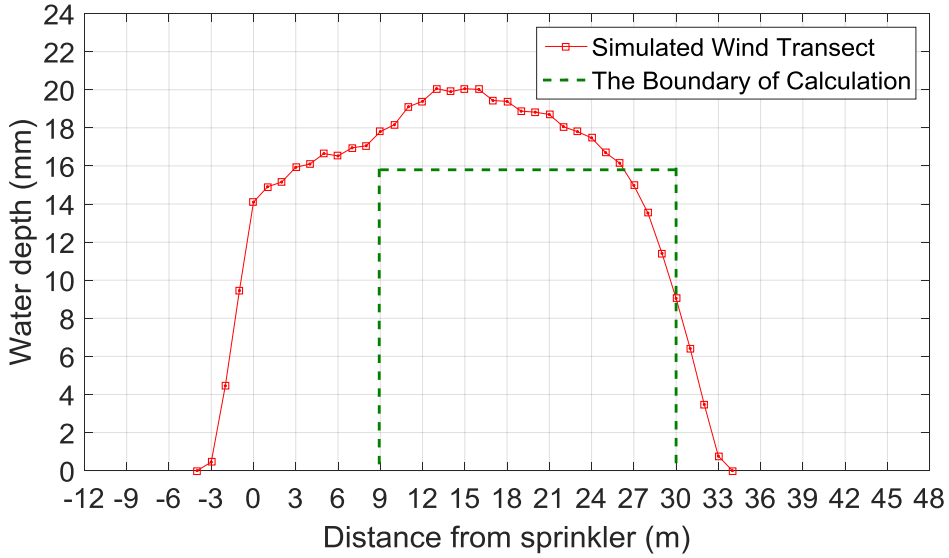

Figure 7-10: Depths of water along the simulated catch-can transect, showing the effect of wind on the transect for an end-gun sector angle of 130° and a side sector angle of 60° when the wind is across the pivot spans, and the machine is moving directly into the wind.

7.4.2 Simulation results for an end-gun travelling across the incoming wind by 45°

The simulation results here are for the pattern and transect under the effect of windy conditions after the centre pivot had rotated 45° clockwise from the original northerly position in the previous section, so that direction of travel is to the south east, or 135° clockwise from north. The wind of constant speed and direction for all tests here is from the East at 1.5 m/s. Figure 7-11 shows the wetted footprint from the end-gun with the chosen standard configuration for this travel direction. The simulated results in this case will be influenced in a way that may occur when the pivot is pointing between northerly and easterly directions, and when the wetted pattern is wind somewhat effected between upwind and crosswind type influences. Figure 7-10 shows that the wetted footprint pattern is compressed and has moved toward the West. The transect is always along the line of the long axis of the centre pivot spans, and will always be perpendicular to the direction of travel. However, the influence of the wind on the transect shape will be different for different directions, as the CP rotates clockwise.

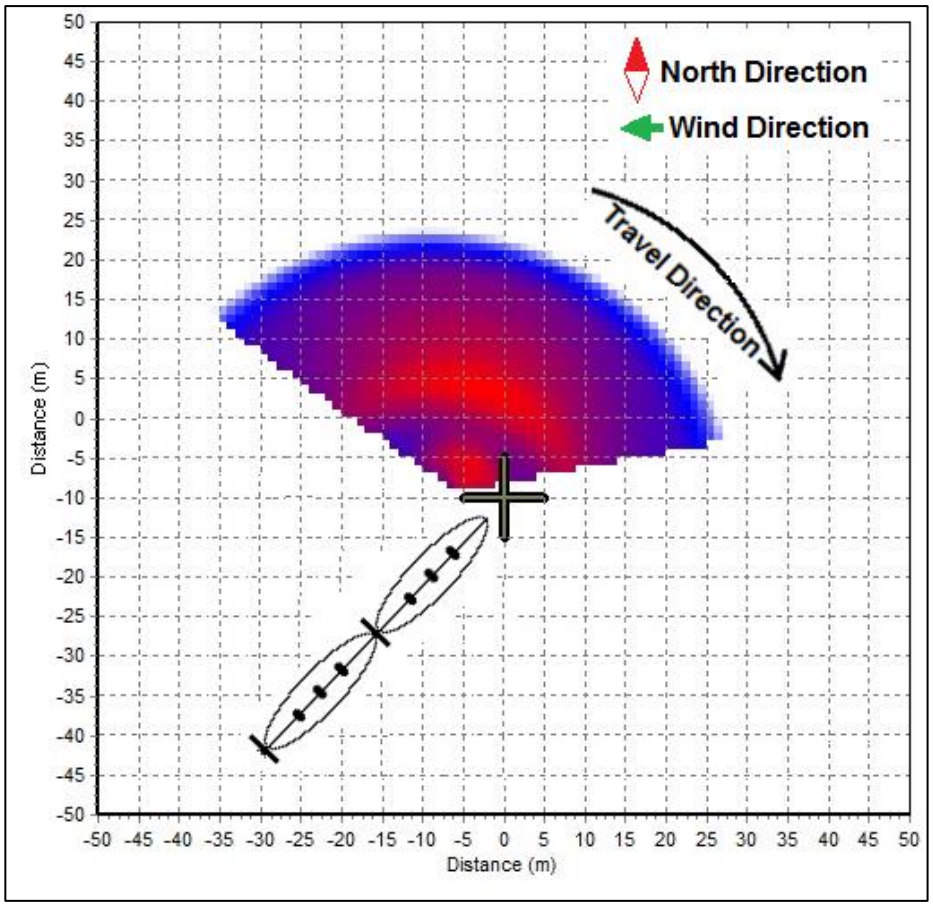

Figure 7-11: The effect of wind on the application pattern for an end-gun when the travelling position was between upwind and crosswind with a travel direction of 135°.

The transect data given in Figure 7-12 shows that the length of the transect decreased sharply from 40 metres at zero wind to 30 metres at a wind speed of 1.5 m/s. The effective irrigated radius decreased sharply from 30 metres to 21 metres, as a result of this sprinkler range shortening. The transect data also show that the water depth changed as a result of the wind pattern distortion and range shortening. The calculated CU_{HH} decreased sharply to 54.0% as a result of the wind movement of the wetted footprint. The simulation results also show the average water depth inside the border of the effective irrigated radius decreased sharply to 12.6 mm.

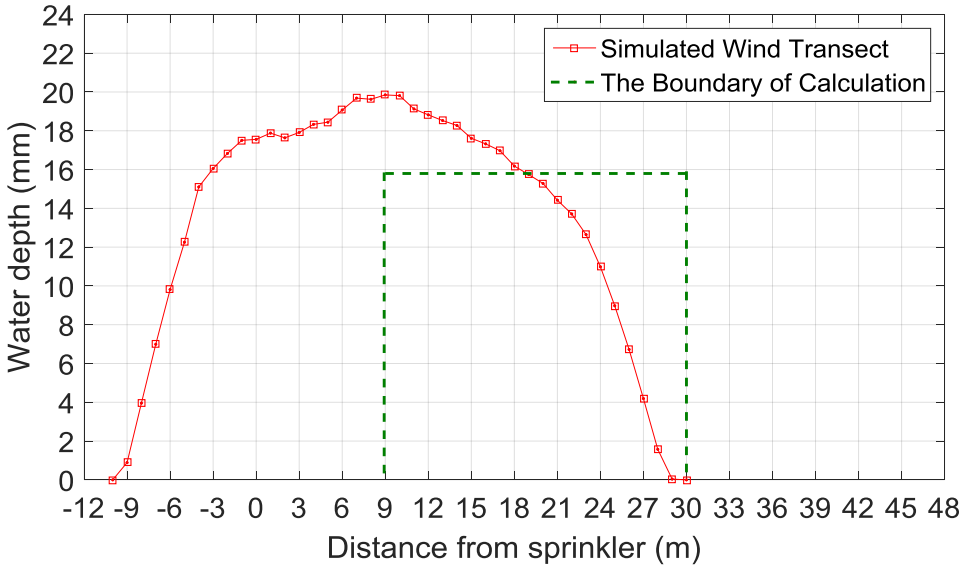

Figure 7-12: The effect of wind on transect for a sector angle of 130° and a side sector angle of 60° when the position of the transect (the pattern) was between a crosswind and upwind effect, on a travel direction of 135°.

7.4.3 Simulation results for the end-gun travelling south in an Easterly wind

The simulation results for the pattern and transect under the effect of windy conditions after the centre pivot has rotated 90° from the North with a direction of travel to the South, are presented here. Figure 7-13 shows the actual position and shape of the simulated wetted pattern under the influence of the Easterly pattern. The transect line in this case is upwind. Therefore, the pattern has compressed and moved toward the West.

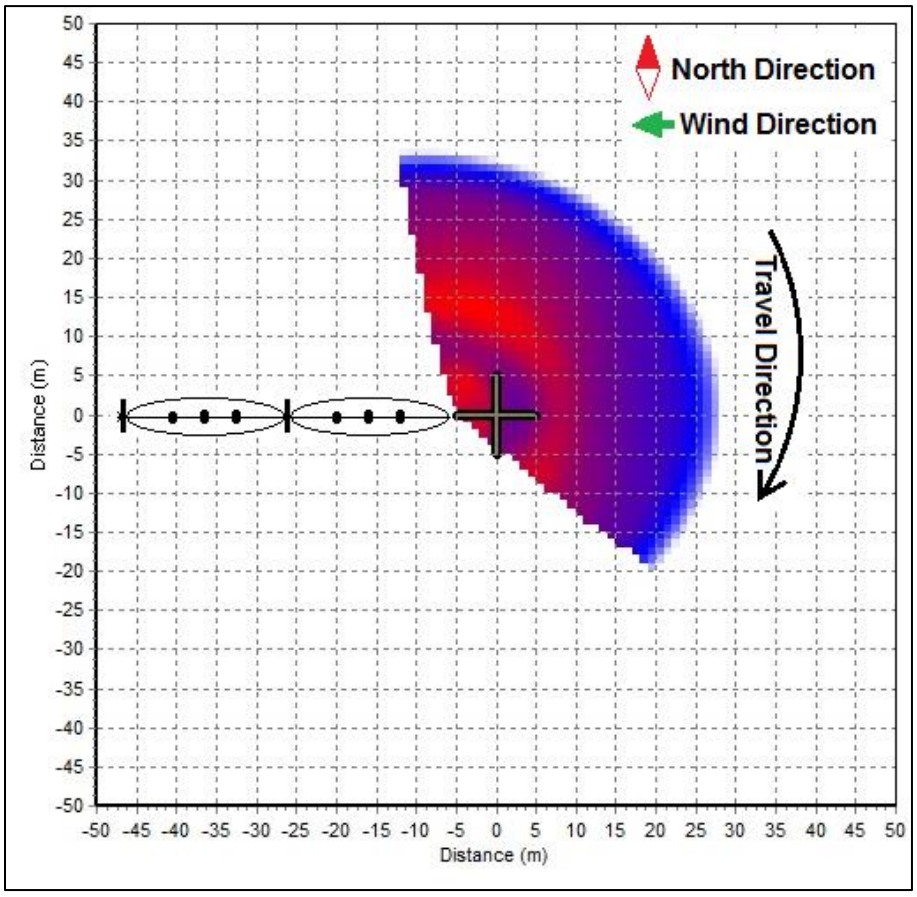

Figure 7-13: The effect of wind on the application pattern for an end-gun with an upwind travelling position and a travel direction of 180°.

The transect data show that the length of the transect decreased sharply from 40 metres at zero wind to 30 metres at a wind speed of 1.5 m/s, as shown in Figure 7-14. The distance that has been sufficiently irrigated decreased sharply from 30 metres to 18 metres, as a result of sprinkler throw range shortening. The water depth sharply changed as a result of wind effect on the wetted pattern, as the transect data reveals. As a result, the CU_{HH} decreased sharply to 47.7% from 95.7% in no-wind. The simulation results also reveal the average water depth decreased sharply to 11.3 mm.

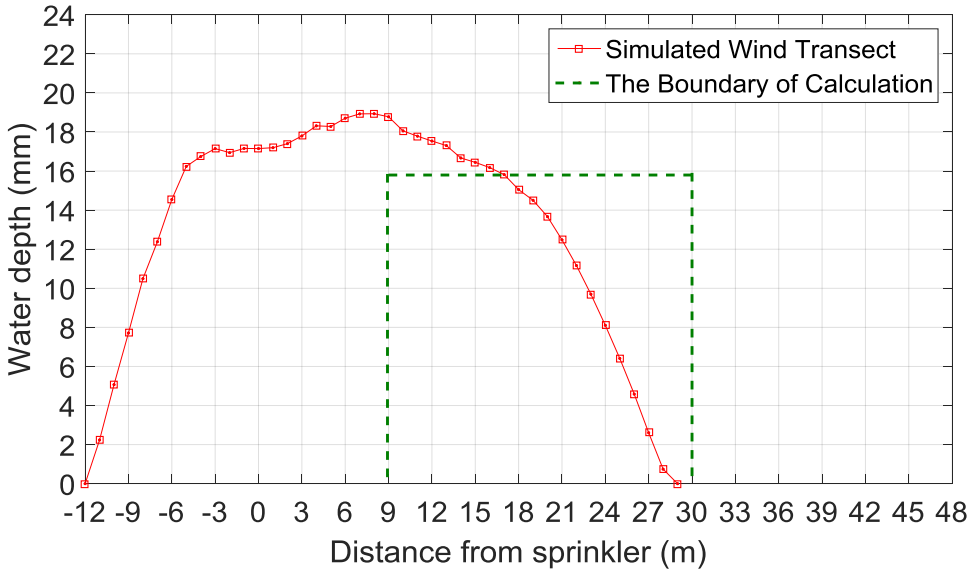

Figure 7-14: The effect of wind on the transect for a sector angle of 130° and a side sector angle of 60° when the position of the pivot was upwind and had a travel direction of 180°.

7.4.4 Simulating the pattern for end-gun travel in a direction of 225°

The simulation results for the wetted pattern and transect under the effect of windy conditions after the centre pivot had rotated 135° and the direction of travel is to the South-West, a heading of 225° are presented in this section for an Easterly wind of constant speed again. Figure 7-15 shows that the wetted pattern moved to the west as before, and as the travel direction has changed with respect to the same wind direction, the real difference will be seen in the resultant water applied to the field. The transect results for this case will be between those for upwind and crosswind cases. In this case, the wind influence on the accumulation of the applied water is completely different compared with the second case presented in Section 7.4.2, as a direct result of the position of the transect with respect to the wind direction.

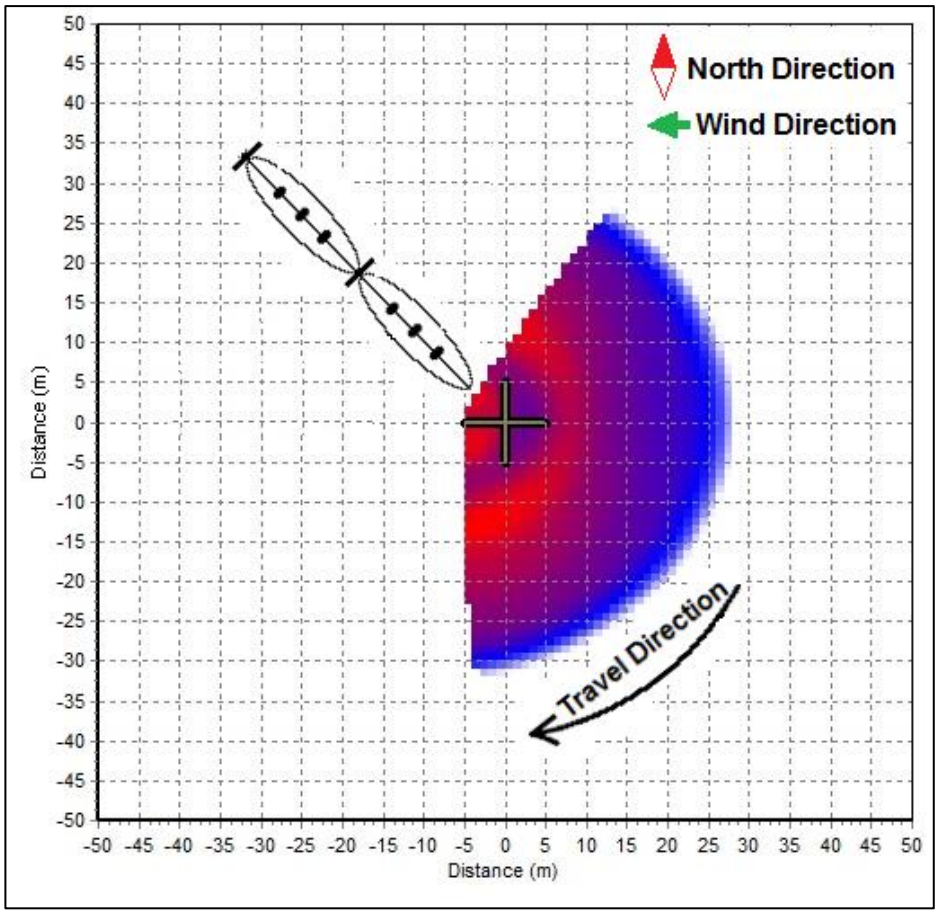

Figure 7-15: The effect of wind on the application pattern for an end-gun when travelling between crosswind and downwind on a travel direction of 225°.

The transect data in Figure 7-16 show that the length of the transect and the effective irrigated radius also decreased to 30 metres and 21 metres, respectively, similar to the simulation results presented in Section 7.4.2, because both simulation cases have similar wind impacts in relation to the full length of throw and crosswind impact. However, the value of the average water depth in the effectively irrigated radius is different, namely, 13.2 mm, because, the side sector angle is asymmetrical to the direction of travel. The CU_{HH} for the effective irrigated radius decreased to 52.8% as a result of the wind influence.

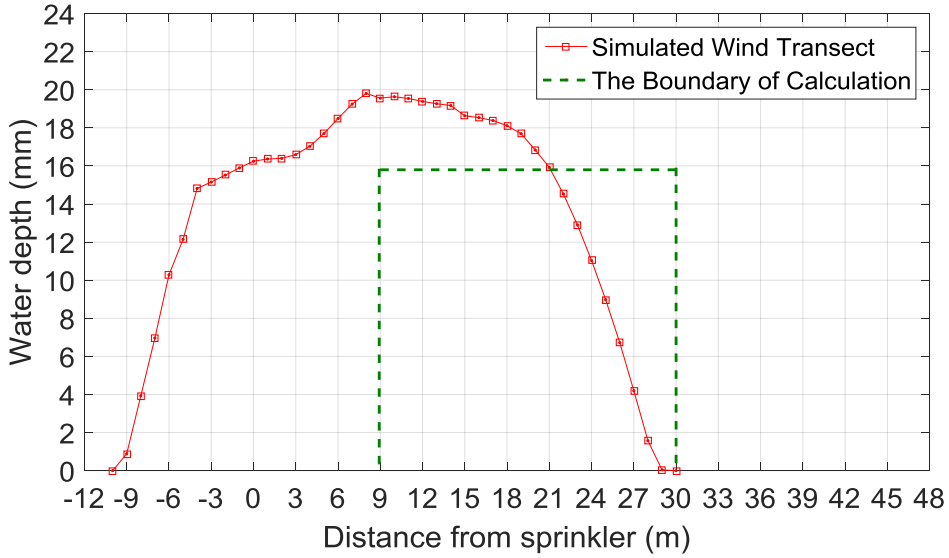

Figure 7-16: The effect of wind on the sprinkler transect for a sector angle of 130° and a side sector angle of 60° when the position of the pivot was between crosswind and upwind with a travel direction of 225°.

7.4.5 Simulating the pattern for end-gun travel direction of 270° in an easterly wind

The simulation results for the wetted pattern and transect under the effect of windy conditions, after the centre pivot had rotated 180° clockwise from the original northerly facing position, clearly indicates that the direction of travel for the end-gun has changed to a westerly direction, 270°. Figure 7-17 highlights that the transect position along the line of the main axis of the centre pivot machine is directly across the easterly wind. However, the wind effect on the wetted pattern for this direction of travel is on the opposite side compared with simulation results presented in Section 7.4.1.

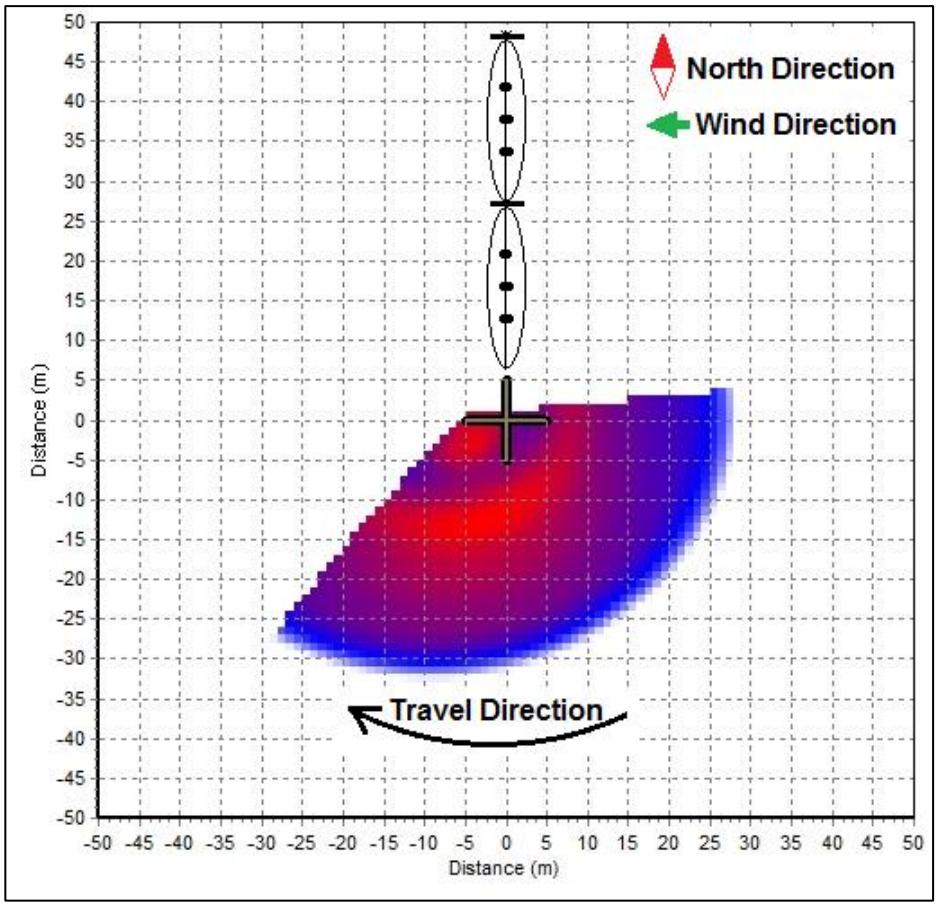

Figure 7-17: The effect of wind on the application pattern for an end-gun when travelling downwind on a travel direction of 270°.

The transect data show that the length of the transect decreased from 40 metres at zero wind to 36 metres at a wind speed of 1.5 m/s, as shown in Figure 7-18. The effective irrigated radius decreased from 30 metres to 27 metres, as a result of range shortening similar to simulation results presented in Section 7.4.1. However, the value of the average water depth under the effective irrigated radius is different, namely, 17.0 mm compared to simulation results with the machine pointing to the North, because the side sector angle was asymmetrical to the direction of travel and the wind direction effect was from the opposite direction. The CU_{HH} decreased to 85.1% and had different values from earlier simulation results.

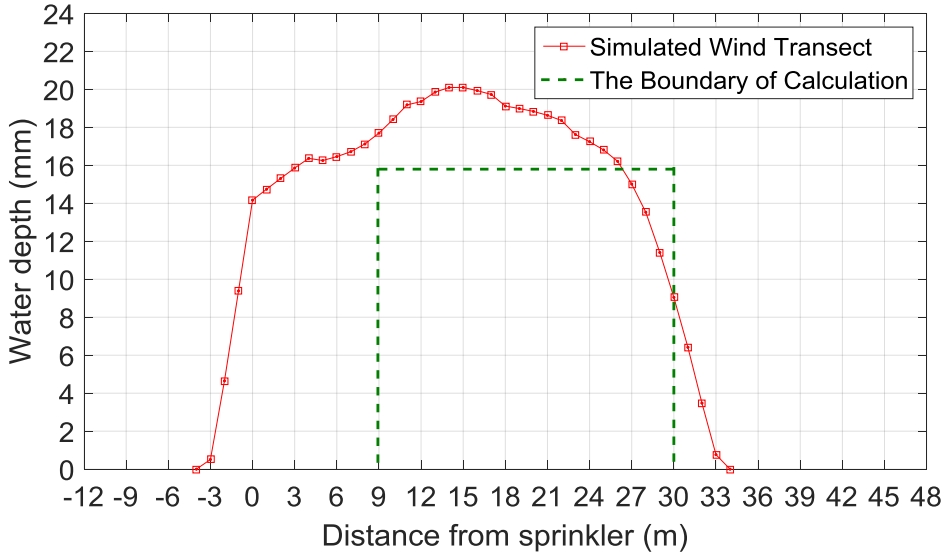

Figure 7-18: The effect of wind on a sprinkler transect with a sector angle of 130° and a side sector angle of 60° when the position of the transect is across the wind, and the end-gun travel direction is 270°.

7.4.6 Simulating the pattern for end-gun travel direction of 315°

The simulation results from TravGUN for the wetted pattern and transect under the effect of windy conditions, after the centre pivot had rotated 225°, when the direction of end-gun travel is altered to the North-West, on a heading of 315° are presented here. Figure 7-19 shows that for the transect position, which is always perpendicular to the direction of travel, the wind effect is between downwind and crosswind. The figure shows that the wetted pattern area was reduced and was moved in a westerly direction, in the same way as each previous case.

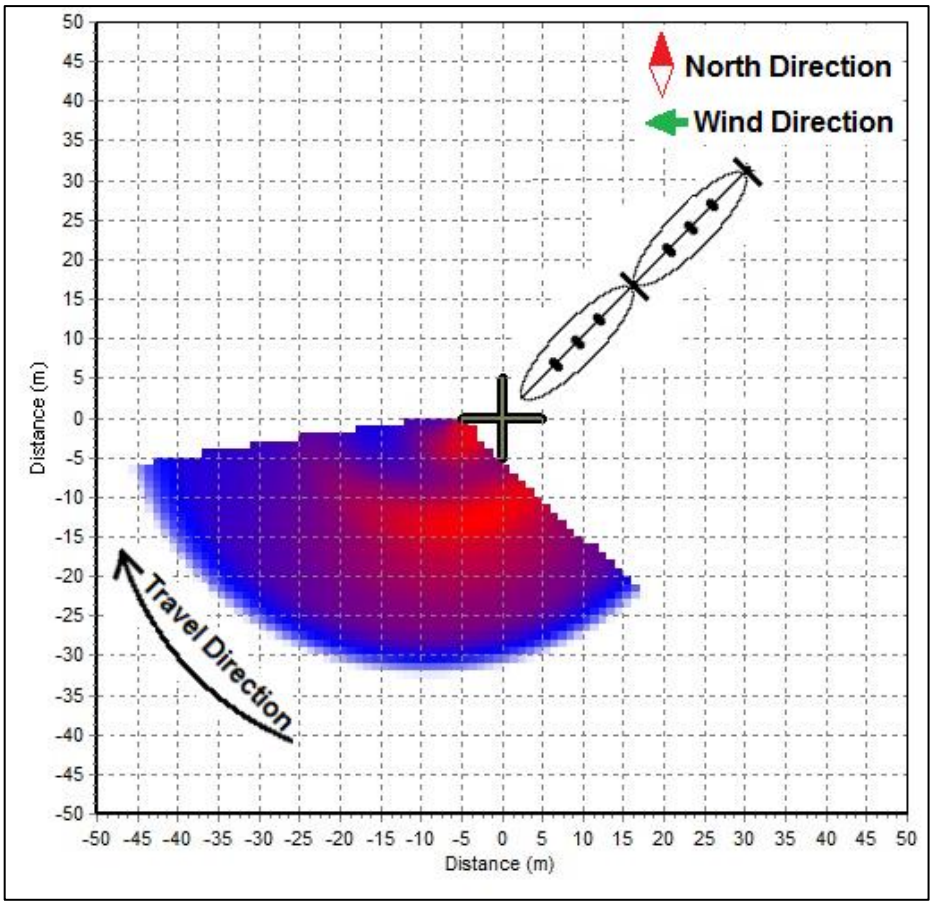

Figure 7-19: The effect of wind on the application pattern for an end-gun when the travel position is between downwind and crosswind on a travel direction of 315°.

However, the transect data shows that the length of the transect increased from 40 metres at zero wind to 42 metres at a wind speed of 1.5 m/s, as shown in Figure 7-20. The effective irrigated radius increased from 30 metres to 33 metres, as a result of sprinkler throw range lengthening. However, the simulation results for the transect data show a reduced water depth in the first collector as a result of the wind effect on the pattern movement. The average water depth under the effective irrigated radius decreased to 16.9 mm. The CU_{HH} for the effective irrigated radius increased to 95.0% as a result of range lengthening.

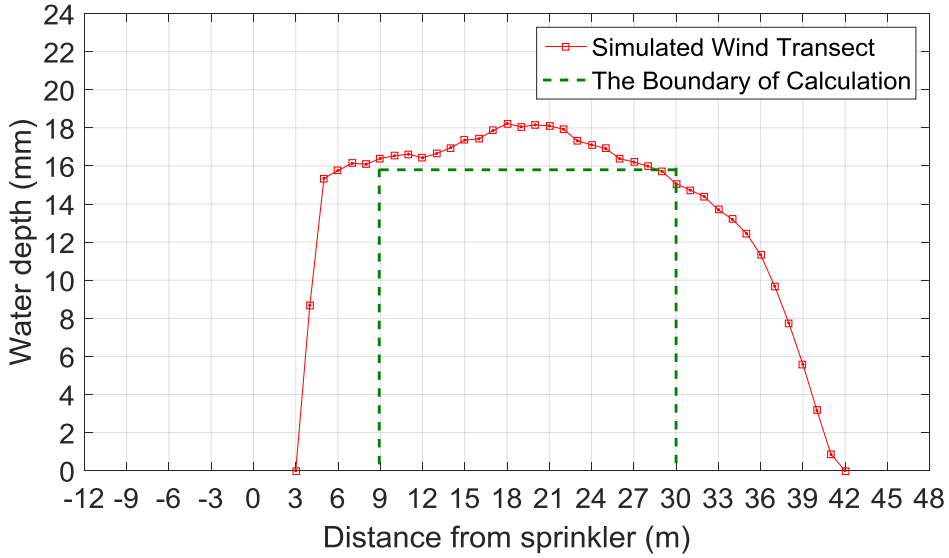

Figure 7-20: The effect of wind on a sprinkler transect with a sector angle of 130° and a side sector angle of 60° when the position of the pivot was between downwind and crosswind, on a travel direction of 315°.

7.4.7 Simulating the pattern for end-gun travel direction of 360°

The simulation results for the wetted pattern and transect under the effect of prevailing easterly wind conditions, after the centre pivot had rotated 270°, are for an end-gun direction of travel to the North, as shown in Figure 7-21. This shows the actual position of the wetted pattern and the travel direction of the end-gun under the prevailing easterly wind directions. The transect alignment extended along the length of the centre pivot, in this case directly downwind.

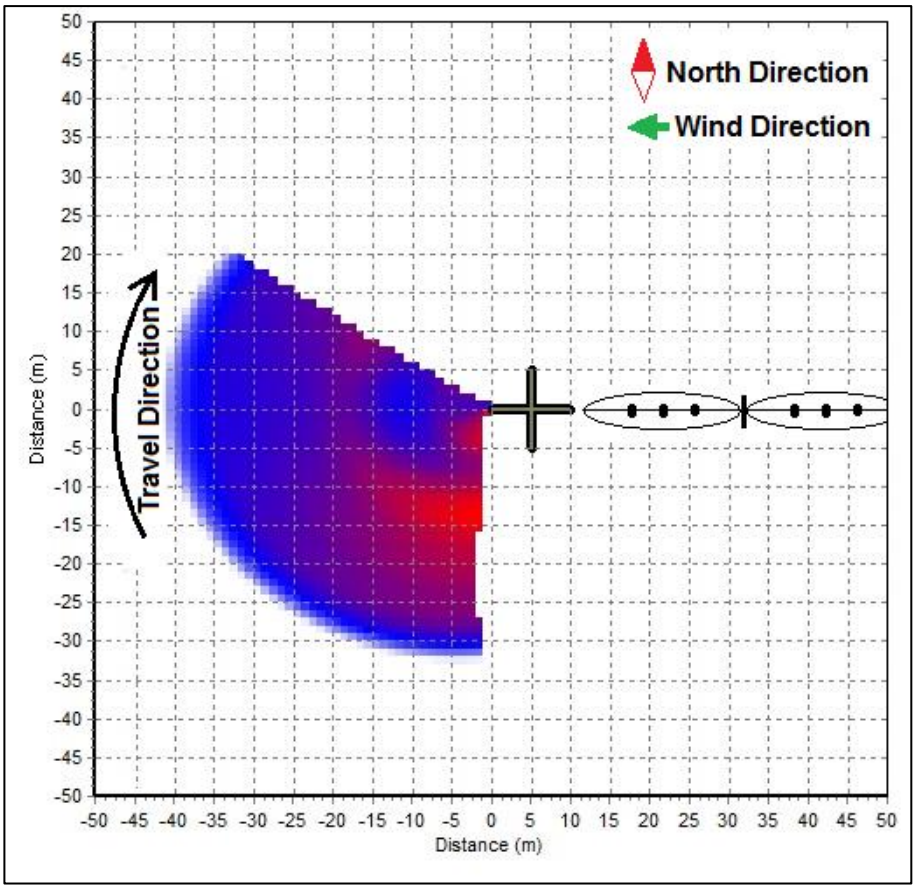

Figure 7-21: The effect of wind on the application pattern for an end-gun when the pivot position was downwind, with an end-gun travel direction of 360°.

The transect data reveal that the length of the transect increased from 40 metres at zero wind to 47 metres at wind speed of 1.5 m/s, as shown in Figure 7-22. The sufficiently irrigated length increased from 30 metres to 33 metres, as a result of sprinkler throw range lengthening. The transect data also show that there was a reduced water depth at the position of the first collector, compared to the no-wind scenario, and the water depth was sharply lower in the second collector going toward the outer radius. The CU_{HH} for the effective irrigated radius increased to 95.2% while the average water depth under the effective irrigated area decreased to 15.6 mm.

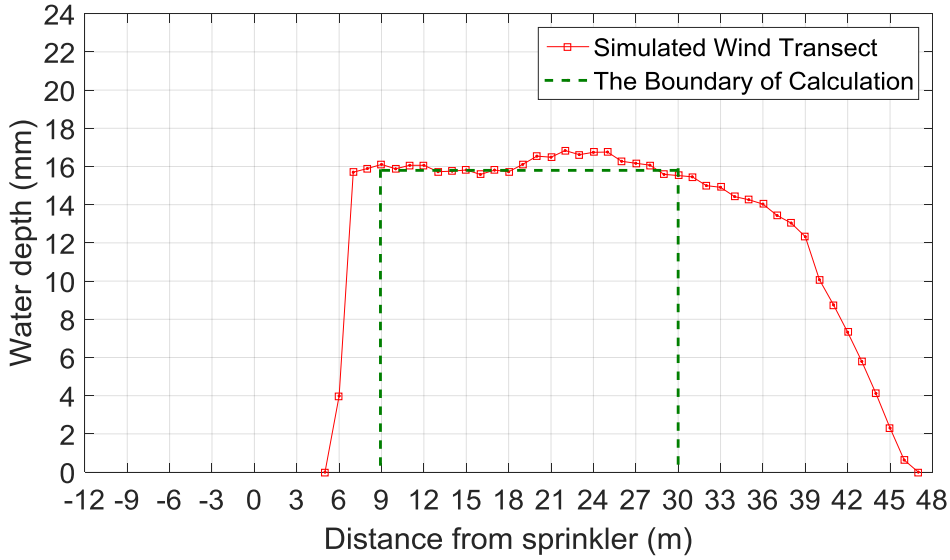

Figure 7-22: The effect of wind on a sprinkler transect for a sector angle of 130° and a side sector angle of 60°, when the position of the transect was a downwind, and the travel direction was 360°.

7.4.8 Simulating the pattern for end-gun travel direction of 45°

The simulation results for the wetted pattern and transect under the effect of prevailing wind conditions after the centre pivot had rotated 315° from its original northerly alignment reveals the direction of travel changed to the North East, or a heading of 45°. Figure 7-23 shows that the travel direction has changed, and the wetted pattern is wind effected in ways somewhat between the upwind and crosswind cases under the prevailing easterly wind. The transect position, as usual, was perpendicular to the direction of travel.

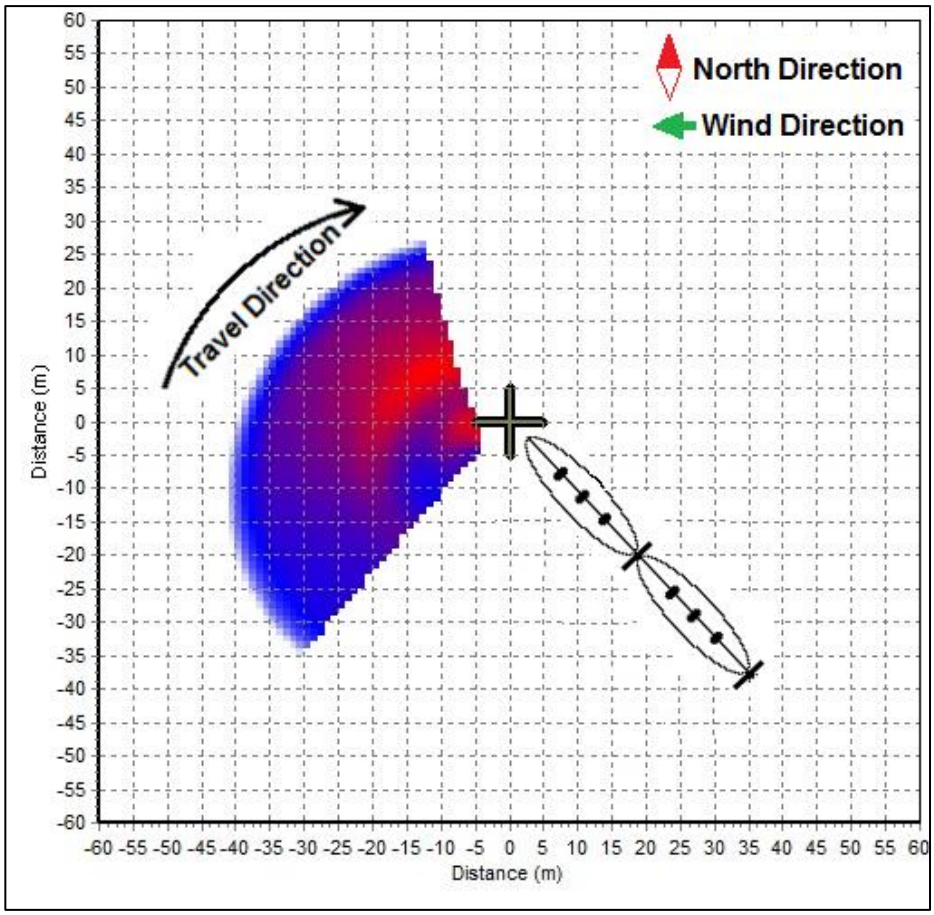

Figure 7-23: The effect of wind on the application pattern for an end-gun when the travelling direction is between crosswind and unwind, on a travel direction of 45°.

The transect data show that the length of the transect increased from 40 metres at zero wind speed to 42 metres at a wind speed of 1.5 m/s, as shown in Figure 7-24. The effective irrigated radius increased from 30 metres to 33 metres, as a result of sprinkler throw range lengthening. However, the simulation result for the transect data again show that there is a reduced water depth at the first collector as a result of wind movement of the wetted pattern. The average water depth under the effective irrigated radius equals 16.6 mm. The CU_{HH} for the effective irrigated radius increased to 95.4% as a result of sprinkler throw range lengthening.

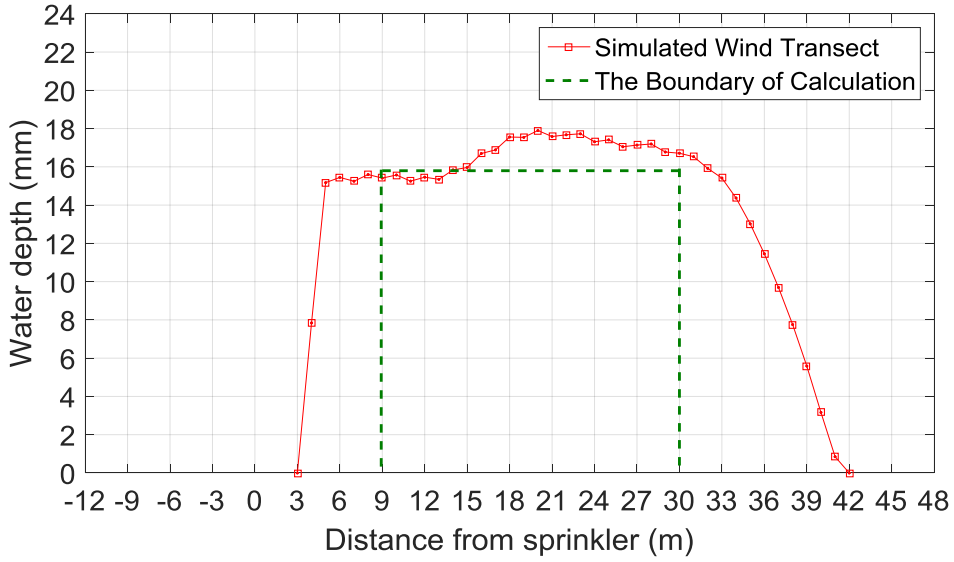

Figure 7-24: The effect of wind on a sprinkler transect for a sector angle of 130°, and a side sector angle of 60°, when the position of the pivot was between a crosswind and upwind, on a travel direction of 45°.

7.4.9 Simulation outcomes

The simulation results for the eight end-gun travel directions under constant wind speed and direction in these eight simulation tests found that end-gun performance was highly deterioration while the end-gun on centre pivot travelling crosswind and upwind.

7.5 Correction factor for arced movement

Simulating the wind effect on an end-gun transect using TravGUN V3.1 (TravGUN with new sub-model) produces an end-gun transect from a sprinkler travelling on a straight path. The TravGUN software was developed for travelling gun machines that travel on straight paths, while TravGUN V3.1 was developed to also produce radial leg data from three transects for wetted sector angles less than 180°, with an asymmetrical side sector angle perpendicular to the direction of end-gun travel. Therefore, the wind transects produced by TravGUN V3.1 need to be adjusted for the

arc like movement of an end-gun on a centre pivot. The best approach to achieve this is to find a correction factor to adjust for the effect of the arc movement.

To calculate the correction factor for the arc movement of an end-gun on a centre pivot, we need to identify the differences between both movement patterns. TravGUN V2.0 produces a transect of applied water depths at different distances from the sprinkler at specific spacing by integrating the sprinkler pattern depths, assuming that the wetted pattern passes over the collectors on a straight path, and that the wetted pattern passes the each collector position in the same distance. However, for an end-gun on a centre pivot, the movement is clearly different across the wetted pattern, and the resultant transect will be similarly impacted. The captured water depths along the transect integrated across the sprinkler pattern are distributed at different radial distances from the end-gun position. Therefore, the applied water depths will be distributed along different circumferential distances whose lengths depend on the radii of the collectors from the end-gun position, as shown in Figure 7-25.

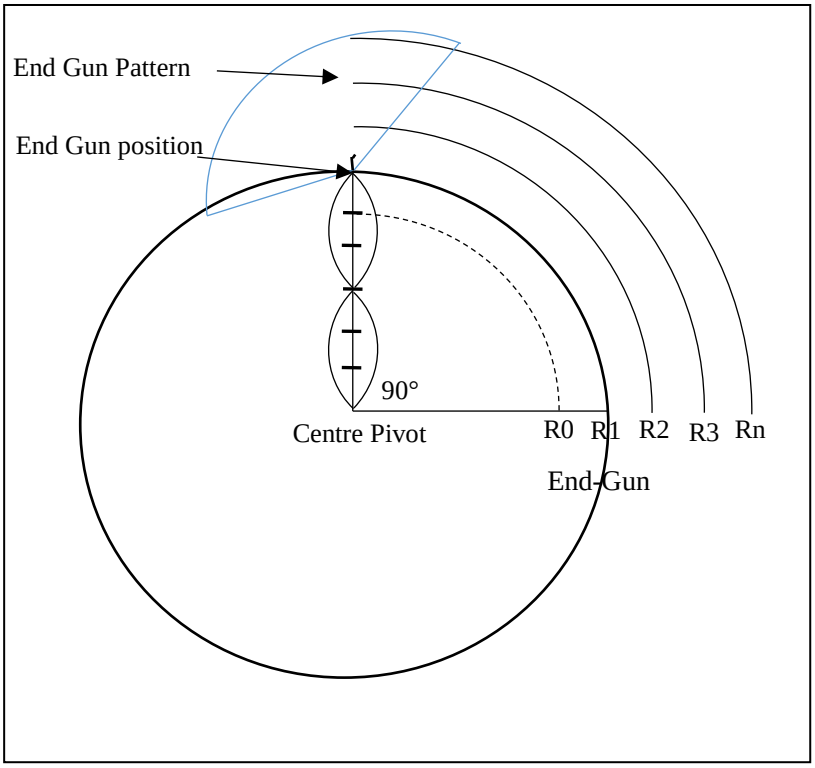

Figure 7-25: A diagram shows the differences in the arc length for end-gun patterns with different radii with the same central angle.

Assuming an end-gun position at R1, the collectors will be at (R2, ... Rn). When, the centre pivot moves through 90°, the end-gun will move the arc length equal to the following Equation:

$$ArcLength1(End-Gun)=\frac{2\pi\times R1_{(End-Gun)}\times 90}{360} \qquad 7\text{-}2$$

In this case, the linear distance at the position of the end-gun is equal to the arc length at the same position because it has the same radius.

The arc length at the first collector is calculated using the following Equation:

$$ArcLength2(collector1)=\frac{2\pi\times R2\times 90}{360} \qquad 7\text{-}3$$

In this case, the pattern will be distributed over an arc length longer than arc length 1, because the radius distance at collector number 1 increases by 3 metres.

The arc length at the last collector will be calculated using the following Equation:

$$ArcLengthN(collectorN) = \frac{2\pi \times Rn \times 90}{360} \qquad 7\text{-}4$$

In this case, the maximum throw of the pattern will be distributed over the longest arc length, because the radius distance at the last collector, n, will increases by 40 metres.

To calculate the proportion of the decrease in applied water depth as a result of increasing the arc length, the value of applied water depth should be multiplied by the ratio of arc length 1 as it is considered to be the first point where the linear distance corresponds with the arc length divided to the arc length 2, 3, . . , n.

The ratio of the decrease can be calculated using the following Equation:

$$TheRatio = \frac{\frac{2\pi \times R1_{(End-Gun)} \times 90}{360}}{\frac{2\pi \times Rn \times 90}{360}} = \frac{R1_{(End-Gun)}}{Rn} \qquad 7\text{-}5$$

In general, the proportion of the decreases in applied water depth can be estimated by dividing the radial distance at the end-gun position on a centre pivot by the radial distances at each collector position under the end-gun. We assume that the radial distance of the end-gun on a centre pivot is the first point of the calculation, and the circumferential length at the end-gun position passing over the radial line of collectors is the same distance as a traveling gun passing over a straight line of collectors. Therefore, the correction factor at the end-gun position will equal one. The correction factor will decrease as the radial distance increases outward from the end-gun position.

However, in the opposite direction toward the centre pivot, the correction will increase as the radial distance decreases toward the pivot point. This will be useful in

calculating the effect of arc movement when an end-gun throws back towards the centre pivot.

7.6 Determining the significance of the curved movement

Three calculations of the correction factor were conducted to explore the significance of the effect of arc movement for different centre pivot radii. The water depth for the optimum transect data under zero wind conditions on a straight path were adjusted using the correction factor for different centre pivot radii of 250, 400 and 550 metres. The results of these tests will be presented in the following section.

7.6.1 Correcting the water depth for a centre pivot of 250 m radius

The transect data for the optimum wetted sector and side sector angle under no-wind speed were generated using TravGUN V3.1 on straight path movement. This transect data was adjusted for a centre pivot radius of 250 metres to represent a curved transect. The water depth for the curve transect decreased by about 1.6 mm. The results of both transects are plotted in Figure 7-26. The RMSE between both transects was calculated and it was found to be 1.43 for centre pivot with a of 250 m radius.

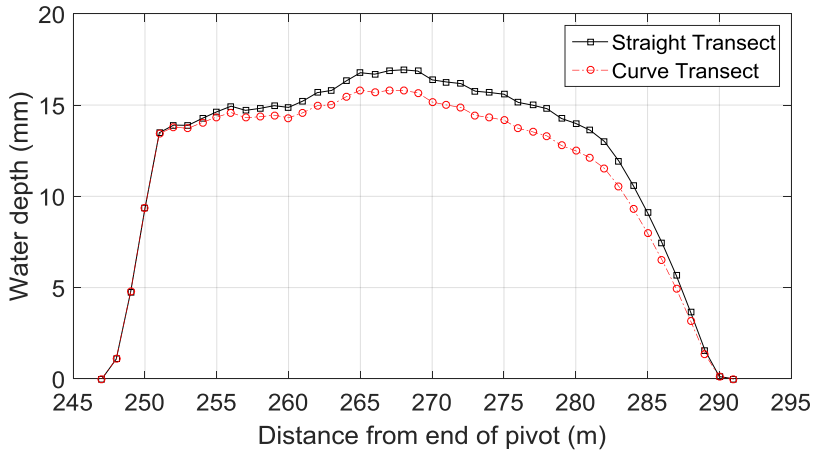

Figure 7-26: The differences between straight and curve transects for a 250 metre long centre.

7.6.2 Correcting the water depth for centre pivot of 400 metre radius

The straight transect data were corrected for a 400 m centre pivot radius. The results of the straight and curved movement were plotted in Figure 7-27. This figure shows that the water depth for the curve transect decreased about 0.96 mm, which is less than for the centre pivot radius of 250 m. The RMSE is 0.93 which is also less than the differences for a pivot radius of 250 m.

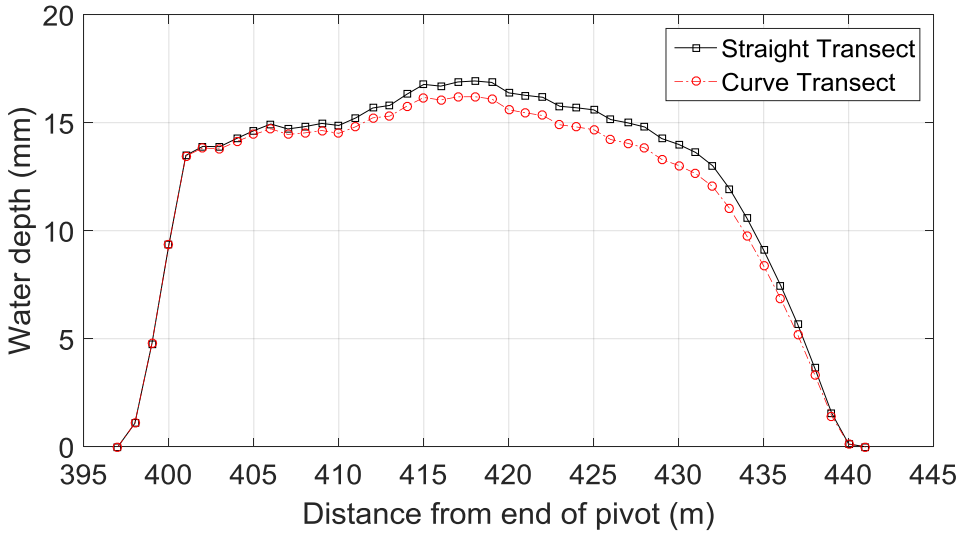

Figure 7-27: The differences between straight and curve transects for centre pivot of 400 m radii.

7.6.3 Correcting the water depth for centre pivot of 550 m radius

The correction factor for a 550 m long centre pivot results in less change in the water depth of the curved transect, at only 0.7 mm, as shown in Figure 7-28. The RMSE was 0.68 which is less than from both centre pivot radii of 250 m and 400m.

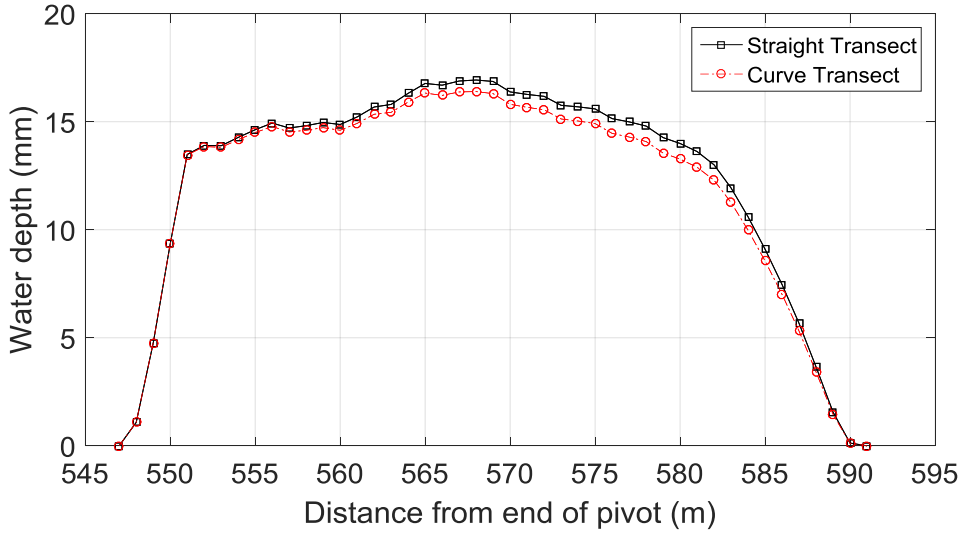

Figure 7-28: The differences between straight and curve transects for a centre pivot with 550 metre radius.

The results of the correction of the transect data for the effect of curved movement reveals that for centre pivot radii less than 400 metre there was a significant effect. The RMSE for this radius was high, and there was decreased water depth about 0.96 mm on an average of about 14mm. The effect on a centre pivot radius of 550 m and longer is not significant on water depths.

7.7 Combining the end-gun pattern with regular centre pivot sprinkler patterns in zero wind

The transect data for the optimized sector and side sector angles of $130°$ and $60°$ for the Nelson 100SR end-gun at zero wind speed was normalized, and then corrected for the arc movement. These data were combined with normalized transect data at zero wind speed for regular centre pivot sprinkler that were Nelson Rotator R3000 green plate sprinklers operating at 148kPa and 2.4 m height on a 4.75 m sprinkler spacing along the last span of the centre pivot (Foley, 2010). Regular centre pivot sprinkler data sets were simulated assuming a centre pivot length of 402.3m, with an end-gun position in the same position as the last regular sprinkler on the centre pivot. The

combined pattern of regular centre pivot sprinkler on the distal span of the centre pivot machine from 354 m radius to 402.3 m, were combined and overlapped with the end-gun pattern and plotted in Figure 7-29.

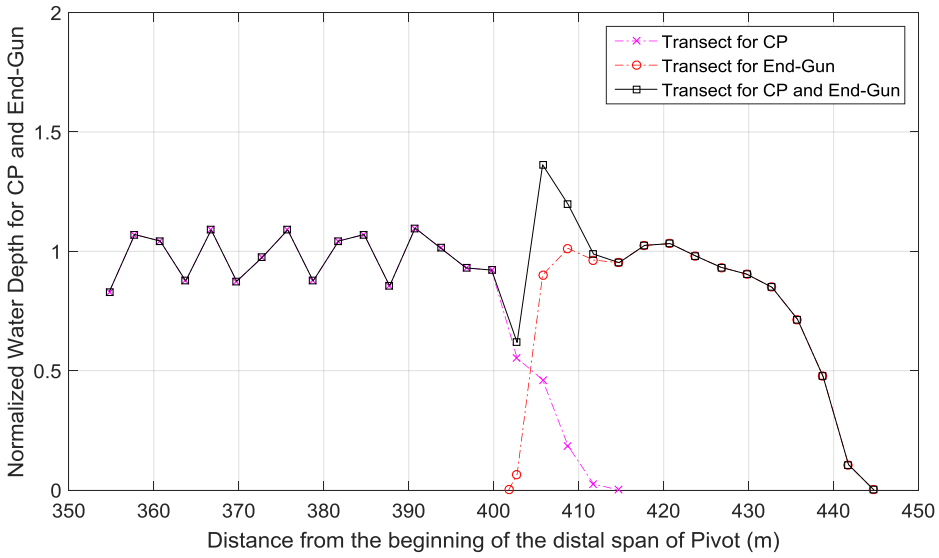

Figure 7-29: The combined application pattern for the centre pivot and end-gun at zero wind speed.

The figure shows, at zero wind speed, that the overlap areas lack uniformity. The first area has low-applied water depth and the second area has over-applied water depth. Therefore, if the position of the end-gun is moved toward the pivot there will be an increase in applied water depth. Conversely, if the position of the end-gun is moved toward the distal of the pivot there will be a decrease in applied water depth in the area that already has low applied water depths. Therefore, the lack of uniformity at the overlapping area at zero wind speed will have a significant impact at any higher wind speed, depending on the position of the centre pivot machine in relation to the prevailing wind direction. The following results in this chapter will reveal the wind effect on the combined pattern of the end-gun and centre pivot, in windy conditions.

7.8 Combining the end-gun wetted pattern with regular centre pivot sprinkler patterns in windy conditions

The following results were produced by overlapping simulated patterns for the centre pivot sprinkler, and the end-gun. The centre pivot sprinkler pattern simulation results were obtained using the mBOSS (moving Boom Overlapped Sprinkler Simulation) software from Foley (2010) to simulate the regular sprinkler patterns for a centre pivot in wind. The patterns for the distal span of the centre pivot machine from 354 m radius to 402.3 m, equal to a quarter mile radius, were simulated for the same wind conditions as for the end-gun in the eight cardinal compass positions as described through Section 7.4 above. The end-gun position is assumed to be at the same position for the last sprinkler at 402.3 m. Applied water depths from both the centre pivot and end-gun were normalized to analyse the uniformity coefficient for the overlapped patterns.

7.8.1 Simulating both patterns for a travel direction of 90°

The combined pattern for simulated results of wind for a centre pivot and end-gun at the first position, when the machine is travelling on a heading of 90°, toward the East, shows slight increases in overlapping values at the end-gun position, as shown in Figure 7-30. The coefficient of uniformity for the overlapped centre pivot and end-gun was 80.5% in the region from 354 metre radius at the beginning of the last span of the centre pivot, out to a radius of 75 % of the end-gun throw.

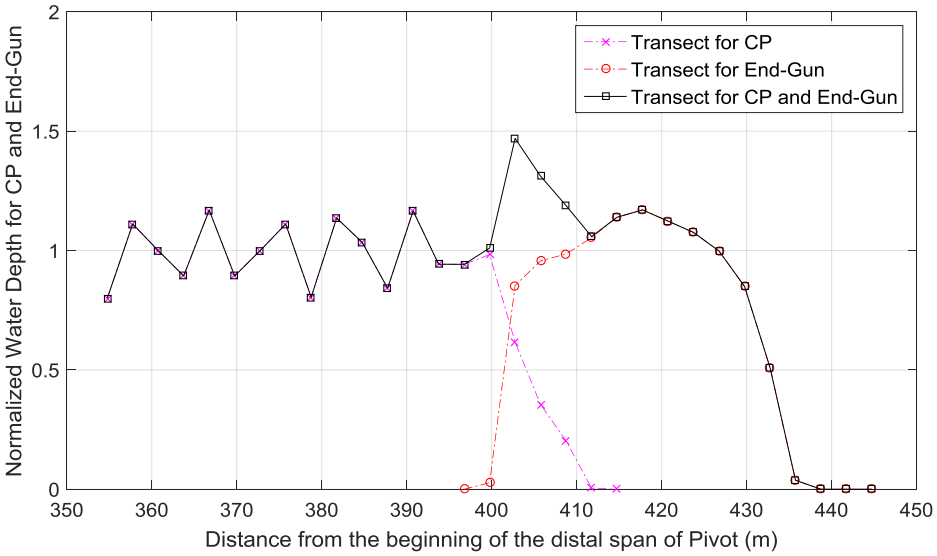

Figure 7-30: The first simulated combined application pattern for a centre pivot and end-gun at a wind speed of 1.5 m/s, with wind direction from East and travel direction of 90°.

7.8.2 Simulating both patterns for a travel direction of 135°

The second travel direction is 135° from the North-West to the South-East. The simulated combined pattern shows increasing applied water depth at the end-gun position as a result of wind drift of the end-gun pattern from the distal point towards the pivot. Because the wind effect on the end-gun pattern was between cross-wind and up-wind, and because the Nelson 100SR end-gun throws the water jet at a high elevation, the end-gun pattern is more prone to wind shift compared with other sprinklers on the pivot. Therefore, the applied water depth at the overlapping area increased, as shown in Figure 7-31. The coefficient of uniformity decreased to 72.2% for the overlapped are of the centre pivot and end-gun.

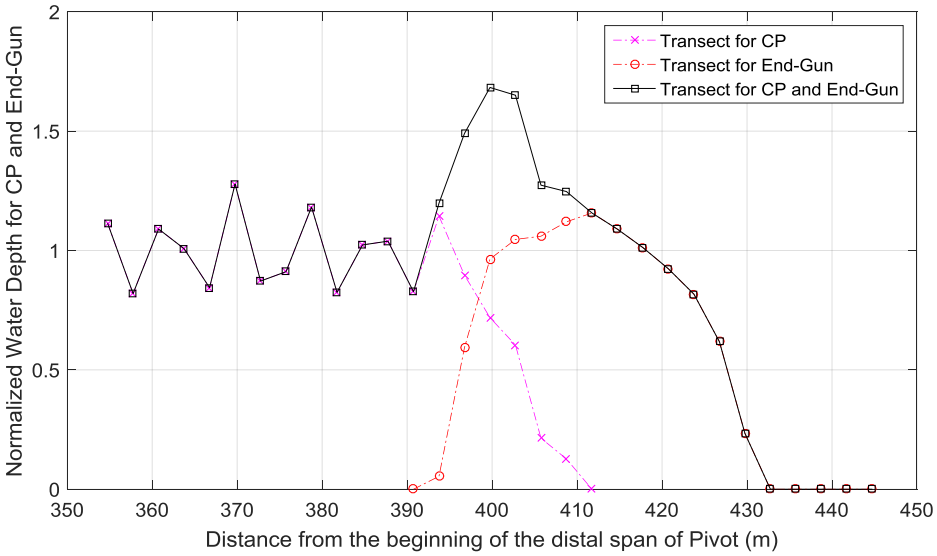

Figure 7-31: The second simulation results showing the combined application pattern for a centre pivot and end-gun at a wind speed of 1.5 m/s, with wind direction from the East, and a travel direction of 135°.

7.8.3 Simulating both patterns for a travel direction of 180°

The third travel direction was 180° from North to South. The simulated combined applied water depth shows a sharp increase in applied water depth at the end-gun position, as shown in Figure 7-32 because the end-gun pattern was upwind and had a high amount of shift from the distal end at the end-gun position towards the pivot direction. The coefficient of uniformity was 73.5% for the combined centre pivot and end-gun irrigation this travel direction.

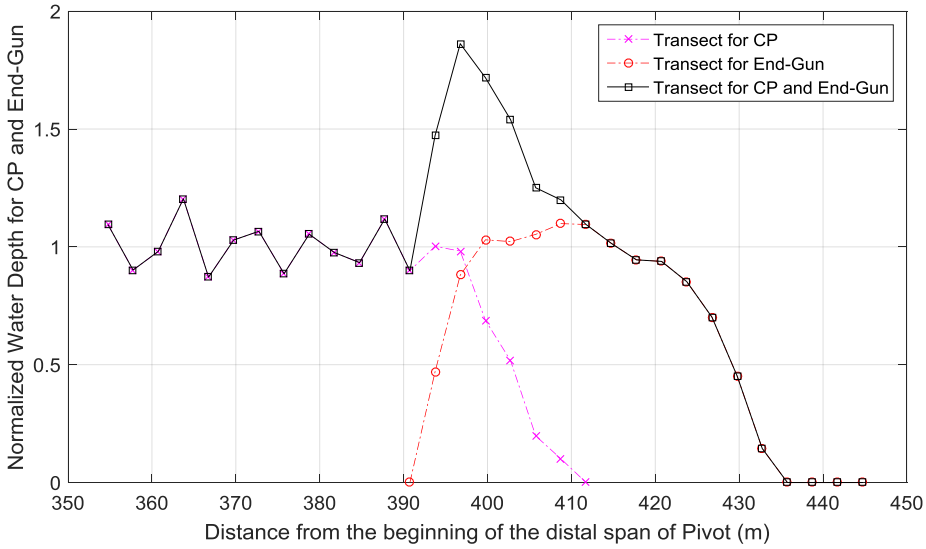

Figure 7-32: The third simulated results for the combined application pattern for a centre pivot and end-gun at a wind speed of 1.5 m/s, with a wind direction from the East, and a travel direction of 180°.

7.8.4 Simulating both patterns for a travel direction of 225°

The fourth travel direction was 225°, from the North-East to the South-West. The simulated combined applied water depth also showed an increase in the applied water depth at the end-gun position, as shown in Figure 7-33. The coefficient of uniformity is 76.3% for both the centre pivot and end-gun irrigated area.

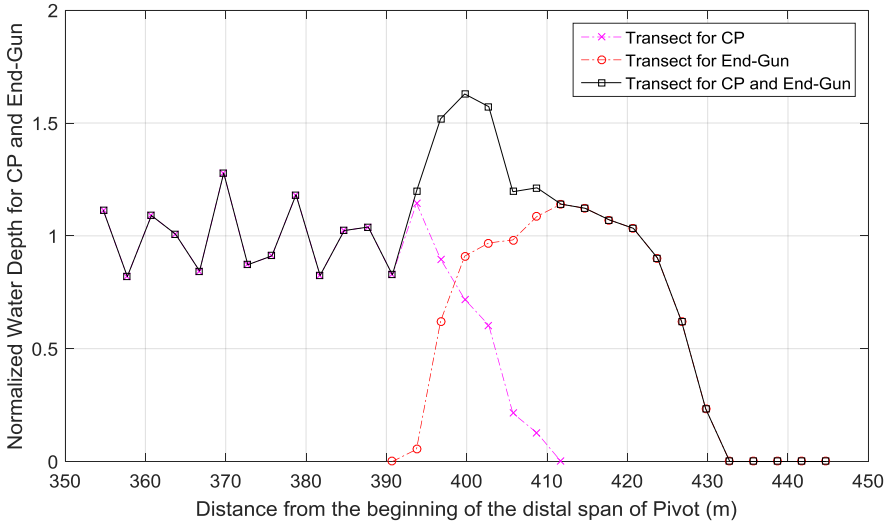

Figure 7-33: The fourth simulated results were for the combined application patterns for a centre pivot and an end-gun, at a wind speed of 1.5 m/s, with a wind direction from the East, and a travel direction of 235°.

7.8.5 Simulating both patterns for a travel direction of 270°

The fifth travel direction was 270°, from East to West. The coefficient of uniformity was improved for this travel direction and found equal to be 81.9% for the combined centre pivot and end-gun applications. However, Figure 7-34 shows both simulated patterns in windy conditions had high applied water depth at the overlapping area.

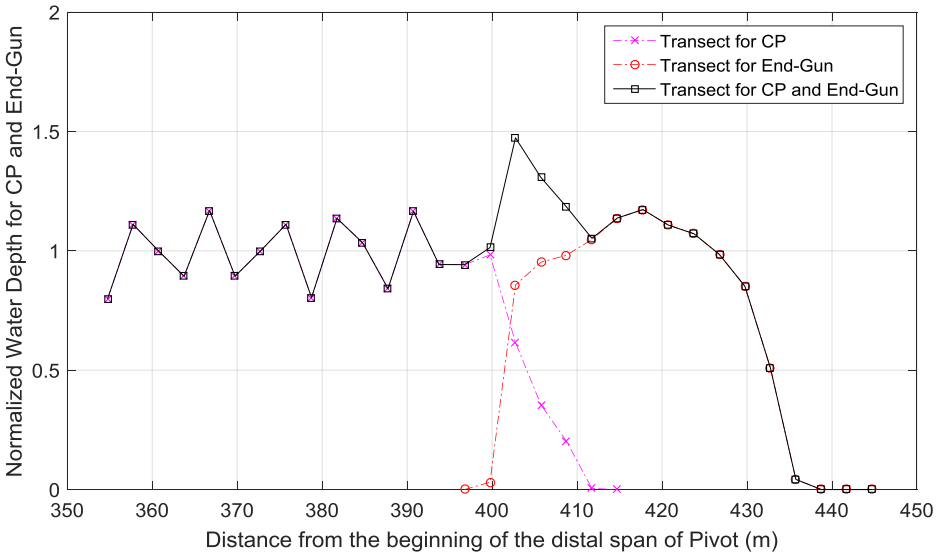

Figure 7-34: The fifth simulated results for the combined application pattern for a centre pivot and end-gun at a wind speed of 1.5 m/s, with a wind direction from the East, and a travel direction of 270°.

7.8.6 Simulating both patterns for a travel direction of 315°

The sixth travel direction is 315°, from the South-East to North-West. Figure 7-35 shows a decrease in applied water depth at the end-gun position. The reason for this reduced depth of applied water is a wind effect on the end-gun pattern between down wind and cross wind. The pattern for the end-gun shifted from the end-gun position towards the outer end because the wind had more influence on the end-gun pattern, whereas the wind had less influence on the sprinkler pattern at the distal end of the pivot. The reason for this variation was that the Nelson 100SR end-gun throws the water at a higher elevation compared to the Nelson rotator R3000 sprinkler with a

green plate at the distal end of the pivot. Therefore, the end-gun pattern drifted more than the other sprinklers at the pivot. However, the coefficient of uniformity slightly increased to 83.6% for the combined centre pivot and end-gun application. Although there was a reduced water depth at the end-gun position, the uniformity of both patterns improved because of the downwind position.

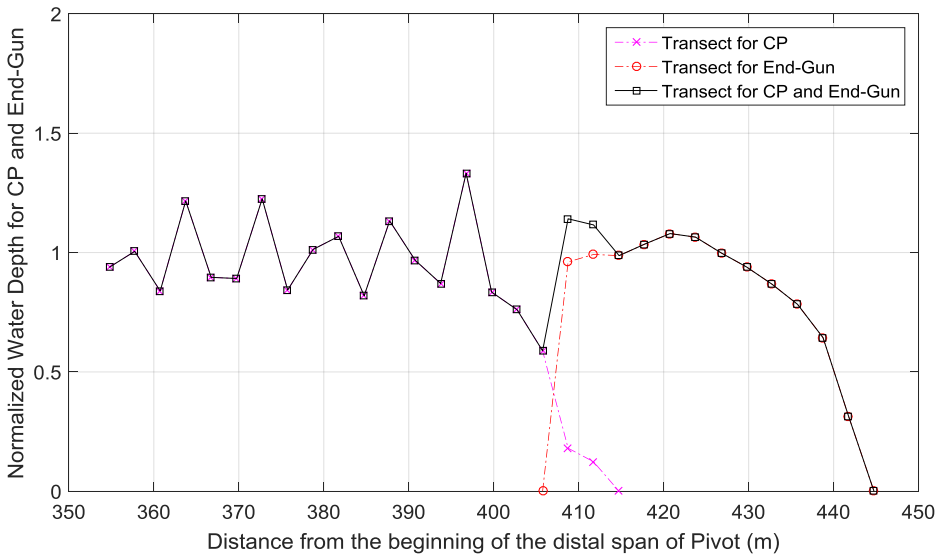

Figure 7-35: The sixth simulated results showing the combined application pattern for a centre pivot and end-gun at a wind speed of 1.5 m/s, with a wind direction from the East, and a travel direction of 315°.

7.8.7 Simulating both patterns for a travel direction of 360°

The seventh travel direction was 360°, from South to North. Figure 7-36 shows a big difference in applied water depths at the end-gun position as a result of wind shift of the patterns, because the end-gun pattern is more prone to wind drift towards the outer end. However, the combined patterns improved in uniformity. As a result, the coefficient of uniformity increased to 84.3% for both the centre pivot and end-gun.

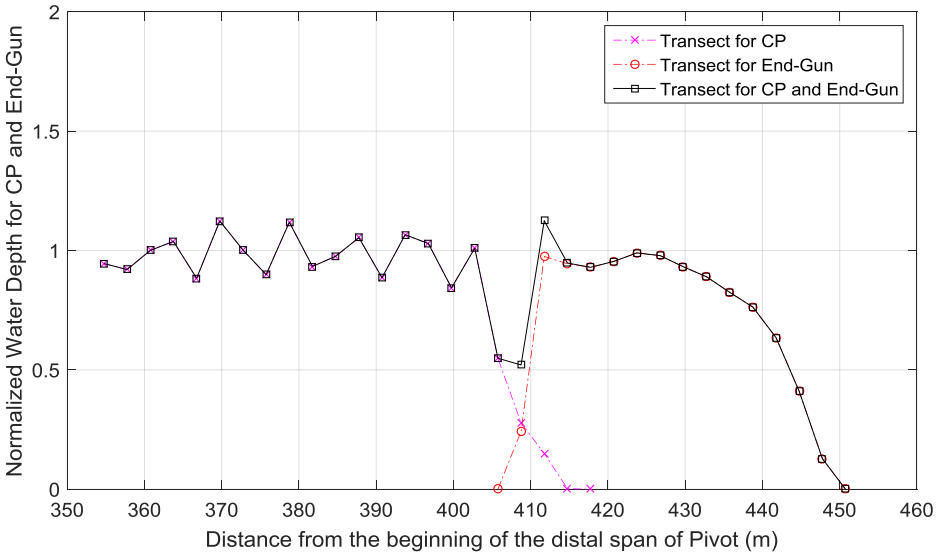

Figure 7-36: The seventh simulated results for the combined application pattern for a centre pivot and end-gun at a wind speed 1.5 m/s, with a wind direction from the East, and a travel direction of 360°.

7.8.8 Simulating both patterns for a travel direction of 45°

The eighth travel direction was a heading of 45°, from the South-West to the North-East. Figure 7-37 shows a reduced depth of applied water at the end-gun position for the combined simulation patterns of end-gun and pivot. The reason for this gap is similar to that for the previous direction of travel. However, the coefficient of uniformity was less at 83.7% for this combined pivot and end-gun irrigation.

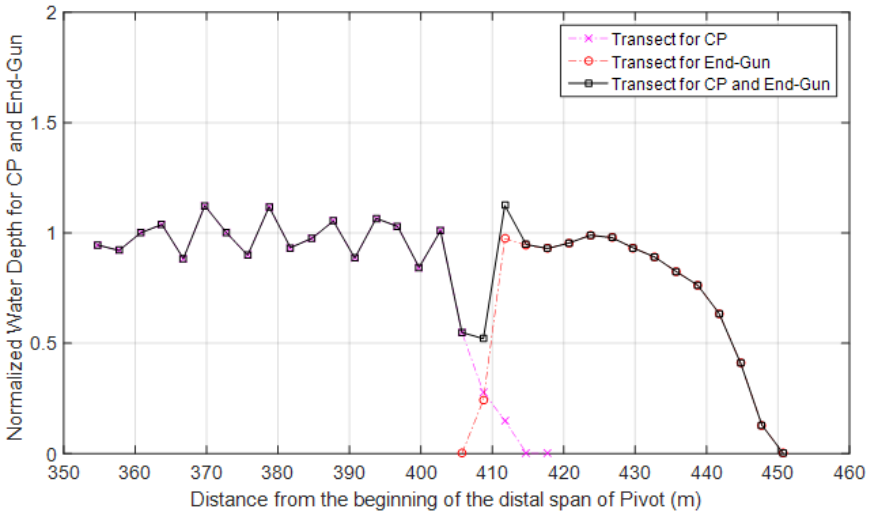

Figure 7-37: The eighth simulation results from the combined application patterns for a centre pivot and end-gun at a wind speed of 1.5 m/s, with a wind direction from the East, and a travel direction of 45°.

The simulation results for the combined patterns at different machine rotation positions shows a large decrease in the CU_{HH} when the machine is travelling upwind and crosswind. Therefore, the wind effect on the combined patterns upwind and crosswind are greater than for downwind.

7.9 The general shapes for different wetted sector angle perpendicular to the direction of travel

The general shapes for simulated transects after using TravGUN V3.1 for a range of wetted sector angles from 60° to 180° for the straight movement with side sector angle perpendicular to the direction of travel are summarised in Figure 7-38. The figure shows that the peak of applied water depth occurred near the centre of the sprinkler when the wetted sector angle was 180°, moving gradually to the outer end when the wetted sector angle decreased to 60°. Conversely, the applied water depth increased as the wetted sector angle decreased as the simulated transects plotted in Figure 7-38. This figure provides a general idea, about how the shape of the transect and the water depth changes when the wetted sector angle changes for a constant side sector angle that is always perpendicular to the direction of travel. This figure could be used as key to maintain the application uniformity in wind conditions by using smaller wetted sector angles when the end-gun pattern is under the influence of a headwind. In this way the maximum applied water depth could be moved to the maximum distance from the sprinkler. When the end-gun pattern is under the influence of a tail-wind, increasing the wetted sector angle should improve the performance. In this way the maximum applied water depth would occur near the end gun sprinkler.

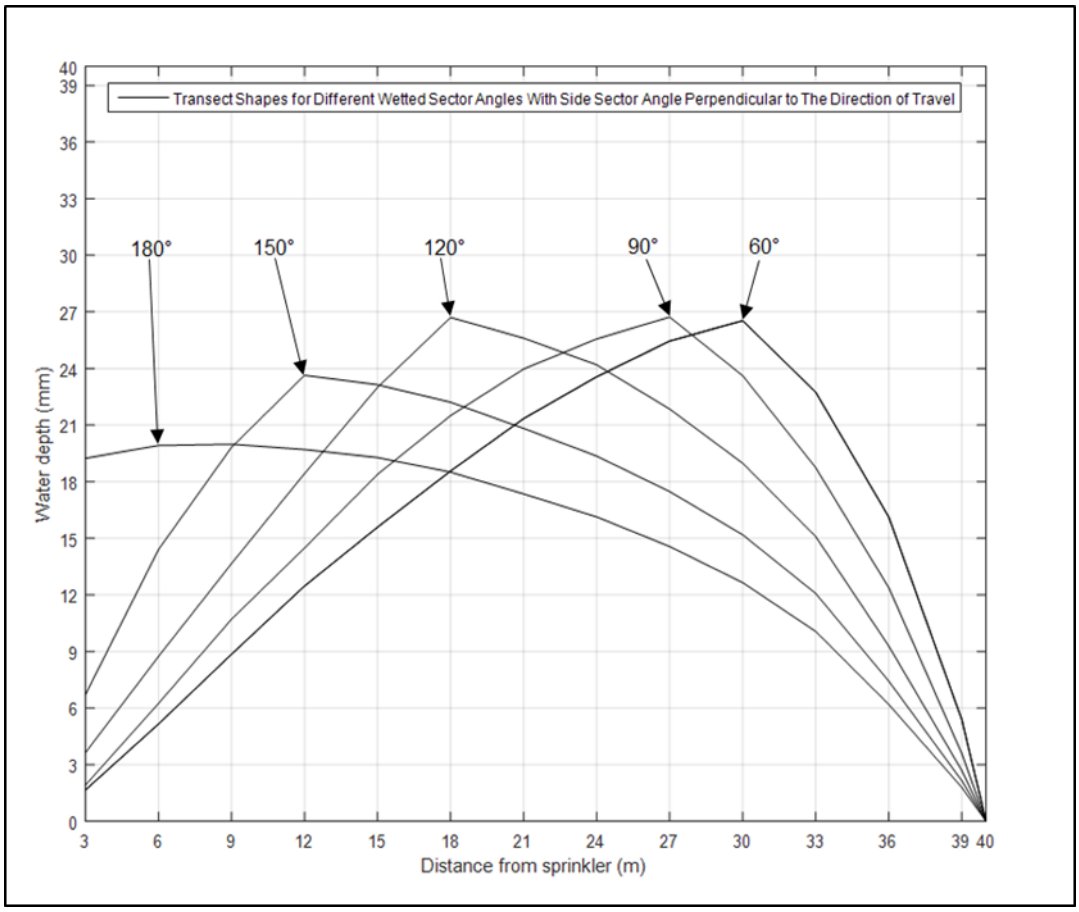

Figure 7-38: Transect shapes for different wetted sector angles, with constant side sector angle perpendicular to the direction of travel.

7.10 Simulating end-gun patterns for curved movement

There is another approach to estimate the effect of the arced movement of the centre pivot that is a little more complex than using the correction factor that was introduced in Section 7.5. This method can be summarised by generating a full matrix of applied water depths at zero wind. This pattern was produced using TravGUN V3.1 for a sector angle of 130° and a side sector angle of 60°. This pattern overlap the centre pivot irrigated circle 5°. The transect produced from the straight movement was calculated by addition of water depth in along lines parallel to the direction of travel at a spacing of one metre. The arced transect can be calculated using the following more complicated calculation process. It was performed by finding the effect of the arc deviation along both the X- and Y-axes for each one metre of machine movement to

pass the transect position. Figure 7-39 shows how the values of the X- and Y-axes are changed.

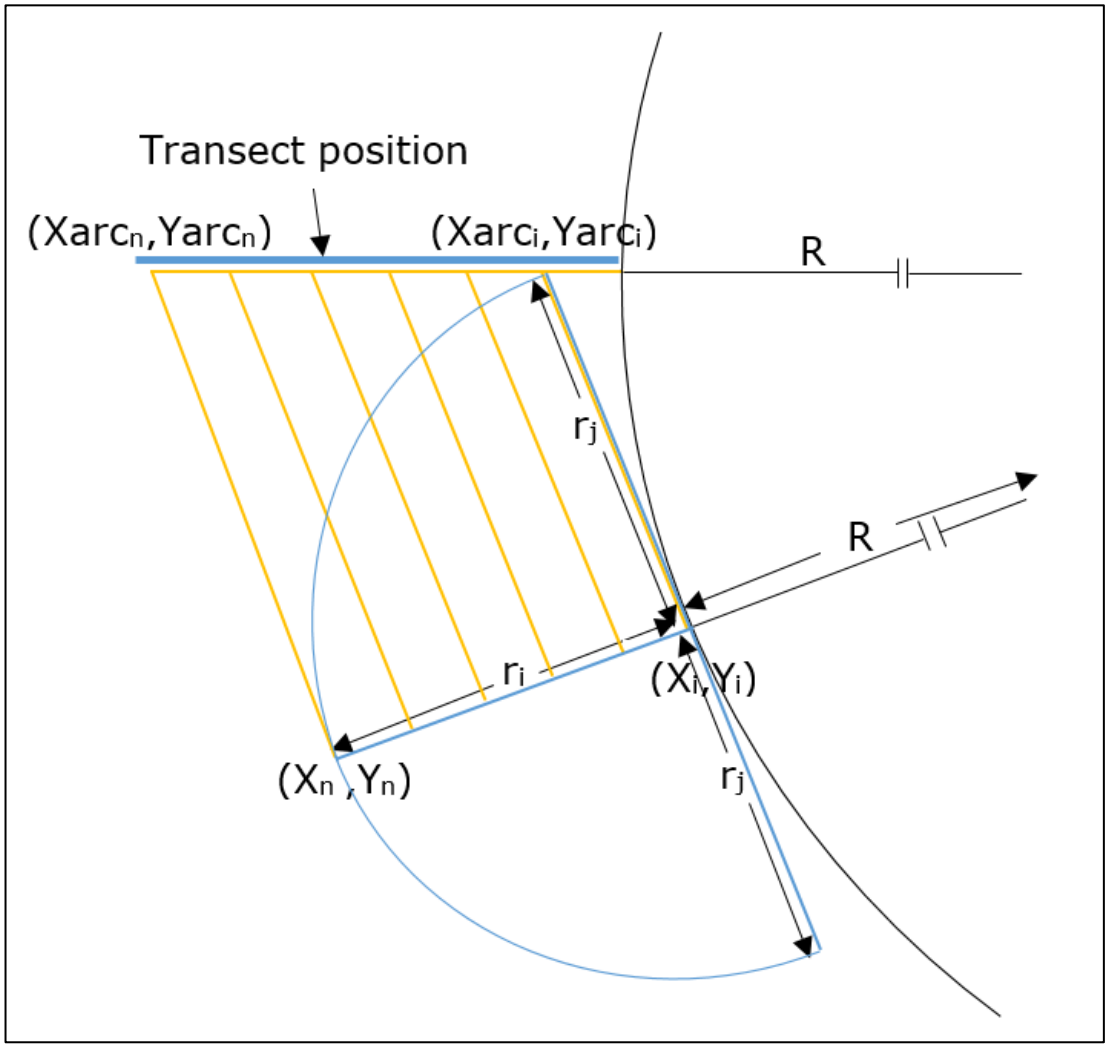

Figure 7-39: Diagram showing how the positions of X, Y points change as a result of the arced movement.

In Figure 7-39 R is the pivot radius,

r is the end-gun radius,

(X_i, Y_i) and (X_n, Y_n) are the original positions of the water depth in the matrix,

and $(Xarc_i, Yarc_i)$ and $(Xarc_n, Yarc_n)$ are the new positions of water depth in the matrix for each one metre movement in the direction of travel.

The values for the change of the arc movement along the X-axis can be calculated using the following Equation:

$$Xarc_{ij} = \sqrt{\left(R + r_i\right)^2 + \left(r_j\right)^2} \qquad 7\text{-}6$$

where i is the indicator for each one metre along the X-axis, and

j is the indicator for each one metre along Y-axis.

The values for the change for the arc movement along the Y-axis can be calculated using the following Equation:

$$Yarc_{ij} = \tan\left(Angle_{arc\,j}\right) \times \left(R + r_i\right) \qquad 7\text{-}7$$

where i is the indicator for each one metre along X-axis, and

j is the indicator for each one metre machine's movement along Y-axis.

The value of $Angle_{arc\,j}$ can be calculated using the following Equation:

$$\tan\left(Angle_{arc\,j}\right) = \frac{r_j}{R} \qquad 7\text{-}8$$

The calculation will begin at the first value of r_j. The pattern will be at the maximum arc angle, and deviated values along both the X and Y-axes, while it passes the supposed transect position, because r_j is at the maximum value. The first value of r_j will be used for all calculations with all values of r_i to produce the first row of $\left(Xarc_i, Yarc_i\right)$. The second value of r_j will be used to produce the second row of $\left(Xarc_i, Yarc_i\right)$ after the machine moves the second metre along the Y-axis. The value of the deviation and the arc angle value will decrease, as much as the machine moves

one metre forward. These processes continue until the value of r_j becomes zero. At this point the first half of the pattern has passed the supposed transect position. Therefore, the values of $(Xarc_i, Yarc_i)$ will be similar to the value of (X_i, Y_i) because the arc angle becomes zero, and the deviation also becomes zero. Next, the second half of the pattern will pass the transect position. The value of the arc angle and the deviation will start increasing again until all of the pattern has passed the supposed transect position.

The values of the applied water depth at $(Xarc_i, Yarc_i)$ will be interpolated and replaced by the applied water depth at (X_i, Y_i) for the original matrix of applied water depths. Then the summation of applied water depths for each one metre distance along the X-axis will represent the arced transect value.

The values of the straight transect data and sampling curved data were normalised and plotted in Figure 7-40 to find the effect of the arced movement, and to compare the results of this approach with the correction factor approach. The figure shows that the applied water depth decreased in both curved sampling and correction factor transects, as a result of the arced movement. However, the water depth in the sampled curved transect decreased more than for the correction factor transect from the end-gun position toward the outer side, while the water depth in the curved sampled transect increased more than for the correction factor transect on the opposite side of the end-gun toward the pivot. However, there is high agreement between both transects, as shown in Figure 7-40. The mean square root error between the curved sampling process and earlier correction factor processed transects, was calculated and was found to be 0.0531.

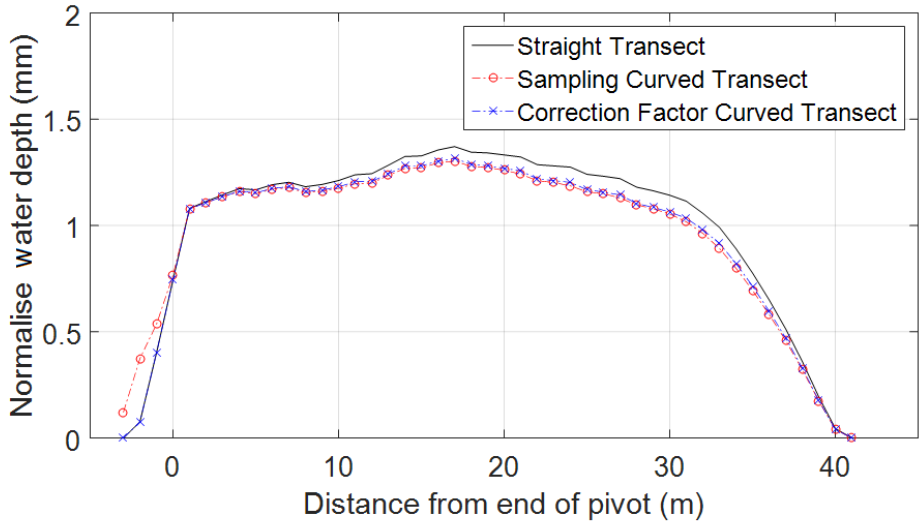

Figure 7-40: A comparison of three transect data sets showing the effect of the arc movement using different approaches including a correction factor.

Both calculation approaches demonstrated the effect of the arced movement of an end-gun on a centre pivot. Regardless, if the effect is not significant for a large radius centre pivot, the effect of the curved movement should be corrected. However, an end-gun on a centre pivot with a radius equal and less than 400 metres will have a high impact on arced movement transect. The time limitation in this study does not permit more e curved sampling for 250 m and 550 m centre pivot radii, to investigate the accuracy of both curved sampling and correction factor. Furthermore, the time in this study does not permit more the curved sampling for the eight simulated wind patterns for combined end-gun and regular pivot sprinkler patterns, so as to calculate the coefficient of uniformity for the entire irrigated pattern.

7.11 Conclusions

This chapter has presented the optimised simulation results for an end-gun on a centre pivot. Firstly, the empirically grounded simulation result under zero wind speed from TravGUN V3.1 reveals that the combination of a wetted sector angle of 130° and a side sector angle of 60° provides the optimum transect for an end-gun on a centre pivot.

This configuration achieved the best overlap, longest sufficiently irrigated distance, and the highest uniformity.

Secondly, simulation results for centre pivot with end-gun moving in an Easterly wind of constant speed for the eight cardinal positions of the compass revealed that the application patterns were distorted, the length of the transect was greatly shortened, and the coefficient of uniformity was decreased while the end-gun was travelling across the wind, and upwind. The simulation results for the end-gun travelling downwind, and across the wind, revealed that the transect length and the coefficient of the uniformity slightly increased.

Thirdly, the effect of the curved movement of the end-gun was adjusted for in the TravGUN V3.1 results using a proposed correction factor. The simulated results adjusted by the correction factor for curved movement, revealed that the applied water depth decreased. This decrease depended on the radius of the centre pivot. The results of the correction factor for three different pivot radii revealed that the curved movement for pivot radii equal and less than 400 m have a significant effect in decreasing the water depth. However, the water depth in the simulated application patterns for radii greater than 400 m were not significantly altered.

Fourthly, the combination of an end-gun pattern and regular centre pivot sprinkler patterns in zero wind conditions revealed that the patterns do not overlap properly. In addition, this problem is worsened under windy conditions in any of the eight positions simulation for the combined patterns.

Fifthly, the simulated results for different wetted sector angles less than 180° perpendicular to the direction of travel in Figure 7-38 could be used to improve the

application uniformity for end-guns on centre pivots in windy conditions using an automatic adjustment of the wetted sector angle.

Finally, the results of another adjustment for the curved sampling of wetted footprints to determine transect data, highlighted water depths that very closely match the results of water depths corrected for curved movement on a 400 m long centre pivot. More study is required to investigate the accuracy of both correction factors for the curved movement of end-guns, and the curved sampling of wetted pattern for different centre pivot radii.

8 CHAPTER EIGHT

Discussion

8.1 Introduction

This chapter discusses the evaluations of end-guns on centre pivot irrigation machines, an investigation of using a new version of the TravGUN model to simulate end-gun performance in wind, and highlights the advantages and the limitations of the existing TravGUN software. It also discusses the limitations associated with collecting data from end-guns on centre pivots, and the development of a new methodology for that purpose. This chapter will then reflect on the objectives and main aim of this dissertation, and how these have been achieved.

8.2 Evaluation of the performance of end-guns on centre pivots

Centre pivot irrigation systems have been used across the world transforming older irrigation systems into some of the most agriculturally productive areas in the world. End-guns are used at the distal end of the pivot to extend the irrigated radius by up to 40 metres. Using ground water and fertilisers through centre pivots is now common practices. So, non-uniform application of irrigation water has a significant and detrimental impact on the crop, the soil and the environment. The irrigated area under the end-gun can equal one quarter of the entire irrigated area of smaller centre pivots, and more regularly accounts for an additional 20% of the an irrigated area. Therefore, it is important to maintain the uniformity for all the irrigated area underneath these

systems. This is especially so when there is a high demand for irrigation water, and a general lack of water resources.

The literature review highlighted the low performance of end guns on centre pivots, but it did not discover any practical solutions or provide useful tools to address this issue. In addition, the literature review highlighted the adverse impact of wind on the performance of large gun sprinklers in terms of uniformity and distortion of the spray pattern. However, there was literature found which investigates the wind effect on the end-gun performance especially when, the end-gun changes its position during the full rotation for the centre pivot system. The results of this research confirm the low performance for the end-guns on centre pivots under wind conditions. The new version of TravGUN V3.1 provides a useful tool to optimize the end-gun performance in different wind conditions and suggest the best end-gun setting according to these wind conditions with minimal cost and effort.

Despite this achievement, there is another challenge of using end-gun on centre pivots. The challenge has mentioned by the literature theoretically and it is the sufficient irrigated area under end-gun. Although the end gun might have a large throw radius, only part of that radius will receive adequate application, which is defined as the sufficient irrigated area. The sufficient irrigated area under end-gun assumed as one third of the total irrigated area under end-gun pattern Keller and Bliesner (1990) and Nelson Irrigation Corporation (2017a). The irrigated area under the end-gun typically represents 20% of the total irrigated area of the centre pivot irrigation system. Therefore, the insufficient irrigated area will be equal to 7% of the total irrigated area of the centre pivot.

In this research through the optimization process, the sufficient irrigated area under end-gun was increased from 2/3 to ¾ of the total wetted area under the gun in no wind

conditions. So, in the optimum case the insufficient irrigated area will be reduced from 7% to 5% of the total irrigated area of the centre pivot irrigated system.

This 5% insufficient irrigated area still has a negative impact on the application efficiency because it represents a water and land area wastage. Water wastage is an important issue whenever there is increasing in the demand for irrigation water. Therefore, this issue will open a new study area for future research to estimate and evaluate the application efficiency and suggest the solution to reduce the wasted water under end-gun on centre pivot and increase water use efficiency.

Based on the above, it is very important to conduct a deep study to evaluate and improve end-gun performance under different wind conditions by developing a novel research approach for this purpose.

8.3 TravGUN limitations

The original TravGUN software has the capability to simulate wind effect on large impact sprinkler patterns from travelling big gun machines under different wind speeds and direction. The original TravGUN model can be calibrated using three sets of transect data, with one in quiescent wind and the other two under different wind speeds and directions. The preliminary investigation of using the original TravGUN to simulate end-gun performance in wind conditions was performed, with 288 simulations for a range of wetted sector angles for 5° intervals from 360° of full circle with side sector angles of 45°, 90°, 180 and 270° respectively. These results highlighted an error during simulation of end-gun patterns that were generally oriented perpendicular to the direction of travel. The literature shows the main differences between travelling gun and end-gun on centre pivot in relation to the direction of travel. In this case, TravGUN does not have the capacity to simulate end-gun pattern in wind

conditions. In addition, the original TravGUN software could not be calibrated from transect data that has been measured on one side of the sprinkler with a side sector angle perpendicular and asymmetrical to the direction of travel.

The new version of TravGUN V3.1 has the capability to calibrate the model from a set of data input from one side of the sprinkler and simulate both travelling gun and end-gun patterns for different wind speed and directions. However, TravGUN V3.1 still has some limitation in relation to simulating the end-gun on centre pivots. These limitations relate to the nature of the curved movement for the centre pivot machine. The original TravGUN display a single pattern in different wind conditions and overlapped pattern for two straight path in 2D chart to optimize the field application under different wind conditions. TravGUN V3.1 does not has the capacity to display the field application for the curved movement and overlapped it with the regular sprinkler on the pivot.

Generally, the effect of curved movement was not considered in the processes of developing the new mathematical model. However, the curved movement have been considered later in Chapter Seven and the theoretical basis was explained. But, did not be applied in the TravGUN V3.1. This can be recommended for future study and development.

8.4 Developing a new mathematical model for big gun sprinklers

The theoretical operation of the TravGUN model (Smith et al., 2008) involves the disaggregation of a transect of catch can values captured under the passage of a large impact sprinkler (big gun) moving parallel to the direction of travel, in zero wind

conditions, to generate a radial leg of applied depths. The operation of a calibrated TravGUN model from the catch can transects, enable users to produce sprinkler wetted patterns for any desired sector, and side-sector angles, for any wind speed and direction combination.

Typically, travelling guns operate with a combination of wetted sector and dry sector angles. The centre of the dry sector angle is commonly parallel to the direction of travel. The TravGUN V2.0 model accepts the input of measured transect data from both sides of the centre travel path of the big-gun sprinkler. The mathematical process to calculate the radial leg data from a zero wind transects occurs on one side of the travel path, using an average of transect data from each side, because the wetted pattern is symmetrical.

The specific characteristics of end-gun operation requires the development of a new mathematical process for measured transect data from one side of the sprinkler where the centre of the dry sector is generally perpendicular to the direction of travel. In addition, the new mathematical process must have the capacity to calculate the radial leg when the centre of the dry sector angle is asymmetrical to the direction of travel. A novel mathematical approach was developed for this purpose.

The processes of developing a new mathematical model for TravGUN include both original equations 2-12 and 2-14 (Smith et al., 2008). The first equation 2-12 was developed to estimate the length of each segment area that contribute in the time required from the machine with the sprinkler pattern to pass transect of the catch cans. The development process covers all the three cases that assumed for any combination of wetted sector and side sector angles in Chapter Three. However, the development

of the second equation was developed to estimate the application rate at each segment area for the first case only which is the most common setting for end-gun.

The new TravGUN sub-model included several developments of algorithms trialled using MATLAB scripts. The final MATLAB script was tested to produce radial leg data from measured transect data at quiescent wind for different combination of wetted sector and side sector angles, similar to usual end-gun operating configurations. The theoretical assumption for the other two cases are not known for any practical use yet. So, the other two cases may be useful for future study.

8.5 New methodology for field tests

An end-gun on a centre pivot has a specific set of operating characteristics, and it overlaps with different sprinkler patterns from the centre pivot spans. In addition, it is attached to the machine at the distal end, at radii up to 400 metres or more. Therefore, it is difficult to measure the transect data for an end-gun separately from the adjacent regular sprinklers on the centre pivot span. Equally it is difficult to measure the transect data of the adjacent regular sprinklers on the centre pivot separately from the end-gun pattern, for the same machine operating speed and water pressure, especially in quiescent wind. This limitation becomes more difficult and increases the cost and the effort when a large number of these data sets are needed for validation of the new sub-model. This challenge and research limitation had been solved by developing a new methodology for data collection.

The new methodology that was described in Chapter Four facilitated the extensive tests and field data collection. However, there are a lot of tests excluded from Chapter Five and presented in the Appendixes for two reasons. The first reason was using taper

ring nozzle that produces small droplet size near the sprinkler. These small droplet are more prone to wind effect and resulting in high variation of applied water depth near the centre of the sprinkler especially for radial leg tests. The second reason is that measurements were performed during variable wind conditions (either wind speed increase or wind direction changes during the test) which was difficult to avoid due to the location and altitude of the experimental site. Therefore, it is very important to review the historical weather condition before choosing the experiment site.

8.6 Field measurements for end-gun configuration

Two types of field measurements were conducted. The first measured data type were for the radial leg of the Nelson 100SR end-gun, from stationary machine tests, to validate the new sub-model. The second measured data type were transect data for several wetted sector and side sector angles perpendicular to the direction of travel under quiescent wind conditions for validation purposes. Another set of transect data type was measured with different wind speeds and directions, for calibration of the wind predictive capacity of the model, and to simulate the end-gun pattern in windy conditions in the later stages of the research.

8.6.1 Radial leg data

The new method of measuring radial leg in open field using three or four lines radially around the sprinkler discover that there is a variation in the applied water between the individual lines. This result shows that measuring the radial leg from one side of the sprinkler does not enough to represent the actual radial leg. Obtaining an accurate radial leg data set is so important for the validation process, because it represents the unique characteristic of any particular sprinkler configuration.

8.6.2 Transect data from straight movement

Twenty-one transect data sets were measured for different combinations of wetted sector and side sector angles for straight travel movement. Twenty tests were measured with a symmetrical side sector angle to the direction of travel, and one was measured with an asymmetrical side sector angle to the direction of travel, to be sure that the new mathematical model was working correctly for any combination of wetted sector and side sector angles. Five of these transect data sets were measured at quiescent wind speeds, and were used for the validation of the new sub-model. As discussed throughout Chapter 6. The other transects were measured under different wind conditions and can be classified into two sets. The first set was chosen while wind speed and direction were constant, and then were used for calibration of the model for the effect of wind and simulating the end-gun pattern under windy conditions in later stages of the research. The model cannot be calibrated correctly from transect data measured during fluctuating wind speed and directions. These other transect data sets that were measured during fluctuating wind speeds and directions, are presented in Appendix B.

Measuring transect data from straight movement for end-gun configuration does not reflect the real transect data for end-gun on centre pivot. However, this method does simplify the complexity of the curved movement of the end-guns on centre pivot. Because, the development of the new mathematical model does not consider the effect of curved movement of end-gun on centre pivot. This method is very important in the validation process at this stage.

8.6.3 Transect data with curved movement

Tests were performed for a sector angle of 180° with a side sector angle perpendicular to the direction of travel for different curved radii, to explore the effect of the curved movement of an end-gun on a centre pivot. Five tests were measured for curved movements. Three of these tests were measured in quiescent wind conditions, and the other two were measured during times with inconsistent wind speed. These wind conditions affected the accuracy if results, so these two tests are presented in Appendix B. The results of the three tests in quiescent wind speeds were for a 200 metre curve radius, 300 metre radius, and 400 metre radius, and were compared with the measured transect data for straight movement for the same sector and side sector angles. A slight decrease in applied water depth occurred at the first collector. The results for these transects did not show an effect of curved movement for the same sector angle, when compared with straight movement. There are a number of reasons that effected the accuracy of these tests. Firstly, wind speed and directions were different during each test. Secondly, the curved movement for the travelling gun were not as smoothly completed as an end-gun on centre pivot. However, this result is consistent with that of (Bittinger & Longenbaugh, 1962). The weather records during this test showed there was a slight increase in wind speed during these tests. Therefore, this result could not be used to identify the actual effect of curved movement. However, the effect of curved movement was modelled later in Chapter Seven using different techniques.

The purpose of measuring radial leg data from different curve movements is to discover the effect of the curved movement of end-gun on centre pivot for the same big gun sprinkler operation conditions for the same sector and side sector angles. The result of these tests did not reflect the effect clearly for more than reasons. Firstly, wind

speed and directions were different during each test. Secondly, the curved movement for the travelling gun were not as smoothly completed as an end-gun on centre pivot. The weather records during this test showed there was a slight increase in wind speed during these tests. Therefore, this result could not be used to identify the actual effect of curved movement. However, the effect of curved movement was modelled later in Chapter Seven using different techniques.

8.7 Validation of the new TravGUN sub-model

The comparison between predicted radial leg data from TravGUN V3.1, using measured transects in quiescent wind conditions (less than 1m/s) for a range of sector angles (80° to 180°) perpendicular and asymmetrical to the direction of travel, against measured radial leg data show very high levels of agreement for the same machine configuration. The comparison graphs through Chapter 6 clearly show that the predicted radial leg have very similar shapes and trends of water depth with radial distance to the measured radial leg. The comparative statistical analyses show low values of RMSE between (0.68 and 0.87). These good results validate the simulation performance levels of the new TravGUN V3.1 software model. The new sub-model adds more capacity to TravGUN to allow measurement of transect data from a new wider range of wetted sector and side sector angles, especially for end-guns on a centre pivots. In addition, the new model has the ability to optimise and simulate end-gun patterns for different wind speeds from any direction.

However, the value of application rate at first point for predicted radial leg shows higher value than measured radial leg. Because, TravGUN calculates the value in the centre of the sprinkler from a linear equation between the two points from the right and left sides in transect. The advantages of the research achievements that provide

useful tools to simulate end-gun performance in different wind conditions from measured transect data, for any end-gun configuration covers the inaccuracy at the first point. This reduces the effort and cost associated with optimisation of end-gun irrigation performance by researchers and industry alike.

8.8 Correction the curved movement

End-guns on a centre pivot move on curved paths. However, the TravGUN model was built for a travelling machine moving along a straight path. The previously described new sub-model to determine the radial leg, process to simulate sector angles relevant to end guns and predict the wind distorted spray pattern all assume a straight path. It was proposed that the curved movement could be accommodated through a simple process.

There have been a number of studies conducted to determine the effect of the curved movement of the sprinkler pattern on centre pivot system. Bittinger and Longenbaugh (1962) concluded that the effect of curved movement considered as linear motion for the centre pivot radius equal five times the sprinkler pattern radius for practical purpose. The results from field tests in this research did not provide an accurate result to determine the effect of curved movement. However, the theoretical analysis and the calculations for the curved movement in Chapter Seven shows there is an effect of the curved movement by decreasing the value of applied water depth. This decreasing depends on the value of the centre pivot radius.

Three calculations for three correction factors for three different centre pivot radii of 250, 400 and 550 metre were performed, to determine the significance of the curved movement on the applied water depths from centre pivot end-guns. The results show

that the curved movement on a radius of 400 metre or less, will decrease applied water depths between 0.96 to 1.4 mm in a 16 mm irrigation, which is about to 8.8% decrease.

There is another approach to estimating the effect of the curved travel movement, by simulating curved transect paths. One estimation using this approach was done for a centre pivot with a radius equal to 400 metres. The results also show applied water depths decreased in similar amount using this approach. These results were compared with the results of the correction factors, for the same centre pivot radius, and show a very similar trend in decreasing water depths compared to straight movement paths. This comparison between different estimation approaches, strongly support the fact that there is an effect of curved movement on the applied water depth underneath irrigated areas from end-guns on centre pivots. However, the significance of the effect of curved movement does strongly depend on the centre pivot radius.

Regardless of the significant or not of the effect of the curved movement, this theoretical analysis should be considered and applied in order to correct the water depth when estimating the radial leg from a transect that measured from real end-gun on centre pivot. Because, TravGUN V3.1 does not calculate the effect of curved movement for end-gun on centre pivot. This issue, needs to be considered for more study and for future development of TravGUN model.

8.9 Using the new model (to solve the problem)

The simulation results for wetted sector and side sector angles under zero wind conditions using the new TravGUN V3.1 revealed that the combination of wetted sector and side sector angles of 130° and 60°, respectively, provide the optimum transect for an end-gun on a centre pivot to achieve the best values of the overlap, the highest average applied water depth, and the highest value of CU_{HH} with the longest effective irrigated radius.

This optimization was based on recommendations from a review of the literature, the industry, and local grower practice for adjustments to the wetted sector and side sector angles. These values of the optimum wetted sector and side sector angles were consistent with those of Solomon and Kodoma (1978). However, these values are not consistent with those of Keller and Bliesner (1990). In addition, these optimised values are not consistent with Nelson Irrigation corporation (2017) recommendations and with local growers' practice for a Nelson end-gun on a centre pivot operating under the same conditions.

The simulation results for end-gun configurations from the literature, Nelson Irrigation Corporation, and local growers' practice were not optimal. The optimum wetted sector angle result was 130° with 60° side sector angle, and this result was consistent with one source in the literature.

8.10 Simulating end-gun pattern in windy conditions

The simulation tests obtained using TravGUN V3.1 under constant wind speed and direction are considered to be credible results for the application pattern and transect for an end-gun on a centre pivot. The transect results demonstrated that the application

pattern was distorted and the length of transect significantly shortened while the end-gun on a centre pivot travelled crosswind and upwind. The transect results also demonstrated that the CU_{HH} for the effective irrigated radius under an end-gun on a centre pivot decreased to between 47.7 to 54.0 % when travelling crosswind and upwind.

Conversely, the transect data from simulation tests for the application pattern for an end-gun on a centre pivot when travelling downwind, and between downwind and crosswind, revealed that the effective irrigated radius and the CU_{HH} increased to 95.2%. However, the average applied water depth for an end-gun on a centre pivot slightly decreased, when the transect position was between a downwind and crosswind influence.

The simulation results from TravGUN V3.1 for eight end-gun travel directions under constant wind speed and direction in this research found that the application uniformity for end-guns on centre pivots were substantially decreased while the end-gun on centre pivot was travelling crosswind and upwind.

8.11 The combination of end-gun and centre pivot patterns

Only analysing end-gun patterns in windy conditions for different directions of travel of the centre pivot, without overlapping these patterns with the other sprinklers on the pivot, does not reflect the real effect of wind for the entire machine, especially in the overlapped area. Therefore, a normalised end-gun pattern was combined and overlapped with a normalised centre pivot pattern in zero wind conditions to present a broader view of both patterns. The combination and overlapping were performed on

the assumption that the end-gun position is at the same position as the last sprinkler at the distal end of the pivot.

The combined patterns for the end-gun and the regular sprinklers on the centre pivot in zero wind conditions, demonstrated that the end-gun pattern did not match the other sprinklers on the centre pivot, especially at the end-gun position and the overlapped area. This is because the characteristics of the Nelson 100SR end-gun sprinkler are completely different from those of the Nelson Rotator R3000 sprinklers with green plates, and are especially impacted due to the higher elevation of the end-gun water jet and its interaction with the air during windy conditions. So, the uniformity issue is exacerbated.

The general features of the combined patterns for both end-gun and centre pivot sprinklers for a prevailing wind conditions increases the applied water depth at the overlapping area at the end-gun position over the average applied water depth. The coefficient of uniformity decreases and shortens the length of the end-gun pattern when the machine rotation is subjected to the effects of prevailing crosswinds and upwinds. The applied water depth at the overlapping area at the end-gun position decreases less than the average applied water depth, increases the coefficient of uniformity and lengthens the end-gun pattern when the machine rotation is subjected to downwind, and in between downwind and crosswind effects. An innovative solution, utilizing some new technology, is needed to solve this issue and enhance the performance of end-guns on centre pivots. This conclusion is consistent with other studies (Agriculture Victoria, 2017; Foley, 2008; Henggeler & Vories, 2009; Smith & North, 2009; Vories et al., 2008).

8.12 Conclusion

The optimisation results revealed that the optimum combination of a 130° wetted sector angle and a 60° side sector angle in zero wind gave best application uniformity, the longest sufficient irrigated radius, with an acceptable overlap of 5° with the regular sprinklers on the distal end of the pivot. The simulation results for eight end-gun travelling directions under a constant wind speed and direction, allowed the discovery that the end-gun performance was badly effected in the directions of end-gun upwind and crosswind travel. At the same time, the application uniformity deteriorated at the overlapping area in all eight end-gun travel directions.

Overall, in this research, significant outcomes have been completed by implementing and achieving a series of logical objectives with acceptably accurate results. This novel research has developed a research methodology including a software programme for researchers and engineers to evaluate end-gun performance in windy conditions, to allow them to develop solutions to increase end-gun irrigation performance.

9 CHAPTER NINE

Conclusions and Future Study

9.1 Conclusions

The main objective of this study was to investigate the performance (application uniformity) of an end-gun sprinkler on a centre pivot irrigation system under different wind conditions, and determine if some improvement can be made to the irrigation performance. A series of theoretical, mathematical calculations and field tests were conducted to achieve this.

A series of logical sub-objectives were also implemented to achieve this goal. Firstly, a new sub-model was developed and combined with TravGUN software to calculate radial leg data for an end-gun by implementing a MATLAB script. This sub-objective was achieved by developing a series of algorithms to increase the capacity of TravGUN V3.1 to calculate radial leg data for any combination of wetted sector and side sector angles and then rotating this radial leg to generate an array pattern for the end-gun. Secondly, a series of twenty five field tests were conducted to measure radial leg data, and a series of catch can transects data for a specific combination of wetted sector and side sector angles for the end-gun, in quiescent wind. These radial leg and transect data sets were used to calibrate the new version of TravGUN. Thirdly, the new sub-model (TravGUN V3.1) was validated using measured transects under different wind conditions. The end-gun pattern was then simulated under a prevailing wind of constant speed and direction for a full rotation of the centre pivot to calculate the coefficient of uniformity at eight end-gun positions, based on the rotation of a centre

pivot irrigation system. Fourthly, the effect of the curved movement of the end-gun on a centre pivot was estimated by multiplying the transect data by a proposed correction factor. Finally, the end-gun pattern was combined with the centre pivot sprinkler patterns under zero wind conditions. Then, eight simulated patterns from a full rotation of a centre pivot irrigation system in windy conditions were combined with eight end-gun patterns, and the coefficient of uniformity was estimated for the combined sprinkler pattern types at each position.

The study concludes that, to achieve the highest uniformity, the optimum sector angle is 130° when combined with a side sector angle 60°. This configuration maintains the overlap with the last sprinkler at the distal end of the pivot. The study found that the end-gun and regular sprinkler patterns overlap on the pivot under zero wind conditions, produces consistently poor uniformity. This issue becomes more complicated in windy conditions because of the nature of the shift and change of the end-gun wetted pattern overlap with the shift and change of the regular centre pivot sprinkler overlap. These is completely different sprinklers interactions for different positions of the centre pivot, in wind different end of machine uniformity results.

9.2 Recommended Future research

1 The new TravGUN V3.1 sub-model was developed in this study to calculate the theoretical length of each segment or part of a segment based on the original equation $l_1 = 2\sqrt{r_0^2 - r_1^2}$ of the TravGUN model for any combination of sector and side sector angles (the three cases described in Chapter Three). The application pattern at each segment or part of a segment that can be calculated using the original equation $\bar{Z}_1 = d_1 V / l_1$ has been developed in this study only for the first case mentioned in Chapter Three. Further development is needed to

increase the capacity of TravGUN software to calculate the application pattern for the three cases that developed in Chapter three.

2 Further developments are required for TravGUN V3.1 to estimate and display the performance factors for the end-gun alone, as well as when combined with a centre pivot, to facilitate and enhance the optimisation requirements.

3 The validated model should be used to make recommendations for end-gun physical settings to maximise irrigation uniformity for the entire centre pivot machine under particular average wind conditions, by selecting the optimum sector and side sector angles. The shapes of different wetted sector angles in Figure 7-38 should be used to enhance the application uniformity under particular wind conditions (crosswind, upwind and downwind) for different machine rotations.

4 There is a need to investigate automated adjustment capacity for end-guns operating in windy conditions to maintain the irrigation uniformity of the entire machine. This requires the following considerations:

- The possibility of adding a small gun operation to automatically fill the gap in applied water depth in the downwind direction and stopping it in the upwind and crosswind directions.
- The possibility of automated adjustment of trajectory angle to maximise water throw in the upwind and crosswind directions and to minimise water throw in the downwind direction, to minimise wind pattern shift.
- The possibility of automated adjustment of the end-gun nozzle bore to change the droplet size to maximise water throw in the upwind and

crosswind directions and to minimise the water throw in the downwind direction to minimise wind drift.

- The possibility of changing end-gun position at the distal end, forward and backward from the pivot to maintain the uniformity according to the opposite direction of wind effect by using automated adjustment.

References

Agriculture Victoria 2017, *Centre Pivot and Lateral Move Systems*, Agriculture Victoria, viewed 5/01/2018, <http://agriculture.vic.gov.au/agriculture/farm-management/soil-and-water/irrigation/centre-pivot-and-lateral-move-systems>.

Al-Naeem, M 1993, 'Optimisation of hosereel rain gun irrigation systems in wind: simulation of the effect of trajectory angle, sector angle, sector position and lane spacing on water distribution and crop yield', Cranfield university.

ASAE S436.1 2003, *ANSI/ASAE S436.1 DEC01 Test Procedure for Determining the Uniformity of Water Distribution of Center Pivot and Lateral Move Irrigation Machines Equipped with Spray or Sprinkler Nozzles*, ASAE, USA.

Bittinger, MW & Longenbaugh, RA 1962, *Theoretical distribution of water from a moving irrigation sprinkler*, American Society of Agricultural Engineers.

Blackmore, B, Griepentrog, H-W & Fountas, S 2006, 'Autonomous systems for European agriculture', in Automation Technology for Off-Road Eguipment, ATOE 2006: *proceedings of theAutomation Technology for Off-Road Eguipment, ATOE 2006*.

Bureau of Meteorology 2015a, *Bureau of Meteorology: Australia's official weather forecasts, Weather Map, Mean Sea Level Pressure (MSLP) map, viewed 26 March 2015*, <http://www.bom.gov.au/australia/charts/synoptic_col.shtml>.

Bureau of Meteorology 2015b, *Bureau of Meteorology: Australia's official weather forecasts, Weather Map Sea Level Pressure (MSLP) map, Interpreting the Mean Sea Level Pressure (MSLP) Analysis, viewed 23 May 2015*, <http://www.bom.gov.au/australia/charts/Interpreting_MSLP.shtml>.

Bureau of Meteorology 2016, *Australia's official weather forecasts, Queensland weather and warnings, Monthly statistics, TOOWOOMBA, viewed 7 June 2016*, <http://www.bom.gov.au/climate/averages/tables/cw_041103.shtml>.

Centralstation 2014, *Centre Pivot Irrigation Australia, Aerial of pivots, Centralstation, viewed 7 January 2018*, <http://www.centralstation.net.au/a-day-at-kilto/>.

Christiansen, JE 1942, *Irrigation by sprinkling*, University of California Berkeley, CA.

Colombo, A, do Prado, G & de Oliveira, HF 2009, 'Modeling wind effects on travelling gun sprinkler water application uniformity', in 2009 Reno, Nevada *proceedings of the2009 Reno, Nevada* American Society of Agricultural and Biological Engineers, p. 1.

Current Result 2018, *Average Annual Wind Speed at Australia Cities, Toowoomba, Queensland, viewed 7 January 2018*, <https://www.currentresults.com/Weather/Australia/Cities/wind-annual-average.php>.

Dalvand, S 1986, 'Effect of pressure on hose-reel raingun performance at various windspeeds', Silsoe, Bedford.

De Lima, J, Torfs, P & Singh, V 2002, 'A mathematical model for evaluating the effect of wind on downward-spraying rainfall simulators', *Catena*, vol. 46, no. 4, pp. 221-41.

Elliott, RL, Nelson, JD, Loftis, JC & Hart, WE 1980, 'Comparison of sprinkler uniformity models', in Journal of the Irrigation and Drainage Division, American Society of Civil Engineers: *proceedings of theJournal of the Irrigation and Drainage Division, American Society of Civil Engineers* pp. 321-30.

Faria, LC, Beskow, S, Colombo, A & de Oliveira, HF 2012, 'Modeling of wind effects on water application uniformity of sprinkler irrigation: medium-sized sprinklers', *Revista Brasileira de Engenharia Agrícola e Ambiental*, vol. 16, no. 2, pp. 133-41.

Faria, LC, Colombo, A, de Oliveira, HF, Beskow, S & Prado, Gd 2012, 'Wind distortion in wetted area of gun sprinklers: extension of modeling to medium-sized sprinklers', *Revista Brasileira de Engenharia Agrícola e Ambiental*, vol. 16, no. 7, pp. 699-705.

Foley, JP 2008, 'Centre pivot and lateral move machines', *WATERpak*, pp. 195-220.

Foley, JP 2010, 'Performance Improvement of Centre Pivots and Lateral Moves', PhD thesis, University of Southern Queensland, Toowoomba, Australia.

Fukui, Y, Nakanishi, K & Okamura, S 1980, 'Computer evaluation of sprinkler irrigation uniformity', *Irrigation Science*, vol. 2, no. 1, pp. 23-32.

Gat, YL & Molle, B 2000, 'Model of water application under pivot sprinkler. I: Theoretical grounds', *Journal of Irrigation and Drainage Engineering*, vol. 126, no. 6, pp. 343-7.

Google Image, *End Gun Sprinkler*, 2014, Created By, Google Image, End Gun Sprinkler, viewed 8 January 2018, <https://www.google.com.au/search?q=www.nespal.org/sirp/waterinfo/state/awd/background/images/irrigation_29.jpg&dcr=0&source=lnms&tbm=isch&sa=X&ved=0ahUKEwjVzt__gMfYAhXCVLwKHWGaCOgQ_AUICigB&biw=1920&bih=1144#imgrc=JEaep_h6KtBpSM:&spf=1515367813625>.

Google Image, *Travelling Big Gun Sprinkler* 2015, Created By, Google Image, Travelling Big Gun Sprinkler Machine, veiwed 2 January 2018, <https://www.google.com.au/search?biw=1920&bih=1144&tbm=isch&sa=1&ei=jblSWs-XOYm38QX0p6G4Dg&q=travelling+Gun+Cart&oq=travelling+Gun+Cart&gs_l=psy-ab.12...0.0.0.6194.0.0.0.0.0.0.0..0.0....0...1c..64.psy-ab..0.0.0....0.LO0cdDA7O00#imgrc=1aQ0TkOAYonB4M:&spf=1515370900402>.

Google Maps 2015, *Toowoomba, Australia, Toowoomba.QLD.4350, viewed 26 May 2016, ,* <https://www.google.com.au/maps/@-27.6086926,151.9308893,322m/data=!3m1!1e3>.

Google Maps 2016, *Street view, Australia, Toowoomba.QLD.4350, viewed 26 May 2016*, <https://www.google.com.au/maps/@-27.5990852,151.9654288,3757a,20y,255.67h,44.4t/data=!3m1!1e3>.

Granier, J, Molle, B & Deumier, J 2003, 'IRRIPARC-Part 1: Modeling spatial water distribution under a sprinkler in windy conditions', in Europen Regional Conference of The International Comission on Irrigation and Drainge: *proceedings of theEuropen Regional Conference of The International Comission on Irrigation and Drainge* pp. 14-9.

Grose, D 1999, 'Mathematical modelling and simulation of irrigation sprinklers', Cranfield University.

Gunston, H & Ali, M 2012, 'Practices of Irrigation and On-Farm Water Management-Volume 2', *Experimental Agriculture*, vol. 48, no. 1, p. 155.

Han, S, Evans, R & Kroeger, M 1994, 'Sprinkler distribution patterns in windy conditions', *Transactions of the ASAE*, vol. 37, no. 5, pp. 1481-9.

Heermann, D & Hein, P 1968, 'Performance characteristics of self-propelled center-pivot sprinkler irrigation system', *Trans Amer Soc Agr Eng*, vol. 2, no. 1, pp. 11-5.

Henggeler, J & Vories, E 2009, 'Evaluating Center Pivot Distribution Uniformity from Catch Can Tests', in ASABE Annual International Meeting: *proceedings of theASABE Annual International Meeting* p. 14.

Hipperson, K 1985, 'Development of Instumentation for Hose-Reel Raingun Irrigators ', Cranfield University, Unpublished dissertation.

India Mart 2014, *Raingun-Sprinkler Irrigation, The First Gear Drive Vari-Angle, viewed 8 January 2018*, <http://www.indiamart.com/raingun-sprinkler-irrigation/raingun-spinklers.html>.

ISO 2003, *ISO 8224-1 Traveller irrrigation machines_ Part 1: Operational characteristics and laboratory and field test methods*, INTERNATIONAL STANDARD.

Jensen, ME 1980, 'Design and operation of farm irrigation systems', *Monograph Series-American Society of Agricultural Engineers (USA) 1980*, no. 3.

Karmeli, D 1978, 'Estimating sprinkler distribution patterns using linear regression', *Transactions of the ASAE*, vol. 21, no. 4, pp. 682-0686.

Keller, J & Bliesner, R 1990, *Sprinkle and trickle irrigation*.

Kincaid, D 1996, 'Spraydrop kinetic energy from irrigation sprinklers', *Transactions of the ASAE*, vol. 39, no. 3, pp. 847-53.

Lacey, TR 2006, 'Improving irrigation effieciency: Raingun performance in field scale vegetable production', Cranfield University, Unpublished PhD thesis.

Lindsay Corporation 2011, *Center Pivots, Zimmatic, Lindsay Corporation, viewed 7 January 2018,*, <http://www.zimmatic.com/7500wd>.

LindsayCorporation 2012, *Center Pivots, Zimmatic, Lindsay Corporation, viewed 7 January 2018,*, <http://www.zimmatic.com/8500p>.

Liu, Z, L. Grabow, G, L. Huffman, R, Osborne, J & O. Evans, R 2012, 'Factors Affecting Uniformity of Irrigation-Type Manure Application Systems', *Applied Engineering in Agriculture*, vol. 28, no. 1, p. 43.

Marco, A, Humpherys, A, Spiess, L & Decroix, M 1989, *The influence of wind on sprinkler irrigation*, International Commission on Irrigation and Drainage.

Martin & et.al 2007, 'Design and operation of sprinkler systems', *Design and operation of farm irrigation systems/Glenn J. Hoffman...{et al.]*.

Merkley, GP & Allen, RG 2004, *Sprinkle & Trickle Irrigation: Lecture Notes*, Biological and Irrigation Engineering Department, Utah State Unive.

Miodragović, RM, Petrović, DV, Mileusnić, ZI, Dimitrijević, AŽ & Radojević, RL 2012, 'Water distribution uniformity of the traveling rain gun', *African Journal of Agricultural Research*, vol. 7, no. 13, pp. 1988-96.

Musa, S 1988, 'A Computer Simulation Methodology for Predicting Water Distribution, Crop Yield, and Economic Return for Mobile Raingun Irrigators (Travellers)', Cranfield University.

Nelson Irrigation 2008, *Pivot Pocket Guide, Water application solutions for CENTER PIVOT IRRIGATION from Pivot to End Gun, viewed 4 July 2017*, <http://fliphtml5.com/clay/gpwi>.

Nelson Irrigarion 2015, *100 Series Big Gun®, viewed 26 January 2015,*, <http://www.nelsonirrigation.com/products/family/big-gun-sprinklers/100-series-big-gun>.

Nelson Irrigation 2010, *Big Gun Sprinkler Nelson, SR100 Big Gun sprinkler, WikimediaCommons, viewed 7 January 2018,* , <https://commons.wikimedia.org/wiki/File:Nelson_Big_Gun.png>.

Nelson Irrigation 2014, *Big-Gun-Multi-Trajectory-Angle, Nelson Irrigation, viewed 5 January 2018,* <http://www.nelsonirrigation.com/media/general/Big-Gun-Multi-Trajectory-A.jpg>.

Nelson Irrigation 2015, *NELSON, SR 100 BIG GUN, Ring Nozzle Data,viewed 23 May 2015,* <http://www.nelsonirrigation.com/media/resources/BG_RING%20DATA.pdf>.

Nelson Irrigation 2016, *Big Gun Performance, Nelson Irrigation, viewed 15 September 2017,* <http://www.nelsonirrigation.com/media/resources/BG_TAPER%20BORE%20DATA.pdf>.

Nelson Irrigation 2017a, *Pivot Point to End Gun - Nelson Irrigation [pdf]*, <http://www.nelsonirrigation.com/media/resources/PIVOT_PP2EG.pdf>.

Nelson Irrigation 2017b, *Center Pivot End Gun Application*, <http://www.nelsonirrigation.com/media/resources/BG_PIVOT.pdf>.

Nelson Irrigation 2018, *P85AS End of Pivot Sprinkler, Typical Added Acres on a 1/4 Mile Pivot*, viewed 8 January 2018, <http://www.nelsonirrigation.com/products/family/end-of-pivot-solutions/p85as>.

Nelson Irrigation Australia 2016, *Nelson Big Gun Nozzle Type, Nelson Product Litrature, Big Guns Product Information & Operation Guides, viewed 8 January 2018*, <https://www.nelsonirrigation.com.au/resources/nelson-pdf-literature>.

Newell, G 2003, 'Traveling gun simulation model TRAVGUN: User's manual and technical documentation: National Centre for Engineering in Agriculture-NCEA', *Toowoomba: University of Southern Queensland*.

Newell, G, Foley, J & Smith, R 2002, *Travelling Gun and Boom Irrigation Machines: Review of Machine Characteristics, Performance Data and Research Issues*, National Centre for Engineering in Agriculture.

Oliveira, HFd, Colombo, A, Faria, LC & Prado, Gd 2012, 'Effects of wind speed and direction on water application uniformity of traveler irrigation systems', *Engenharia Agrícola*, vol. 32, no. 4, pp. 669-78.

Oliveira, HFEd, Colombo, A, Faria, LC, Beskow, S & Prado, Gd 2013, 'SIA: Modelo para simulação da irrigação por aspersão - Calibração e validação', *Revista Brasileira de Engenharia Agrícola e Ambiental*, vol. 17, pp. 253-60.

Omary, M & Sumner, H 2001, 'Modeling water distribution for irrigation machine with small spray nozzles', *Journal of Irrigation and Drainage Engineering*, vol. 127, no. 3, pp. 156-60.

Pair, CH 1970, *Sprinkler Irrigation*.

Palacin, J, Salse, J, Clua, X, Arnó, J, Blanco, R & Zanuy, C 2005, 'Center-pivot automatization for agrochemical use', *Computers and Electronics in Agriculture*, vol. 49, no. 3, pp. 419-30.

Prado, G & Colombo, A 2007, 'Análise da uniformidade de aplicação de água pelo aspersor Plona-RL250 em sistemas autopropelidos de irrigação', *Irriga*, vol. 12, no. 2, pp. 249-62.

Prado, G, Colombo, A, Barreto, AC, Matos, Fd & Ferreira Júnior, J 2008, 'Uniformidade de aplicação de água pelo aspersor PLONA-RL250 em sistemas estacionários de irrigação', *Irriga*, vol. 13, pp. 220-34.

Prado, Gd 2008, 'Modelagem da aplicação de água com canhões hidráulicos sob diferentes condições de vento', PhD thesis, Federal University of Minas Gerais, Minas Gerais, Brazil.

Prado, Gd & Colombo, A 2010, 'Determining sprinkler patterns from water distribution tests of traveller irrigation systems', *Engenharia Agrícola*, vol. 30, no. 2, pp. 232-43.

Prado, Gd & Colombo, A 2013, 'Sprinkler radial water distribution profiles interpolation', *Revista Brasileira de Engenharia Agrícola e Ambiental*, vol. 17, no. 4, pp. 355-61.

Prado, Gd, Colombo, A, Oliveira, HFd & Faria, LC 2012, 'Water application uniformity of self-propelled irrigation equipment with sprinklers presenting triangular, elliptical and rectangular radial water distribution profiles', *Engenharia Agrícola*, vol. 32, no. 3, pp. 522-9.

Prado, Gd, Faria, LC, de Oliveira, HF & Colombo, A 2013, 'Effect of trajectory angle on technical characteristics of a gun sprinkler', *Revista Brasileira de Engenharia Agrícola e Ambiental*, vol. 17, no. 7, pp. 689-97.

Rapp, E, Chanasyk, D.S. and B.C. Horvath 1979, 'Simulated Model of Center Pivot Sprinkler Irrigation Systems', *Can. Agric. Eng.*, vol. 21, pp. 141-5.

Richards, P & Weatherhead, E 1993, 'Prediction of raingun application patterns in windy conditions', *Journal of Agricultural Engineering Research*, vol. 54, no. 4, pp. 281-91.

Seginer, I, Nir, D & Bernuth, Rv 1991, 'Simulation of wind-distorted sprinkler patterns', *Journal of Irrigation and Drainage Engineering*, vol. 117, no. 2, pp. 285-306.

Shull, H & Dylla, A 1976a, 'Traveling gun application uniformity in high winds [Sprinkler irrigation system]', *Transactions of the ASAE*, vol. 19, no.2, pp.254-258.

Shull, H & Dylla, A 1976b, 'Wind effects on water application patterns from a large, single nozzle [irrigation] sprinkler', *Transactions of the ASAE*, vol. 19,no.3,pp.501-504.

Smith, A & North, S 2009, *Planning and managing centre pivot and linear move irrigation in the Southern Riverina*, Cooperative Research Centre for Irrigation Futures.

Smith, R, Gillies, MH, Newell, G & Foley, JP 2008, 'A decision support model for travelling gun irrigation machines', *Biosystems engineering*, vol. 100, no. 1, pp. 126-36.

Solomon, K & Kodoma, M 1978, 'Center pivot end sprinkler pattern analysis and selection', *Transactions of the ASAE [American Society of Agricultural Engineers]*, vol. 21.

Solomon, K & Bezdek, JC 1980, 'Characterizing sprinkler distribution patterns with a clustering algorithm', *Transactions of the ASAE*, vol. 23, no. 4, pp. 899-902, 6.

Solomon, KH 1987, *Sprinkler irrigation uniformity*, ASPAC, Food and Fertilizer Technology Centre.

Southorn, N 1998, *Farm Irrigation*, Butterworth-Heinemann.

Tarjuelo, J, Montero, J, Honrubia, F, Ortiz, J & Ortega, J 1999, 'Analysis of uniformity of sprinkle irrigation in a semi-arid area', *Agricultural Water Management*, vol. 40, no. 2, pp. 315-31.

Time And Date 2016, *Timeanddate Toowoomba Queensland Australia, Distance Calculator to/from Toowoomba, viewed 7 June 2016*, <http://www.timeanddate.com/worldclock/distanceresult.html?p1=955&p2=47>.

Trailco T200-2 2018, *Trailco Irrigation, T200-2 Traveller, viewed 15 January 2018*, <https://www.google.com.au/search?q=trailco+T200-2&rls=com.microsoft:en-AU:IE-Address&biw=1600&bih=805&source=lnms&tbm=isch&sa=X&ved=0ahUKEwiUvMqp1oDNAhWlL6YKHZ2mCvIQ_AUIBigB#imgrc=603DNAMB70TFPM%3A>.

Von Bernuth, R 1983, 'Nozzling considerations for center pivots with end guns', *Transactions of the ASAE*, vol. 26, no. 2, pp. 419-0422.

Von Bernuth, R 1988, 'Effect of trajectory angle on performance of sprinklers in wind', *Journal of Irrigation and Drainage Engineering*, vol. 114, no. 4, pp. 579-87.

Von Bernuth, R & Gilley, J 1984, 'Sprinkler droplet size distribution estimation from single leg test data', *Transactions of the ASAE*, vol. 27, no. 5, pp. 1435-41.

Vories, E & Von Bernuth, R 1986, 'Single nozzle sprinkler performance in wind', *Transactions of the ASAE*, vol. 29, no. 5, pp. 1325-30.

Vories, E, Von Bernuth, R & Mickelson, R 1987, 'Simulating sprinkler performance in wind', *Journal of Irrigation and Drainage Engineering*, vol. 113, no. 1, pp. 119-30.

Vories, E, Tacker, P, Stephenson, D, Bajwa, S & Perry, C 2008, 'Performance of a Variable Rate Center Pivot System', in World Environmental and Water Resources Congress 2008: Ahupua'A: *proceedings of theWorld Environmental and Water Resources Congress 2008: Ahupua'A* pp. 1-10.

Wade Rain 2018, *Big Gun Irrigation, Wade Rain Irrigation Systems, viewed 8 January 2018*, <http://www.waderain.com/index.php?page=big_gun>.

Weatherzone 2015a, *Weatherzone: Weather-Australia 7 day forecastes and radar, App, Toowoomba weather, viewed 25 May 2015*, <http://m.weatherzone.com.au/qld/darling-downs/toowoomba>.

Weatherzone 2015b, *Weatherzone: Weather-Australia 7 day forecastes and radar, Toowoomba weather, viewed 22 May 2015*, <http://www.weatherzone.com.au/qld/darling-downs/toowoomba>.

Wigginton, D, Foley, J, Schultz, J & Van Niekerk, R 2011, 'Review of Centre Pivot and Lateral Move Installations in the Queensland Murray Darling Basin', *National Centre for Engineering in Agriculture Publication 1004167/1, USQ, Toowoomba*.

WillyWeather 2017, *Toowoomba Wind Forecast*,

<http://wind.willyweather.com.au/qld/darling-downs/toowoomba.html>.

Appendix A

Radial Leg at Wind

A.1 Introduction

This appendix includes some radial leg data that were measured at different wind conditions when they did not match the expectation for quiescent wind conditions. These data are shown in this section to provide general information about the difficulty of analysing complicated data and how perfect data were achieved in this study.

A.2 Measuring radial leg data from stationary full circle

These data were measured from three lines of collectors placed radially around a stationary sprinkler with 120° between each line. The test descriptions are organized by the date and time of the measurement.

A.2.1 Measuring radial leg data test one on 15/3/2015 at 7:20 pm

The average radial leg data from the three lines for test one looks very confusing (see Figure A-1. This is because the test was performed during high wind speeds and changing wind directions as shown in Figure A-2. The figure shows wind speed increasing during measurement. Therefore, the data between the three lines were interpolated and plotted as shown in Figure A-3. This figure shows that the sprinkler pattern had drifted down-wind effects in different directions. The data for this test were not used for validation in this study because wind direction was not constant during the test.

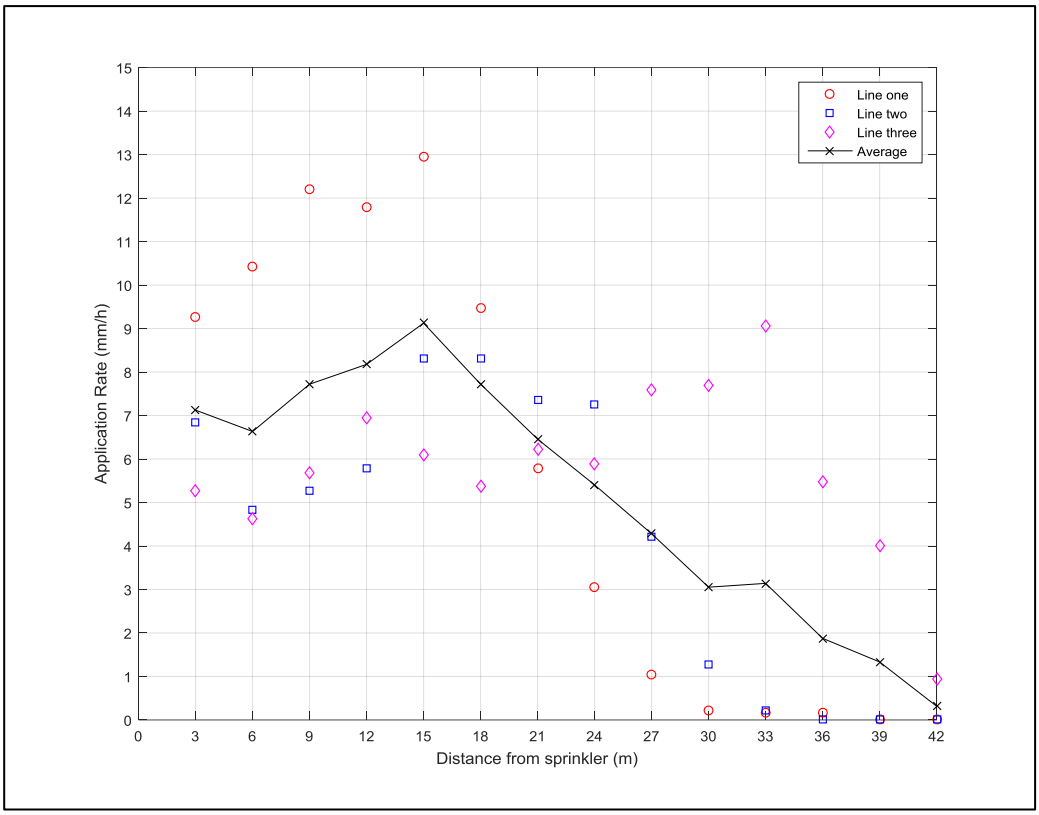

Figure A-1: Radial leg data test one collected from three lines of collectors placed around a stationary sprinkler.

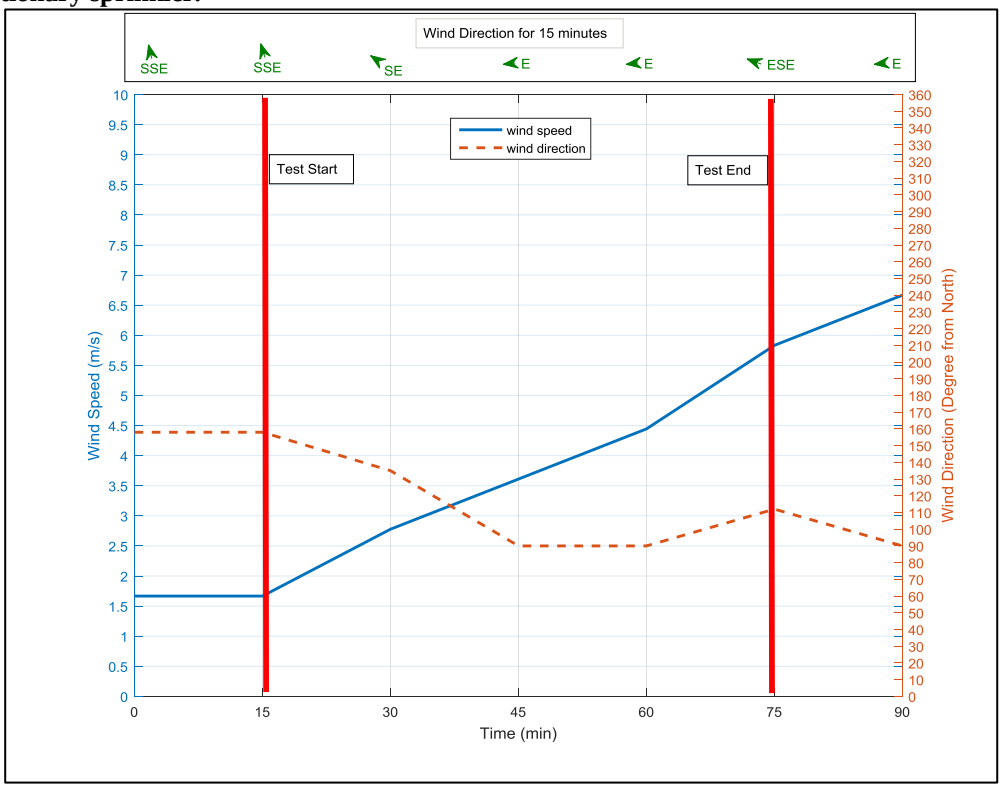

Figure A-2: Weather conditions (wind speed and direction) for radial leg test one.

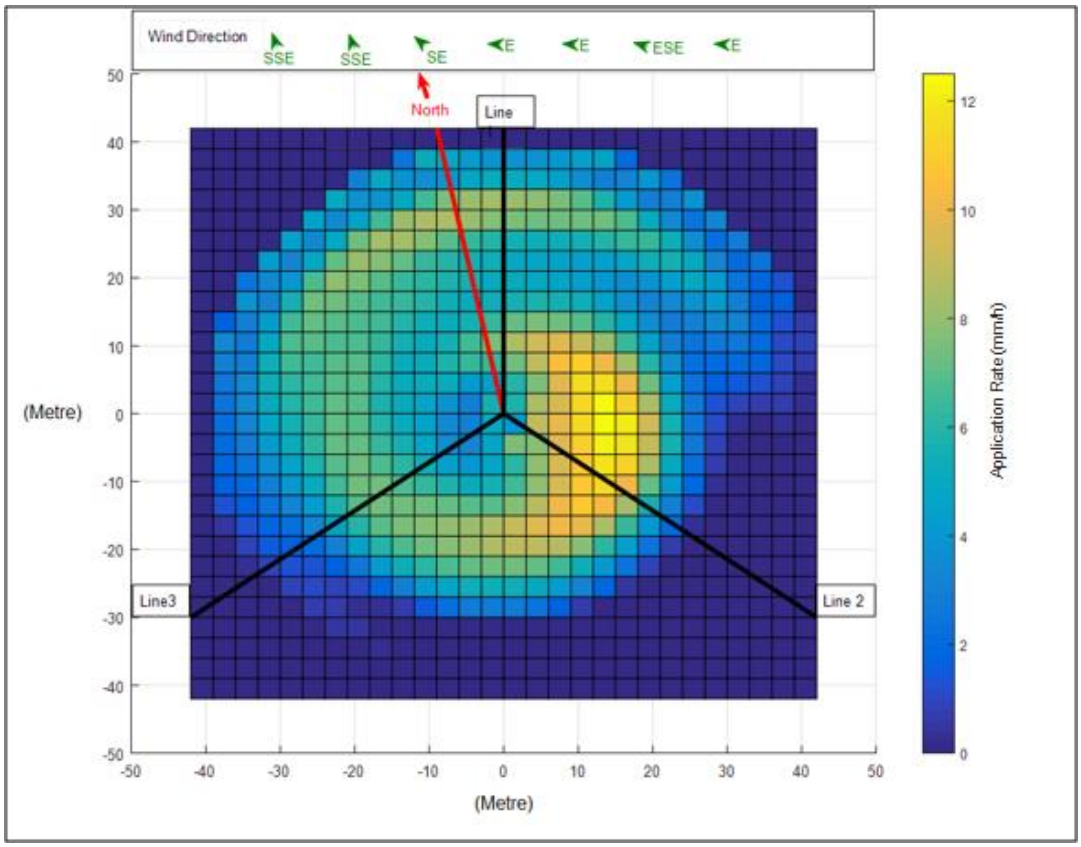

Figure A-3: Surface plot for radial leg test one shows the effect of wind on distortion sprinkler pattern.

A.2.2 Measuring radial leg data test two on 18/3/2015 at 4:00 am

The second test was also performed during high wind speed and wind direction also changed during the test. The radial leg data from the three lines appear confusing, as shown in Figure A-4. Weather conditions in Figure A-5 show wind speed as less than in test one, but it is still high. Wind direction changed during the test as well. Figure A-6 shows the sprinkler pattern drifted in different directions.

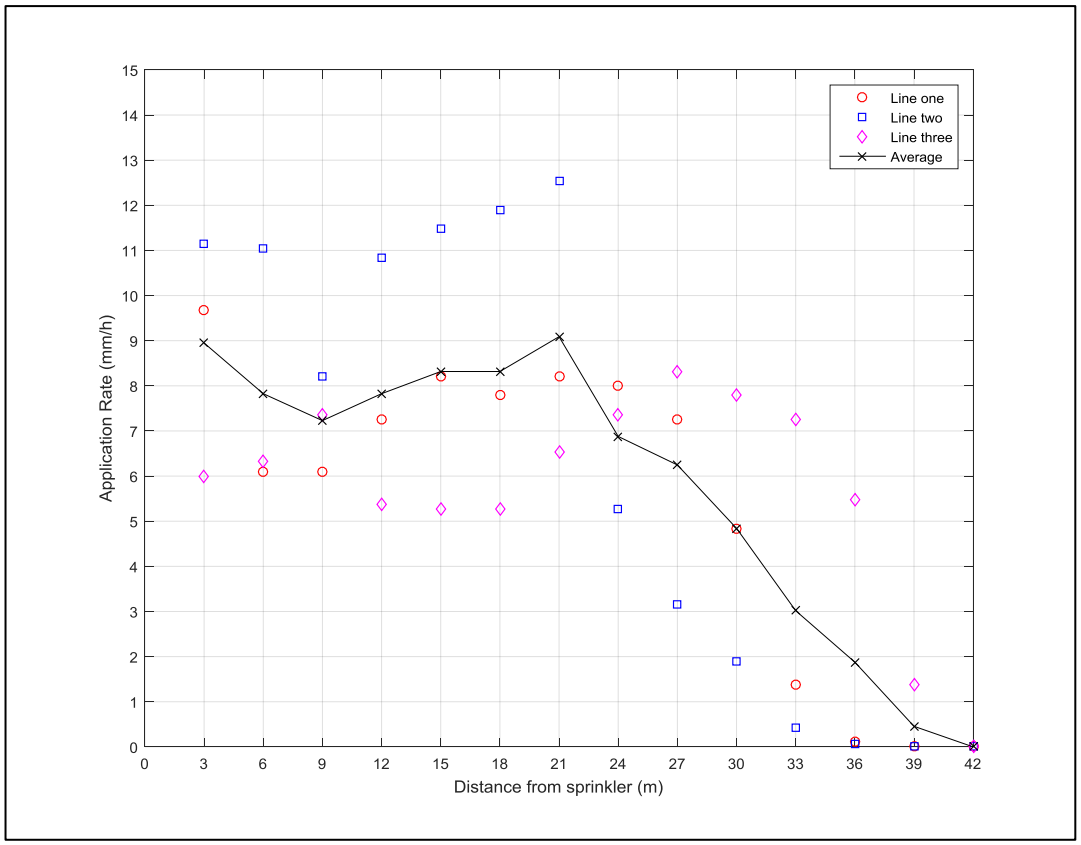

Figure A-4: Radial leg data for test two collected from three lines of collectors placed around a stationary sprinkler.

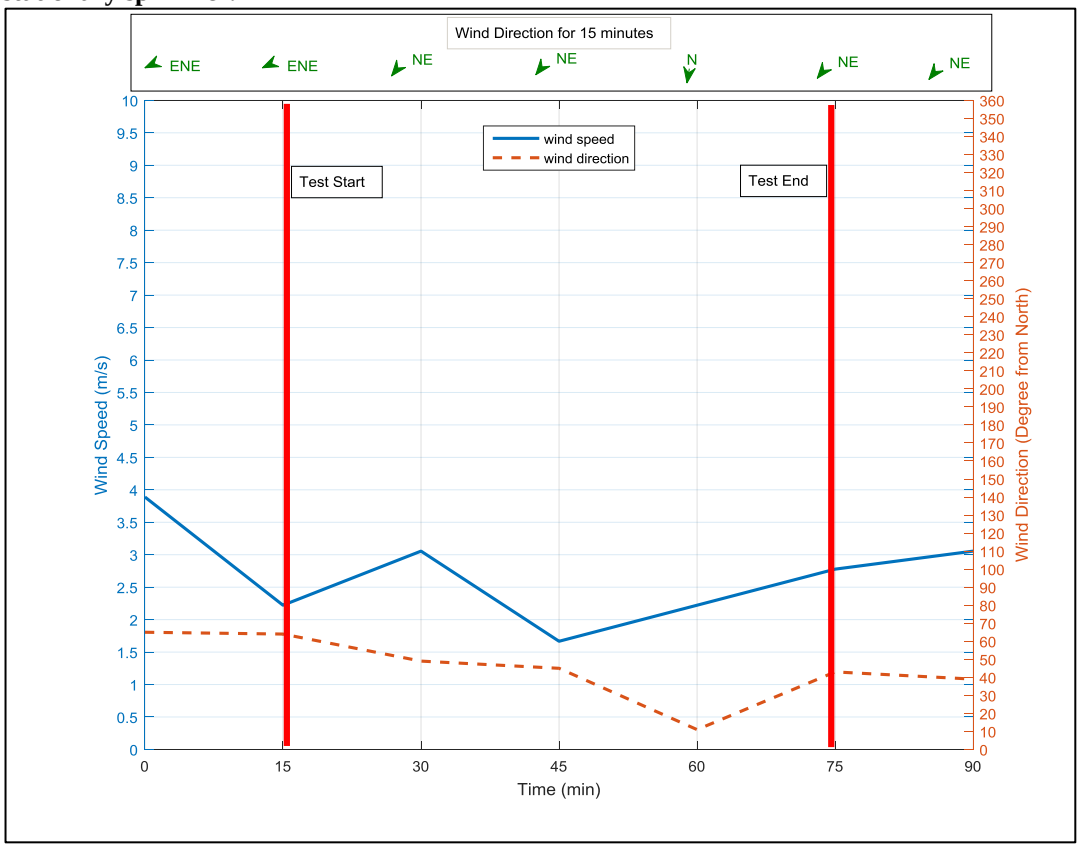

Figure A-5: Weather conditions (wind speed and direction) for radial leg test two.

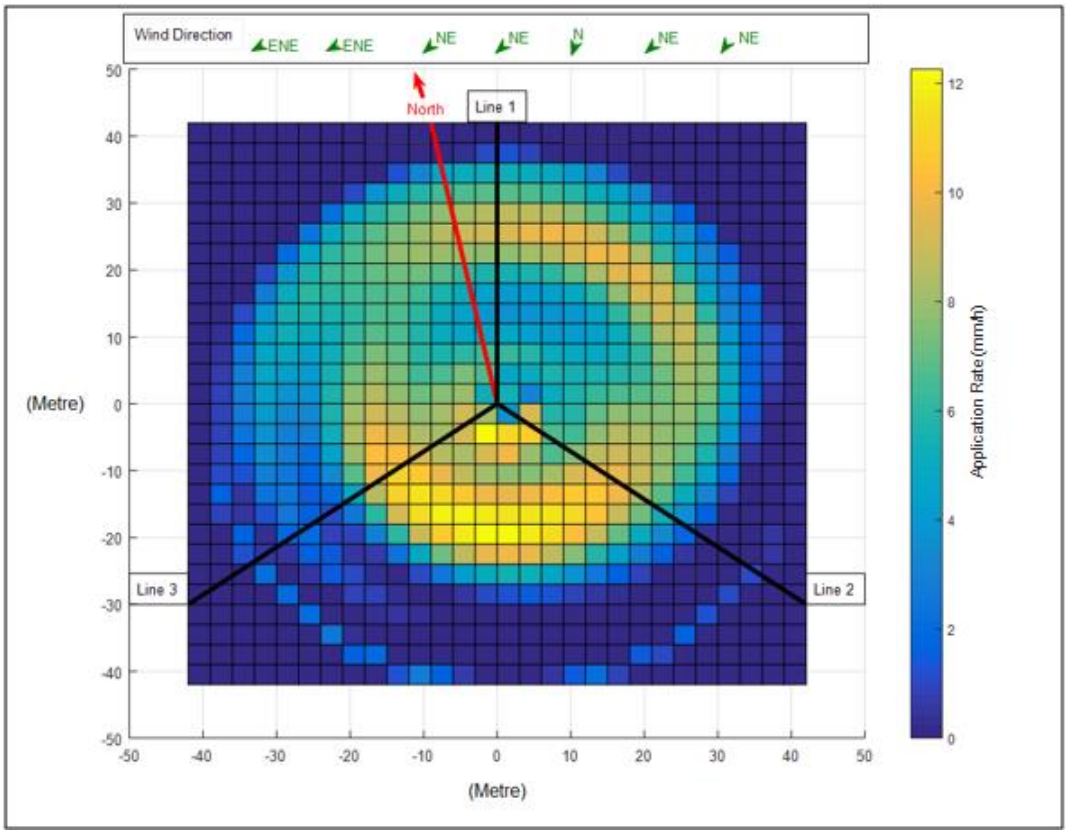

Figure A-6: Surface plot for radial leg test two shows the effect of wind on distortion sprinkler pattern.

A.2.3 Measuring radial leg data test three on 18/3/2015 at 6:30 pm

The shape of the average radial leg data for test three appears like a normal radial leg, as shown in Figure A-7. However, weather data in Figure A-8 indicate that wind speed and direction changed during the test. The sprinkler pattern in Figure A-9 shows the pattern drifted toward the downwind average wind direction.

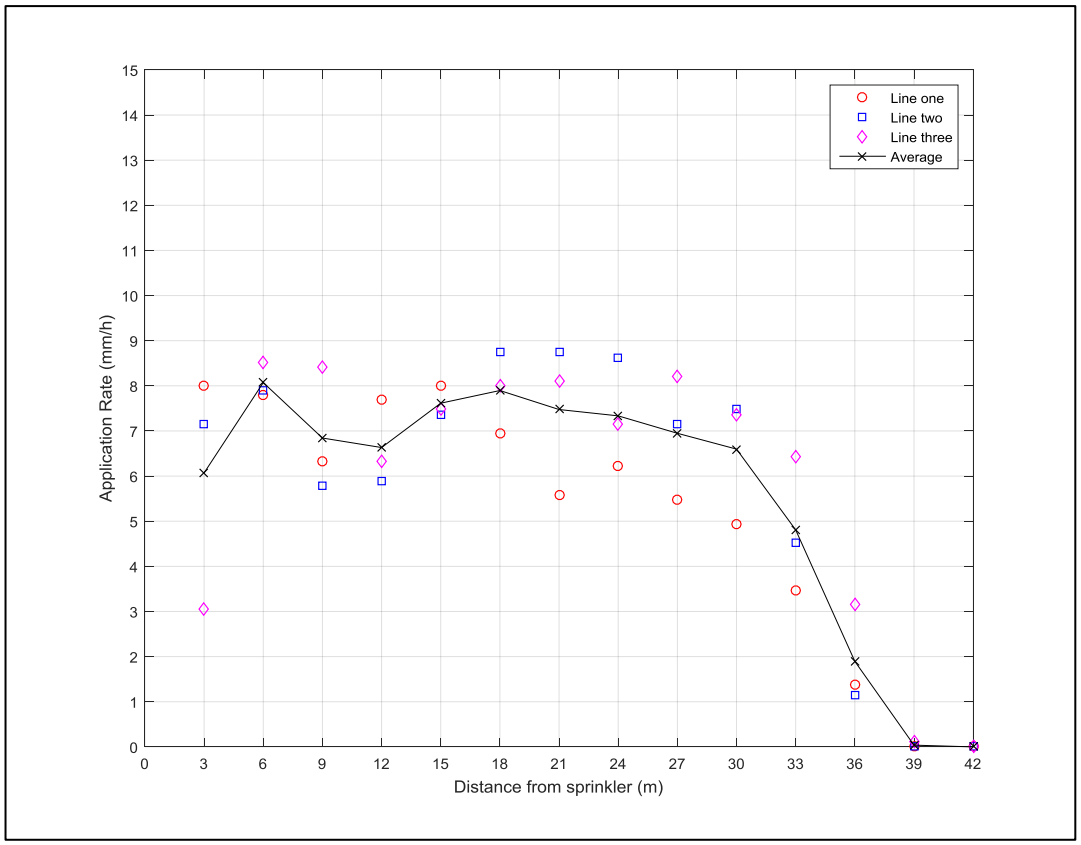

Figure A-7: Radial leg data for test three collected from three lines of collectors placed around a stationary sprinkler.

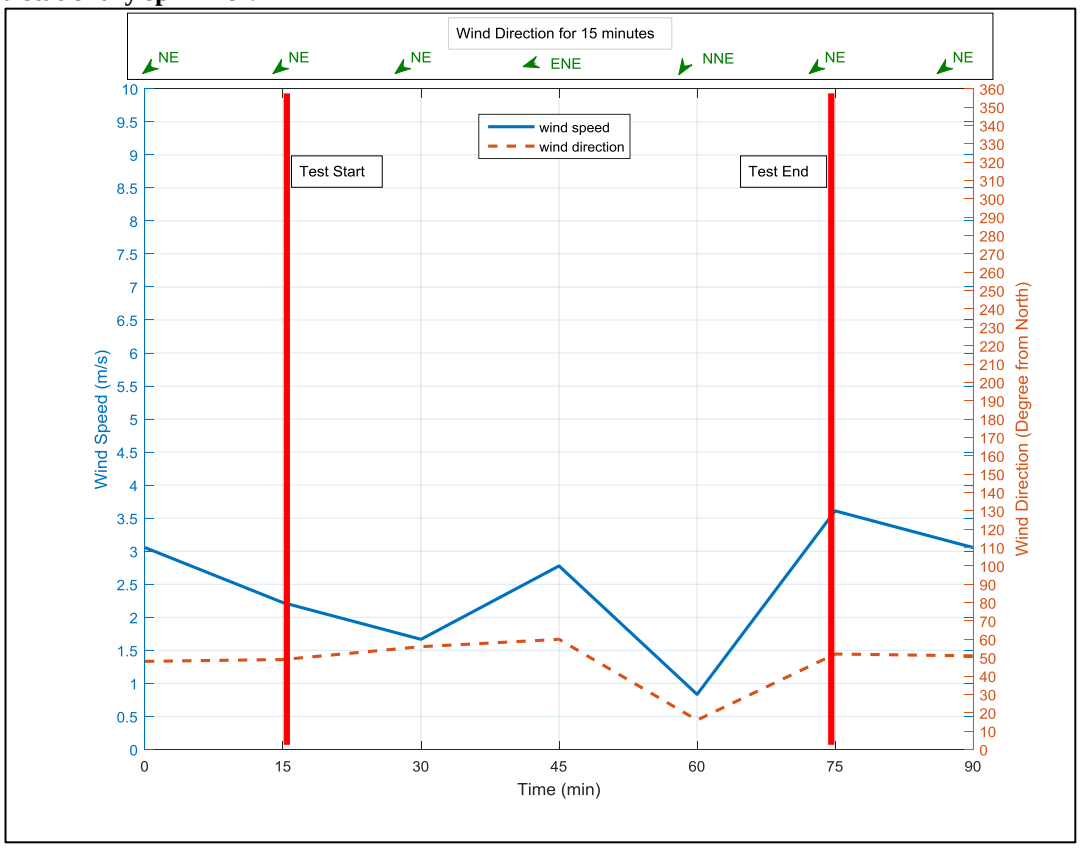

Figure A-8: Weather conditions (wind speed and direction) for radial leg test three.

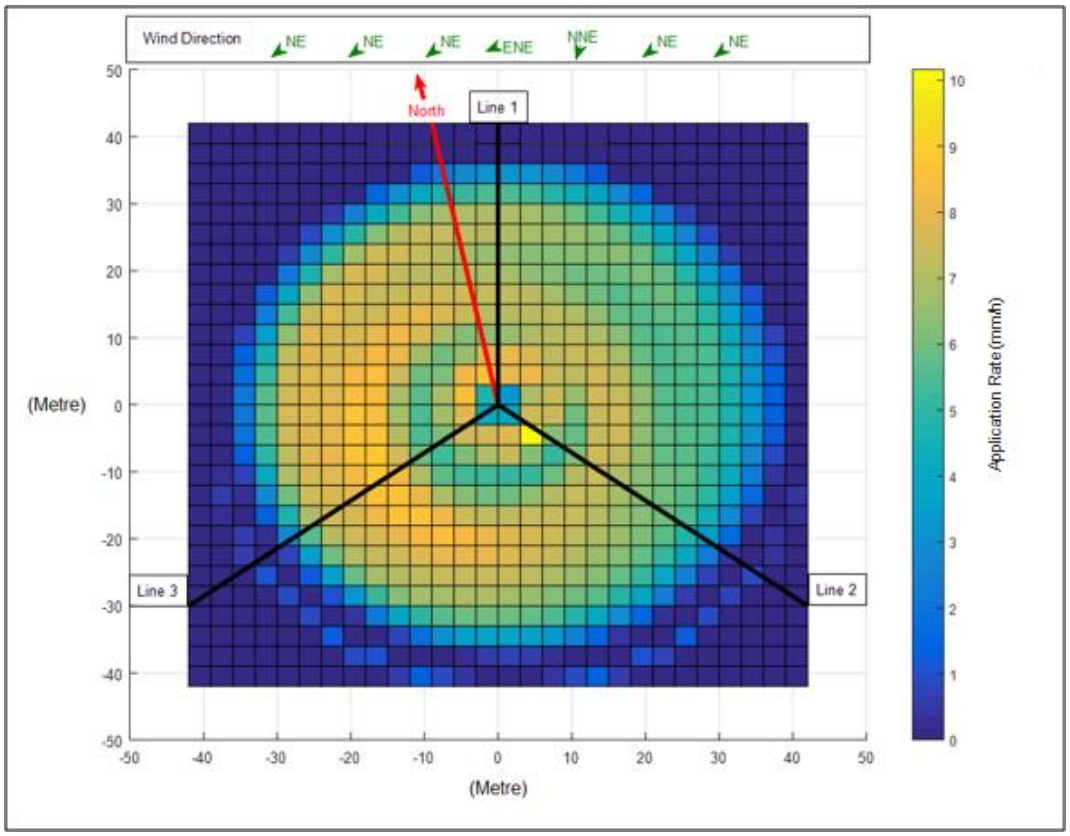

Figure A-9: Surface plot for radial leg test three shows the effect of wind on distortion sprinkler pattern.

A.2.4 Measuring radial leg data test five on 18/3/2015 at 9:30 pm

The shape of radial leg data for this test appears to be more acceptable compared with previous tests. However, the variation between the individual lines was high, as shown in Figure A-10. Wind speed and direction were changed considerably during the second half of the test, as shown in Figure A-11. The sprinkler pattern in Figure A-12 shows the pattern drifted downwind in different direction.

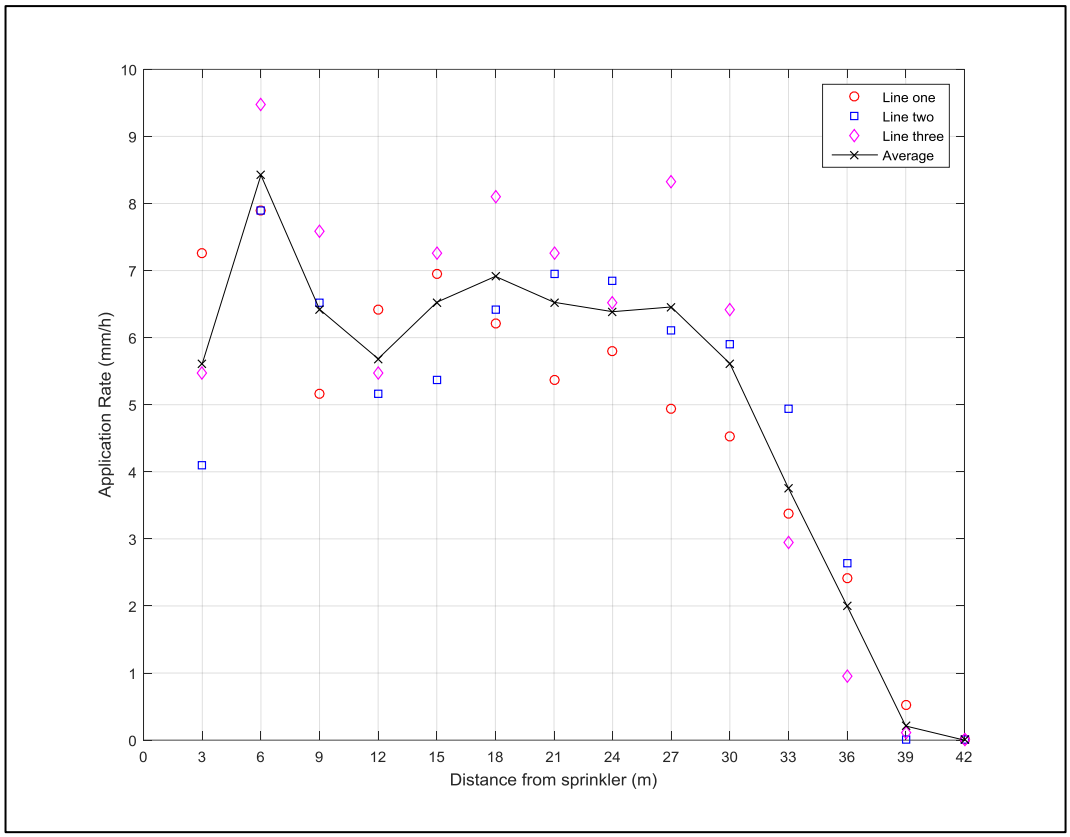

Figure A-10: Radial leg data for test five collected from three lines of collectors placed around a stationary sprinkler.

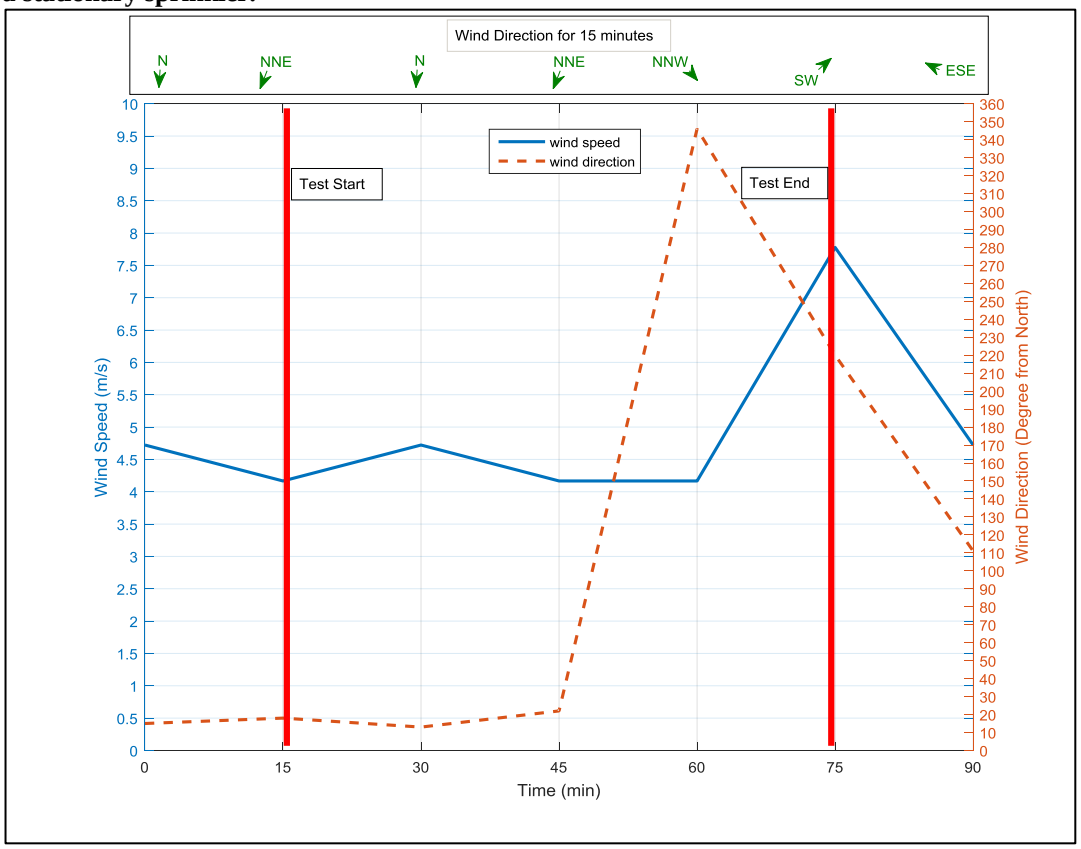

Figure A-11: Weather conditions (wind speed and direction) for radial leg test five.

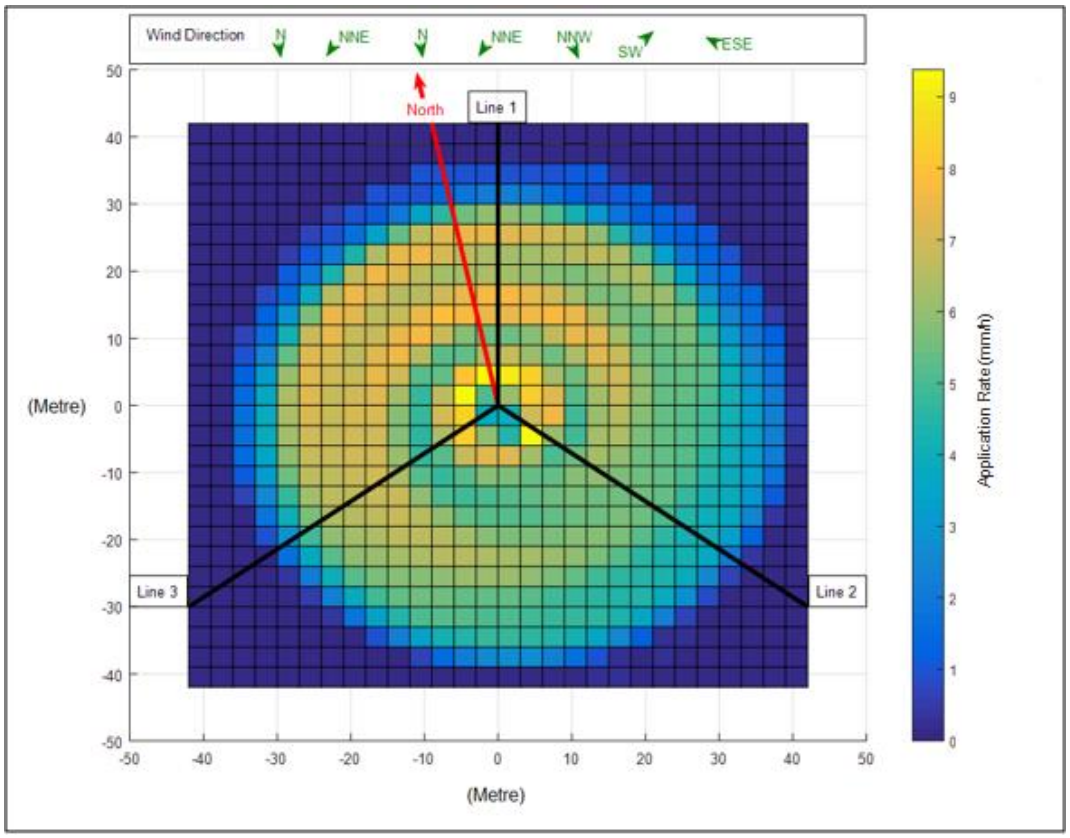

Figure A-12: Surface plot for radial leg test five shows the effect of wind on distortion sprinkler pattern.

Appendix B

Transect data at Wind

B.1 Introduction

This appendix includes some transect data that were measured at different wind conditions which did not match the expectation for quiescent wind conditions. These data are shown in this section to give general information about how the shape of the transect changed with different wind conditions.

B.2 Measuring transects in straight movement

These transect data were measured at high wind speeds. The tests are organized by the test sequence number of the same sector and side sector angles, as shown in Chapter Five.

B.2.1 Transect test number eight

The test was performed on Monday 27 April 2015 from 6:15 pm to 8:00 pm with a sector angle of 180° and a side sector angle of 270°. Figure B-1 summarizes the test layout and wind directions. Figure B-2 shows that wind speed was very high and wind directions were highly variable during the test. Figure B-3 shows the transect shape was very different from transect data in test number four. The figure shows water depth sharply decreased at the collectors at distances of 21, 24, 26, 30 metres from the sprinkler as a result of wind drift and range shortening.

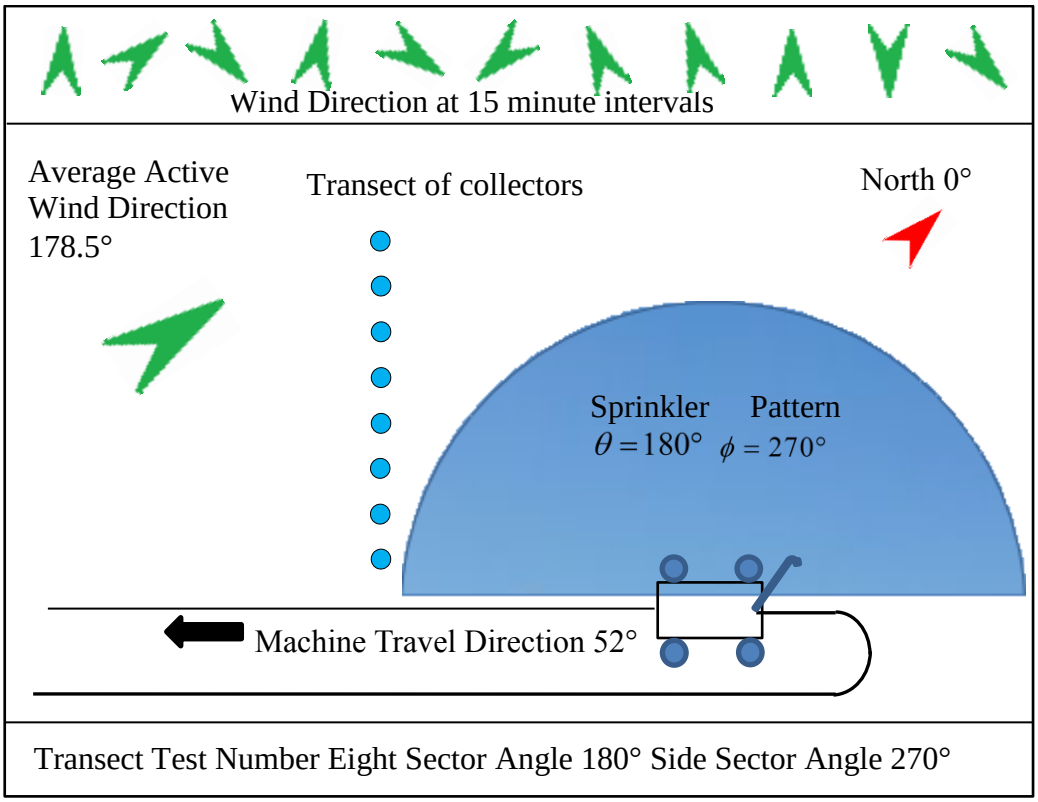

Figure B-1: Transect test number eight shows test layout, the combination of sector and side sector angles and other directions relevant to that test.

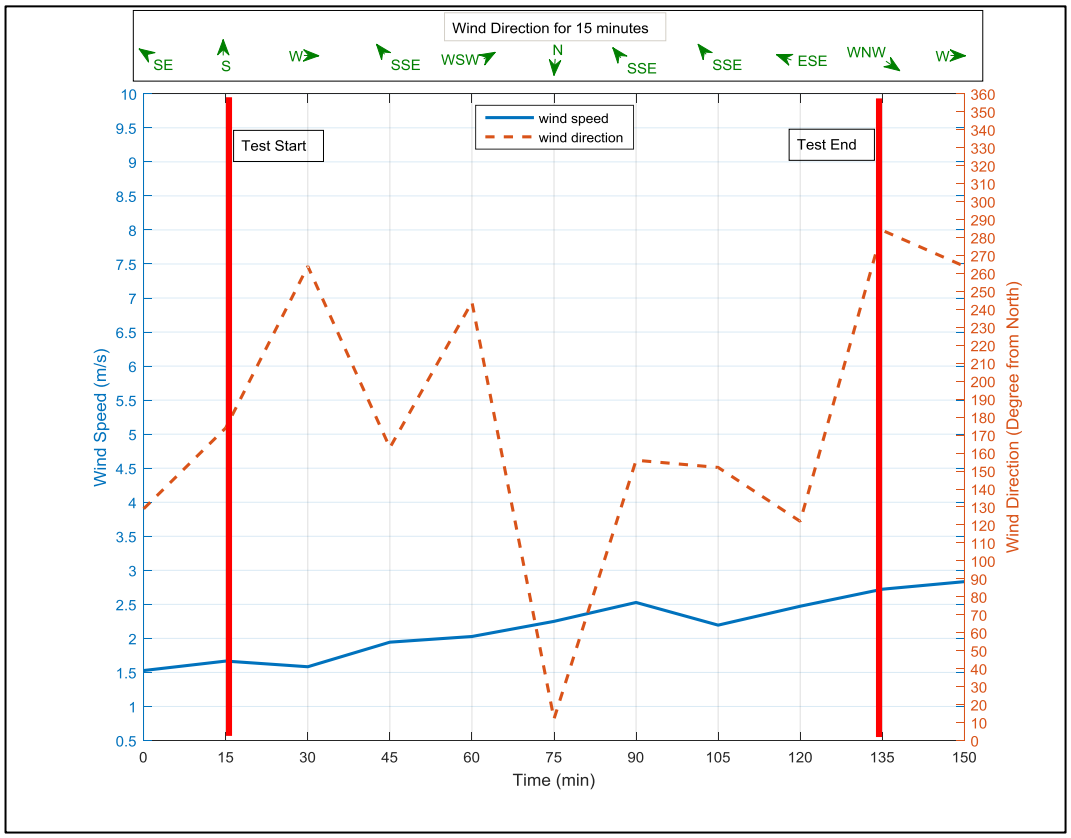

Figure B-2: Weather conditions (wind speed and direction) for transect test number eight.

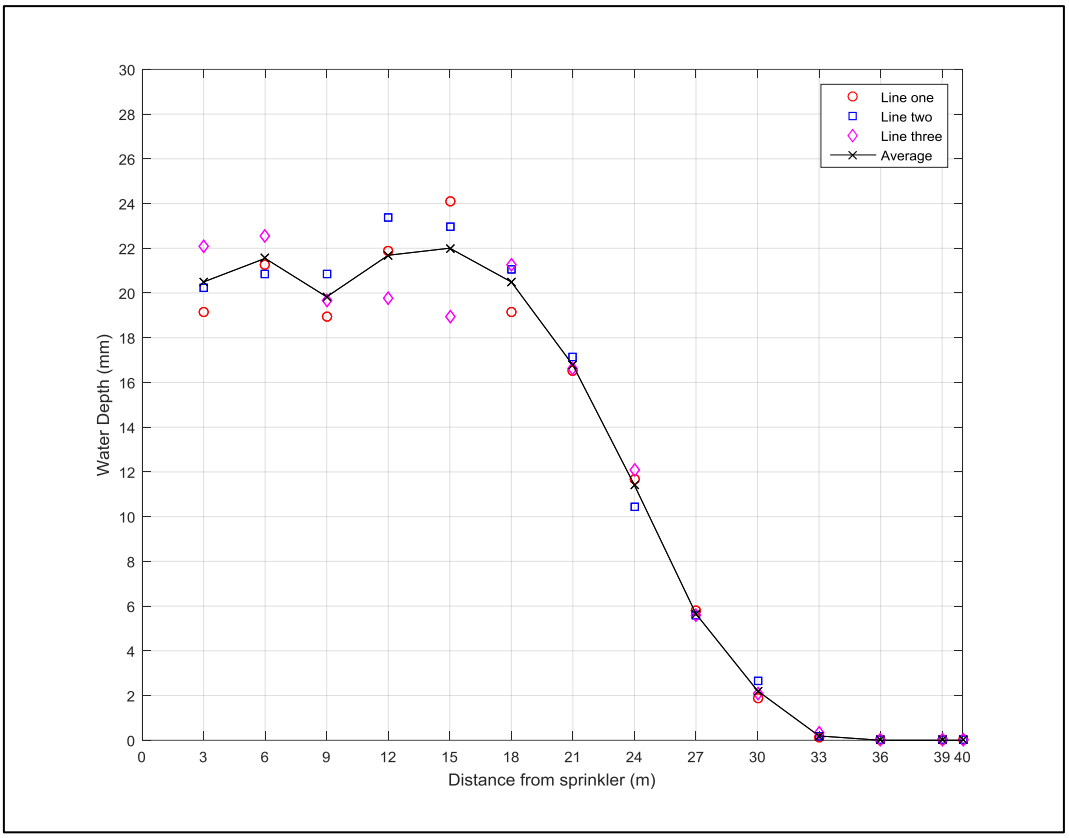

Figure B-3: Transect data for test number eight for the combination of 180° sector angle and 270° side sector angle.

B.2.2 Transect test number nine

The test was performed on Sunday 3 May 2015 from 7:45 pm to 9:30 pm with a sector angle of 180° and a side sector angle of 270°. Figure B-4 summarizes the test layout and wind directions. Figure B-5 shows wind speed was low during the test but the wind gusted during the test. Wind direction changed slightly during the test. These weather conditions changed the transect shape, as shown in Figure B-6. The figure shows water depth decreased sharply in the collectors at distances of 36 and 39 metres from the sprinkler.

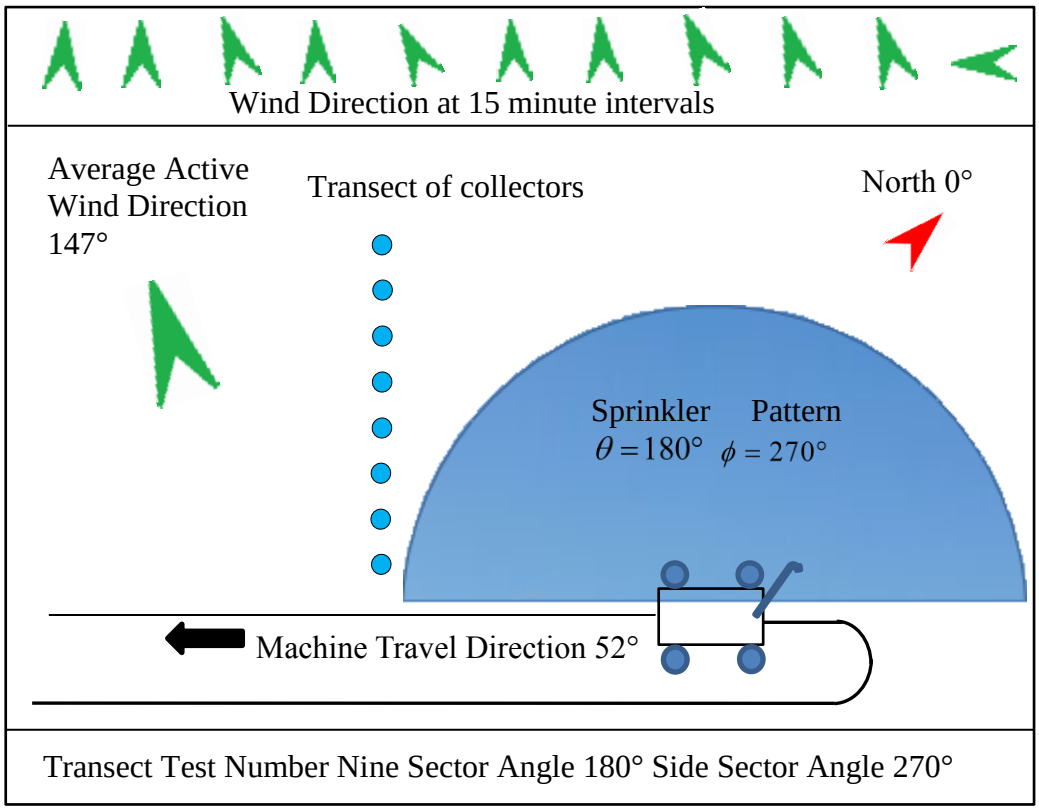

Figure B-4: Transect test number nine shows test layout, the combination of sector and side sector angles and other directions relevant to that test.

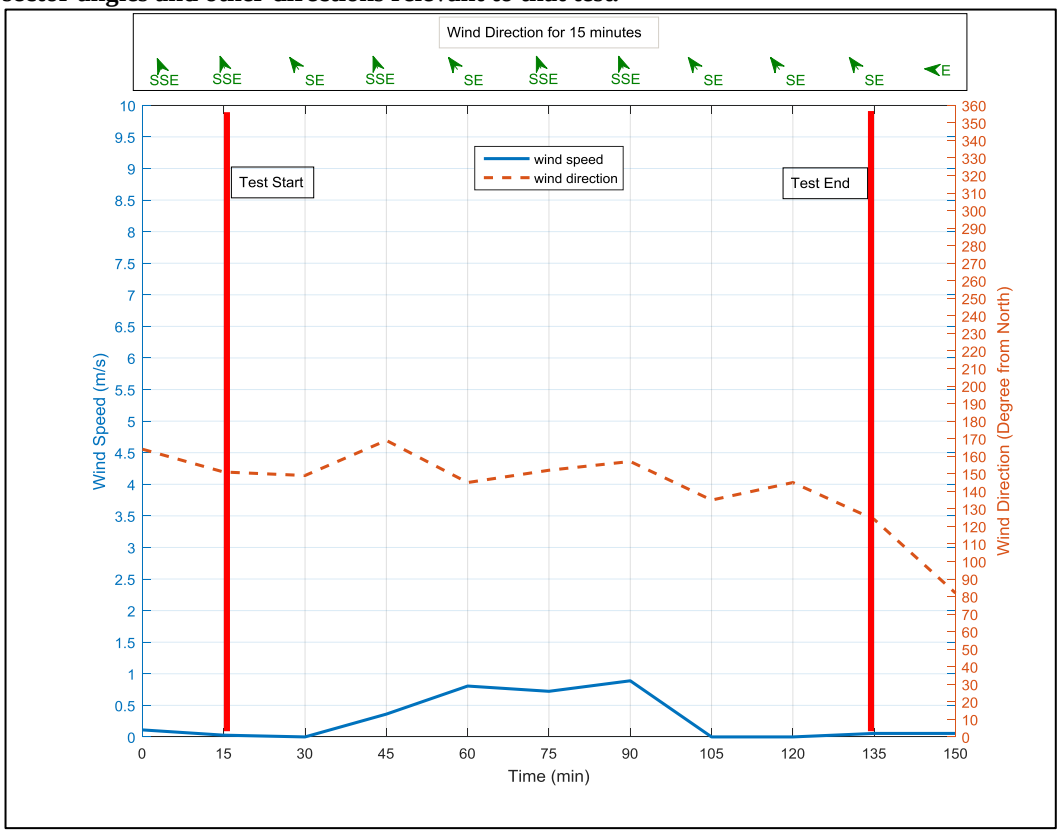

Figure B-5: Weather conditions (wind speed and direction) for transect test number nine.

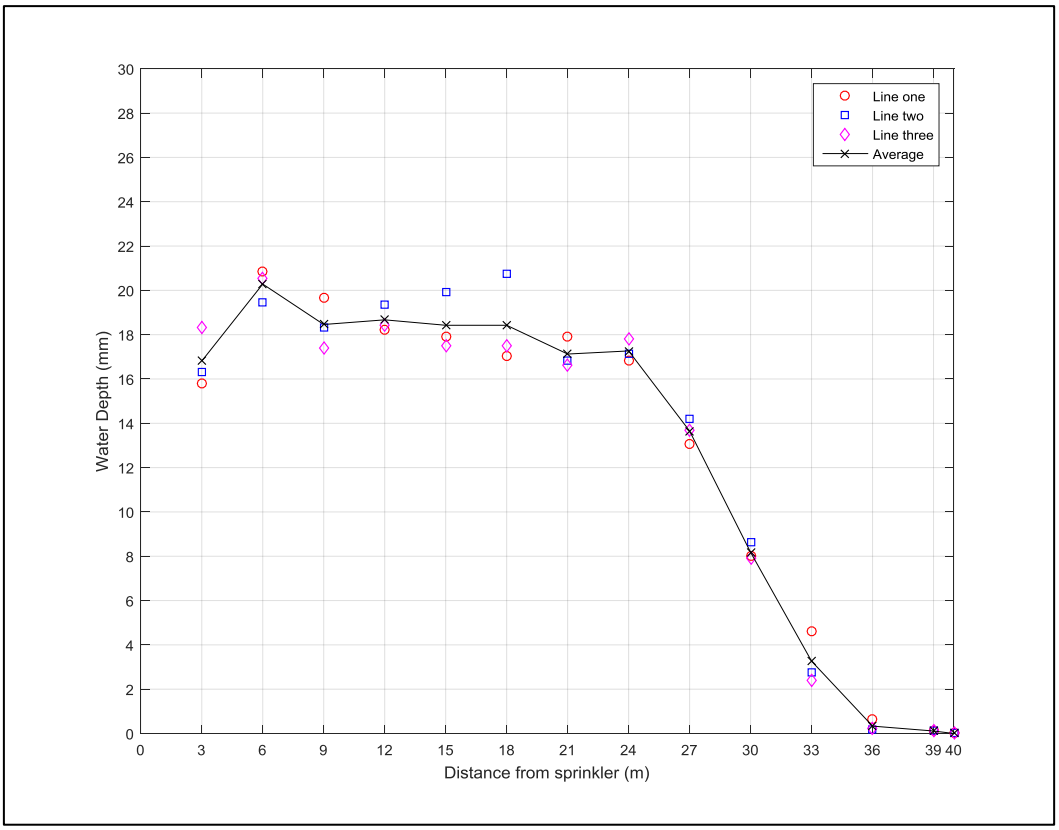

Figure B-6: Transect data for test number nine for the combination of 180° sector angle and 270° side sector angle.

B.2.3 Transect test number twelve

The test was performed on Wednesday 6 May 2015 from 1:15 am to 2:55 am with a sector angle of 140° and a side sector angle of 270°. Figure A-7 shows the test layout and average active wind direction. Figure B-8 shows wind speed was high during the test and wind direction changed slightly. Figure B-9 shows the shape of transect data changed as a result of wind drift. Water depth was much less in collectors at 36 and 39 metres from the sprinkler.

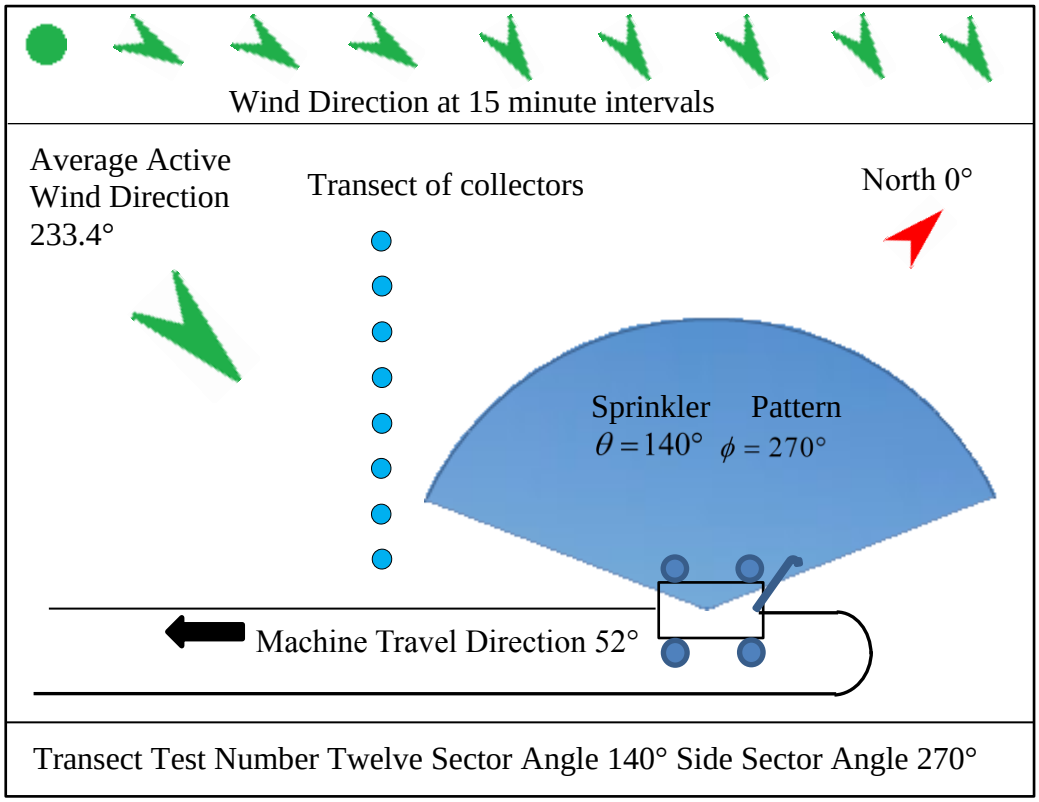

Figure B-7: Transect for test number twelve shows test layout, the combination of sector and side sector angles and other directions relevant to that test.

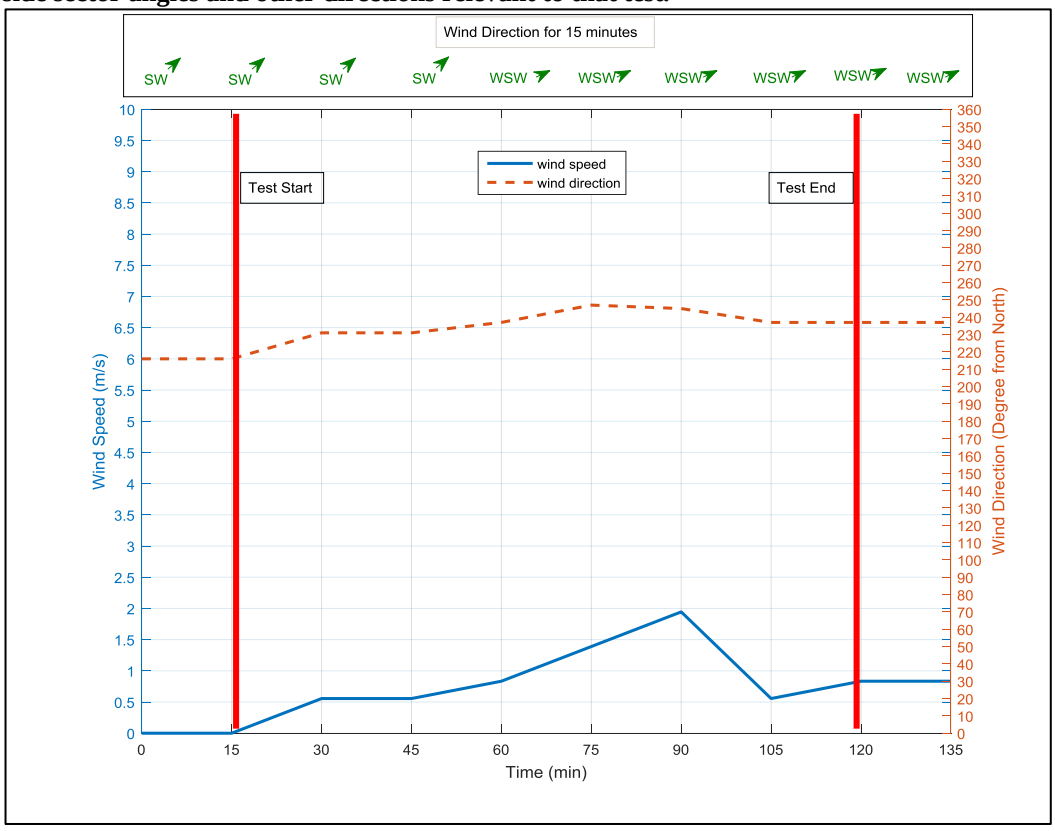

Figure B-8: Weather conditions (wind speed and direction) for Transect test number twelve.

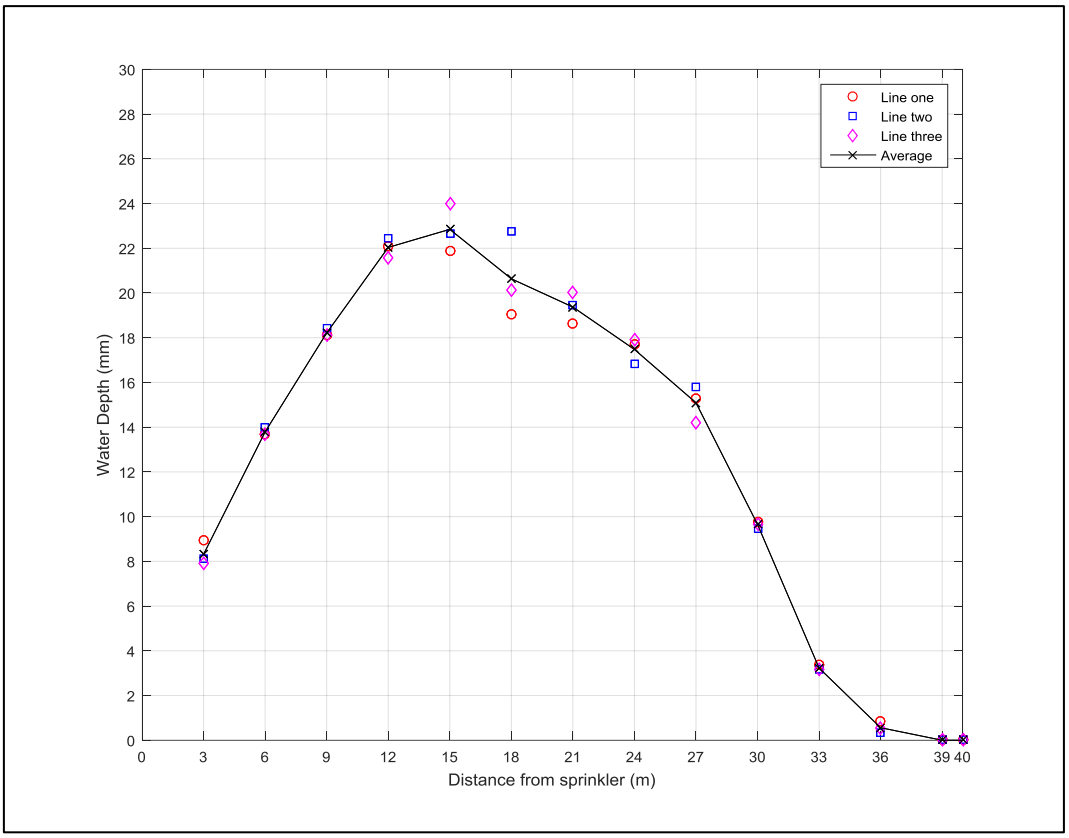

Figure B-9: Transect data for test number twelve for the combination of 140° sector angle and 270° side sector angle.

B.2.4 Transect test number five

The test was performed on Thursday 23 April 2015 from 5:45 pm to 7:30 pm with a sector angle of 105° and a side sector angle of 270°. The test layout in relation to sector and side sector angles and all direction relevant to test conditions are shown in Figure B-10. Weather data in Figure B-11 show wind speed was high during the test. Wind direction changed slightly. The wind speed and direction effects on the water depth along the transect are shown in Figure B-12 . Water depth had decreased sharply in the collectors at distances of 36 and 39 metres from the sprinkler.

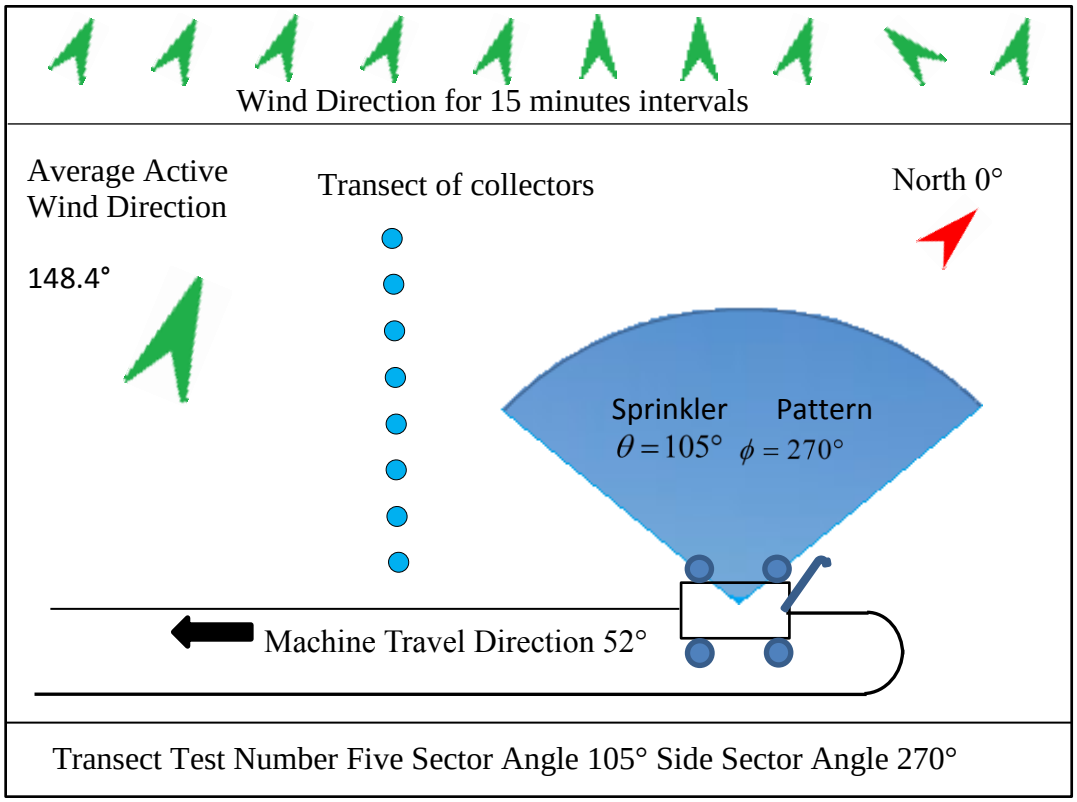

Figure B-10: Transect test number five shows test layout, the combination of sector and side sector angles and other directions relevant to that test.

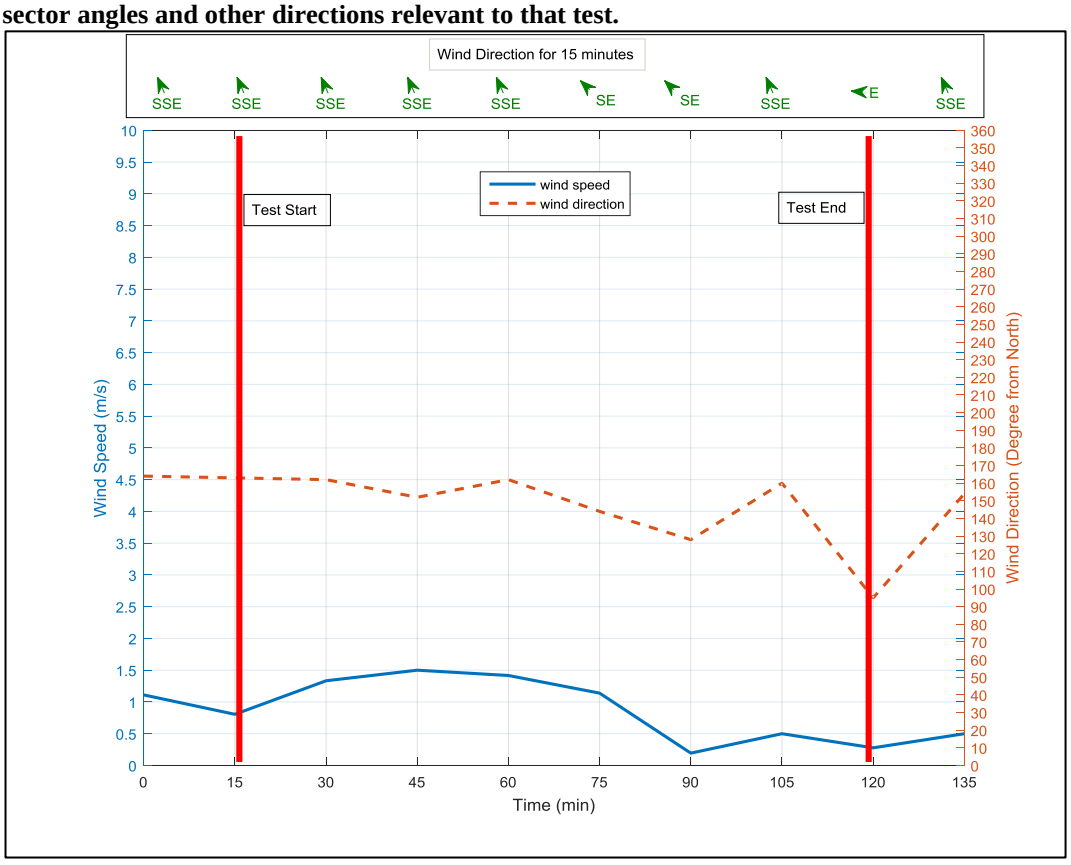

Figure B-11: Weather conditions (wind speed and direction) for transect test number five.

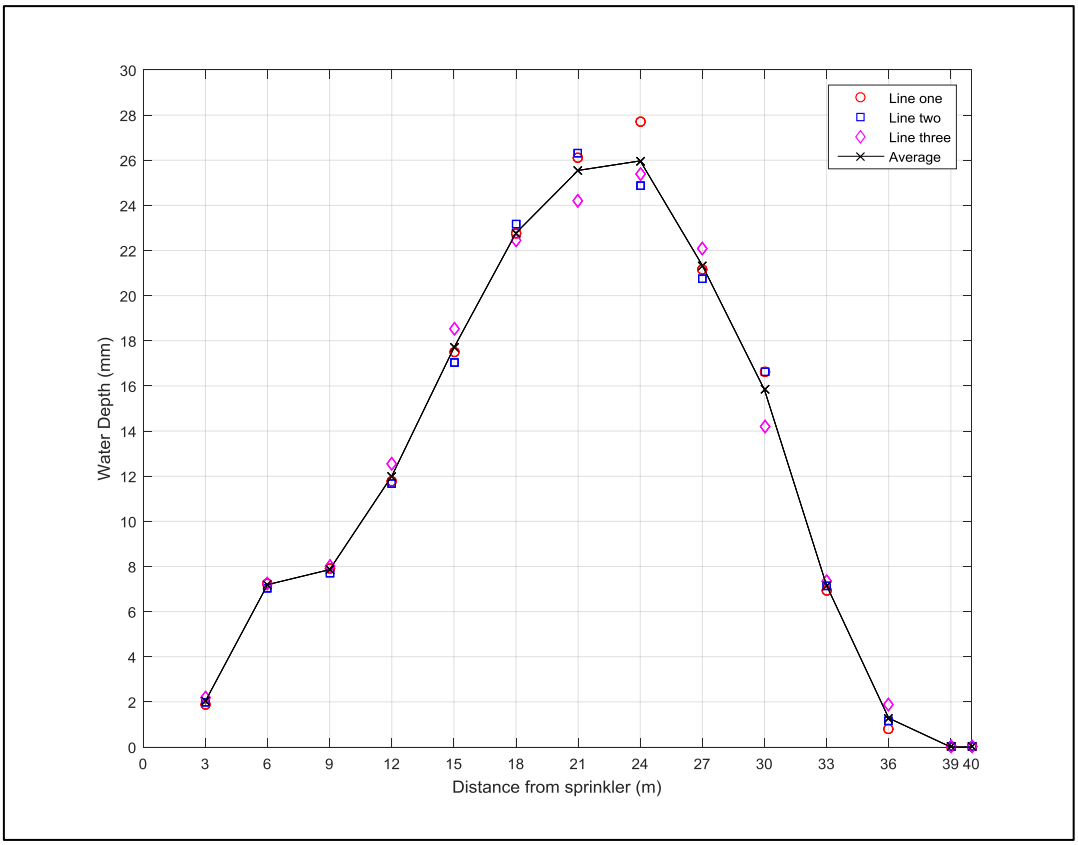

Figure B-12: Transect data for test number five for the combination of 105° sector angle and 270° side sector angle.

B.2.5 Transect test number six

The test was performed on Thursday 23 April 2015 from 10:45 pm to 12:15 am with a sector angle of 105° and a side sector angle of 270°. The test layout is shown in Figure B-13. Wind speed was high during the test, as shown in Figure B-14. Wind directions changed markedly during the test.

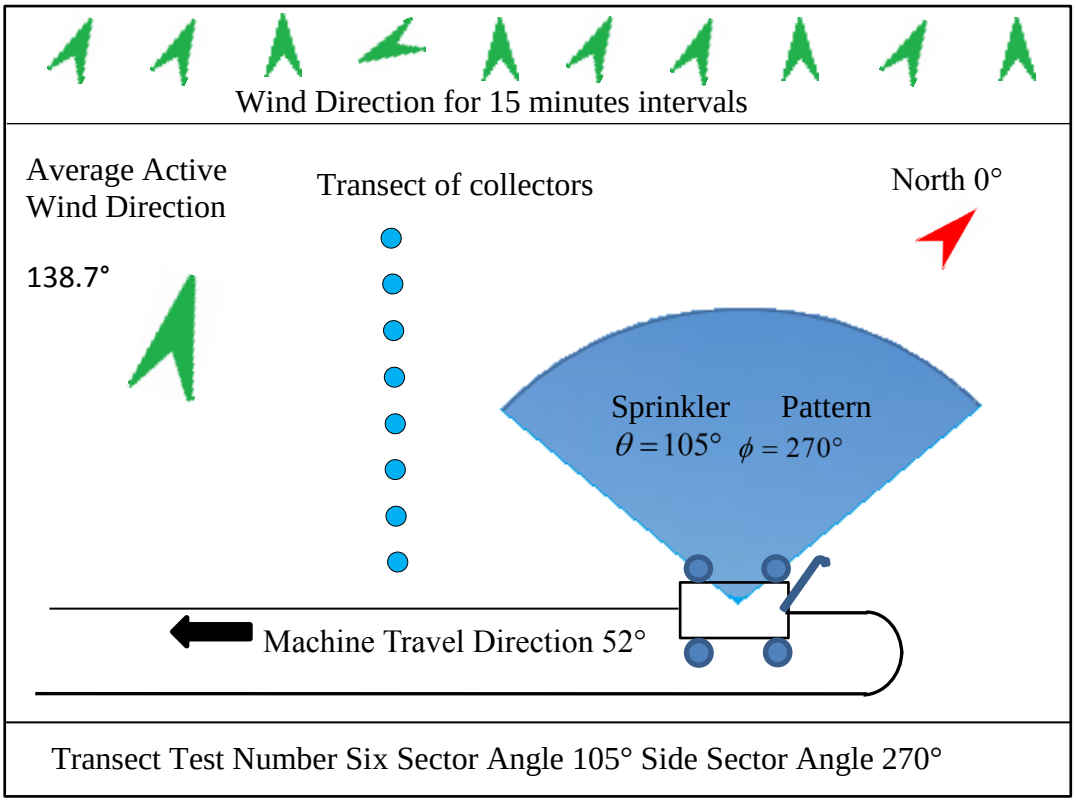

Figure B-13: Transect test number six shows test layout, the combination of sector and side sector angles and other directions relevant to that test.

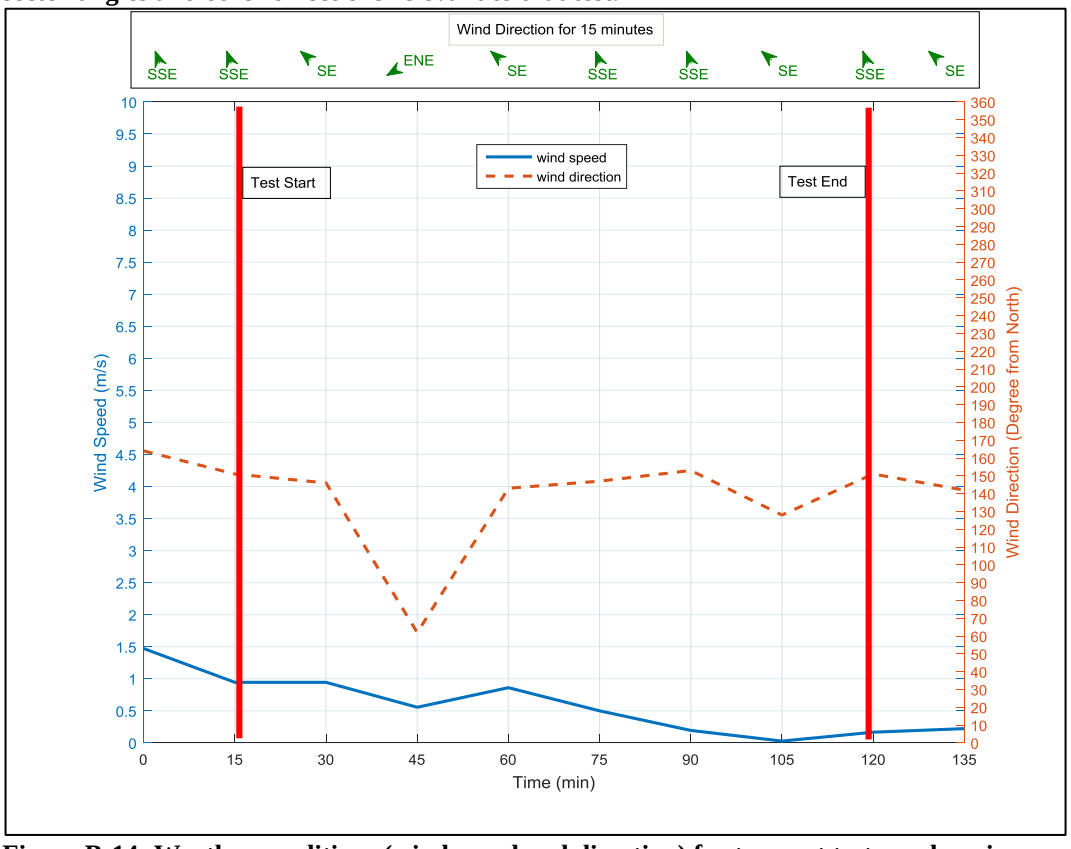

Figure B-14: Weather conditions (wind speed and direction) for transect test number six.

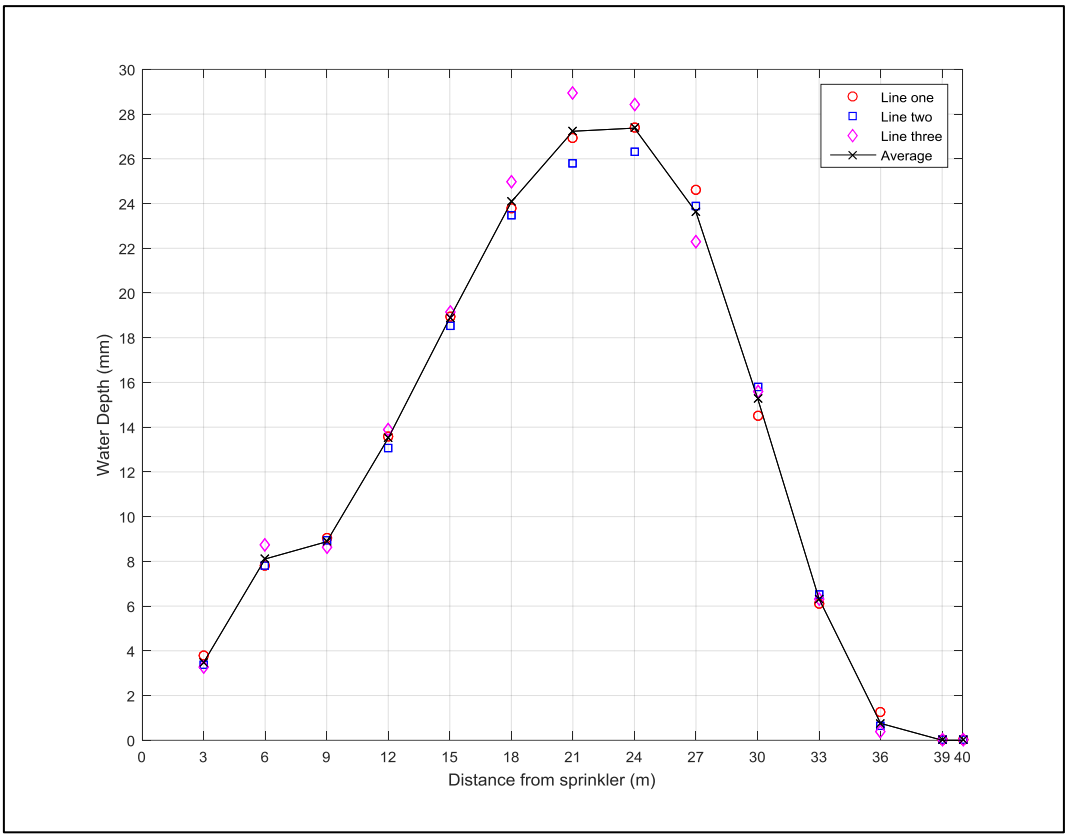

Figure B-15: Transect data for test number six for the combination of 105° sector angle and 270° side sector angle.

B.2.6 Transect test number one

The test was performed on Thursday 19 March 2015 from 9:00 pm to 10:36 pm with a sector angle of 80° and a side sector angle of 270°. The test layout is shown in Figure B-16. Wind speed was very high during the test and wind direction changed during the test, as shown in Figure B-17. Water depth was very different between the three lines of the transect as shown in Figure B-18.

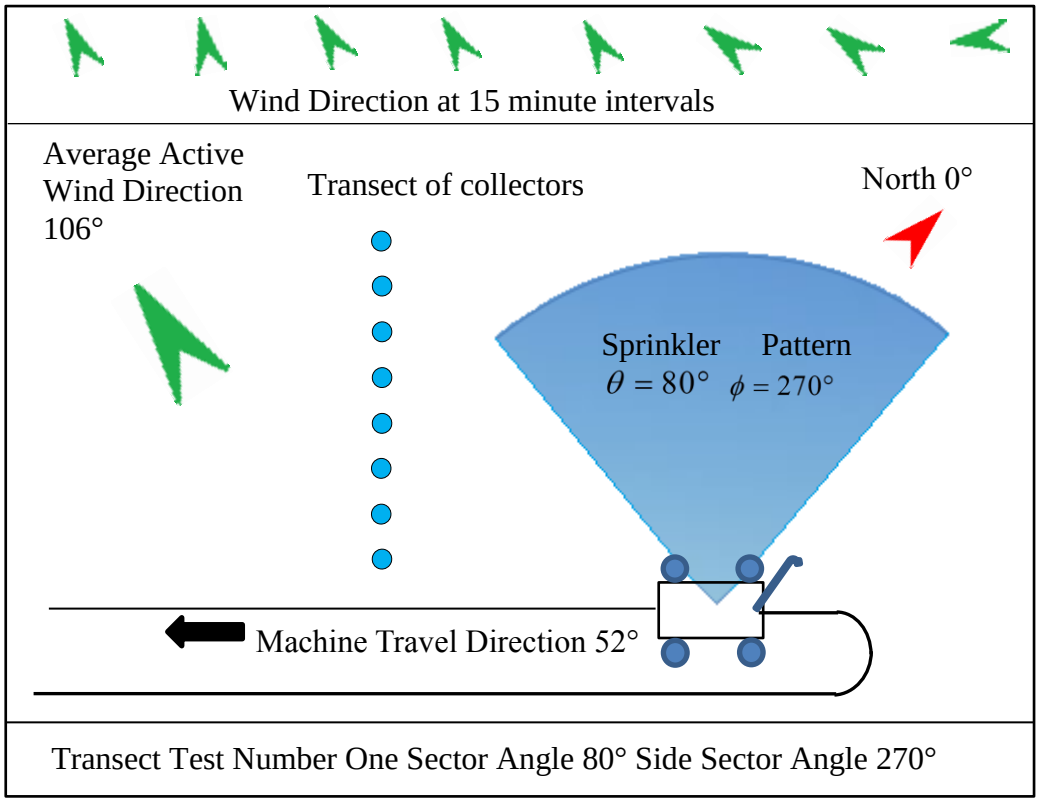

Figure B-16: Transect test number one shows test layout, the combination of sector and side sector angles and other directions relevant to that test.

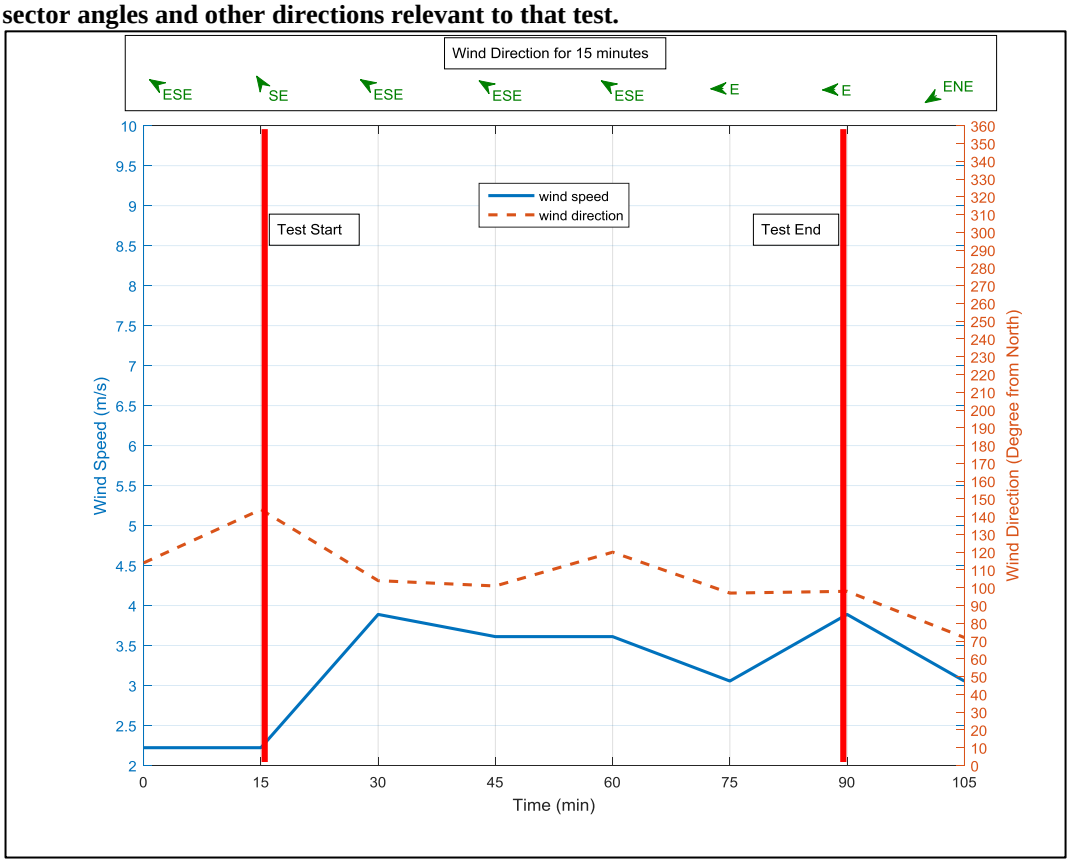

Figure B-17: Weather conditions (wind speed and direction) for transect test number one.

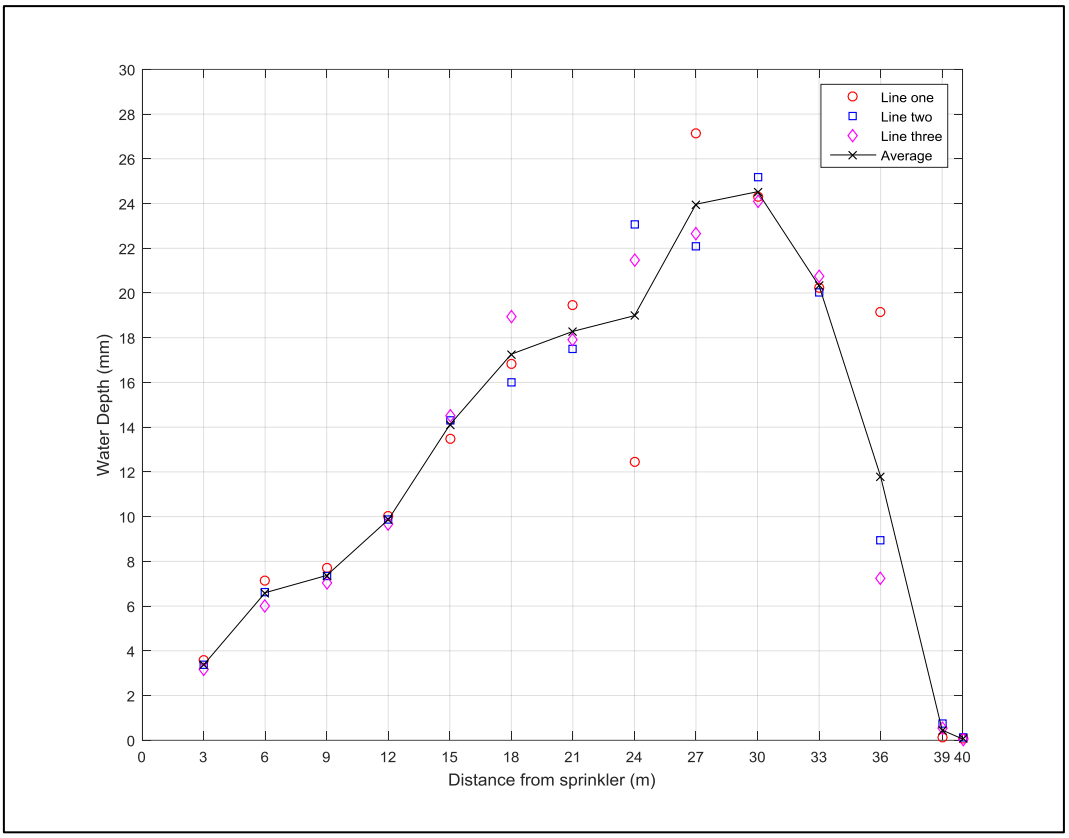

Figure B-18: Transect data for test number one for the combination of 80° sector angle and 270° side sector angle.

B.2.7 Transect test number two

The test was performed on Wednesday 25 March 2015 from 5:00 pm to 6:35 pm with a sector angle of 80° and a side sector angle of 270°. Figure B-19 shows the test layout similar for test one. Wind speed and direction were different during the test. Figure B-20 shows wind speed dropped to zero. However, average wind speed was very high. Wind direction was highly variable, as shown in Figure B-20 . The shape of the transect is different from the other test for the same sector and side sector angles as a result of the differences between wind speed and direction in both tests. Figure B-21 shows water depth in the transect is different from the other test.

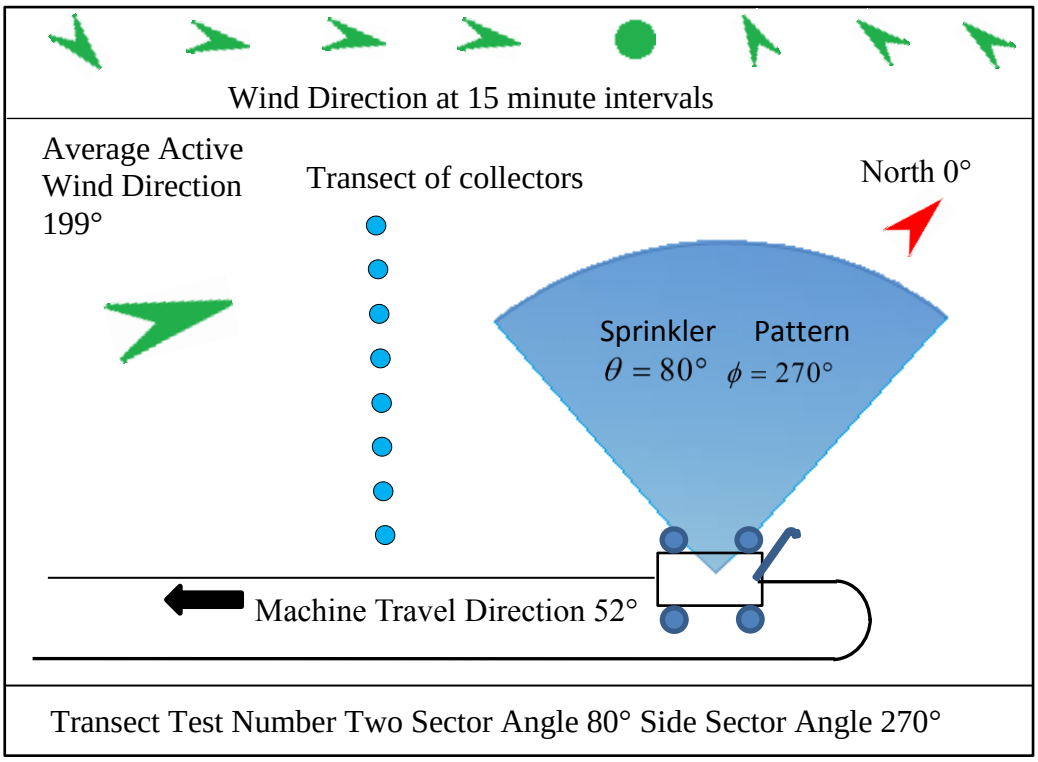

Figure B-19: Transect test number two shows test layout, the combination of sector and side sector angles and other directions relevant to that test.

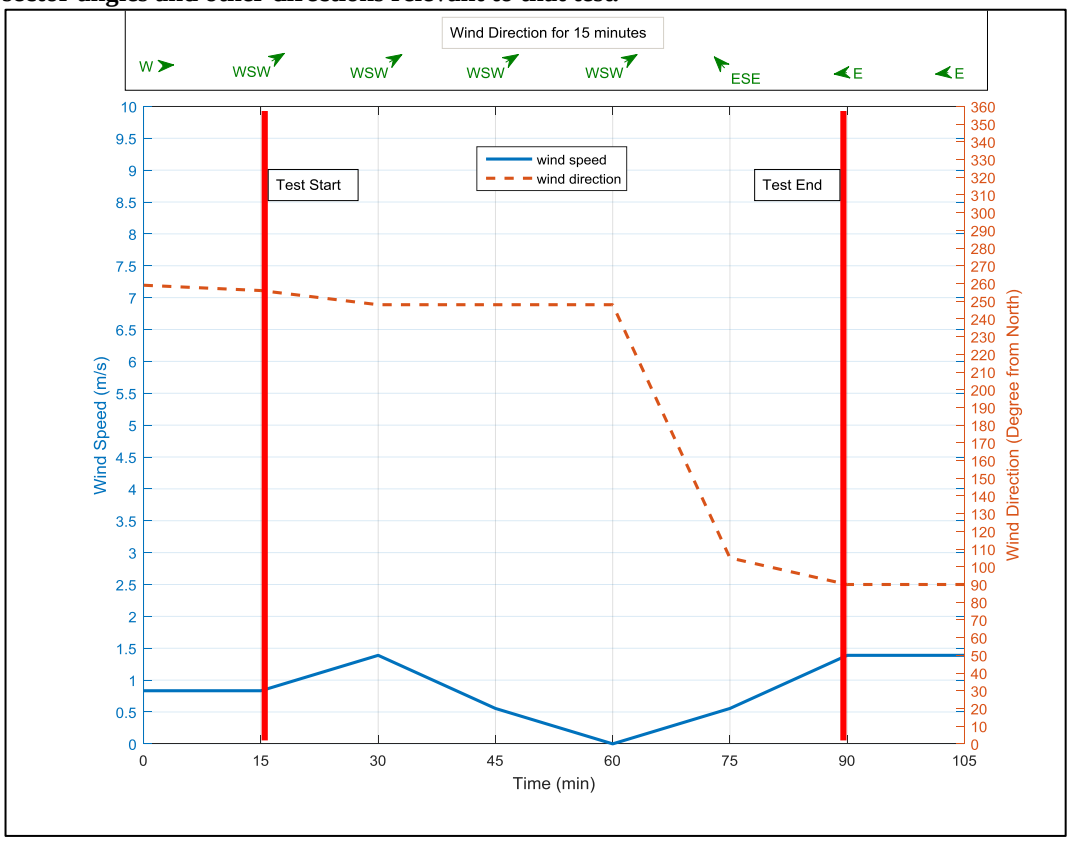

Figure B-20: Weather conditions (wind speed and direction) for transect test number two.

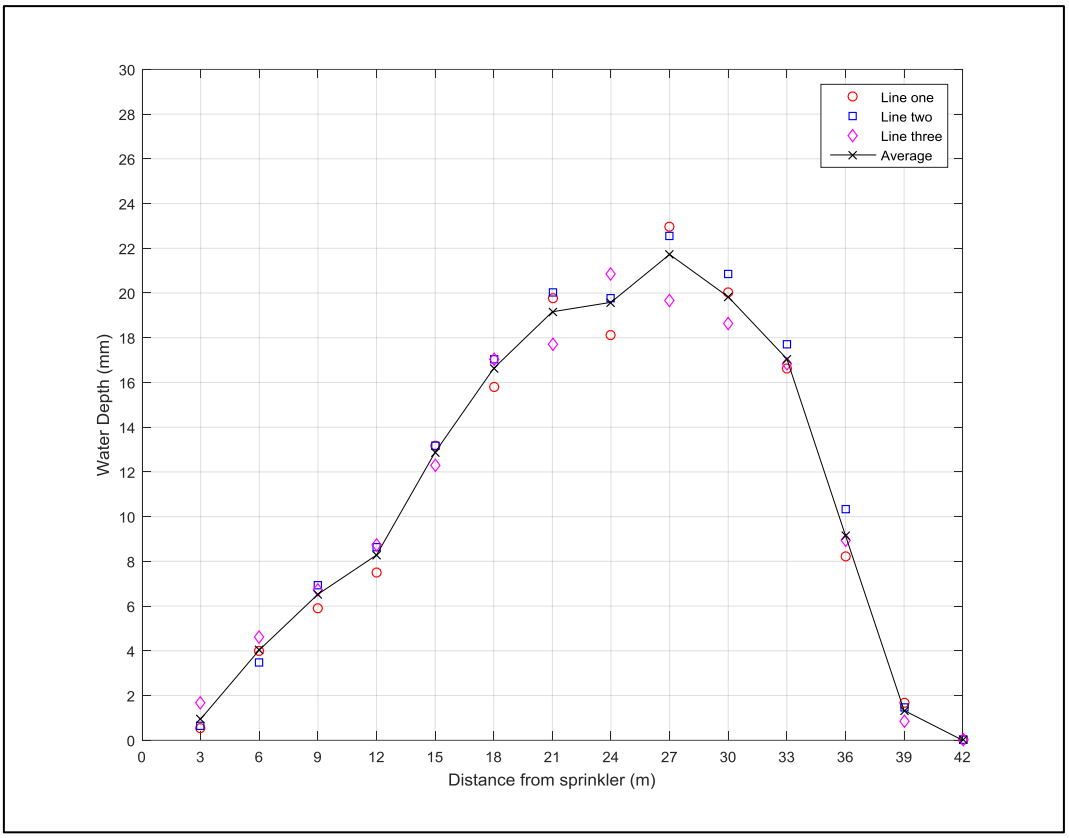

Figure B-21: Transect data for test number two for the combination of 80° sector angle and 270° side sector angle.

B.2.8 Transect test number three

The test was performed on Thursday 26 March 2015 from 6:00 pm to 7:15 pm with a sector angle of 80° and a side sector angle of 270°. Figure B-22shows the test layout is similar to tests one, two and ten. However, weather conditions are different. Figure B-23 shows that wind speed was very high and wind direction very variable during the test. Figure B-24 shows a different transect shape as a result of wind speed and direction effects.

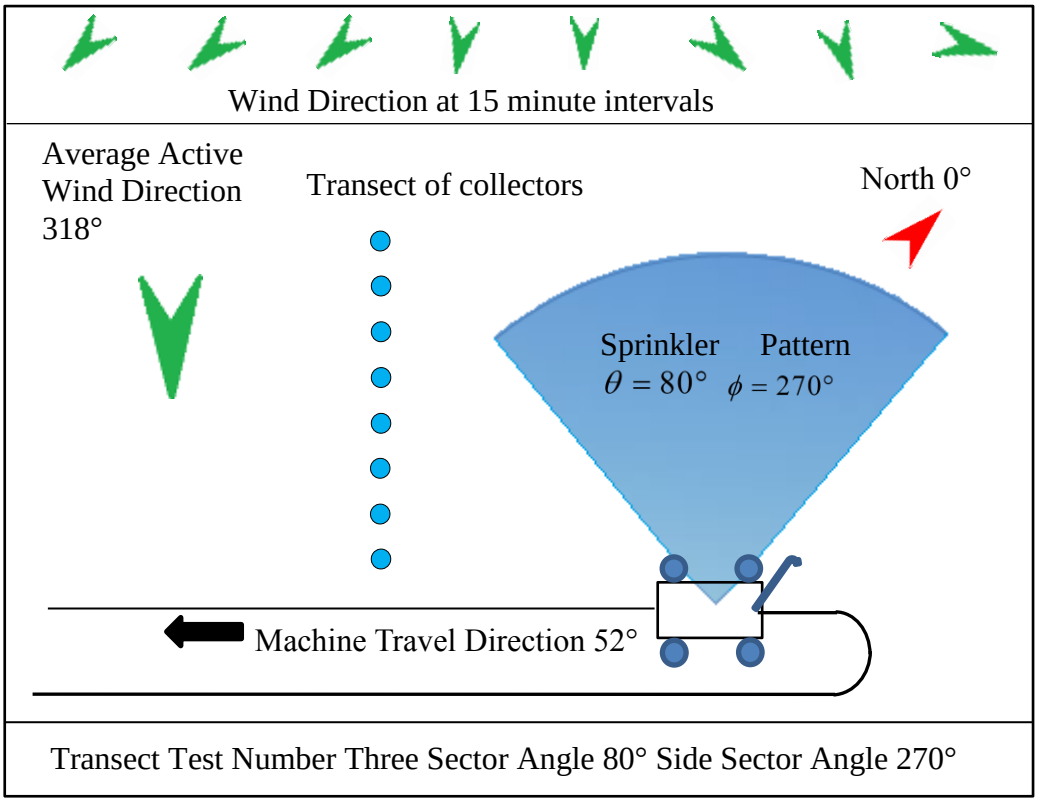

Figure B-22: Transect test number three shows test layout, the combination of sector and side sector angles and other directions relevant to that test.

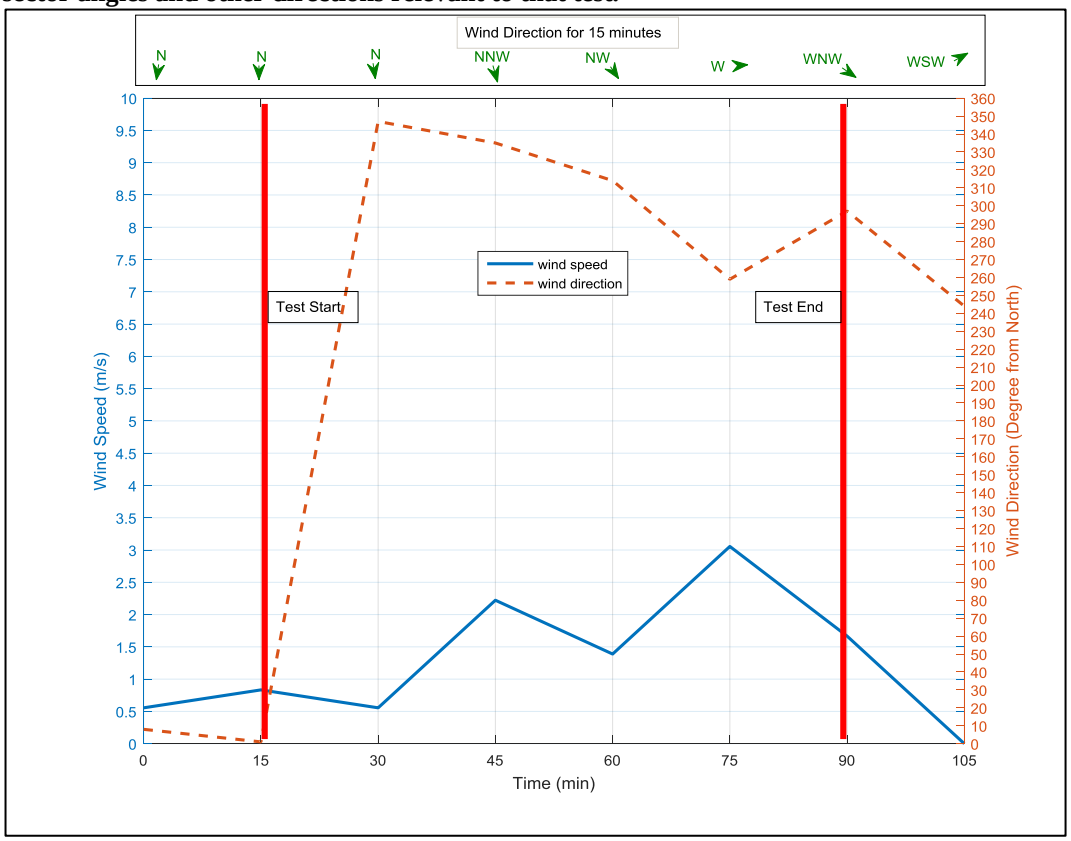

Figure B-23: Weather conditions (wind speed and direction) for transect test number three.

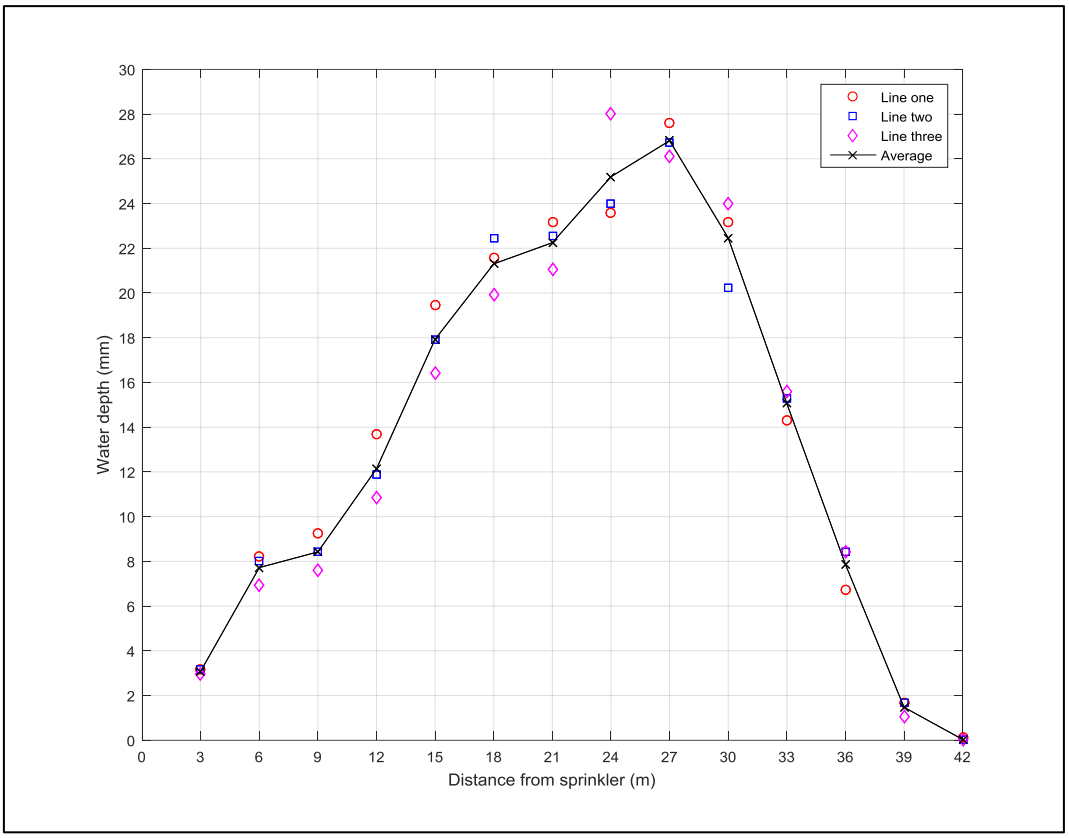

Figure B-24: Transect data for test number three for the combination of 80° sector angle and 270° side sector angle.

B.3 Measuring transect in curve movement

Two tests in curve movement were performed in high wind speed conditions. These tests are included in this appendix to provide a general idea of the change in shape of transects in wind. The tests have the same sector and side sector angles but the curve radii are different.

B.3.1 Transect test number sixteen

The test was performed on Tuesday 9 June 2015 from 10:45 pm to 12:30 pm with a sector angle of 180° and a side sector angle of 270°, and a curve radius of 300 metres. Figure B-25 shows the test layout and the average wind direction for the sprinkler pattern in relation to a northerly direction. Figure B-26 shows wind speed and direction

during the test. The figure shows wind speed was high and wind directions were highly variable during the test. Figure B-27 shows water depths were varied greatly between the three lines of collectors as a result of changing wind direction during the test.

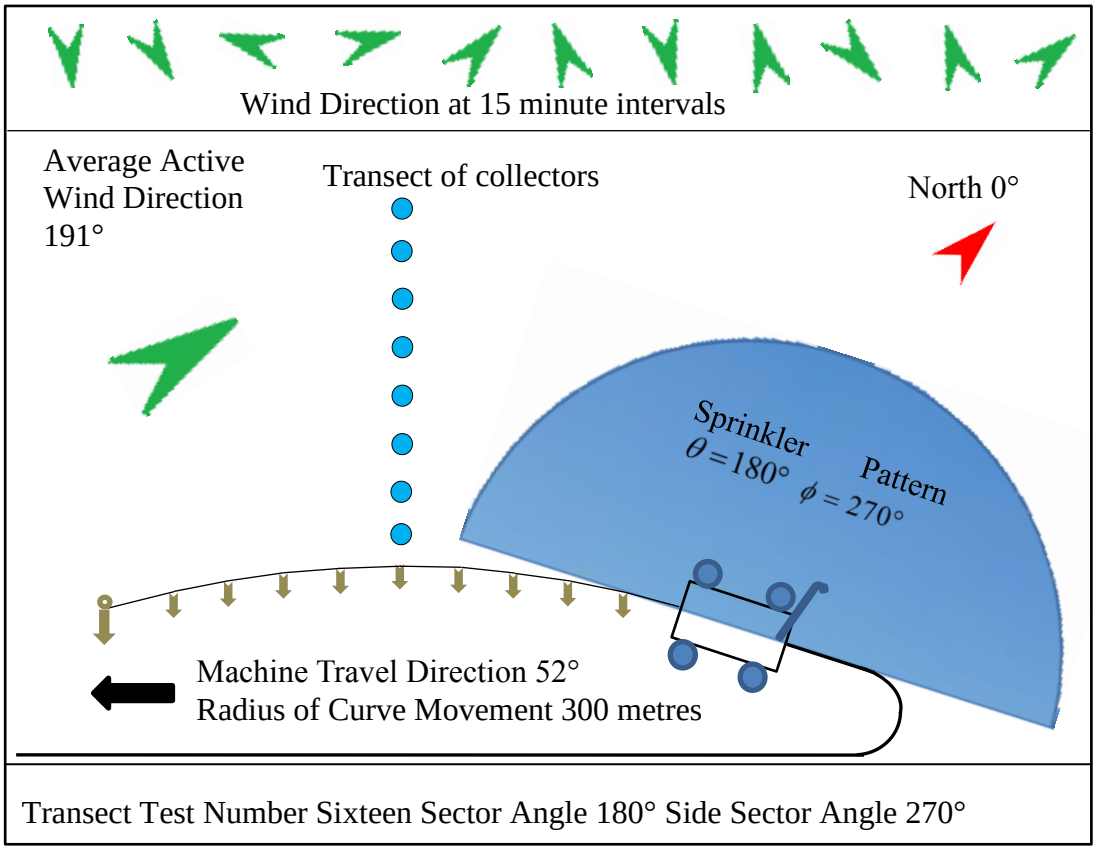

Figure B-25: Transect test layout for a curvature movement of 100 metres radius and weather conditions during test number sixteen.

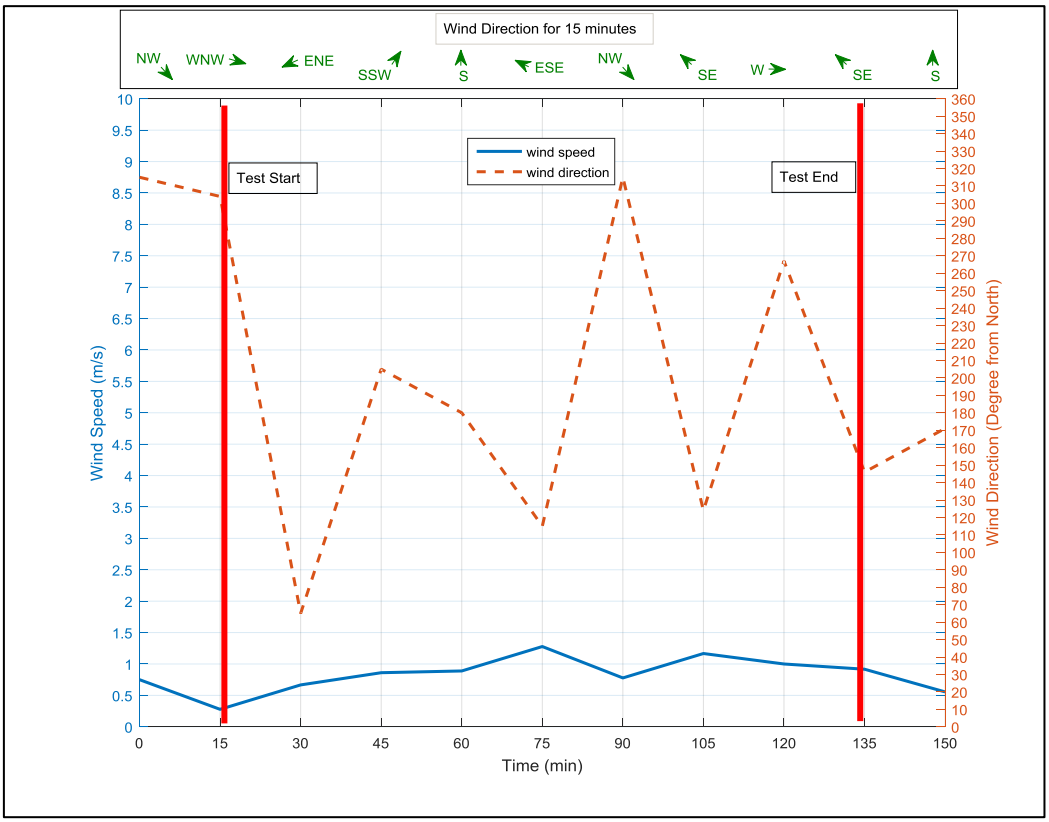

Figure B-26: Weather conditions (wind speed and direction) for transect test number sixteen.

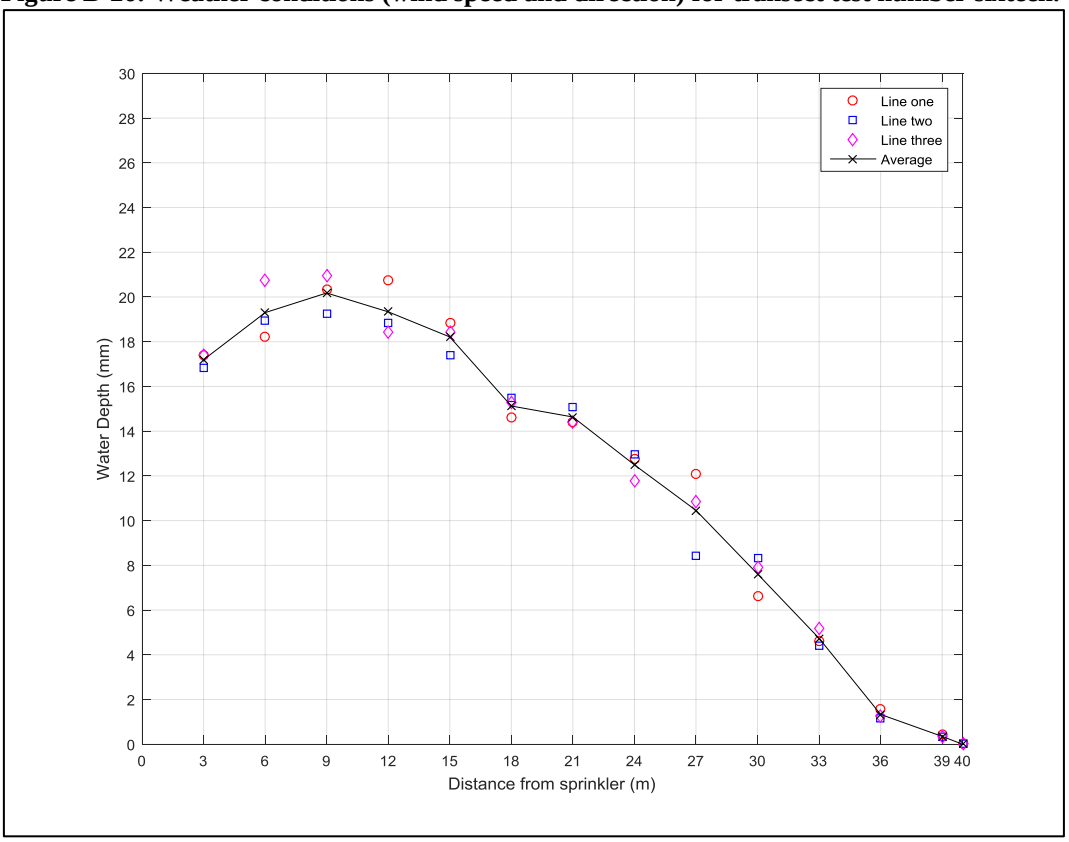

Figure B-27: Transect data for a curve movement of 100-metre radius and the combination of a 180° sector angle and 270° side sector angle for test number sixteen.

Appendix C

Record Zero Wind Speed

C.1 Introduction

This appendix includes records of zero wind speed that were recorded while monitoring weather forecasts before and during the tests.

C.1.1 Second record of zero wind speed

The second record of zero wind occurred on 24 April 2015. Figure C-1 shows that the region of the experimental site was not under the influence of any different pressure system surrounding the experimental site as the isobar was too wide around it.

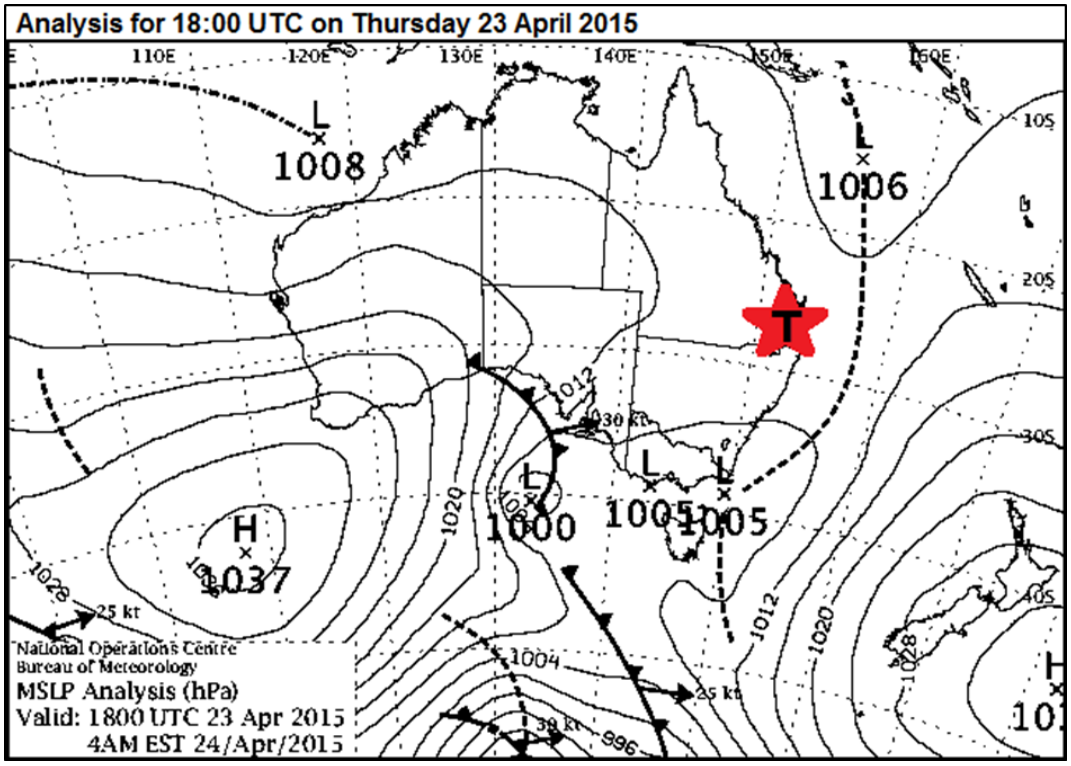

Figure C-1: Synoptic pressure systems surrounding the experimental region (Bureau of Meteorology, 2015) record two.

The remote monitoring of wind speed and direction during that time shows the long period taken for the wind speed to reach zero. Figure C-2 reveals the length of time, approximately 7 hours, until the wind speed became zero. Images (A), (B), (C) and (D) show that wind speed reached zero on Friday at 3:30 am.

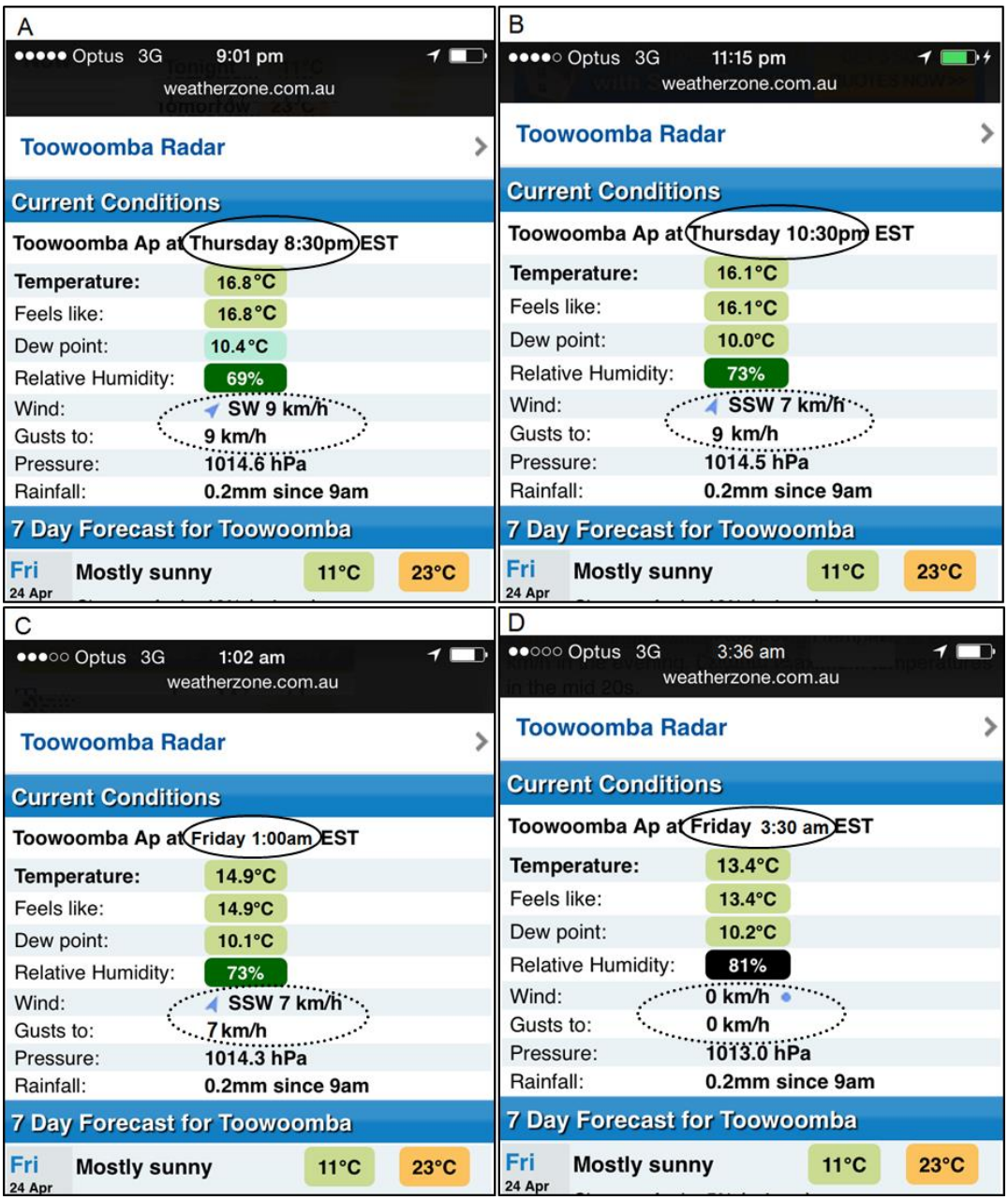

Figure C-2: Four screenshots showing current wind speed decreasing gradually at that date until it reached zero. The solid circle displays the time and the dotted circle displays wind speed (Weatherzone, 2015) record two.

The period of zero wind speed was recoded for 90 minutes as shown in Figure C-3. Zero wind speed started at 3:30 am as shown in image (A) and continued until 5:00 am as shown in image (B) Figure C-3.

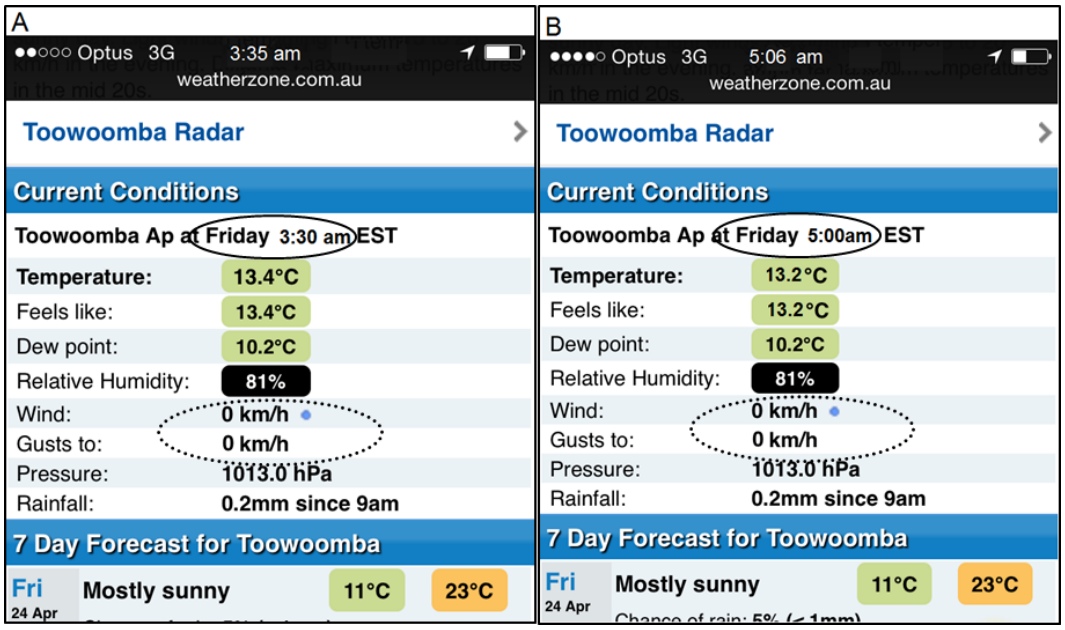

Figure C-3: Two screenshots at different times show periods of zero winds of more than one (Weatherzone, 2015) record two.

C.1.2 Third record of zero wind speed

The third record of zero wind speed occurred from the afternoon of 5 May to the morning of 6 May 2015. It was recorded as the longest period of zero wind speed. Figure C-4 shows that the region of the experimental site was not part of the influence of any different pressure system surrounding the experimental site at that time as the isobar was too wide around it.

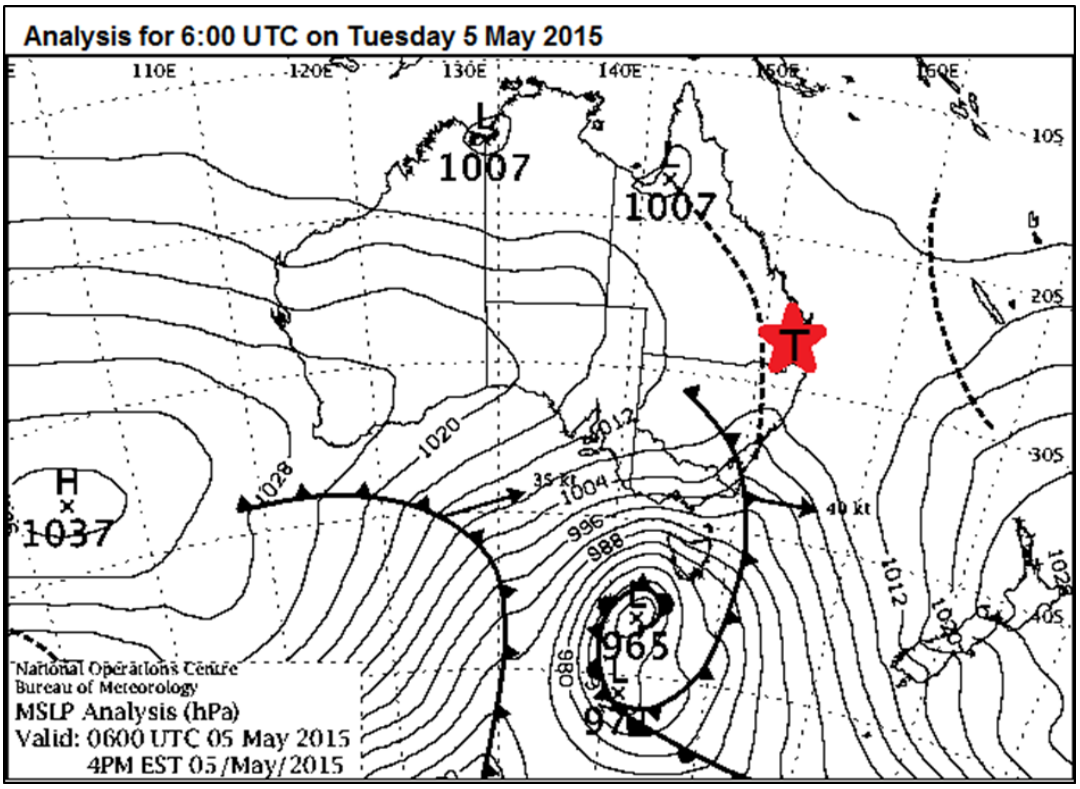

Figure C-4: Synoptic pressure systems surrounding the experimental region (Bureau of Meteorology, 2015) record three.

The figure shows the extension of the isobar of the high-pressure system to the West of the region of the experimental site was too distant. The centres of two low pressure systems to the South-West and North-West of the region of the experimental site were also too distant.

The period of remote monitoring showed wind speed slowing before it reached zero, as shown in Figure C-5 . Image (A) in this Figure shows wind speed was 4 km/h at 5:30 pm and wind gusts were 6 km/h. Wind slowed to 2 km/h after one hour as shown in image (B) of Figure C-5, but wind gusts reached 6 km/h. Image (C), Figure C-5, was taken at 7:35 pm and shows wind speed as zero at 7:30 pm. However, at that time there were still wind gusts up to 2 km/h. Image (D), Figure C-5, shows that wind speed became zero at 8:30 pm on Tuesday 5 May 2015.

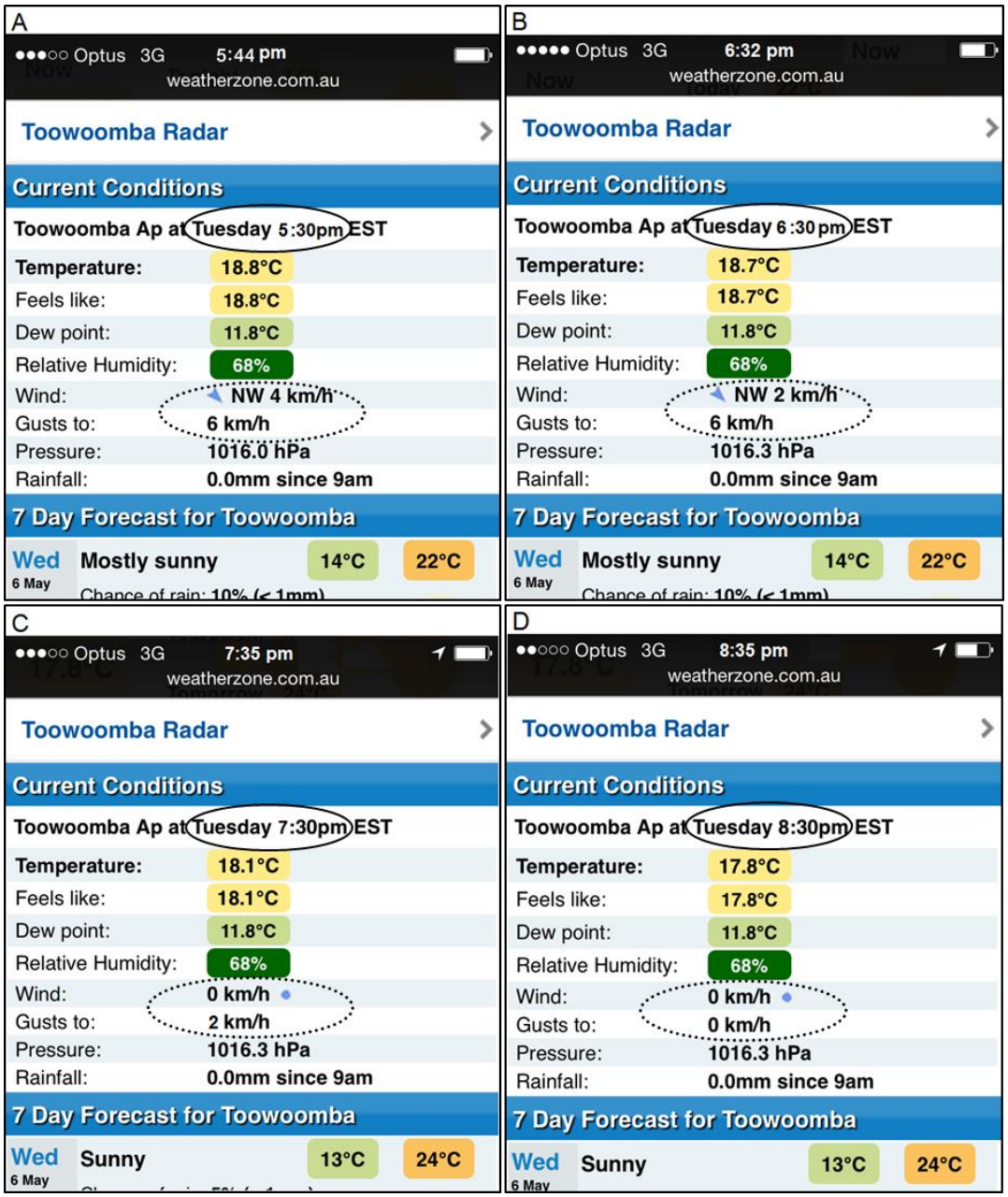

Figure C-5: Four screenshots show that current wind speed decreased gradually at that date until it became zero, (Weatherzone, 2015) record three.

The period of zero wind recorded was the longest that night, as shown in Figure C-6. However, wind gusts and wind speed increased slightly during that night. It began at 8:30 pm on Tuesday 5 May 2015, as shown in Figure C-5 image (D), and continued for more than 180 minutes, as shown in Figure C-6 image (D), which was taken at 8:35 pm. Figure C-6 image (A) was taken at 11:36 pm. There were wind gusts up to 6 km/h at 12:00 am, as shown in image (B), then wind speed slowed to zero at 1:00 am, as

shown in image (C). After that, zero wind speed continued to 1:30 am, as shown in image (D).

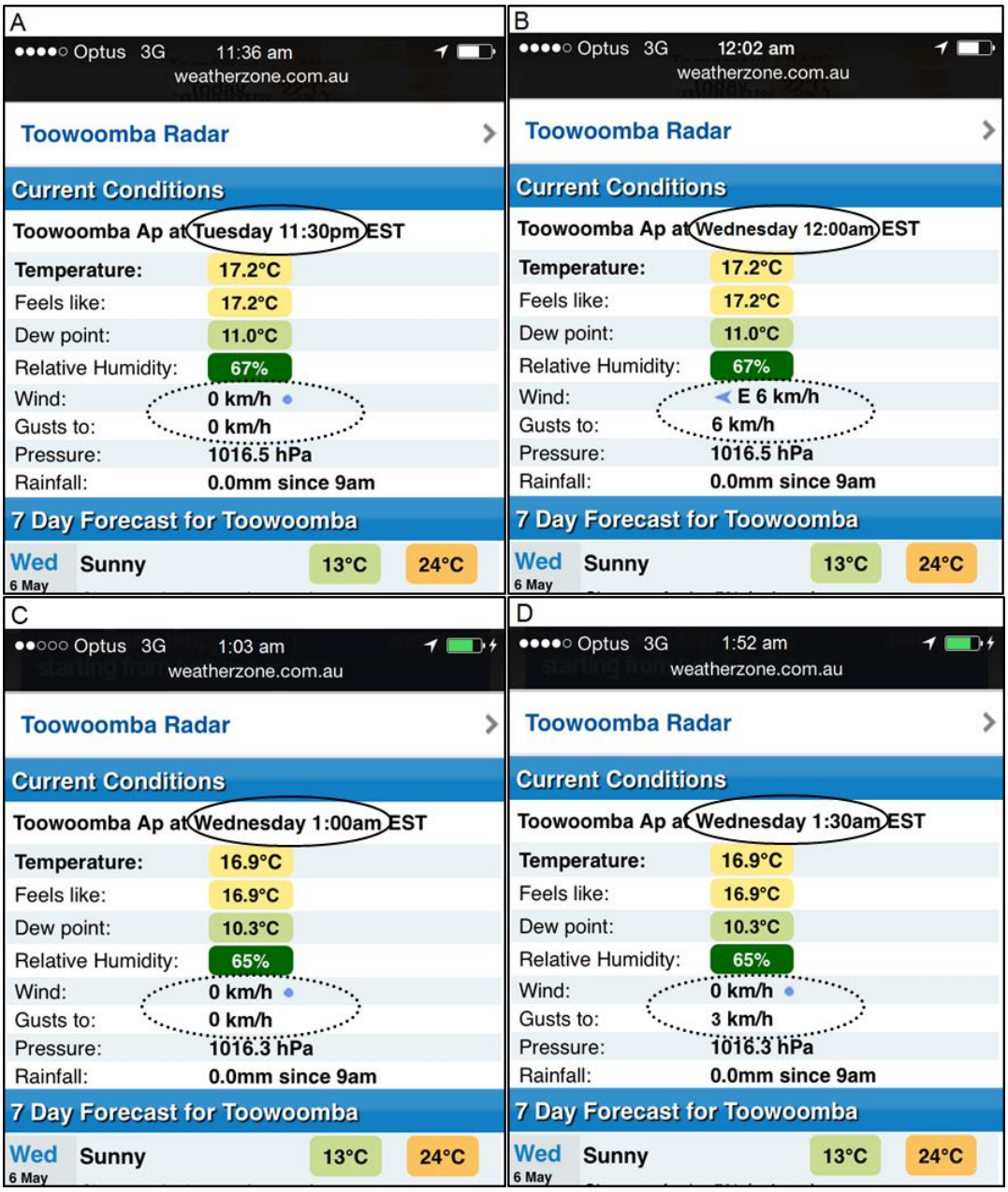

Figure C-6: Four screen shots at different times shows the period of zero wind and wind gusts during that time (Weatherzone, 2015) record three.

C.1.3 Fourth record of zero wind speed

The fourth record of zero wind speed occurred from the afternoon of 29 May to the morning of 30 May 2015. During this period wind speed dropped to zero for 150 minutes before the wind started gusting and increased in speed after approximately 60

minutes. After that, wind speed fell to zero for 120 minutes, as shown in the following figures. Figure C-7 shows that the region of the experimental site was not part of the influence of any different pressure system surrounding the experimental site and the isobar was too wide around it.

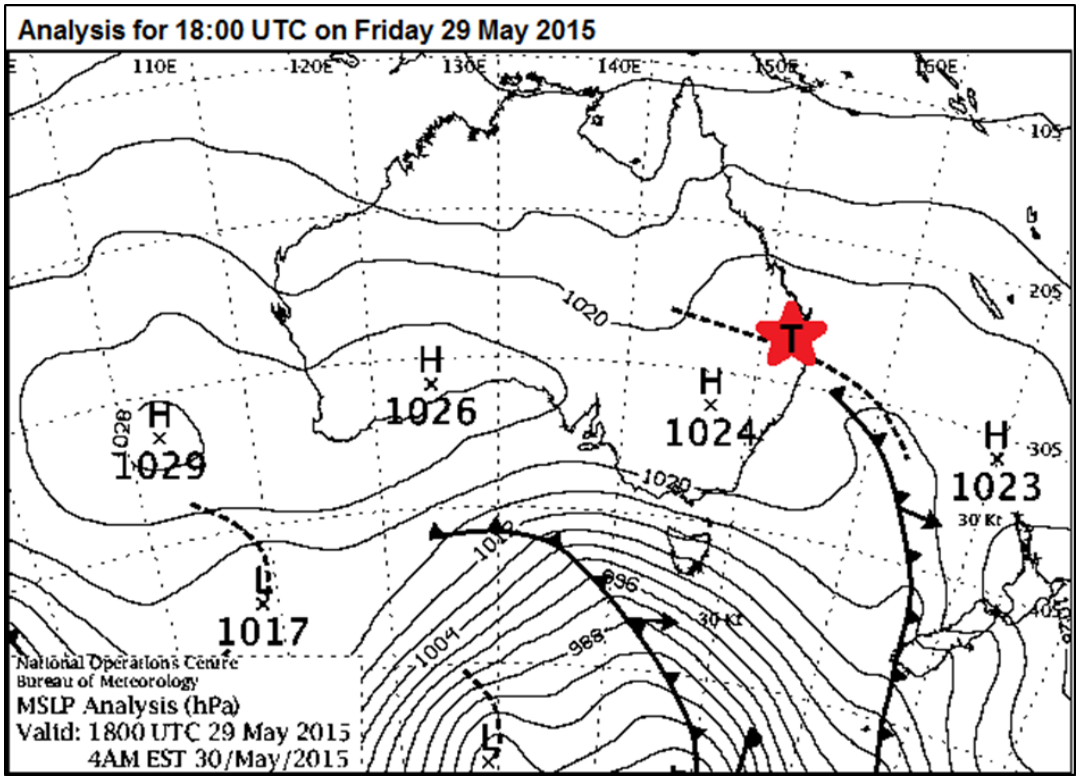

Figure C-7: Synoptic pressure systems that surrounded the experimental region (Bureau of Meteorology, 2015) record four.

The remote monitoring of wind speed continued for more than four hours before wind speed became zero, as shown in Figure C-8. Image (A) in this Figure shows wind speed was 9 km/h at 5:00 pm. After one hour, the wind slowed to 5 km/h, as shown in image (B) Figure C-8. Image (C), Figure C-8 was taken at 7:35 pm and shows wind speed at 7:30 pm fell to 4 km/h. Image (D), Figure C-8, shows wind speed became zero at 9:30 pm on Friday 29 May 2015.

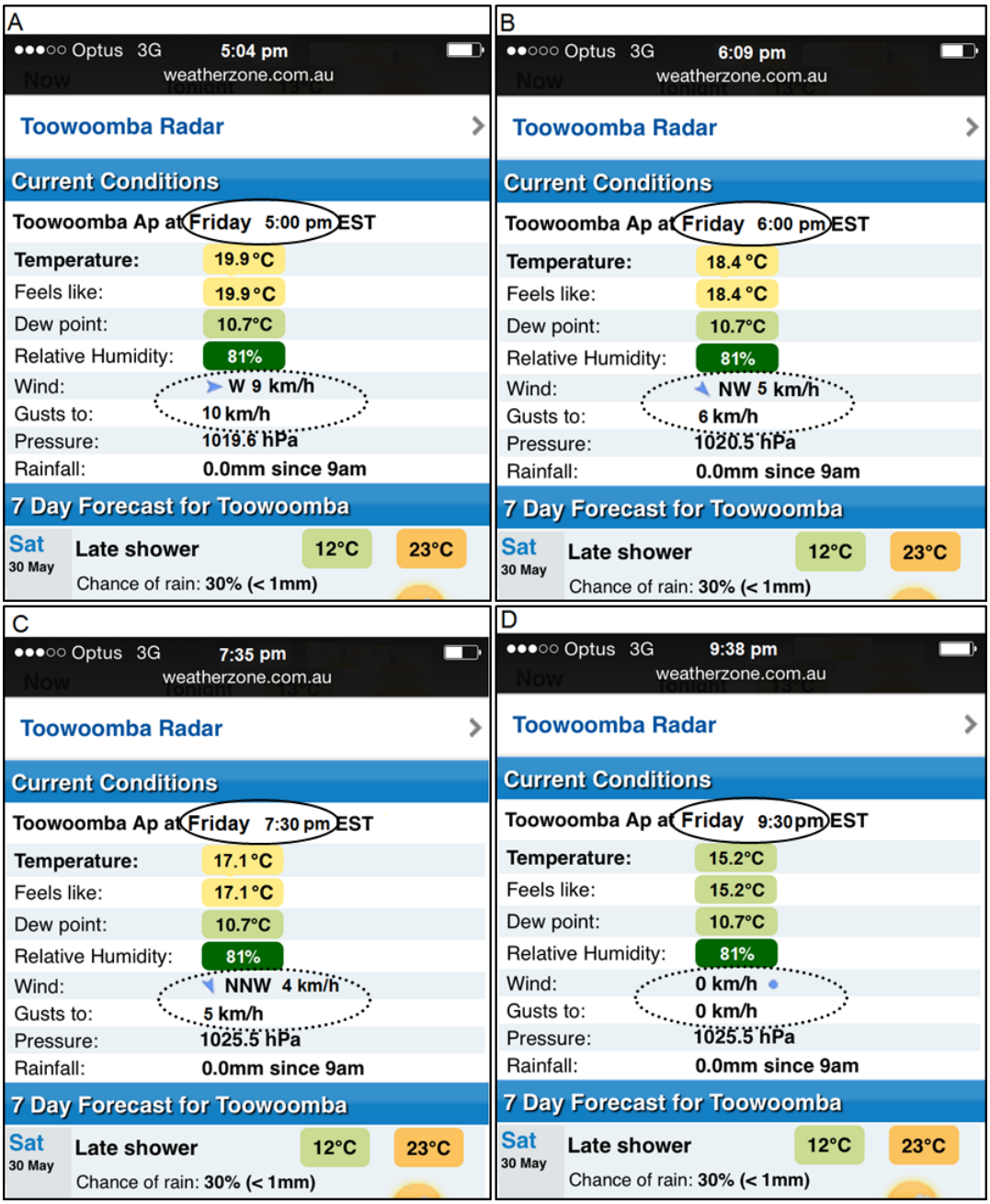

Figure C-8: Four screenshots showing current wind speed decreased gradually until it became zero, (Weatherzone, 2015) record four.

The period of zero wind recorded was more than 150 minutes on that night, as shown in Figure C-8 and Figure C-9. It began at 9:30 pm on Friday 29 May 2015, as shown in Image (D) Figure C-8, and continued to 12:00 am on 30 May 2015, as shown in Figure C-9 Image (A). The wind started to gust and speed up, as shown in Figure C-9 images (B) and (C). Image (D) shows that wind speed decreased to zero at 2:30 am but, there were still wind gusts up to 4 km/h.

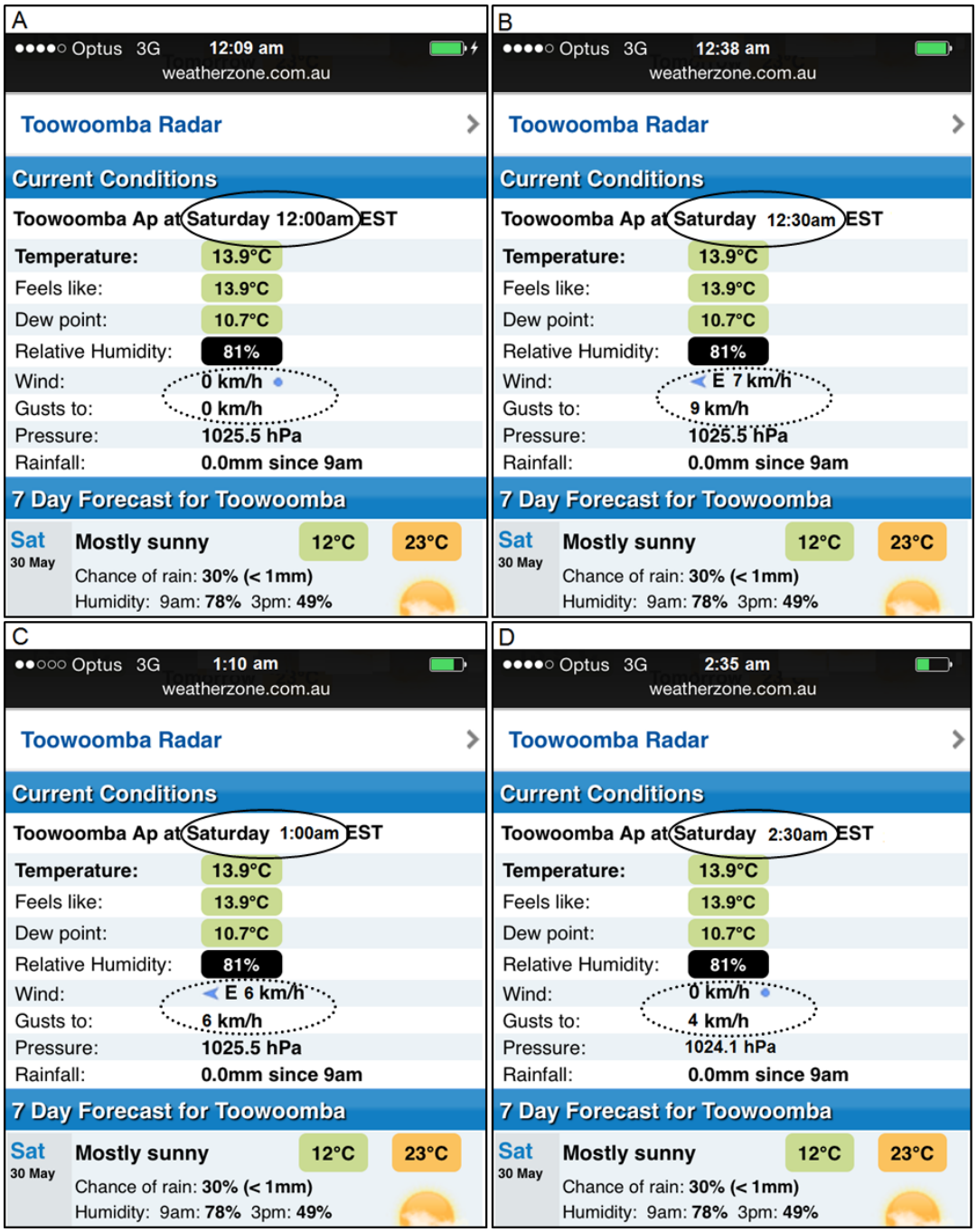

Figure C-9: Four screenshots at different times, showing the period of zero wind and wind gusts during that time (Weatherzone, 2015) record four.

Figure C-10 shows zero wind continued until 3:00 am, image (A), and was still zero until 4:30 am, image (B).

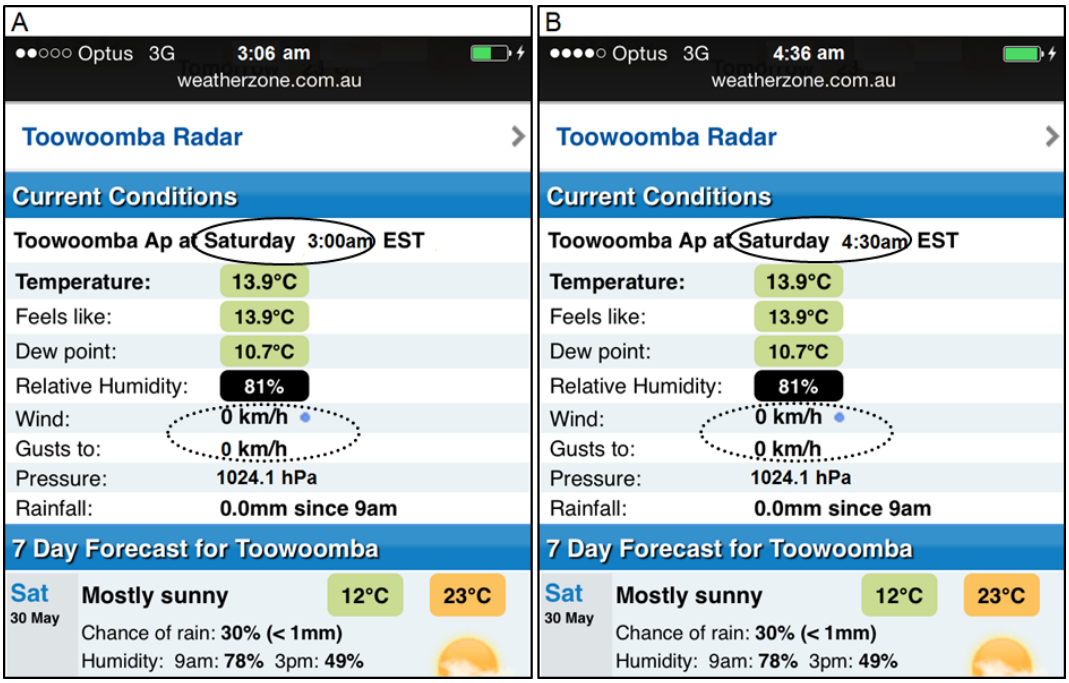

Figure C-10: Two screenshots at different times, showing the period of zero wind as 120 minutes (Weatherzone, 2015) record four.

C.1.4 Fifth record of zero wind speed

The fifth record of zero wind speed occurred during the afternoon of Saturday 30 May 2015 between 5:30 pm and 7:00 pm. Figure C-11 shows that the experimental region was still not part of the high pressure systems that were stationed far away to the South-West and the two high pressure systems to the North and South-East of the region of the experimental site. However, the distance between the isobars was too wide near the experimental region.

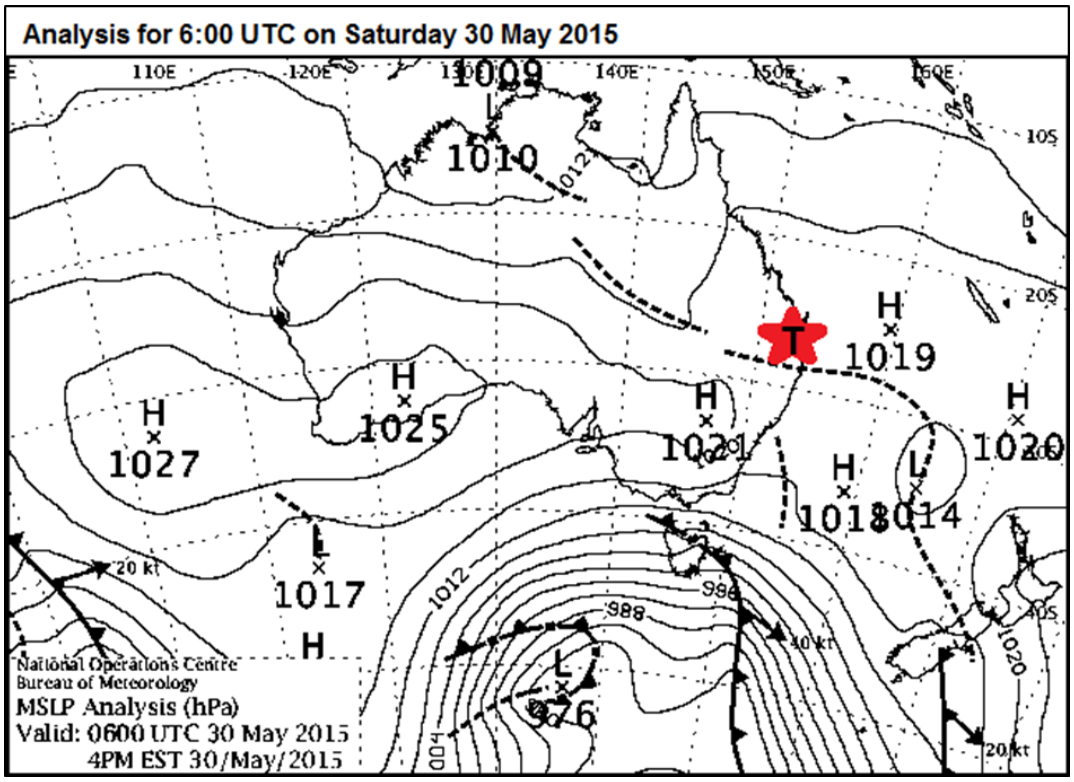

Figure C-11: Synoptic pressure systems that surrounded the experimental region (Bureau of Meteorology, 2015) record five.

The period of remote monitoring of wind speed at that date shows a short period of monitoring stages until wind speed became zero. It took one hour and 30 minutes until wind speed became zero. Image (A) Figure C-12 shows wind speed became 9 km/h at 4:00 pm on Saturday 30 May 2015. Image (B) shows wind speed slowed to 7 km/h at 4:30 pm, but there were still wind gusts to 13 km/h. Image (C) shows wind speed became 9 km/h at 5:00 pm with wind gusts to 13 km/h. Image (D) shows wind speed became zero at 5:30 pm on Saturday 30 May 2015.

Figure C-12: Four screenshots showing current wind speed decreasing gradually until reaching zero, (Weatherzone, 2015) record five.

The period of zero wind recorded was 90 minutes, as shown in Figure C-12 and Figure C-13. It started at 5:30 pm on Saturday 30 May 2015 as shown in Figure C-12 image (D) and continued for more than 90 minutes, as shown in images (A) and (B).

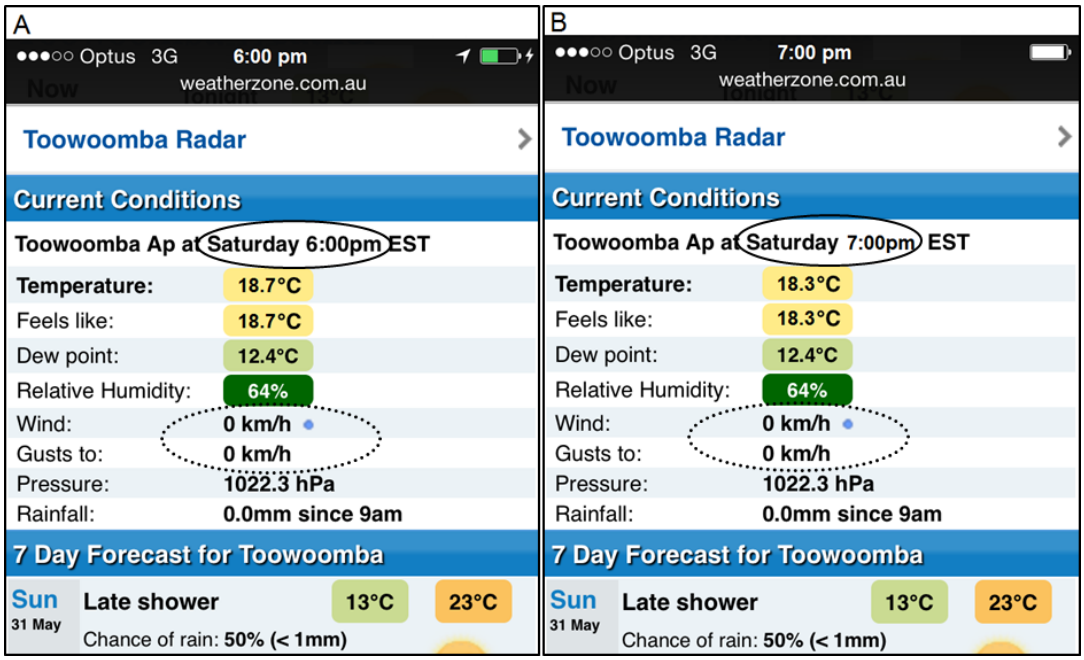

Figure C-13: Two screenshots at different times show the period of zero wind was 90 minutes (Weatherzone, 2015) record five.

C.1.5 Sixth record of zero wind speed

The sixth record of zero wind speed was during the afternoon of Wednesday 15 July to early morning Thursday 16 July 2015. Figure C-14 shows that the region of the experiment was not part of the influence of the two low pressure systems that were stationed at the South and South-West of the region of experimental site.

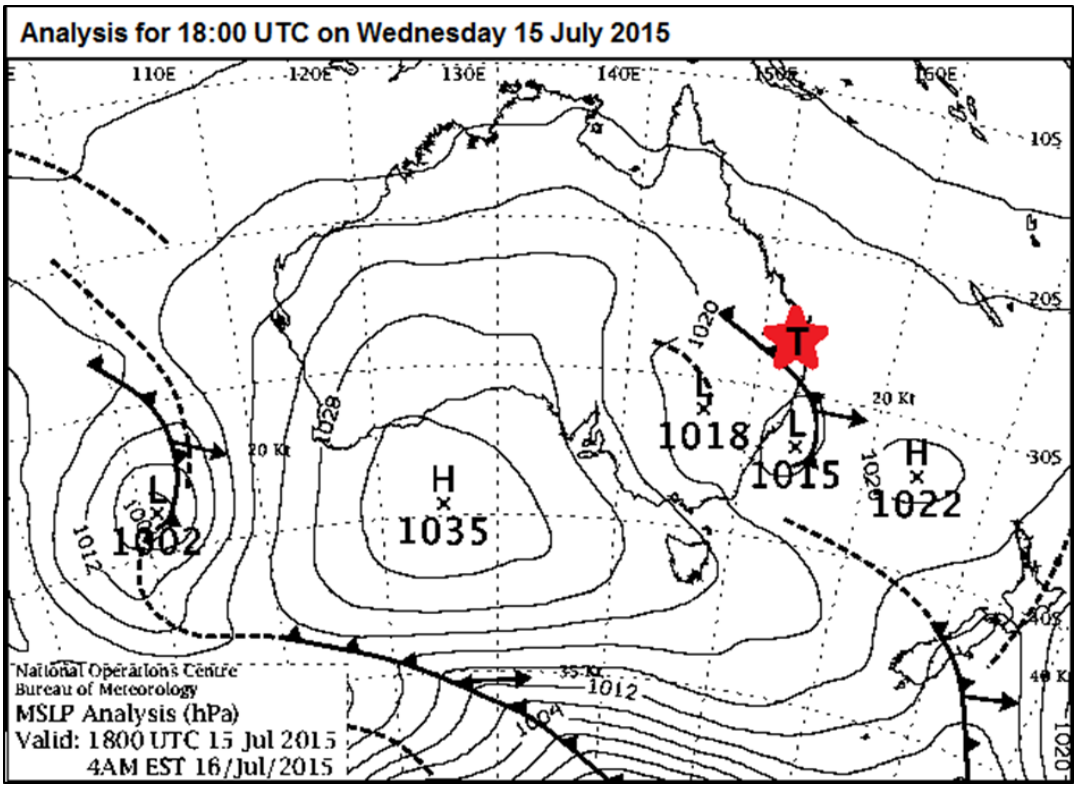

Figure C-14: Synoptic pressure systems that surrounded the experimental region (Bureau of Meteorology, 2015) record six.

The period of remote monitoring of wind speed at that date shows a short period of monitoring stages until the wind speed reached zero. Figure C-15 reveals a time of one hour until the wind speed reached zero. Image (A), in Figure C-15 shows wind speed was 7 km/h at 7:30 pm on Wednesday 15 July 2015. Image (B) shows wind speed increased to 9 km/h at 8:00 pm. Image (C) shows wind speed and wind gusts dropped to zero at 8:20 pm. Image (D) shows wind speed continued to be zero at 9:10 pm on Wednesday 15 July 2015. The period of zero wind speed was recorded as 50 minutes. However, wind gusts and wind speed increased to 6 km/h at 9:30 pm, as shown in image (A). Wind speed dropped to zero again at 10:00 pm in image (B).

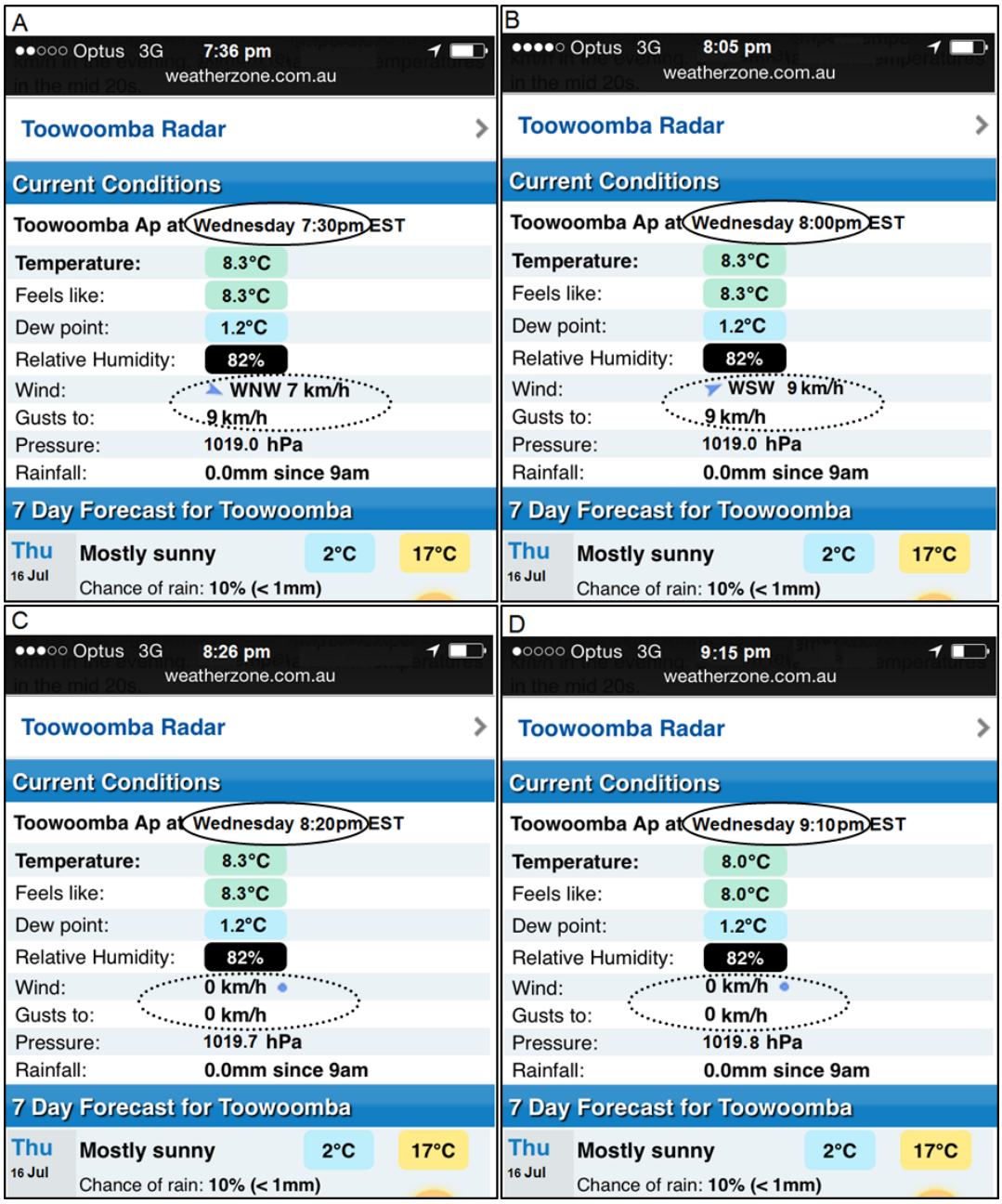

Figure C-15: Four screenshots show current wind speed decreasing gradually at that date until reaching zero, (Weatherzone, 2015) record six.

The period of zero wind continued for 50 minutes, as shown in image (C). After that wind gusted to 6 km/h and wind speed increased to 2 km/h at 11:00 pm on Wednesday 15 July 2015, as shown in image (D). Wind speed then fluctuated between 6 km/h at 12:00 am and 4 km/h at 1:07 am on Thursday 16 July 2015, as shown in Figure C-17, images (A) and (B), respectively. Wind speed then dropped to zero from 1:10 am to

4:00 am as shown in images (C) and (D) respectively. The period of zero wind recorded was more than 150 minutes.

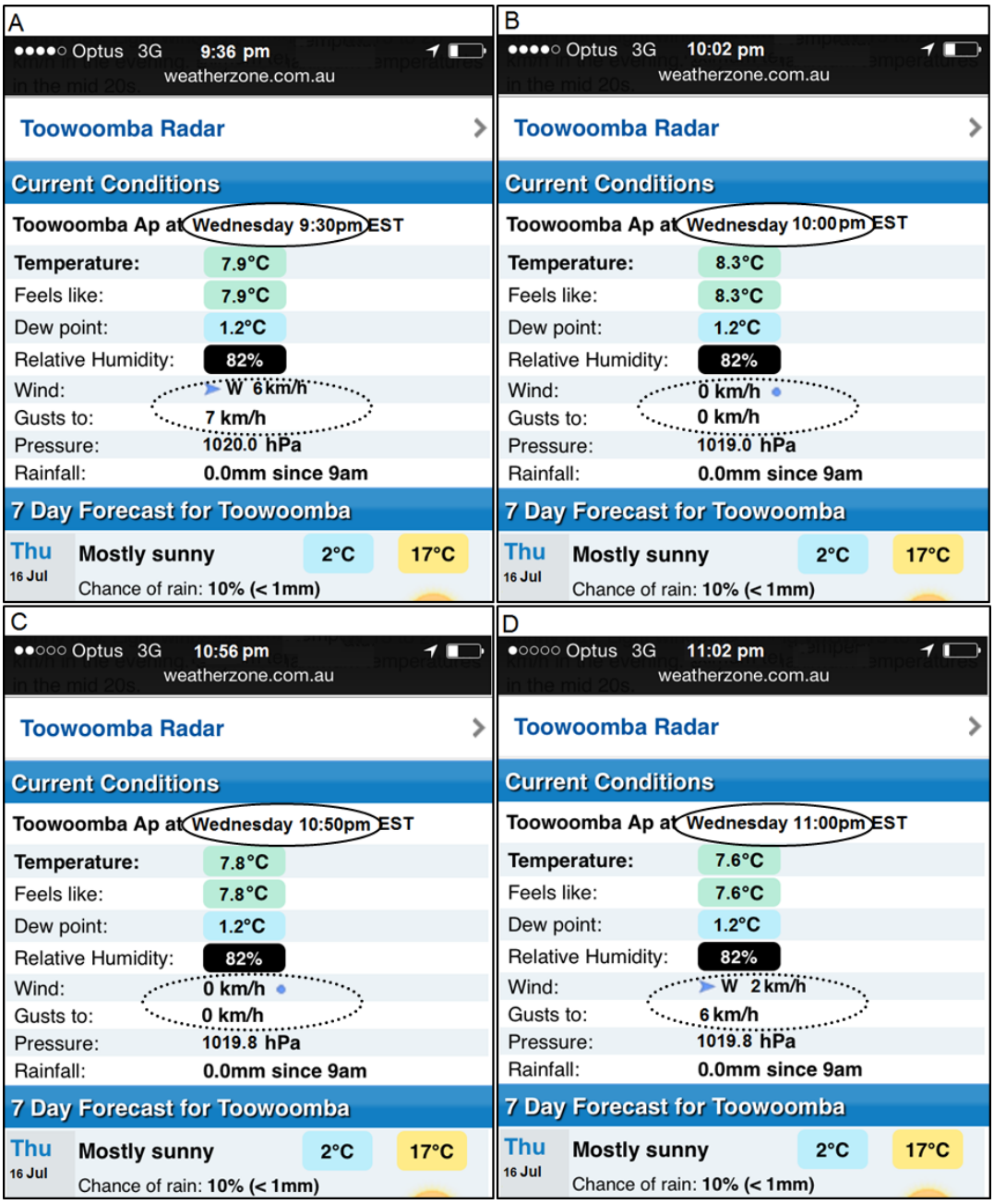

Figure C-16: Four screen shots at different times show wind speed fluctuated at different times on that date (Weatherzone, 2015) record six.

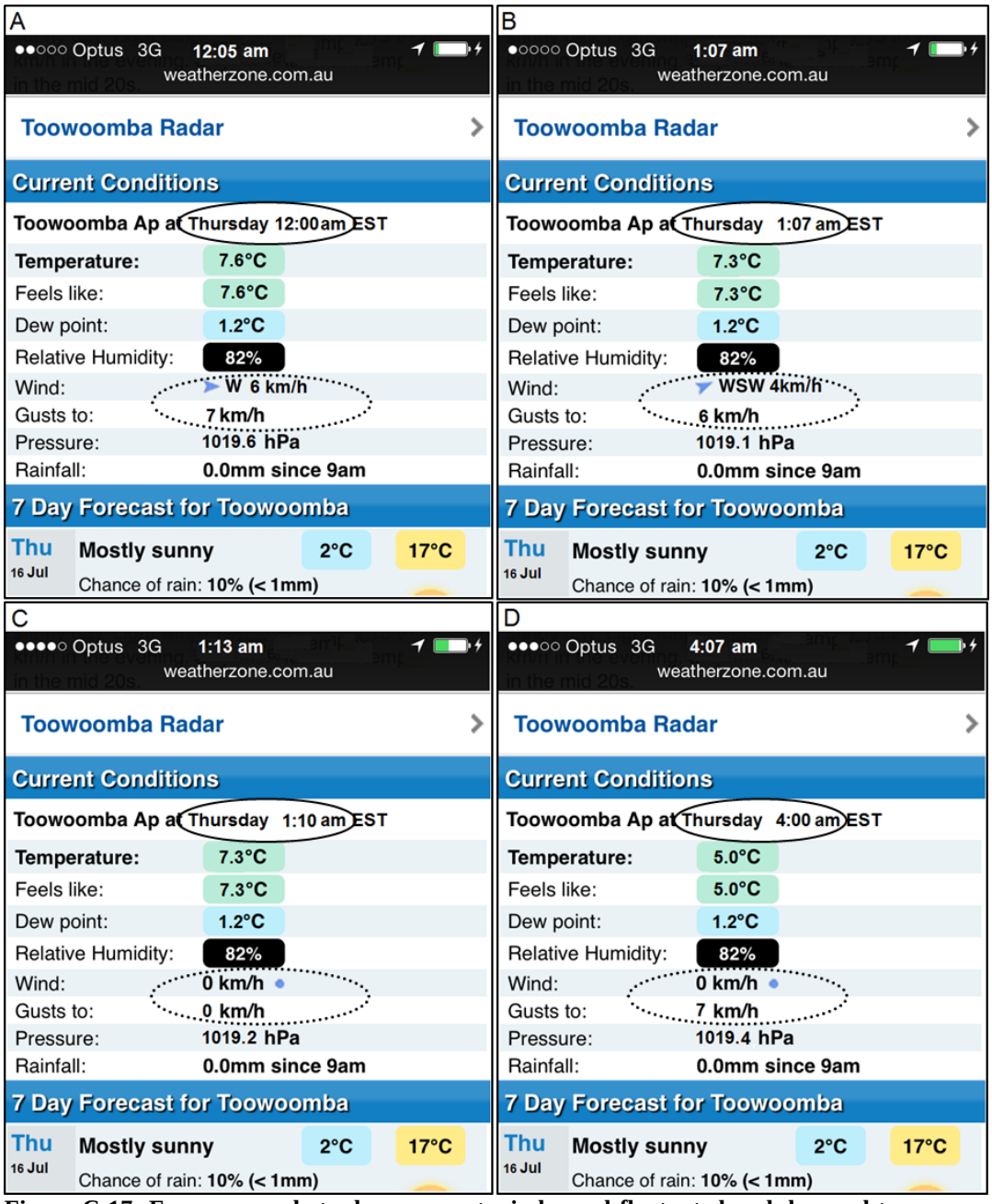

Figure C-17: Four screen shots show current wind speed fluctuated and dropped to zero on that date (Weatherzone, 2015) record six.